Carbon isotope stratigraphy of the interglacial Umberatana Group, Adelaide Fold Belt, South Australia.

By Jamie M. Burgess, B.Sc.(Hons.)

Department of Geology and Geophysics
The University of Adelaide

Submitted in partial fulfilment of the requirements for the degree of Doctor Of Philosophy in Geology at the University of Adelaide.

December, 1999

TABLE OF CONTENTS

All maps but Figure 2; Australian Grid Reference PARACHILNA 1:250 000 (SH 54-13)

LIST OF FIGURES page

LIST OF TABLES

LIST OF PLATES

ABSTRACT

The use of stable isotope geochemistry to aid the stratigraphic correlation of Neoproterozoic successions has only been in practice for the last two decades. Hitherto, rocks of this age were thought to have been too altered to allow their carbon isotopic compositions to be used for such purposes. Isotope chemostratigraphy is particularly helpful in the Neoproterozoic where biostratigraphic control is less well constrained than for Phanerozoic sequences, if available at all. This mode of geochemistry has also served to further our knowledge of the palaeoclimates and extant biogeochemical systems during this pivotal time in Earth history.

Carbon isotope signatures have been used extensively in the Phanerozoic to interpret environments in both a sedimentological and secular context. The carbon isotope record through the Neoproterozoic reveals variation and absolute $\delta^{13}C$ values that are quite anomalous in comparison to the Phanerozoic record. Relative to PDB, hugely positive interglacial values (up to +10‰) are bracketed by negative values (as low as -5‰) near glacial horizons.

The lithostratigraphic record of the Adelaide Fold Belt is well known and has long been a reference for Neoproterozoic investigations. The latest Cryogenian Sturtian to Marinoan interglacial succession is by far the thickest and most complete such interglacial sequence in the world, attaining a cumulative thickness in excess of 4km. As such, it provides an excellent opportunity for chemostratigraphic study and the compilation of a secular C-isotope curve for use in inter-regional correlation.

Careful examination of conventional thought regarding sample quality reveals the overuse of Phanerozoic models to gauge diagenetic alteration. Indeed such models cannot be used when interpreting the unique biogeochemistry of the Neoproterozoic. Whilst interbasinal and intercontinental chemostratigraphic correlations have been attempted using very sparse data sets, until now there have been few locally intensive studies aimed at elucidating regional geochemistry.

The resultant secular C-isotope profile for the interglacial succession in the Adelaide Fold Belt exhibits an overall climb to highly positive values of +8 to +10‰, before a marked negative excursion prior to the Marinoan glaciation. This compares favourably with the fragmentary curves documented from late Cryogenian interglacial successions

elsewhere, notably northwest Canada and Namibia. The increased density of C-isotope data in the Adelaide Fold Belt profile reveals higher-order perturbations of up to 4‰ that reflect changes in palaeobathymetry attributable to glacioeustatic fluctuation of sea level and local diapiric activity. The lower-order interglacial positive excursion is explicable in terms of increased marine primary productivity and high net rates of burial of organic carbon relative to carbonate carbon. A corollary of this hypothesis is a steady increase in atmospheric oxygen levels, eventually manifest in the appearance of redbed (oxidised) sediments late in the interglacial succession.

This study demonstrates the need for refinement of the established approach to interbasin stratigraphic correlation based on C-isotope geochemistry. High data resolution is desirable and correlation should take into account lithostratigraphy and sequence stratigraphy rather than solely relying on data trends or absolute $\delta^{13}C$ values. Stable isotope signals observed through the Neoproterozoic are not well understood and their precise meaning is still open to considerable debate.

STATEMENT

This thesis contains no material which has been accepted for the award of any other degree or diploma in any university and, to the best of my knowledge and belief, it contains no material previously published or written by any other person except where due reference is made in the text.

I give my consent to this copy of my thesis, when deposited in the University Library, being available for loan and photocopying.

J. M. Burgess

Acknowledgements

I recall sitting on an outcrop just east of Brachina Gorge in August 1994 with Prof. Bill Galloway and the late Dr. Bill Stuart. Dr. Nick Lemon, giving us his trade mark whistle-stop tour of the area's geology, I think may have even been off chasing his G-pick after demonstrating "hammer-golf" to our visiting friend from Austin. However the preceding conversation was undoubtedly geological, causing W.G. to pass comment on the sizeable amount of work Nick must have done for his PhD: W.S.-"Yep, he did a lot of good work". W.G.-"Makes me kinda think I let my students get away with a fair bit". For whatever motivates Nick Lemon in life, I believe a lot of young people are grateful. No amount of thanks may return the wisdom and friendship he bestows on precocious young scientists year after year. I thank him, his wife Robyn and sons Philip and David and wish them all centuries, if only on the back yard pitch. I thank Robyn's family at Gum Creek; Gordon and Beryl, Bill, Ralph, Nutmeg and others for their hospitality during my field work.

Great thanks are due also to Assoc. Prof. David McKirdy and Dr. Richard Jenkins for likewise displays of generosity. Their friendship, wisdom, honesty, support and encouragement has been critical throughout the term of this candidature. I sincerely thank Assoc. Prof. Victor Gostin for his advice, availability and contagious zest for life and the geosciences. I have benefitted from discussions with Professors Bill Galloway, Larry Frakes and Detlev Leythauser and they are sincerely thanked for their time and thoughts.

Many thanks to John Stanley, David Bruce, Wayne Mussared and especially Dr. Keith Turnbull for their advice and support through various phases of this work. I thank Gerald Buttfield and the other office staff for their support, advice and humour on all matters, especially administrative.

I thank Bernd Michaelsen for memorable laboratory stints, for wisdom imparted and humour shared. I thank my co-students Garry Adams, Rosemary Paull, Meshack Kagya, Khaled Arouri, Xinke Yu, Miles Davies, Bruce Schaefer, Paul Polito and a cast of literally hundreds of other students that made my time at the department enjoyable.

Chris Cubitt once told me that getting married had to be the ultimate distraction to thesis writing. I thank the true love of my wonderful wife Helen and her belief in kindness and the human spirit.

Only higher powers may understand the all-pervading unconditional love of the Burgess family in which it is my honour in life to share.

1. INTRODUCTION

The unique biogeochemical systems at work during the Proterozoic Eon (2500 – 544 Ma) gave rise to some of the most profound transformations in Earth history, most significantly the evolution and radiation of megascopic organisms. Geologically, the Proterozoic is characterised by several intense global glaciations and the tectonic evolution of the supercontinent Rodinia ~1.05 - 0.7 Ga (Kaufman, 1997; Li et al., 1995). From the biological perspective, the Proterozoic witnessed many landmark events. It saw the development of multicellular organisms at 1.7 Ga (Shixing and Huineng, 1995); the evolution of the eukaryotic cell at ~1.7Ga (Mendelson and Schopf, 1992); the advent of sexual reproduction at 900 Ma, and the evolution of macroscopic animals by 549Ma (Grotzinger et al., 1995). It is also speculated that microbiotas had even begun to inhabit terrestrial environments during the Proterozoic (Horodyski and Knauth, 1994; Fairchild et al., 1996)

The formation worldwide of Neoproterozoic epicontinental rift basins supports a hypothesis of the break-up of the global supercontinent Rodinia (Powell et al., 1994). In contrast to the Phanerozoic, the strontium isotope record of the Neoproterozoic documents anomalous $^{87}Sr/^{86}Sr$ values and dramatic secular variation, providing further evidence of radical tectonic activity (Derry et al., 1992). Piecing together this supercontinent has led the world's geologists on a continuing quest to correlate Mesoproterozoic orogenic belts and Neoproterozoic sedimentary stratigraphy, in order to better understand the evolution of the Earth during this period.

Over the last decade and a half, stable isotope geochemistry has been exploited as a way of improving stratigraphic resolution in sedimentary sequences with limited fossil control (Knoll et al., 1986). By measuring the variation of $\delta^{13}C$ over time (ie. through a succession of age-constrained sedimentary strata) and comparing this with other measured "secular curves", it has been possible to obtain a stratigraphic resolution greater than that provided by fossils alone (Kaufman and Knoll, 1995).

Since determination of primary stable C and O-isotope ratios in Proterozoic sedimentary rocks has traditionally been thought impossible due to their age and presumed advanced metamorphism, it has become necessary to quantify the degree of alteration and decide what amount of geochemical metamorphic "overprint", if any, exists. It is now known that "primary" stable isotopic signatures can be obtained from rocks with

a wide range geochemistries and varying degrees of metamorphism (Wickham and Peters, 1993).

The study of C-isotope ratios in Proterozoic marine carbonate and coeval organic matter has revealed globally synchronous variations that correspond to glacial-greenhouse (and vice versa) transitions (Knoll et al., 1996). It has also unveiled anomalous $\delta^{13}C$ values, not thought possible by Phanerozoic standards. When combined with palaeomagnetic studies, several of the negative excursions reflect severe global glaciation extending to low palaeolatitudes (Schmidt and Williams, 1995; Kaufman, 1997). The carbon isotopic record in the Proterozoic contains the highest and lowest values ever reported (Hoffman et al., 1998).

Stable C-isotope measurements have also been helpful in elucidating the factors which control the evolutionary transformations evident in the Proterozoic biosphere. Models of the Neoproterozoic carbon cycle have been significant in demonstrating the growth of the organic carbon reservoir (Des Marais et al., 1992) and in establishing the important role of sulphate-reducing bacteria in the terminal Proterozoic ocean (Logan et al., 1995).

The sedimentary rocks preserved in the Adelaide Fold Belt span the period 802 – 515 Ma and have a cumulative thickness in excess of 20 km (Fanning et al., 1986; Preiss, 1987). These rocks are among some of the best studied in Australia and provide a global benchmark for several important events in Earth history including the Sturtian and Marinoan glaciations and the evolution of the famous Ediacaran fauna. The lithostratigraphic units contained therein are relatively well constrained in terms of their regional and interregional equivalents and serve as a framework from which to build chemostratigraphic profiles. The Neoproterozoic part of the Adelaide Fold Belt succession contains well-preserved, characteristic glacial and interglacial sediments. It is these sediments that form the focus of the present study.

This thesis uses continuous exposure in drill core and outcrop with uneqivocal continuity but relies on correlations established by other workers to tie between the sections analysed. It was considered beyond

the scope of this thesis to reinterpret the stratigraphic succession but merely use the available data as a “ladder” and place the isotopic analyses on the “rungs”. This thesis aims first to test the contemporary application of C-isotope stratigraphy on several different local scales. Then, with a composite dataset for a specific interval of time, it seeks to compare the constructed interglacial C-isotope profile with those from key late Cryogenian successions on other continents (Kaufman and Knoll, 1995). It also evaluates various ideas regarding the origins of the observed C-isotopic signals so that the systematics of Neoproterozoic chemostratigraphy may be better understood.

2. GEOLOGICAL AND GEOCHEMICAL BACKGROUND

2.1 Stable C-isotope geochemistry

Whilst the elemental chemistry of seawater has changed little during the Phanerozoic, the isotopic composition of carbon, oxygen, sulphur and strontium in the oceans have varied dramatically over this same period (Holser, 1984). These isotopic variations are inextricably linked to tectonic and biogeochemical change. A thorough explanation of molecular and isotopic biogeochemistry of these elements can be found in Summons and Hayes (1992).

Carbon is the element that forms the basis of living matter and as such, remains a focus for geologists striving to elucidate the history of life. The rate of primary biological productivity, and the relative rates at which carbonate carbon (C_{carb}) and organic carbon (C_{org}) are buried, are parameters crucial in evaluating $\delta^{13}C$ data. Both are equally able to cause fluctuations in C-isotopic composition (Hayes, 1983; Holser, 1987).

The fixation of CO_2 by autotrophic-photosynthetic organisms is characterised by the preferential uptake of the lighter ^{12}C isotope. Photosynthetic fractionation of the stable carbon isotopes by such biota causes the observed difference in the isotopic composition of co-existing Neoproterozoic carbonate carbon and organic carbon, which has been shown to be relatively constant at 28.5‰ (Knoll et al., 1986). Although near-primary $\delta^{13}C$ of organic matter (kerogen) can be reliably measured (provided its atomic H/C ratio is >0.2: McKirdy and Powell, 1974), carbonate carbon isotopic signatures have been most often determined, with covariance between the two being used as verification of sample quality (Kaufman and Knoll, 1995).

The breakdown of organic matter in the Neoproterozoic water column has been indentified as a process crucial to the proper interpretation of secular C-isotope data. Logan et al. (1995) postulated that the presence of an unusual $\delta^{13}C$ signature (n-heptadecane > kerogen > pristane) observed in Neoproterozoic sediments was a result of the high degree of reworking of sinking algal organic matter by heterotrophic sulphate-

reducing bacteria (Figure 1A). It was further postulated that the advent of metazoans and faecal pellets in the Cambrian enabled the quick removal of organic matter from the water column and the shift of the sulphate-reducing process to the substrate (Figure 1C). The enhanced burial of photosynthetically-derived organic material in marine sediments would increase concentrations of dissolved oxygen in the upper levels of the water column, enabling its eventual escape to the atmosphere.

This theory was expanded upon by Knoll et al. (1996) who saw the drawdown and consumption of CO_2 in the surface waters of the Neoproterozoic ocean as a likely mechanism for driving the greenhouse-glacial climatic transition. The removal of CO_2 from the atmosphere reduces the capacity for greenhouse, facilitating the growth of continental ice sheets and sea ice and stimulating ocean circulation and turnover (Figure 1B).

Important implications of this model include increasing the concentrations of CO_2, HCO_3^- and H_2S in the deeper part of the Neoproterozoic ocean. With the localisation of organic productivity high in the water column and the release of isotopically lighter carbon via organic matter remineralisation in the deep ocean, an overall exaggeration of the known variation of $\delta^{13}C$ with depth (Kroopnick, 1985) would be expected. The model incorporates a sluggish interglacial ocean overturn and chemical stratification of the water column based on redox state. The presence of banded iron formations (BIFs) in many late Proterozoic successions suggests that the deep ocean was anoxic if only irregularly (Beukes and Klein, 1992).

Recently, an alternative hypothesis by Hoffman et al. (1998) postulated that the $\delta^{13}C$ signals observed in the Neoproterozoic carbonate record were in part the result of a virtual standstill of the hydrologic cycle during glaciation. The “Snowball Earth” hypothesis implies that virtually the entire Neoproterozoic ocean closed-over with sea ice, preventing chemical exchange between the ocean and atmosphere during glaciation. Build up of atmospheric CO_2 via subaerial volcanism over the course of the glaciation would eventually reach critical amounts and deglaciation would be nearly instantaneous. Large amounts of

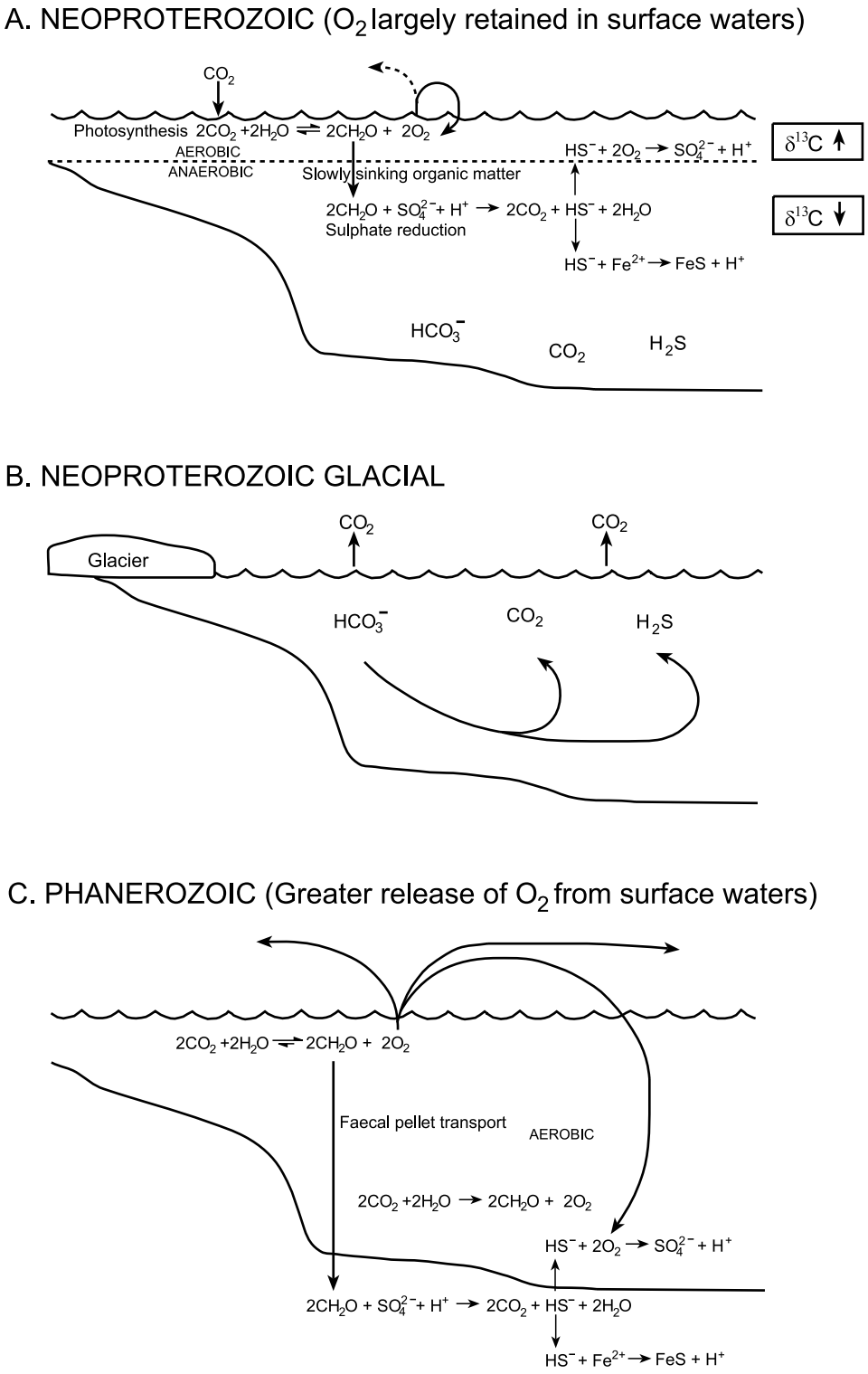

Figure 1. Models of the Proterozoic and Phanerozoic biogeochemical cycle highlighting the importance of oxidation of organic matter by sulphate-reducing bacteria. 1A: chemically stratified ocean. 1B: post-glacial overturn of oceanic water. 1C: organic matter “bypasses” water column to substrate (modified after Logan et al., 1995 and Knoll et al., 1996).

atmospheric CO_2, with isotopically light carbon, given relatively sudden access to the ocean would be readily dissolved, thereby facilitating widespread (cap) carbonate precipitation with negative $\delta^{13}C$ values (Hoffman et al., 1998).

Variations of $\delta^{13}C$ and $\delta^{18}O$ with environment of deposition have traditionally led geochemists working on Phanerozoic systems to derive the origins of carbonate cements on the basis of isotopic data alone (Veizer and Hoefs, 1976). Due mainly to the degree to which $\delta^{18}O$ readily alters with diagenesis and neomorphism, it is now recognized that this is not altogether possible with many Neoproterozoic sections (Kaufman and Knoll, 1995). Studies have shown that in a stratified Neoproterozoic ocean, carbonates precipitated below the surface level of mixing are depleted in $\delta^{13}C$ by 4-6‰ relative to shallow water carbonate (Kaufman et al., 1990; Winter and Knauth, 1992). Although the large number of sections outlined in Kaufman and Knoll (1995) appear to record no apparent facies-related variation of carbonate $\delta^{13}C$, it is acknowledged that the data may show geographic variations of 1-2‰. Notwithstanding any such local variation in $\delta^{13}C$ signal, it appears likely that the overall variation observed through Neoproterozoic successions records a globally valid secular trend.

2.1.1 Evaluation of sample quality

A protocol for rigorously evaluating the quality of C-isotope chemostratigraphic data is set out by Kaufman and Knoll (1995). Various causes of alteration of primary $\delta^{13}C$ signatures in Neoproterozoic carbonates are indentified. These include: post-depositional interaction with organic matter, equilibration with fluids of different isotopic composition and decarbonation reactions in the presence of silicate minerals. Oxidation of organic matter by aerobic and sulphate-reducing bacteria releases isotopically light CO_2 that can be important in the precipitation of diagenetic carbonate. As a result, diagenetically-altered carbonates will have a reduced $\delta^{13}C$ signal. The CO_2 given off as a result of the decarbonation reaction between carbonate and silica will be isotopically heavy, resulting in the overall lowering of $\delta^{13}C$ in the remaining carbonate (Shieh and Taylor, 1969).

The formation of dolomite has commonly been thought to involve the chemical alteration of calcite by saline Mg-bearing fluids. Study of Neoproterozoic dolomites has found that most were formed from pore fluids isotopically similar to those from which the coexistent calcite precipitated. Thus, many dolomites normally retain the $\delta^{13}C$ of their precursor calcite (Kaufman and Knoll, 1995).

Commonly, plain light and cathodoluminescence microscopy is used to assess extent of diagenetic cements and alteration. Knowledge of oxygen and carbon systems may also be utilized in assessing sample quality. The elemental abundances of Mn, Sr, Mg and Fe in limestones, have also been used as indicators of diagenetic alteration. Through such alteration, Mn and Fe are enriched and Sr and Mg are depleted. The criteria of acceptability proposed by Kaufman and Knoll (1995) are by no means rigid. Carbonate samples with $\delta^{18}O < -10‰$ and/or Mn/Sr ratios > 10, normally considered to indicate unacceptable levels of alteration, may nonetheless be deemed to have acceptable (near primary) C-isotope signatures that record secular changes in sea water chemistry (Narbonne et al., 1994; Pelechaty, 1998).

Logically, the least altered samples are likely to be those which have undergone minimal heating during catagenesis and metamorphism. Even so, Wickham and Peters (1993) showed that Neoproterozoic rocks within the amphibolite facies (450°C+) in western North America, recorded primary or at least pre-metamorphic $\delta^{13}C$ values.

Organic matter (kerogen) is a sensitive indicator of thermal alteration and as such may provide an index of the level of heating experienced by the host rocks. Measurement of the ratio of atomic hydrogen to carbon in kerogen, where present, is a very useful sample screening procedure (McKirdy and Powell; 1974; McKirdy et al., 1975; Hayes et al., 1983).

The use of petrology to aid microsampling of separate carbonate phases has worked well where suitable lithofacies are available (eg. Narbonne et al., 1994). Microsampling enables avoidance of carbonate phases thought to be altered. However, there is no reason to believe that measurement of $\delta^{13}C$ via whole-rock digestive techniques cannot yield high quality data provided that the sample selection process is thorough.

An explanation of the screening protocol and analytical method used in this study is contained in Appendix 1.

The samples included in this study are generally micrites which show no obvious sign of recrystallisation. Moreover, they were collected from an area where kerogens have atomic H/C ratios greater than 0.2 and therefore retain near-primary δC_{org} values (McKirdy et al., 1975, Cooper, 1991). Many of the sediments, however, show evidence of deposition under reducing conditions and, as a consequence, the iron contents of their carbonates are elevated.

Finally, quite a deal of information can be obtained simply from the comparison of the C and O isotope curves themselves. If $\delta^{13}C$ of carbonate shows covariance with $\delta^{13}C$ of coexisting organic matter with a modal separation of ~28‰, this will indicate the likely preservation of primary isotopic signatures since no alteration process will alter both parameters by the same magnitude in the same direction (Knoll et al., 1986). Indeed, if absolute C-isotope values for stratigraphic equivalents correspond across a region, then those values can be assumed to be primary, recording the ambient compositions of marine carbonate and organic matter.

2.2 The Adelaide Fold Belt: a geological overview

Over thirteen kilometres of largely shallow water Neoproterozoic sediments are exposed in the north-south oriented Adelaide Fold Belt in South Australia. Historically the basin has been called the Adelaide Geosyncline, sharing many elements in common with the miogeosyncline of Kay (1947). Preiss (1987) discusses the nature of the basin in a full description of its sediment fill and tectonic history. The geometry of the basin suggests that its central zone, exposed in the central Flinders Ranges, may be described as an aulacogen located between two continental blocks, the Gawler craton to the west and the Curnamona Cratonic Nucleus to the east (Figure 2). Re-evaluation of its tectonic history has given rise to the alternative terms ‘Adelaide Fold Belt’ (Jenkins, 1990) and ‘Adelaide Fold-Thrust Belt’ (Flottmann et al., 1994).

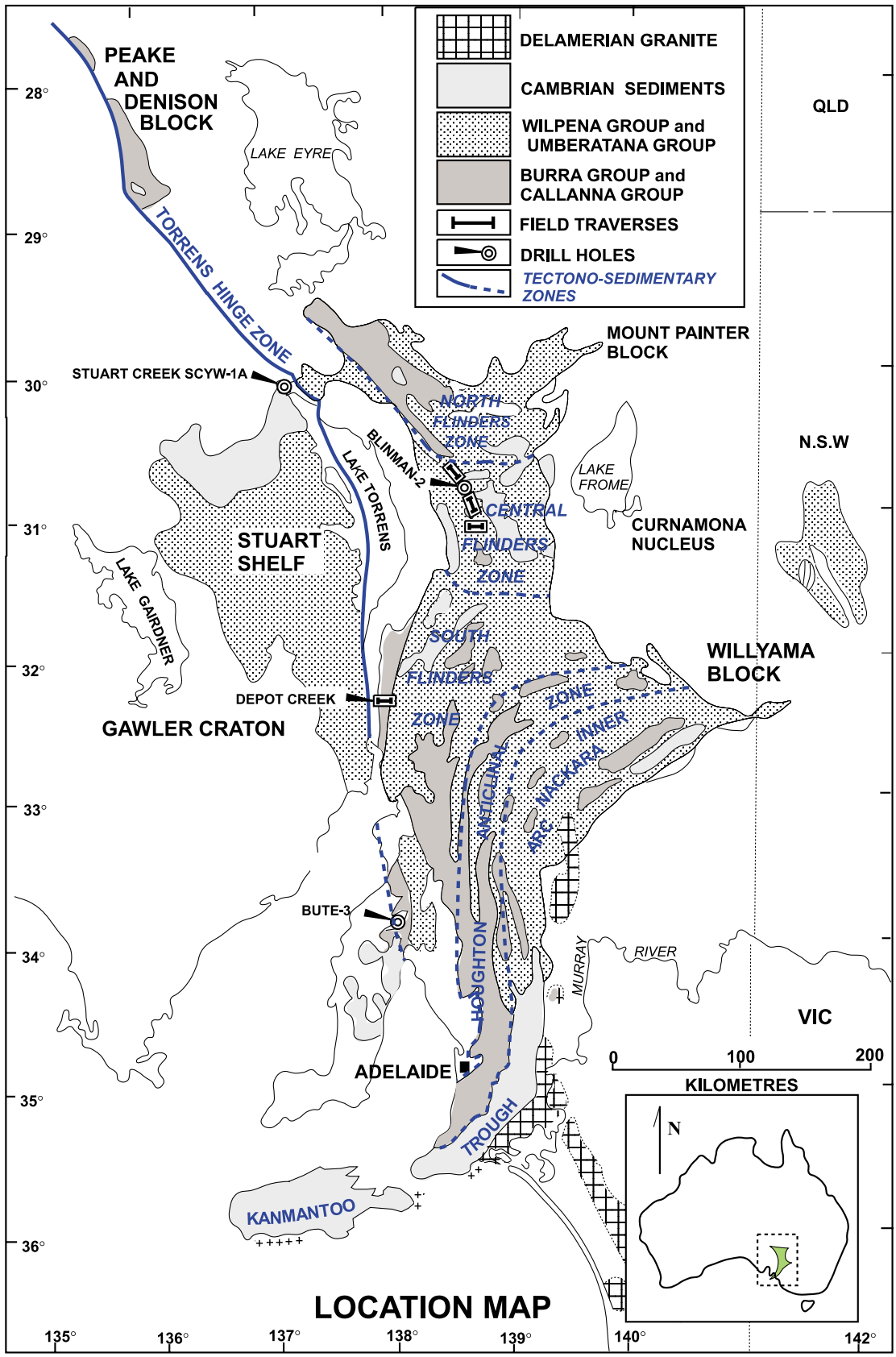

Figure 2. The Adelaide Fold Belt, South Australia. (Tectono-sedimentary zones after Rutland et al., 1981)

The formation of an epicontinental rift, the first stage in the development of the Adelaide Fold Belt, began before significant breakup of the global supercontinent Rodinia around 700 Ma. Various stages of the basin's subsequent evolution are interpreted as reflecting tectonic movements on a grander scale (Powell et al., 1994).

The Adelaide Fold Belt displays many characteristics of a rift that developed into a passive margin, as reflected in the twofold, lithostratigraphic subdivision of its Neoproterozoic sequence (Preiss, 1985; Figure 3). The Warrina Supergroup (Callanna and Burra Groups) is largely restricted to a fault-bounded rift, whereas deposition of the Heysen Supergroup (Umberatana and Wilpena Groups) spread on to the Stuart Shelf and is reflective of passive margin-style sedimentation.

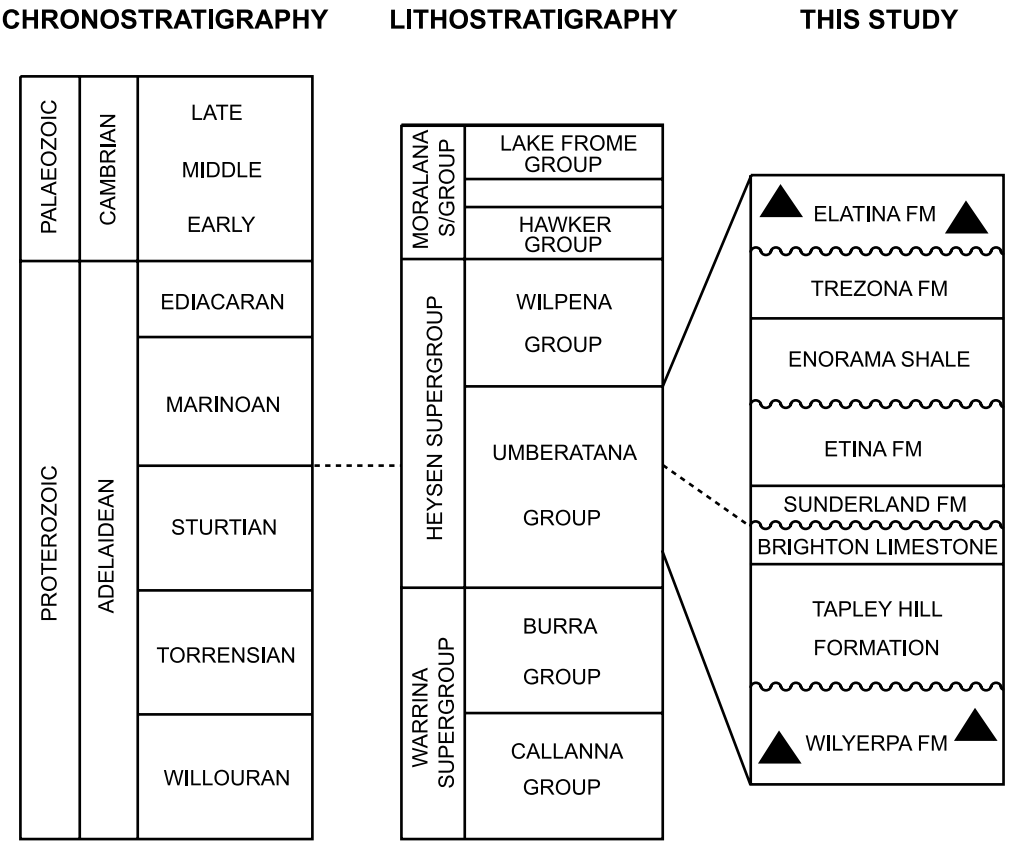

Figure 3. Summary of Umberatana Group stratigraphy, Central Flinders Ranges (after Lemon, 1988).

The Warrina Supergroup encompassses the bottom half of the Adelaidean sequence. It comprises restricted playa and salina deposits interbedded with redbeds and basic volcanics (Callanna Group) which

give way to sandy clastics interfingering with dolomite and unusual magnesite beds (Burra Group). A reliable age of 802 ± 10 Ma exists for the Rook Tuff of the Callana Group (Fanning et al., 1986). The Heysen Supergroup comprises the Sturtian to Marinoan glacial and interglacial units of the Umberatana Group; and the post-Marinoan redbed siliciclastics and ramp-style carbonate deposits of the Wilpena Group.

The extensive Sturtian glaciation is represented by at least two distinct pulses of sediment deposition in the basin now preserved as the Adelaide Fold Belt. This is thought to represent either two distinct glacial phases (Coates and Forbes, 1977) or, more likely, an overall waxing and waning of a single glacial event (Young and Gostin, 1988). Basal hematitic boulder tillite fines up to a red ironstone shale facies, a global event seen on four other continents (Derry et al., 1992). Locally, a hiatus preceded the deposition of the dolomitic siltstones, yellow-brown lithic sandstones and diamictites of the Wilyerpa Formation throughout the wider basin. The exceptionally low $^{87}Sr/^{86}Sr$ ratios and occurrence of vast iron rich sediments during the Sturtian, described by Derry et al. (1992), may be accounted for by the increased influence of hydrothermal fluids on seawater chemistry, a likely by-product of the contemporary tectonic activity.

The description of the Adelaidean succession was initially attempted in rock-time units by Mawson and Sprigg (1950), but the application of this description failed due to lack of definitive time markers. The lithostratigraphic subdivision of Thomson et al. (1964) has served well but is currently under revision. The application of sequence stratigraphic concepts has allowed some time constraint to be re-injected into description of the succession but this is yet to be finalised (Preiss et al., 1998).

Deposition of the interglacial Umberatana Group is reflective of sea level fluctuation on different scales. Reclassification of Umberatana Group stratigraphy (Preiss et al., 1998) has raised questions about the limits of stratigraphic subdivision based on sequence-mapping and, in particular, the relative importance placed on recognised sequence boundaries. Attempts to quantify periodicity and the causal effects of depositional cyclicity (e.g. Krapez, 1996) have hitherto not been applicable to most

Precambrian sequences due to the lack of absolute geochronological control.

The Sturtian Series of the Adelaide Geosyncline (Mawson and Sprigg, 1950) comprises the glacigenic sediment and the post-glacial Tapley Hill Formation and Brighton Limestone. Representing initial transgression associated with the melting of the Sturtian ice cap, the Tapley Hill Formation is one of the first units in this system to be deposited on the Stuart Shelf to the west. Deposition of the dolomitic Tindelpina Shale Member marks the onset of post-Sturtian transgression and represents a typical "cap" carbonate to the underlying diamictites of the Wilyerpa Formation. Within the Tapley Hill Formation, facies variants reflecting shallowing over intrabasinal highs in the central Flinders Ranges take the form of the Mount Caernarvon Greywacke and Wockerawirra Dolomite Member.

Deposition of the succeeding Brighton Limestone, a stratigraphic equivalent of the Wockerawirra Dolomite at shelfal localities, represents a fall in sea level of significant proportions. The Brighton Limestone is characterised by a gradation from silty limestone to intraclastic and stromatolitic limestone and finally ooid shoals. An increase in dolomite content towards the top of the section confirms shallowing-upward to an exposure surface. This is a significant sequence boundary which marks the end of the Sturtian (Lemon, 1988; Preiss, 1996).

The next 1500 m of sedimentation in the Central Flinders Zone shows a series of repetitions of the Brighton Limestone paracycle, shallowing upward through limestones to exposure and then deepening into calcareous shale. This part of the interglacial succession is dominated by shallow water limestones and the redevelopment of paracycle-depositional systems involving various degrees of hiatus and exposure.

In contrast to the predominantly suboxic environments of deposition represented by the lower part of the Umberatana Group, the top 1000 m of the section comprises mostly oxidised red shales and limestones and provides strong evidence for the stratification of the late Cryogenian ocean. The onset of the Marinoan glaciation was accompanied by the

lowering of base level, and exposure and erosion of significant amounts of the uppermost interglacial limestone unit, the Trezona Formation.

The Marinoan glacial deposits of the Elatina Formation were first described and identified as being younger than the Sturtian tillites by Mawson (1949). Up to 1500 m thick, the Elatina diamictites are mainly pink to brownish red pebbly sandy siltstone with a dolomitic silty matrix and low clast density. The Marinoan glacigenic sediments are capped by a fine grained, pink cap dolomite, the Nuccaleena Formation.

The Marinoan is the likely Adelaidean equivalent to the first of the well documented Varanger glacial episodes, recorded in the Northern Hemisphere. The two-fold Varanger glacigenic succession is most notably represented in Svalbard by the Elbobreen (E2) and Wilsonbreen Formations and in East Greenland by the Ulvesø and Storeelv Formations respectively (Knoll et al., 1986; Fairchild and Spiro, 1987). The same glacial events are also represented by the Smalfjord and Mortensnes Formations in Finnmark, Norway, that also give their names to the respective glacial stages (Harland et al., 1989, Fairchild and Hambrey, 1995).

The Nuccaleena Formation “cap dolomite” marks the base of the Wilpena Group. The majority of the lower Wilpena Group is dominated by siliciclastics, mainly thick red deep-water shales and massive delta-front sands. The deep-water, red and black shale of the Bunyeroo Formation in the middle Wilpena Group contains the Acraman impact ejecta horizon (Preiss, 1987); and rare clasts thought to be possible dropstones, indicating a cool water environment of deposition and making it a possible equivalent of the second Varanger glacial episode (Jenkins and Nedin, 1998).

The upper half of the Wilpena Group consists of a thick sequence of silty limestones of the Wonoka Formation and sandstones of the Pound Subgroup, the latter containing the famous Ediacaran Fauna (Preiss, 1987).

2.3 Sampling strategy

In order to sample limestones from the Umberatana Group of the Adelaide Fold Belt with minimal metamorphic overprint, the Central Flinders Zone (Rutland et al., 1981) was targeted. Weak metamorphism in this area (Lemon et al., 1992) increases to biotite grade greenschist facies towards the northeast in the North Flinders Zone (McKirdy et al., 1975).

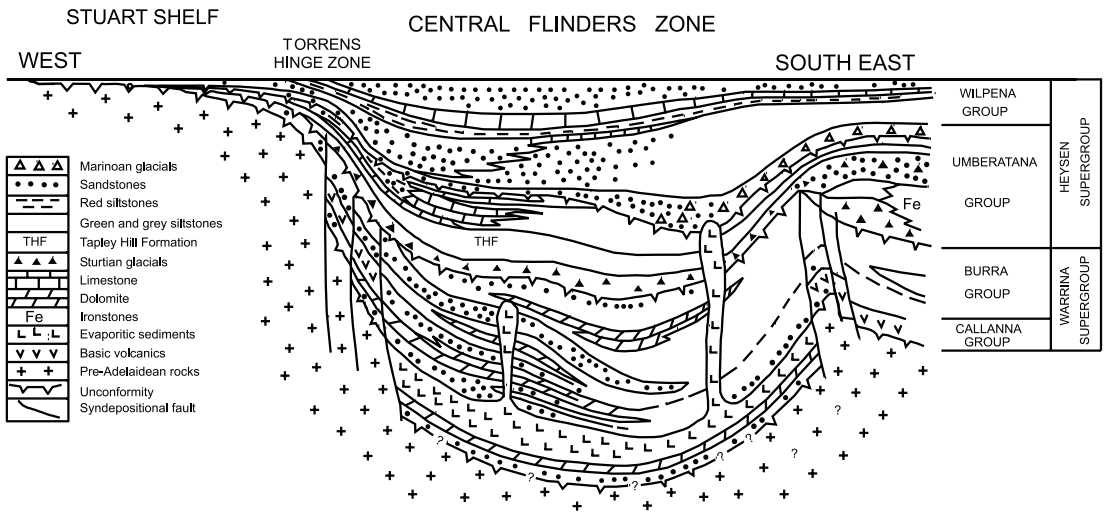

Figure 4. Interplay of facies in the central Flinders Ranges (adapted from Lemon, 1996)

It is theoretically possible to sample a calcareous rock throughout the whole interglacial succession (Figure 4). Times of transgression and high sea level stand, such as during deposition of the thick Tapley Hill Formation and the Enorama Shale, are represented by condensed (with respect to their comparable basinal facies thickness) proximal carbonate facies, such as the Brighton Limestone and Woocalla Dolomite on the Stuart Shelf. As the post-Sturtian sea level began to drop and these shelfal limestones were deposited, stratigraphically-equivalent limestones were also formed over or around intrabasinal topographic highs, e.g. above ascending diapirs (Figure 4). Careful mapping of these areas adds to the inventory of carbonate rocks suitable for sampling for interglacial chemostratigraphic purposes.

It is expected that shelfal limestones such as the Brighton Limestone, as well as other thicker platform carbonate units like the Etina Formation,

have undergone some degree of alteration due to burial diagenesis, as well as exposure to meteoric waters after uplift and erosion, bringing their geochemical integrity into question. In an attempt to quantify these effects, beds of the Trezona Formation were sampled at three different locations, where compaction, lithification and exposure to meteoric influence can be assessed. By documenting the nature and magnitude of C and O isotopic alteration due to karstification immediately below demonstrable exposure surfaces, it is possible to place limits on the likely alteration of the other carbonate units sampled.

3. DIAPIRS AND DOLOMITE

3.1 Introduction

The isotopic signature of sediments older than the Umberatana Group was investigated because it is known that older rocks are reworked to positions higher in the succession. They are discussed here to provide some quality control on isotopic values derived from rocks containing these older sediments as reworked clasts.

The presence of breccias that exhibited stratigraphic disorder was first noted in the Flinders Ranges by Howchin (1922). Their occurrence in the Adelaide Fold Belt follows the deposition of graben-controlled continental playa and salina style evaporites (source material) overlying redbeds of the basal Callanna Group. These sediments are interbedded with typical early-rift basic extrusive volcanics and evaporitic carbonates which form the bulk of diapiric debris observed in the central Flinders Ranges (Preiss, 1987; Lemon, 1988).

Diapirism occurs when shale or evaporitic sediment is subjected to substantial loading by sediment of greater density and a pressure gradient exists within the source horizon. Overburden pressures accentuate the density contrast as the less dense material becomes bouyant and mobile. This disrupted material will most often mobilise xenoclasts of surrounding strata creating a brecciated appearance in outcrop.

The effect of diapirs on local sedimentation at various times in the history of the Adelaide Fold Belt has been well documented by Lemon (1988). He grouped 16 diapiric breccia bodies in the central and northern Flinders Ranges, into six different “families” based on their order of development. This was primarily determined by how they affected the surrounding sediments, including incorporation of diapirically-derived detritus and the development of local bedding characteristics such as slumping and unconformities. In the central Flinders Ranges, the Blinman and Enorama Diapirs are among the oldest and have had a profound influence on the interglacial sediments of the Umberatana Group in their immediate vicinity.

According to the model proposed by Lemon (1988) for sedimentation in moderate to shallow water depths around diapirs, change in sea level is reflected in the facies that are exposed at the sediment-water interface (Figure 5). At times of low relative sea level, sub-aerial exposure of the

diapir will result in erosion and be manifested in the inclusion of reworked diapiric xenoclasts in the surrounding sediment. Times of sea level high stand initiate pulses of diapiric movement by increasing the load on the diapir-source and surrounding beds, creating slumps and turbidite facies in peripheral sinks. The increased relief on the diapir allows fringing reefs and saline lagoon facies to develop beside and atop the diapir, respectively.

The effect of salt diapirs on regional salinity is well studied in modern terrains such as the Mexican Gulf Coast of North America (Hanor, 1994). In this subsurface setting (>1 km depth), greatly increased salinities are observed in pore water fluids over many kilometres vertically and tens of kilometres laterally, having a pronounced effect on the chemical reactions occurring within the surrounding sedimentary sequences.

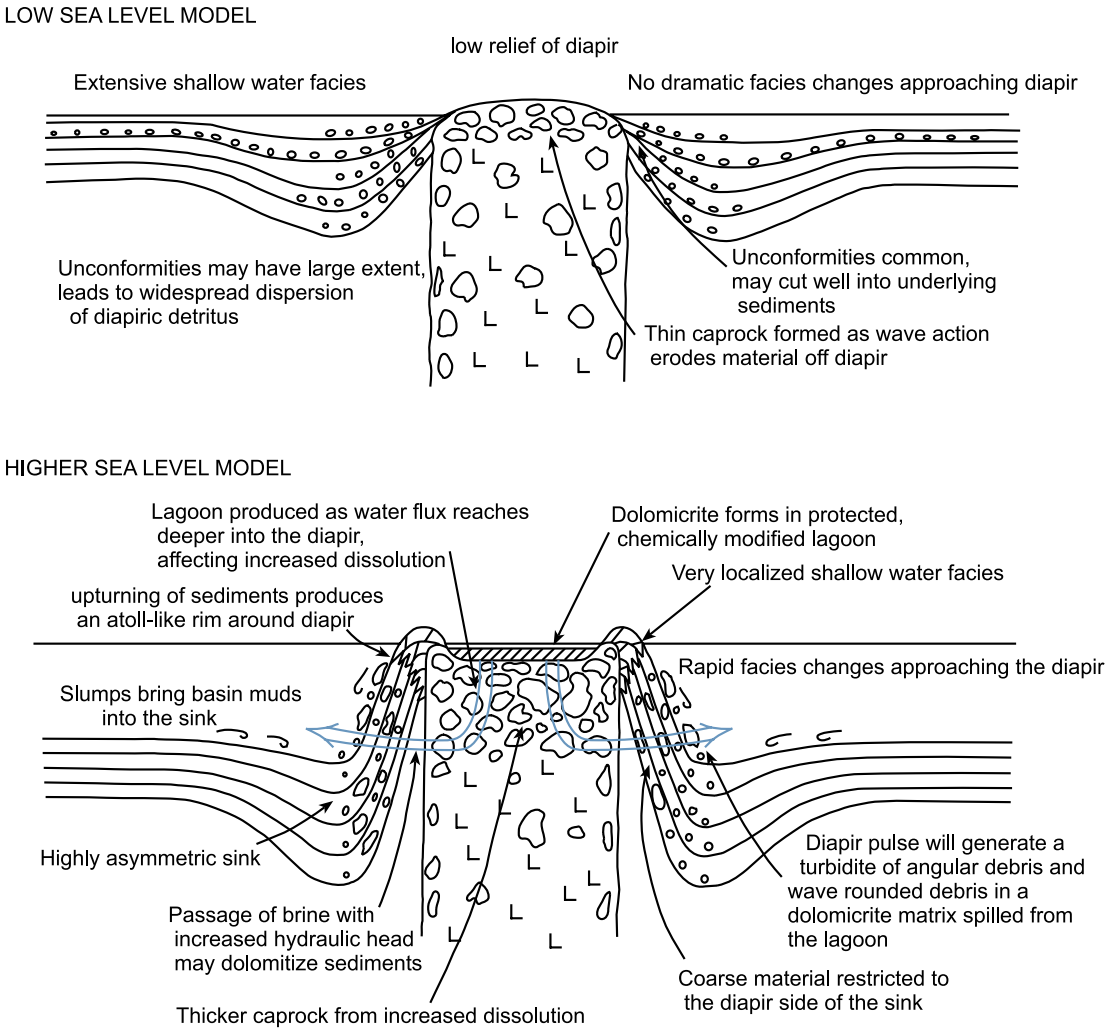

Figure 5. Models for exposed diapirs (from Lemon, 1988).

At a transgressive surface in the Enorama Shale, largely devoid of shallow water carbonate, Lemon (1988) documented increasing concentrations of dolomite toward the Enorama Diapir for up to 2-3 km. Increased dolomite content in the sediments surrounding the diapir was attributed to either *in situ* dolomitisation via a typical brine-reflux method, or supply of detrital dolomite in the form of dolomitic diapir xenoclasts or dolomicrite directly precipitated out of water in the lagoon on top of the diapir then swept into the surrounding sediment.

The stable isotope compositions of these "diapirically"-derived dolomites will most likely reflect their respective environments of formation and may be responsible for affecting the geochemistry and mineralogy of surrounding limestones. More importantly, this may have a substantial effect on the interpretation of their C-isotopic data.

A consideration of the potential influence of diapiric rocks and diapirically-modified sea water chemistry is important in the context of this thesis because the lower part of the interglacial sequence in the Central Flinders Zone are only exposed where pushed upwards by diapir emplacement. In short, these sequences are exposed only around diapirs.

3.2 Diapiric xenoclasts; an insight into displaced Callanna Group

The majority of xenoclasts observed in the breccias of the Blinman and Enorama Diapirs are from different parts of the Curdimurka Subgroup, the upper Callanna Group (Figure 6). The Willouran sediments of the Callanna Group in the Worumba area east of Hawker, are thought to have been deposited between 1100 and 800 Ma, with the Torrensian Burra Group being deposited after that and before 750 Ma (Preiss, 1985). At the base of the Callanna Group, a localised debris facies is overlain by widespread extrusive basaltic volcanics of the upper Arkaroola Subgroup. The succeeding Curdimurka Subgroup is characterised by siltstones with halite casts, as well as further basic volcanics that pass laterally into diapiric breccia (Thomson et al., 1964). The graben-controlled sedimentation of the Callana Group records a cyclical facies variation based upon pyritic and carbonaceous siltstones, well-bedded siltstones and sandstones with halite casts, stromatolitic limestone and dolomite, evaporitic dolomite with cryptalgal lamination and evaporite mineral pseudomorphs. Known thicknesses of this group range from nearly 2 km in the Worumba area to over 8 km in the far northwestern reaches of the fold belt, as exposed in the Peake and Denison Ranges (Preiss, 1987).

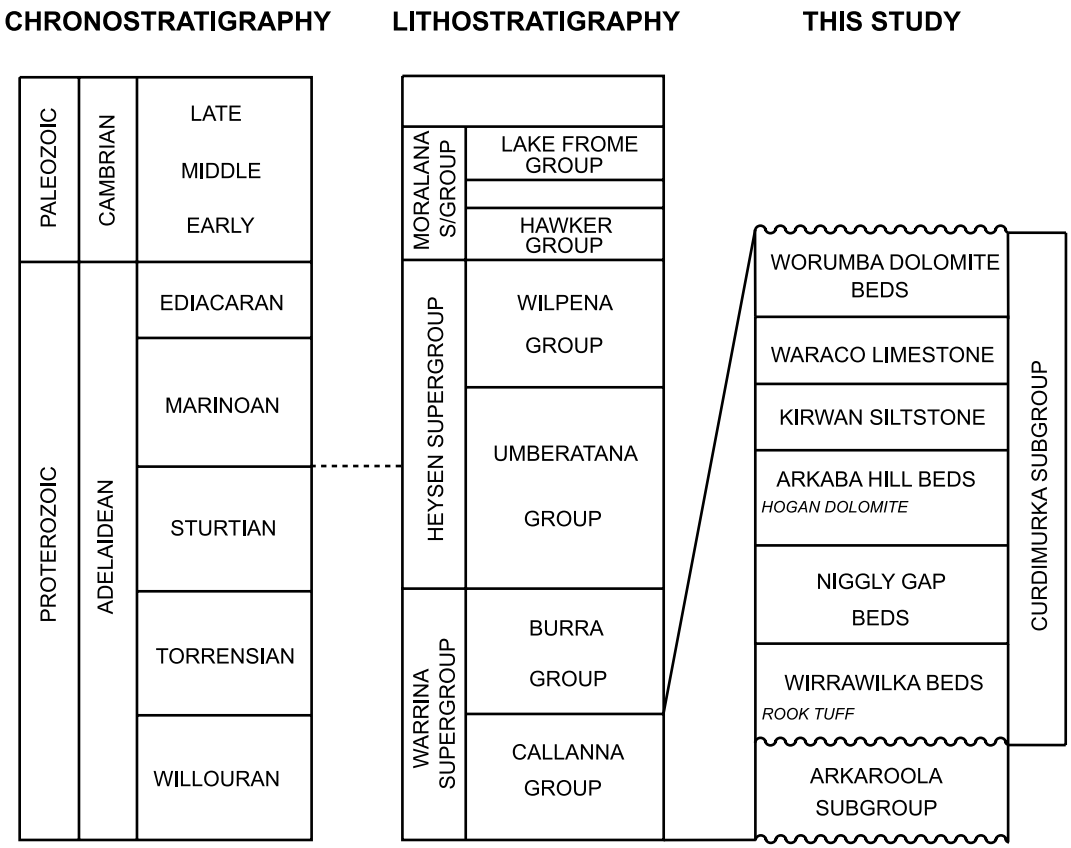

Figure 6. Generalised Callana Group stratigraphy (after Preiss, 1987).

The Curdimurka Subgroup is exposed in the Worumba area as a series disjointed blocks. Preiss (1985) found sufficient continuity between these blocks to erect a stratigraphy for the subgroup. There is enough lithological similarity between the blocks in the Worumba area and the xenoclasts found in the diapiric breccias, to suggest that they have the same origin. Curdimurka Subgroup deposition begins with the Wirrawilka Beds that record a regression from permanently submerged, grey pyritic siltstone to commonly graded silt and cryptalgal and fenestral laminated intertidal to supratidal dolomicrite deposited in an overall playa lake or restriced marine setting. The Niggly Gap Beds are the most significant post-volcanic sediments in the area, comprising immature micaceous and feldspathic sandstones closely interbedded with carbonaceous siltstone and shale. The overlying Arkaba Hill Beds consist of a lower finely laminated siltstone unit grading up into a shallow-water carbonate unit. The upper unit includes both limestone and dolomite characterised by cryptalgal lamination, low-relief stromatolite mounds, psuedomorphs after gypsum, tepee structures and laminar fenestral fabrics indicative of low-energy mud and carbonate flats with slight intertidal influence and intermittent sub-aerial exposure. The carbonates of the Arkaba Hill Beds conformably grade into dark grey, finely laminated, carbonaceous siltstone of the Kirwan Siltstone. This unit also contains black chert lenses and early diagenetic pyrite,

indicating that it was deposited in a subaqueous environment under reducing conditions. Regression followed with the deposition of the Waraco Limestone as three distinctive units: a basal grey limestone with black chert, a pale stromatolitic dolomite marble, and an upper siltstone. At the top of the Curdimurka Subgroup are the Worumba Dolomite Beds. These consist of cream to pale brown, cryptomicrobially laminated dolomite overlain by finely laminated dark siltstone which is in turn overlain by buff to pale grey cryptomicrobially laminated dolomite.

The xenoclasts in the Blinman Diapir are up to 3 km long, mostly comprising grey micaceous shale and sandstone interbedded with red, heavy-mineral laminated sandstone and cupriferous dolomite with abundant halite casts. As such they closely resemble the Niggly Gap Beds of the Worumba Anticline. The xenoclasts of the Enorama Diapir are dominantly rafts of basic volcanic with brecciated sediments resembling the Arkaba Hill Beds and the Niggly Gap Beds (Preiss, 1987).

3.2.1 Previous geochemical investigations

Samples from the Arkaba Hill Beds, Kirwan Siltstone and Worumba Dolomite from the Worumba Anticline area east of Hawker were sampled by McKirdy et al. (1997) for investigation of their organic carbon contents. These samples were taken from the darker siltstone units of their respective formations, representing euxinic environments of deposition ideal for preservation of organic matter.

The one sample from the Arkaba Hill Beds recorded a total organic carbon (TOC) value of 0.35% and a $\delta^{13}C_{org}$ of -28.03‰. Assuming a ~28.5‰ difference between organic matter and coexisting carbonate (Knoll et al., 1986), this would correspond to an equivalent $\delta^{13}C_{carb}$ of approximately +0.5‰.

Six samples from the dark Kirwan Siltstone yielded TOC values in the range 0.17 - 0.45% (mean = 0.31%). One $\delta^{13}C_{org}$ measurement was recorded at -26.6‰, corresponding to an equivalent $\delta^{13}C_{carb}$ of +1.9‰.

The three samples from the Worumba Dolomite yielded TOC values in the range 0.23 - 0.43% (mean = 0.35%). One sample yielded $\delta^{13}C_{org}$ of -25.0‰ equating to a $\delta^{13}C_{carb}$ of +3.5‰.

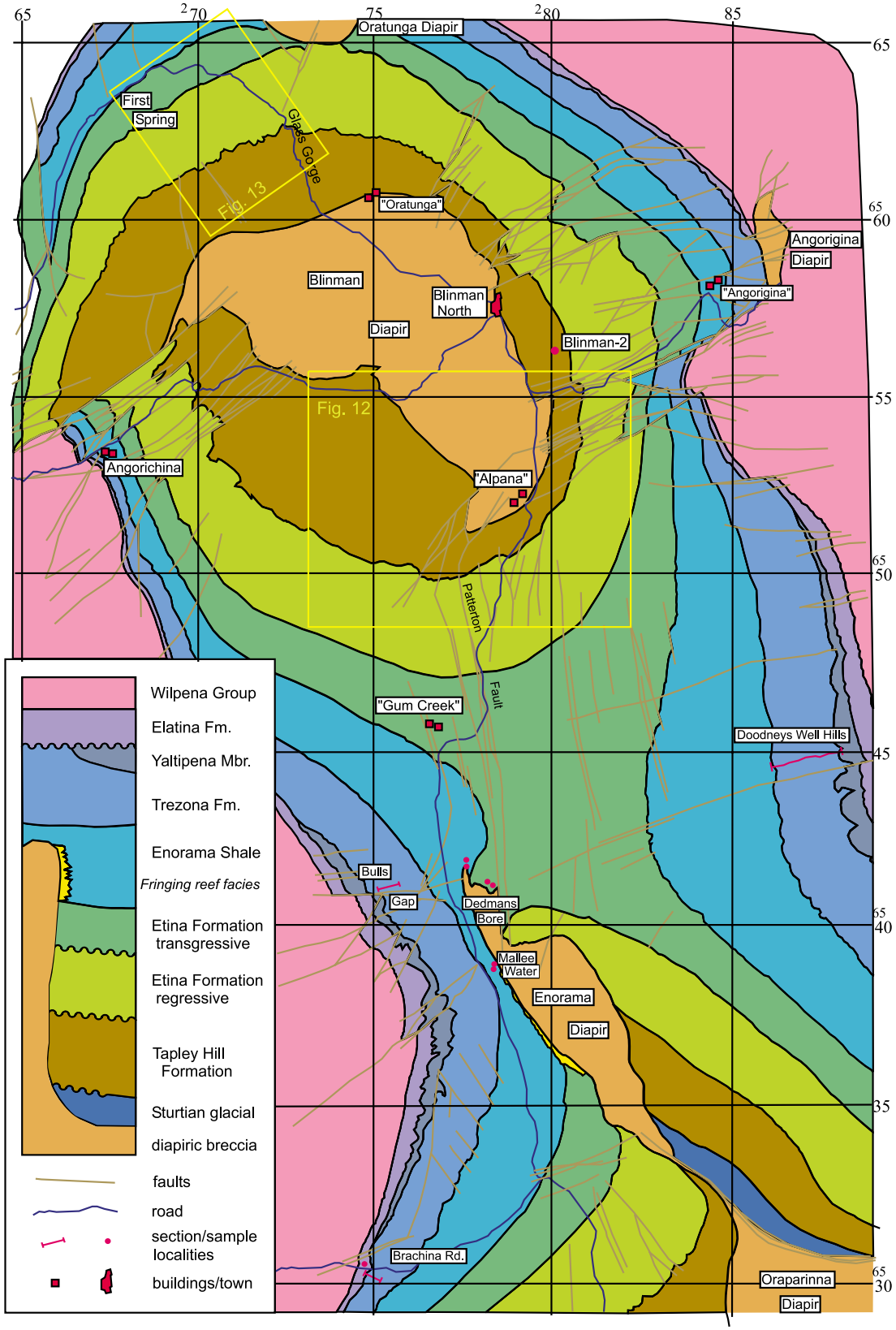

Figure 7. General geology, central Flinders Ranges (After Lemon, 1988, A.M.G. Co-ordinates).

3.2.2 Sampled xenoclasts

Four dolomites known to be from the Enorama Diapir were sampled. Two of these are samples of a fenestral, sabkha-type dolomite that occur as large float boulders in the creek directly to the east of Dedmans Bore (1041-108 and 109: Plate 1A). One is a yellow-weathered dolomitic limestone from within the diapiric breccia at Dedmans Bore (1041-110) and another is dolomitic float from further south at Mallee Water (1041-113: Figure 7). Their isotopic compositions are shown in Table 1.

Sample	δ^{13}Ccalc	δ^{18}Ocalc	δ^{13}Cdol	δ^{18}Odol
1041-108			+1.8‰	-5.5‰
1041-109			+1.7‰	-6.3‰
1041-110	-4.8‰	-4.3‰	+2.9‰	-5.6‰
1041-113			+3.3‰	-10.9‰

Table 1. Carbon and oxygen isotopic compositions of diapiric xenoclasts.

The only reference by Preiss (1985) to the sabkha-typical fenestral fabric observed in samples 1041-108 and 109 occurs near the top of the Wirrawilka Beds. The light-buff colour of these samples is also in accord with the described lack of carbonaceous material of the Wirrawilka Dolomite. It is acknowledged that accurate stratigraphic correlations based on rock type and diagenetic fabrics alone may not be reliable in this case because of the laterally impersistent nature of the source beds. Moreover, supratidal evaporite facies are observed at other levels in the Curdimurka Subgroup.

The gritty dark yellow immature dolomitic limestone (1041-110) has dispersed limonite from weathering of scattered heavy sulphides. It is likely to originate from rocks of the same description at the base of the Niggly Gap Beds. Carbonaceous material is also common at this level, the post-depositional oxidation of which may be the cause of the light δ^{13}C signature exhibited by the recrystallized calcite of this sample.

Sample 1041-113 is a ripple-worked to cryptomicrobially-laminated, buff arenaceous dolomite that has no truly characteristic features may indeed fit almost anywhere within in the Curdimurka Subgroup stratigraphy. It contains talc laths, produced by reaction of chert with dolomicrite, that appear to be pseudomorphs of anhydrite after gypsum within micritic layers (Plate 1B). It also contains early chloritic stylolites and late-stage fractures healed by dolosparite cements. The onset of talc

Plate 1A. Float boulders of fenestral dolomite, samples 1041-108 and –109, Dedmans Bore. δ^{13}Cdol +1.8‰ and +1.7‰, δ^{18}Odol –5.5‰ and –6.3‰ respectively.

Plate 1B. Talc laths, pseudomorphs of anhydrite after gypsum, produced by reaction of chert with dolomicrite. Diapiric xenoclast sample 1041-113, δ^{13}Cdol +3.3‰ and δ^{18}Odol –10.9‰, plane polarised light, 4X mag.. Field of view is 4.2mm wide.

formation at lower greenschist facies temperatures (350-400˚C), the absence of dedolomitisation and only subtle recrystallisation of arenaceous parts of this rock together indicate that this rock has not undergone severe metamorphism .

The occurrence of talc is documented throughout the Adelaide Fold Belt. It accompanies asbestos deposits at Robertstown and in the Enorama Diapir and is a common metamorphic mineral in the Callana Beds of the Northern Flinders Ranges (McBriar, 1949; Wymond and Wilson, 1951; Coats and Blissett, 1971). Talc was observed as an accessory mineral of both xenoclasts and diapiric breccia interstices by Mount (1975). The timing of its formation with respect to emplacement of the diapirs remains ambiguous. Mount (op. cit.) concluded that the talc is a product of the very low grade dedolomitisation (decarbonation) reactions in the siliceous metadolostones found within diapiric cores.

Talc was not observed in the other three xenoclasts sampled in this study. Nevertheless dedolomitization is likely to have occurred in sample 1041-110 as indicated by its high calcite content and light $\delta^{13}C$ signature. If indeed the same reaction has occurred in sample 1041-113, but to a lesser degree, then the original $\delta^{13}C$ value for this sample would undoubtedly have been greater than that observed.

Although the stable isotope compositions of these samples are largely as would be expected for carbonate minerals precipitated in evaporative settings, the inexact stratigraphic origin must remain uncertain due to differing degrees of alteration and the similarity of the carbonate facies deposited throughout the Curdimurka Subgroup.

The incorporation of diapiric xenoclasts of this kind into Umberatana Group sediments was assessed petrographically as discussed in Chapters 4-7. Although diagenesis of carbonate minerals is notoriously subtle and indeed the cement stratigraphy of a sample like 1041-113 is just as complex as that of any interglacial limestone, the clastic nature of any included xenoclasts is easily recognizable.

3.3 Lagoonal Dolomicrite

The development of lagoonal environments atop exposed diapirs is documented by Lemon (1988). The abundance of dolomicrite matrix in conglomerates and dolomicrite slumps in deep water shales observed around the Patawarta, Beltana, Blinman, Enorama and Oraparinna diapirs indicates a source of dolomite mud over or around the diapirs.

Resistant lenses of yellow-weathering dolomicrite can be observed at various levels in the stratigraphy around the Enorama Diapir. Lemon (op. cit.) postulated that dolomite "whitings" (after Haines, 1987) precipitated directly out of sea water in these lagoons and was washed into surrounding sediment following pulses of upward diapiric movement influenced by sea level rise.

Although lagoonal dolomite mud is easily observed as discrete lenses its wider incorporation the matrix of other units in smaller concentrations has possibly been understated. Its presence in sediments containing dolomite from other sources, and its affect on the isotope geochemistry of the host rock, will be more difficult to determine than is the case for diapiric xenoclasts.

The geological and geochemical relationship of this dolomite mud to the fringing reef facies of the Enorama Shale will be discussed in Chapter 6.

3.3.1 Dolomicrite samples

Samples of four dolomicrites were taken from the Dedmans Bore and Mallee Water areas around the Enorama Diapir (Figure 7). Yellow-brown sandy limestones 1041-111 and 1041-112 are from 50 and 150 metres, respectively, into the Patterton Shale Member of the Etina Formation along the Dedmans Bore section (section 10, Lemon, 1988) on the northeastern side Enorama Diapir. Sample 1041-37 comes from the lower third of the Enorama Shale directly north of the Enorama Diapir and Dedmans Bore. A dark red argillaceous dolomicrite 1041-114 was taken close to a conglomerate bed half way through the Enorama Shale at Mallee Water to the west of the Enorama Diapir. The isotopic compositions of these samples are presented in Table 2.

Sample	δ^{13}Ccalc	δ^{18}Ocalc	δ^{13}Cdol	δ^{18}Odol
1041-111	-0.5‰	-9.9‰	+1.2‰	-6.4‰
1041-112	+1.2‰	-3.5‰	+4.6‰	-2.7‰
1041-37	+4.0‰	-5.9‰	+6.4‰	-6.1‰
1041-114			-3.1‰	-4.7‰

Table 2. Carbon and oxygen isotopic compositions of lagoonal dolomicrites.

Sample 1041-111 is a coarsely crystalline, yellow-brown dolomitic marble. The existence of this carbonate-rich horizon within the transgressive-deeper water facies of the Patterton Shale is characteristic of the occurrence of lagoonal dolomicrite. Petrographic evidence indicates that extensive dedolomitisation of this rock has occurred,

leaving poikilotopic calcite spar overprinting a relic stylolitic dolomicrite fabric (Plate 2A). The extensive recrystallisation of this rock is most likely related to its close proximity to faults associated with diapir development. Large shear stresses act upon compacted sediments in the development of such structures.

Sample 1041-112, at a higher stratigraphic position and further away from the diapir, is more finely crystalline and has therefore probably been subjected to a lower degree of alteration. The carbon isotopic composition of these first two samples (Table 2) gives an indication of the degree to which these rocks have been altered. The depletion of the calcite in ^{13}C relative to dolomite is as expected from decarbonation reactions. The extent to which the C-isotopic compositions of the dolomite in these samples reflect its original signatures is difficult to determine. The fabric and isotopic compositions of these two samples, however, will serve as a good reference for suspected metamorphism of other dolostones in the Central Flinders Zone.

Sample 1041-37 contains xenotopic dolomite with rare thin calcite veins. Minor diagenesis has occurred resulting in overgrowth cement on siliciclastic grains that commonly include microscopic dolomite rhombs. This dolomicrite contains a high amount of feldspar which is most likely derived from diapiric breccia. It also contains detrital iron minerals, including hematite, and cyanobacterial flakes that are probably storm debris originating from a diapir-fringing stromatolite reef facies.

Dolomicrite 1041-114 was sampled at a stratigraphic level that is approximately half way through the Enorama Shale. It was deposited immediately after a bed of conglomerate associated with a pulse of upward movement of the diapir. This sample has a dark red colour resulting from a high proportion of ferric-iron in the mud matrix. The red mud was probably mixed into the dolomicrite by turbulent flow into the basin where red mud is the background sediment. However, what appear to be mostly elongate clasts up to 4 mm long (mean = 0.5 mm) containing no matrix of this kind are in luminescence-continuity with surrounding dolomicrite. They are most likely clasts of partially cemented lagoonal dolomicrite that remained intact, having been washed down the side of the diapir with oxidised muds from shallow waters. Inclusion of diapiric xenoclasts with varying cathodoluminescence signatures, including a clast with evaporite mineral pseudomorphs (Plate 2B), is likely to have a proportional effect on the measured stable isotope compositions of the host rock. In this case it would appear that if there has been any isotopic overprint from the observed small number of diapir

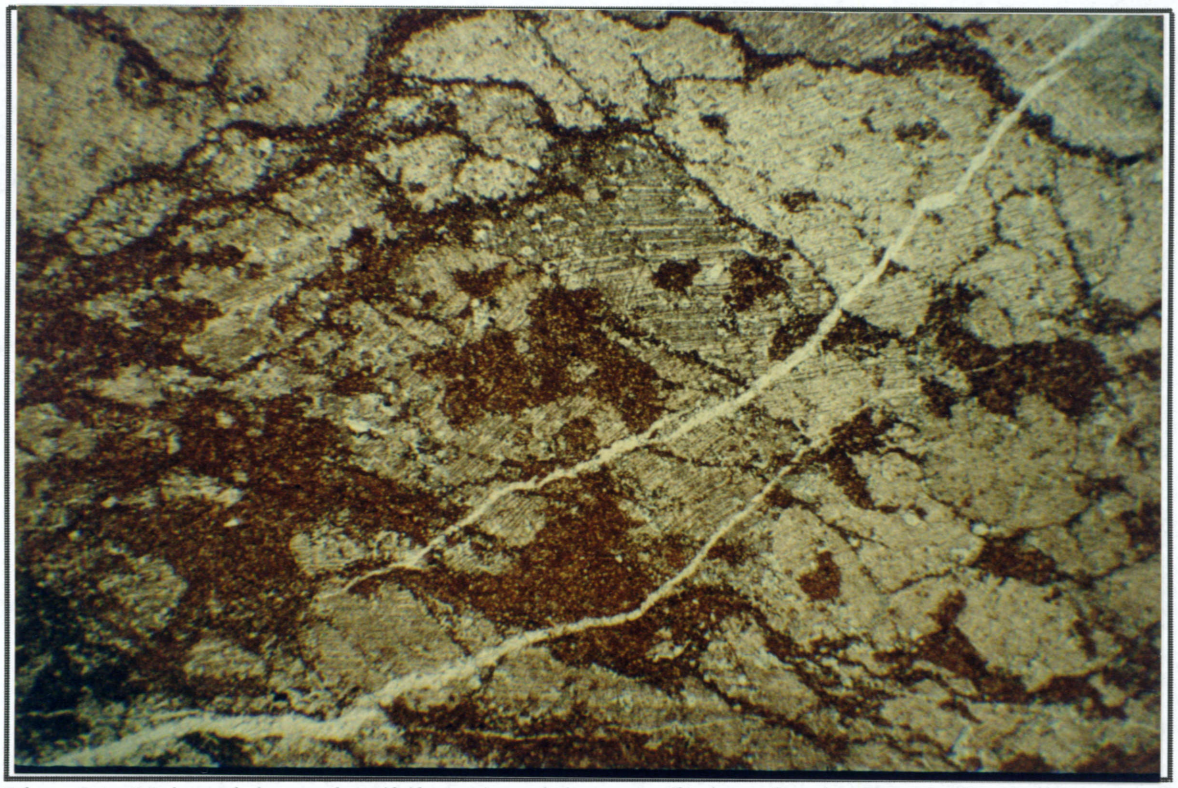

Plate 2A. Vein calcite and poikilotopic calcite spar (light colour) overprinting relic stylolitic dolomicrite fabric (orange). Dedolomitization in lagoonal dolomicrite in Patterton Shale, sample 1041-111, δ^{13}Ccal –0.5‰, δ^{18}Ocal –9.9‰, δ^{13}Cdol +3.3‰, δ^{18}Odol –10.9‰, plane polarised light, 4X mag.. Field of view is 4.2 mm wide.

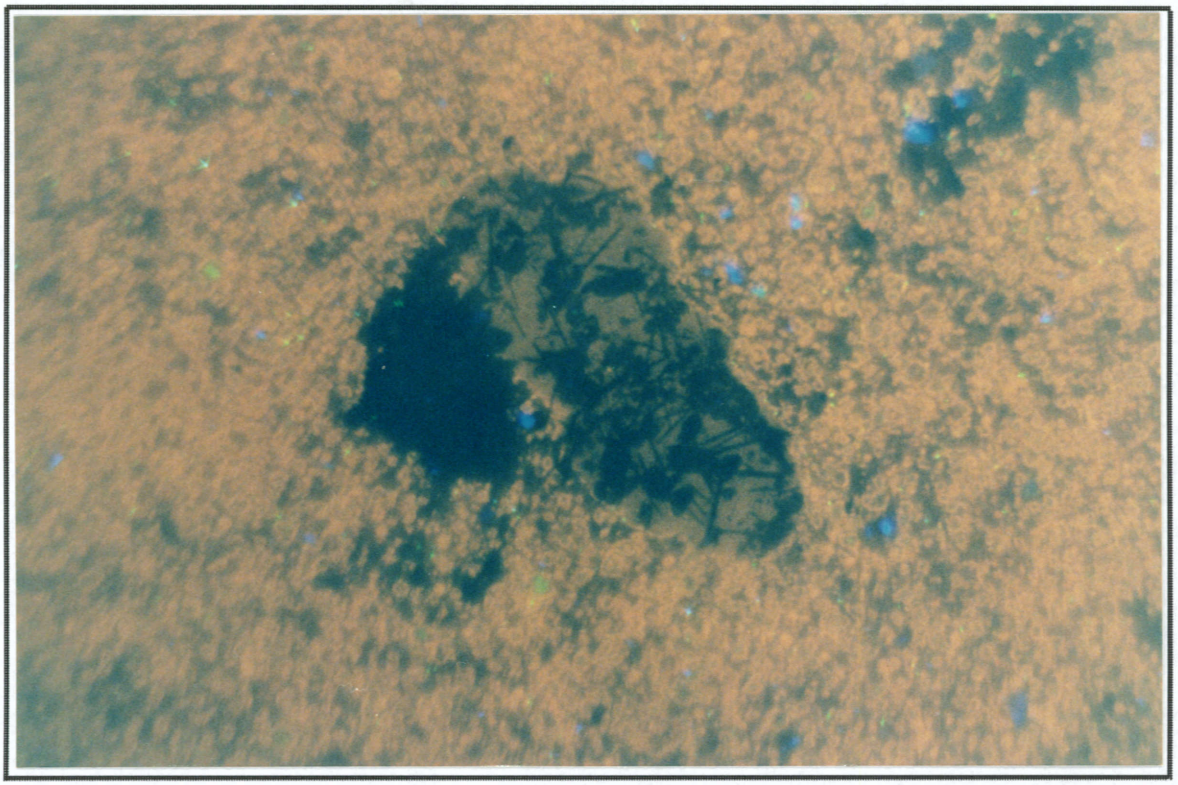

Plate 2B. Diapiric xenoclast with evaporite pseudomorphs in lagoonal dolomicrite. Sample 1041-114, δ^{13}Cdol -3.1‰ and δ^{18}Odol –4.7‰, 15kV, 203μA, 2.9 seconds, 20X mag.. Field of view is 1.25 mm wide.

xenoclasts (observed range of $\delta^{13}C$ = +2 to +3‰ from limited sampling), then the $\delta^{13}C$ of the background dolomicrite will be somewhat less than -3.1‰.

3.4 Discussion.

Diapiric xenoclast geochemistries are complex and largely unpredictable. However, this is to be expected given the varying diagenetic maturity, as well as their unclear but variable stratigraphic origins. It can at least be observed that most Callanna Group rocks have $\delta^{13}C_{carb}$ signatures in the low positive range (+2 to +3‰) and that these can be assumed to be carried into the sediments higher in the stratigraphic column into which they are subsequently incorporated.

The range of $\delta^{13}C$ observed in lagoonal dolomicrite is much greater and may possibly reflect primary stratigraphic variation. The C-isotopic signatures of dolomicrite vary from >+4.6‰ (allowing for the effect of decarbonation) in the upper Etina Formation, through +6‰ in the overlying Enorama Shale and back to <-3.1‰ (allowing for xenoclast inclusion) in the mid-Enorama Shale.

If the presence and amount of either of these forms of dolomite can be established petrographically then it should be possible to predict the degree to which they effect local mineral and stable isotope geochemistries.

4. WILYERPA AND TAPLEY HILL FORMATIONS AND BRIGHTON LIMESTONE

4.1 Introduction

The Tapley Hill Formation is a well-sorted, dark bluish grey, slightly calcareous or dolomitic, often pyritic, siltstone (Preiss, 1987). It commonly has a concordant or disconformable contact with the underlying Sturtian glacial units, and the transgressive to high-stand nature of its deposition means that it is distributed widely throughout the Adelaide Fold Belt. Indeed the Tapley Hill Formation is generally interpreted as having a deep oceanic environment of deposition and has equivalents both within Australia and on other continents. Regional facies variation of the Tapley Hill Formation was controlled by changing sea level and contrasting basin topography. Its thickness exceeds 3.5 km in some depocentres and it extends onto the Stuart Shelf. It is the first unit within the Adelaidean succession to spread beyond the fault boundaries of the early rift and has been equated with the start of a passive margin phase of deposition within the Adelaide Fold Belt (Preiss, 1983; Lemon, 1996).

In the central Flinders Ranges, the Tapley Hill Formation commonly overlies the glacigenic Wilyerpa Formation. The Wilyerpa Formation comprises dolomitic silts and sands that are interbedded with and overlain by, yellow weathering diamictites and lithic sandstones and conglomerates (Lemon, 1988).

A typical post-glacial transgressive cap carbonate occurs at the base of the Tindelpina Shale Member in the form of finely bedded, micritic (often detrital) dolomite with dark grey siltstone interbeds. This organic-rich and pyritic member indicates a very rapid transition into deep water and suboxic environments of deposition. At shelfal localities, this transition had probably slowed somewhat allowing the deposition of peloid grainstones up to 15 m thick (Preiss, 1987).

Reflecting sea level fluctuation and facies change on a paracyclic scale, shallowing over intrabasin topographic highs of the Blinman and Oraparinna Diapirs gave rise to the deposition of the Mount Caernarvon Greywacke Member. This buff to grey, well sorted, very fine feldspathic sandstone is generally flat laminated but also shows ripple cross-lamination as an indication of the shallowing that brought about its deposition (Lemon, 1988).

Regression during the later stages of the post-Sturtian high stand gave rise to shallow-water carbonate facies in the form of the Brighton Limestone in shelfal localities, and the Wockerawirra Dolomite in the Central Flinders Zone. Eventual low stand and exposure resulted in the first sequence boundary of the interglacial succession (Figure 3). The Brighton Limestone reflects a steadily shallowing transition from calcareous shales into shallow water stromatolites, followed by high-energy intraclastic and ooid limestones before being capped by supratidal fenestral dolomites. At locations on the Stuart Shelf, the top of the Brighton Limestone is a buff colour reflecting oxidation upon exposure. An increase in carbonate content with shallowing and change from siltstone to limestone with stromatolites, ooids and intraclasts is repeated several times in the overlying Etina Formation (Lemon, 1988).

In the Central Flinders Zone (Rutland, 1981), the shallow water Wockerawirra Dolomite is the stratigraphic equivalent of the Brighton Limestone. This buff to pale-yellow, fine grained dolomite may be mapped as two separate bodies in the peripheral sinks around the Blinman Diapir, each with its own separate parasequence boundaries.

4.2 Previous geochemical investigations

The Tapley Hill Formation has come under scrutiny by mineral and petroleum geologists, as well as those with academic interests. The Tapley Hill Formation is renowned for its stratabound ore deposits (Lambert et al., 1980) and the preserved organic matter which makes the Tapley Hill Formation a prospective hydrocarbon source rock (Cooper, 1991). It has also been the focus of previous chemostratigraphic studies (e.g. Strauss et al., 1992; McKirdy et al., 1995).

The upper Sturtian glacial units contain up to 20% carbonate, mainly in the form of dolomitic matrix but also as dolostone clasts from pre-glacial units such as those of the Burra Group. Crossing and Gostin (1994) measured isotopic signatures from the Appila Tillite along the Emeroo Range (South Flinders Zone: Figure 2) and found that its dolostone clasts mostly retained the positive $\delta^{13}C$ signatures (mean ~ +4‰) of their corresponding precursor rock unit. The dolomitic "rock-flour" matrix, however, was considered likely to have been subjected to alteration in the presence of isotopically-light melt fluids, explaining its somewhat more negative $\delta^{13}C$ signature (mean ~ -1‰). The post-glacial calcareous muds of the Tapley Hill Formation returned $\delta^{13}C$ values ranging from -2‰ immediately above the Appila Tillite to +3.8‰ higher in the section.

McKirdy et al. (1975) measured the thermal maturity and C-isotopic composition of organic matter in the Tindelpina Shale Member from locations throughout the southern and northern Flinders Ranges. They reported $\delta^{13}C_{org}$ values that increased from -24.2‰ to -14.7‰ with increasing metamorphic grade from west to east across the fold belt.

Williams (1979), citing data from Veizer and Hoefs (1976), reported $\delta^{13}C$ and $\delta^{18}O$ values of +1.8‰ and –5.5, respectively, for a dark grey laminated dolostone at the base of Tapley Hill Formation in the Emeroo Range area.

In contrast to the geochemical study of Sumartojo (1974), that indicated open marine environments of deposition, ^{34}S-enriched sulphide isotopic compositions led Lambert et al. (1980, 1984) to conclude that the Tapley Hill Formation was deposited in a restricted marine or possibly lacustrine setting. Since then, further sulphur isotopic studies in Neoproterozoic successions have shown an anomalous enrichment in ^{34}S (Logan et al., 1995; Strauss, 1997) discrediting this assessment. Indeed, given that it represents a sea level high stand, it is unlikely that the Tapley Hill environment was restricted at all. Consequently, its S-isotope signature presumably reflects that of the global ocean. Lambert et al. (1980, 1984) also reported carbonate $\delta^{13}C$ values ranging from -4.3‰ to +4.6‰ for the Tapley Hill Formation.

Singh (1986) examined the Balcanoona Formation (an equivalent of the Brighton Limestone) in the Northern Flinders Zone. He presented C and O-isotope data for the Brighton Limestone ($\delta^{13}C$ = +2 to +4‰, $\delta^{18}O$ = -12 to -8‰) and Balcanoona Formation ($\delta^{13}C$ = +1 to +9‰, $\delta^{18}O$ = -13 to -4‰).

4.3 Drillhole sections

4.3.1 Blinman-2

The exploration well Blinman-2 was drilled on the eastern flank of the Blinman Diapir in the Central Flinders Zone (Figure 2) by Frontier Exploration Ltd. in 1991. The well targeted the carbonaceous sediments of the Tapley Hill Formation with the aim of discovering economic accumulations of hydrocarbons and even rafts with metallic mineralisation such as that hosting the Blinman copper mine. Reaching a total depth of 2031 metres in the glacial sediments of the Wilyerpa Formation, Blinman-2 showed minor methane in fracture porosity.

The chemostratigraphy of the Blinman-2 well initially produced by Cooper (1991) has been expanded upon by McKirdy et al. (1995, 1997) and is presented herein as Figure 8.

The Tapley Hill Formation in the vicinity of Blinman-2 has obviously been subjected to sufficient heat to produce dry gas (methane). An atomic H/C ratio of 0.54 for a kerogen sample from 1316.7 m depth was recorded by Cooper (1991). This corresponds to a vitrinite reflectance of 2% or a palaeo-temperature of around 150°C. This atomic H/C value from the Central Flinders Zone compares favourably with the sub-graphitic values (McKirdy et al., 1975) from the southern and northern parts of the Flinders Ranges. It argues for the retention of near original $\delta^{13}C_{org}$ values in the Blinman-2 drillhole section.

The $\delta^{13}C$ values of dolomite in the glacigenic Wilyerpa Formation below 1930 m depth in Blinman-2 are in the range -5.3‰ to -3.0‰, as expected for carbonate precipitated from isotopically light glacial melt water. Positive $\delta^{13}C_{carb}$ values of ~ +1.5‰ at 1800-1860 m depth correspond to a Holowilena Ironstone equivalent and are interpreted as having a restricted lacustrine environment of deposition (Cooper, 1991). Organic carbon in the Wilyerpa Formation has $\delta^{13}C$ values of -30.1‰ to -28.4‰ which are consistent with the slightly negative values recorded for the co-existing carbonate.

The Tapley Hill Formation in Blinman-2 consistently contains upwards of 20% carbonate, mostly in the form of dolomite. There is no bedded dolomite at the base of the Tapley Hill Formation but the Tindelpina Shale Member displays elevated organic (TOC up to 1.1%) and carbonate contents in the 1550-1620 m interval (Cooper, 1991).

Preiss (1987) reported that the micritic dolomite from the very base of the Tindelpina Shale Member appeared to have been deposited by settling and indeed need not represent a shallow environment of deposition. He further qualified this by saying that the facies of equivalent units in locations towards the Stuart Shelf are more likely to reflect shallow water deposition. Substantial carbonate "factories" are inferred for the detrital carbonate deposited in the Tapley Hill Formation (Preiss, 1987; Lemon, 1988). The great proportion of its dolomite at Blinman-2 may be attributed to diapirically-sourced salts providing Mg^{2+} for direct precipitation of dolomite in local shallow-water shelf environments.

The geochemical analyses of organic matter in the Tindelpina Shale conducted by McKirdy et al. (1975) led these workers to conclude that it was derived from aquatic photosynthetic micro-organisms. The settling of this organic detritus through calm deep waters led to its burial in fine-grained sediments flooring a post-glacial ocean enriched in isotopically light carbon. The result at Blinman-2 is TOC values of up to 1.2% (Figure 8).

The $\delta^{13}C$ of the coexisting carbonate record typically negative post-glacial "cap carbonate" values of -1.7‰ and -5.0‰. Immediately thereafter the carbonate isotope signal in the Tindelpina Shale Member trends toward positive values of +1.5‰, and there is a parallel trend in $\delta^{13}C_{org}$ from –28.9 to –26.2‰ (Figure 8). The signal is complicated somewhat by the large amount of diapirically-derived debris in turbidites and the slumping and apparent reworking of sediment over the 1200-1500 m interval. Cooper (1991) concluded that the very high pyrite content of the sample at 1212 m. ($\delta^{13}C_{dol}$ = -2.9‰) suggested an increase in the amount of ^{13}C-depleted early diagenetic carbonate resulting from bacterial sulphate reduction.

Mapping of the Tapley Hill Formation surrounding the Blinman Diapir by Lemon (1988) revealed local thickness variations associated with development of peripheral sinks and shallow platforms related to upward movement of the diapir. As well as numerous conglomerates, slumps and turbidites surrounding the diapir, giving evidence of its activity, the slump diamictite encountered in Blinman-2 between 1050-1200 m depth documents a major pulse of diapir movement. The sudden flux of material into the diapir gave rise to deepening of the sea floor adjacent to the structure and creation of peripheral 'sinks' conducive to the preservation and burial of organic matter. The resultant black, finely laminated shale has a TOC of up to 1.2% and in all respects resembles the Tindelpina Shale Member.

The amount of carbonate in sediments above the slump diamictite (Figure 8) varies widely. The turbiditic sample taken from immediately above the breccia at 1032 m contains 2% carbonate in the form of oolitic limestone diapir xenoclasts of likely Callana Group origin (Cooper, 1991). The recrystallised ferroan dolomite of the intraclasts in this sample has a $\delta^{13}C$ value of –5.5‰ which is somewhat anomalous with respect to the overall secular profile shown in Figure 8. The upward pulse of diapir movement undoubtedly caused local shallowing directly over the diapir, and perhaps on saddles between the peripheral sinks, which allowed for greater precipitation of carbonate and probably

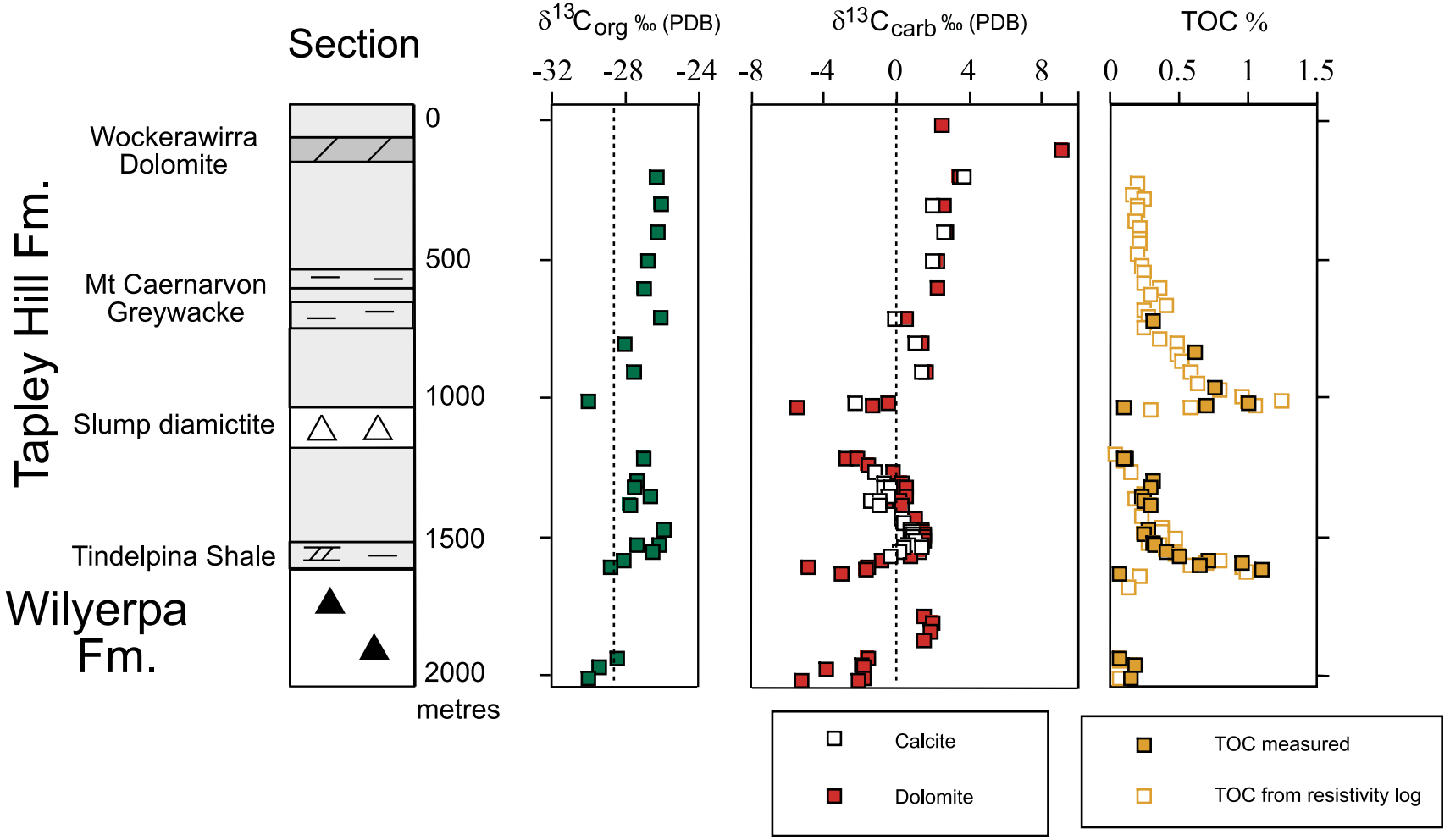

Figure 8. Chemostratigraphy of Wilyerpa and Tapley Hill Formations: Blinman-2 drill hole, Central Flinders Zone (after Cooper, 1991, and McKirdy et al., 1995)

increased organic productivity. The greater amount of carbonate (65%) in the finely laminated black shale at 1022.3 m depth, with a TOC value of 0.6%, possibly reflects this proximity to carbonate production.

The negative carbonate C-isotopic compositions at this level (above and below the slump diamictite: Figure 8) require a local input of isotopically light carbon. To better understand the possible causes of this negative excursion, a number of important observations must first be emphasized. The enhanced burial and preservation of organic matter directly above the slump diamictite, and indeed throughout much of the Tapley Hill Formation at Blinman-2, is directly correlatable to develpoment of a suboxic environment by way of greater water depth and/or increased salinity. For the majority of the interval of deep turbiditic sediment i.e. 1200-1500 m, from the top of the Tindelpina Shale Member to the base of the thick slump diamictite, TOC is generally above 0.22% (mean = 0.26%) whilst above the slump diamictite, preserved organic matter tends to decrease with decreasing water depth.

The $\delta^{13}C$ of coexisting carbonate and organic matter exhibit nearly perfect covariance throughout Blinman-2 with a mean separation of 28.0‰ (Appendix 1), very close to that prescribed as the photosynthetic fractionation effect (Knoll et al., 1986). It would thus seem unlikely that any major alteration has affected these isotopic signatures. It is interesting to note that $\Delta^{13}C$ ($\Delta^{13}C = \delta^{13}C_{carb} - \delta^{13}C_{org}$) in the interval 1200-1500 m averages 26.7‰ whereas in the interval overlying the slump diamictite (200-1010 m) it averages 28.9‰. The apparent reduced fractionation effect in the deeper water sediments is most likely attributable to the oxidation of slowly sinking organic matter by sulphate-reducing bacteria. The development of framboidal pyrite and, to a lesser degree, the isotopically light diagenetic carbonate cements observed in the organic-rich sediments of Blinman-2 (such as those seen in the sample at 1212 m) may be linked to this process. Free-floating bacterial heterotrophs of this kind are interpreted to have extended below the carbonate lysocline in Neoproterozoic oceans (Logan et al., 1995) which presently is at 4.5 km depth (Scoffin, 1987).

Having established the likely $\delta^{13}C$ signal of Callanna Group diapiric xenoclasts from the Enorama Diapir as low positive (Chapter 3), the isotopic composition of xenoclasts from the Blinman Diapir may nonetheless be entirely different. Indeed, given the $\delta^{13}C_{dol}$ signature in the clast at 1032 m depth, it is possible, that the diapir may have acted, for a period of time, as a local sink for isotopically light carbon. The ascent of the diapir and the increased hydraulic head due to high sea

level would promote diapiric breccia dissolution and force fluid through the diapir and out into the surrounding sediment, having quite an unpredictable effect on their carbonate isotope geochmistry.

The typical post-glacial positive trend in $\delta^{13}C$ continues through the upper 1000 m of Tapley Hill Formation. Slight deviations back to -0.2‰ (calcite) and +0.5‰ (dolomite) at 710 m depth in the Mount Caernarvon Greywacke probably reflect the clastic nature of this unit. The seemingly dramatic jump to +9‰ in the Wockerawirra Dolomite at 95 m depth probably reflects the restricted depositional setting of this supra- to intertidal fine grained, yellow to grey dolomite. The return to a more modest $\delta^{13}C_{dol}$ value of +2.2‰ at 35 m should not be surprising as access to open ocean water returned with the sea level fluctuation reflected in the third-order stratigraphic parasequences at the top of the Tapley Hill Formation.

4.3.2 Stuart Creek SCYW-1A

Drilled by AMOCO Ltd in 1981 and located on the Stuart Shelf of the northern Adelaide Fold Belt (Figure 2), Stuart Creek SCYW-1A reached a total depth of 1450 m in Sturtian Tillite. It intersected 160 m of well bedded, dark grey calcareous/dolomitic Tapley Hill Formation with up to 3% disseminated pyrite. The top 20 m of Tapley Hill Formation comprises dark grey siltstone interbedded with dolomite/limestone which grades upwards into 45 m of grey stromatolitc limestone and dolomite with local interbedded fine sandstone assigned to the Brighton Limestone. The drillhole intersected a further 100 m of upper Umberatana Group siliciclastics which were in turn overlain by 840 m of Wilpena Group sandstone and shale and 200 m of Cambrian limestone and shale.

Sixteen samples from the Tapley Hill Formation and Brighton Limestone interval were analysed for TOC content and $\delta^{13}C$ of their organic matter by McKirdy et al. (1995). The chemostratigraphy of this interval of SCYW-1A is presented in Figure 9.

The dramatically thinner Stuart Shelf section of Tapley Hill Formation observed in SCYW-1A nonetheless shows much the same geochemical profile as Blinman-2. Organic matter $\delta^{13}C$ values show a typical post-glacial gradual positive trend from -33.8‰ immediately overlying glacial diamictite up to -27.3‰ in the basal Brighton Limestone. Preserved organic matter is also highest in the basal Tapley Hill Formation with TOC up to 0.7% diminishing with subsequent regression.

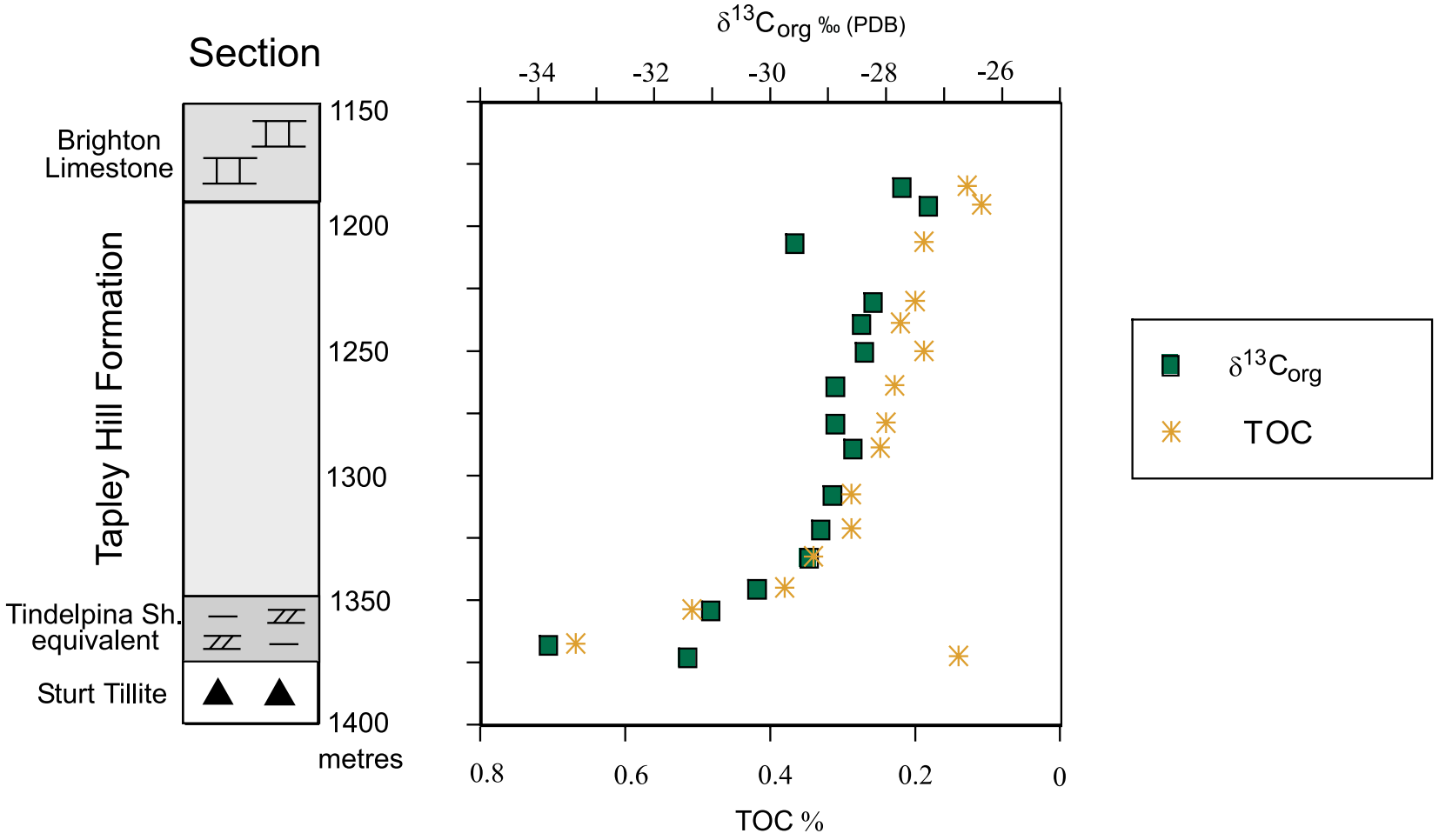

Figure 9. Chemostratigraphy of the Tapley Hill Formation and Brighton Limestone: SCYW-1A drill hole, Stuart Shelf (from McKirdy et al., 1995)

4.3.3 Bute-3

Located on a basement high on the northern Yorke Peninsula (Figure 2), Bute-3 was a stratigraphic hole drilled in 1970 by the then South Australian Department of Mines and Energy. It reached a total depth of 163 m in Mesoproterozoic metasiltstone, intersecting 18 m of finely laminated grey dolomite and siltstone and shale of the Woocalla Dolomite, equivalent to the Mount Caernarvon Greywacke, 33 m of black laminated slaty shale and siltstone as Tapley Hill Formation and 23 m of grey siltstone and pebble conglomerates of a unit equivalent to the basal Brighton Limestone. The top 50 m of the well section comprises limestone of Cambrian age.

Bearing in mind the less complete section, the chemostratigraphy of Bute-3 (Figure 10) is comparable to that of the upper part of the previous two wells discussed. Although the thinnest section of the three holes, in Bute-3 the Tapley Hill Formation displays a highest TOC of 0.4% and most negative $\delta^{13}C$ of organic matter of -29.8‰ grading to less negative values up section. This is typical of a post-glacial succession.

4.3.4 Discussion

The chemostratigraphy of the drillholes largely reflects their respective depositional setting. Blinman-2 is located where the sea floor was topographically lower and steadily subsiding. It therefore records a thicker section, greater facies variation including a large pulse of diapir movement and thus a more complex geochemistry. Although it appears as if sulphate reduction may be responsible for a slightly negative overprint just below 1200 m, the $\delta^{13}C_{carb}$ data otherwise record a typical post-glacial climbing trend from –4‰ to +4‰ (or +9‰ in the Wockerawirra Dolomite Member).

SCYW-1A was drilled at a more proximal location on the Stuart Shelf resulting in a thinner, more condensed section. Being a topographic high, the Bute-3 locality was not flooded until well after deposition of the Tapley Hill Formation began at Blinman-2 and SCYW-1A. Moreover, as sedimentation ceased in the two basin-margin locations, it continued in the Blinman area where the extra section records a continuation of positive trend in $\delta^{13}C_{carb}$. The resultant carbon isotope curves are a valid record of global post-glacial secular trends in ocean chemistry distorted, to varying degrees, by local facies variations.

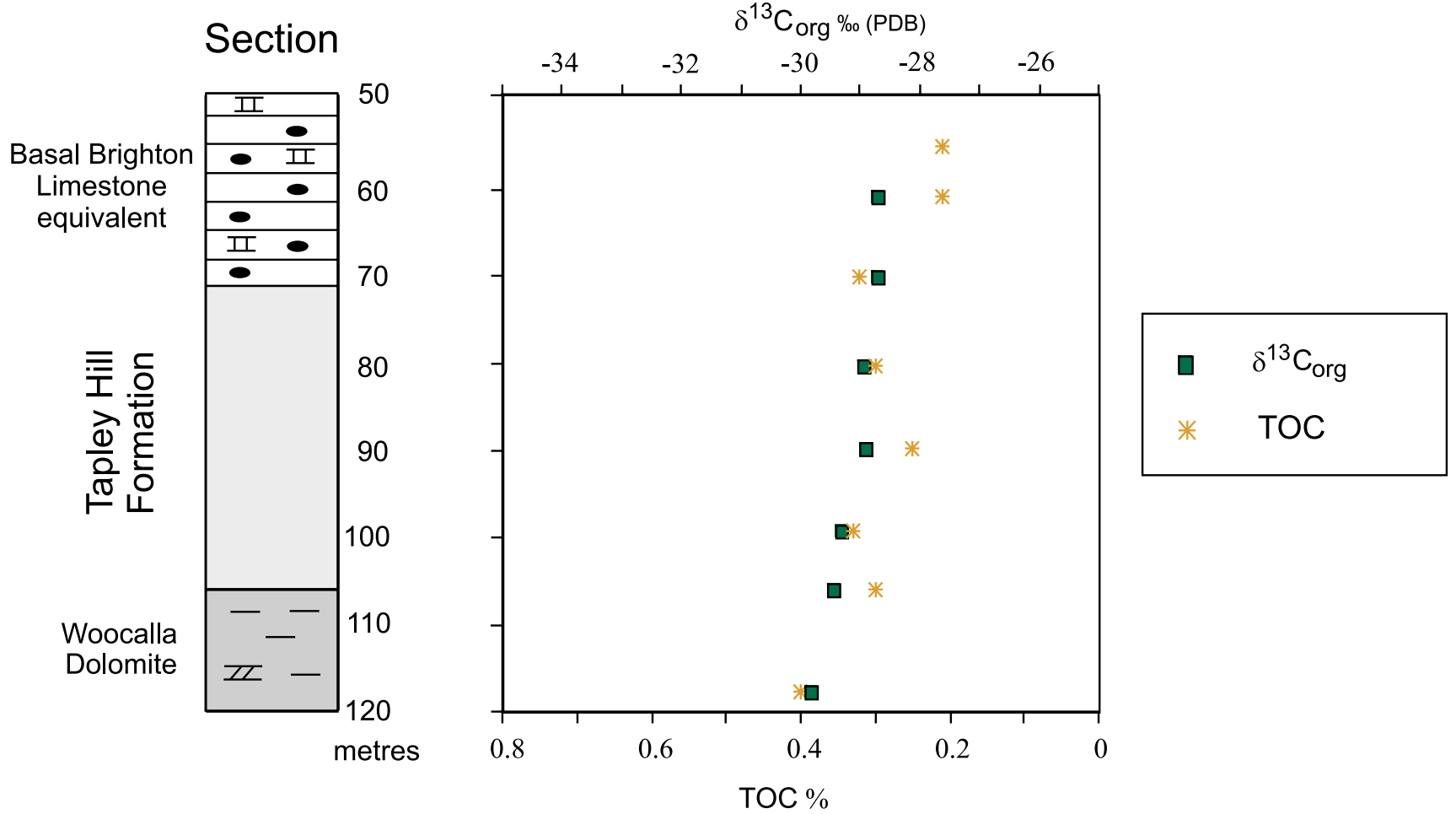

Figure 10. Chemostratigraphy of the Tapley Hill Formation and Brighton Limestone: Bute-3 drill hole (from McKirdy et al., 1995)

Enhanced preservation of organic matter (TOC > 0.2%) in the lower half of the Tapley Hill Formationcan be linked directly to the post-Sturtian glacial sea level high stand.

4.4 Brighton Limestone

The reference section for the shelf-deposited Brighton Limestone in this study is located north-northeast of Spencer Gulf at Depot Flat (Figure 2). At this location the Brighton Limestone is relatively thick (130 m) indicating that active subsidence accompanied sea level fall (Lemon, 1988).

Almost certainly largely the stratigraphic equivalent of the Wockerawirra Dolomite, the Brighton Limestone includes reworked intraclastic limestones but does not have the intraclastic diversity of the sediments surrounding diapirs in the Central Flinders Zone.

At this locality, Lemon (1988) documented gradation from deep calcareous shale to stromatolitic and shallow ooid intraclastic limestones, with an increase in carbonate and dolomite content up section. The section is capped by a pink supratidal fenestral dolomite.

In thin section, samples near the top of the Brighton Limestone exhibit multiple carbonate mineral phases (Plate 3) although X-ray diffraction analysis indicates dominant amounts of calcite and only minor dolomite (Appendix 3). Staining with Alizarin Red reveals an early interstitial dolomicrite phase that binds an ooid framework. Ooids have undergone little to moderate recrystallisation and later stage and pore-occluding calcite cements have varied cathodoluminescent signatures. The dolomite cement observed near the top of the Brighton Limestone is clearly very early as intraclasts of cemented ooid limestone are reworked into ooid limestone that has later cement (see “grapestone” Plate 3B).

The isotope chemostratigraphy of the Brighton Limestone section (Figure 11) illustrates general coincidence of the $\delta^{13}C$ profiles of the calcite and dolomite mineral phases. This may be interpreted as dolomite forming from calcite as an immediately post-depositional event, thereby retaining the $\delta^{13}C$ signature of its precursor, as suggested by Kaufman and Knoll (1995). Secondly, the whole-rock digestion technique employed in this study (Appendix 1) discriminates between calcite and dolomite but samples an aggregate of any coexisting calcite

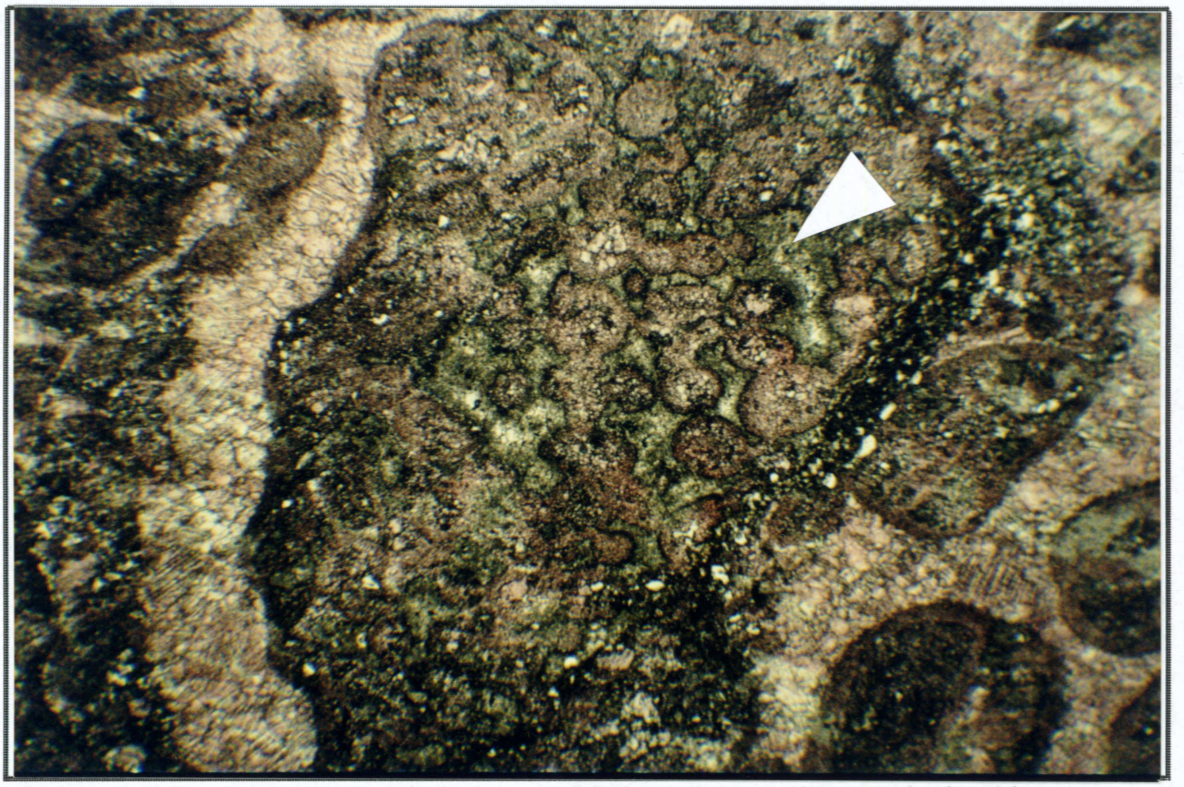

Plate 3A. Dolomite exists as a dark, intra-ooid phase (arrow), in reworked ooid limestone. Sample 1041-17, upper Brighton Limestone at Depot Flat, 115 metres, δ^{13}Ccal –3.3‰, δ^{18}Ocal –9.3‰, δ^{13}Cdol +4.0‰, δ^{18}Odol –7.1‰, pl.pol., 4X mag.. Field of view is 4.2mm.

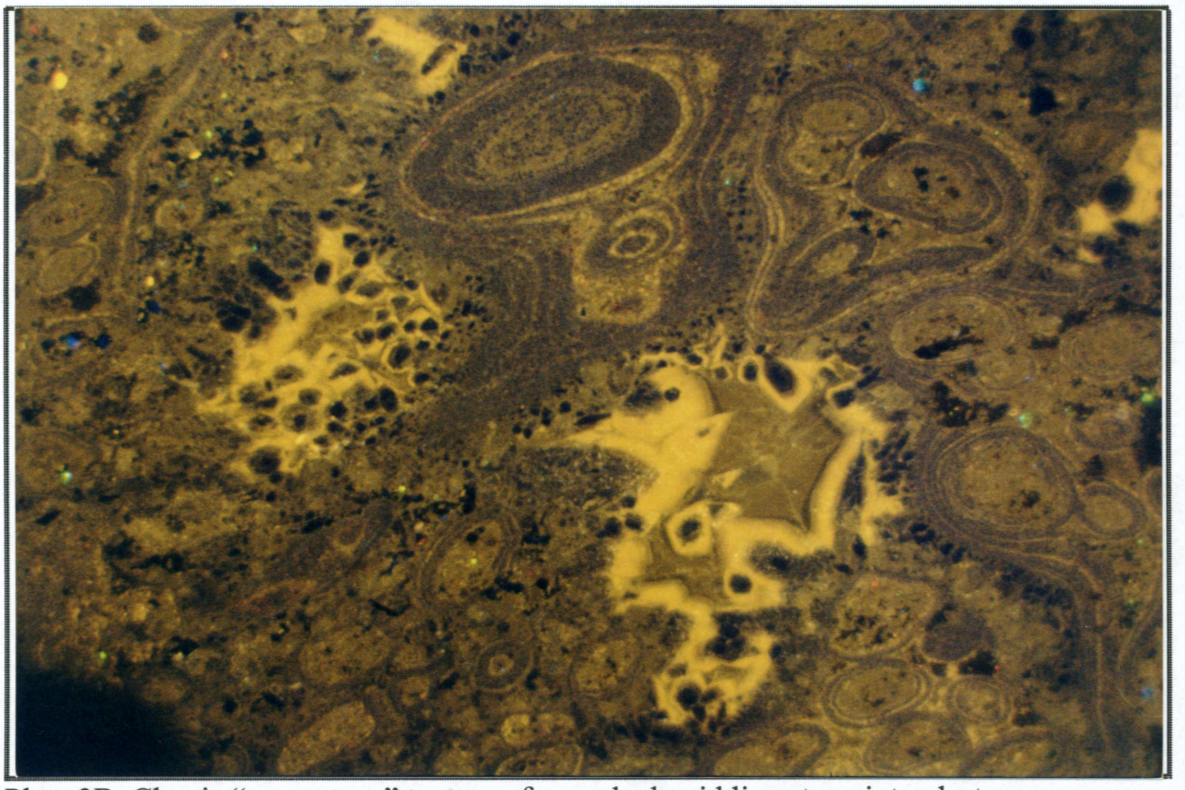

Plate 3B. Classic "grapestone" texture of reworked ooid limestone intraclasts cemented together by stages of microspar and late stage calcite spar. Same sample as plate 3A, 15kV, 201μA, 3.2 seconds, 10X mag.. Field of view is 2.3mm.

phases. The reproducibility of the Brighton Limestone data suggests that any late-stage calcites also retain the $\delta^{13}C$ of their precursor mineral phase, regardless of their cathodoluminescence signature and trace element chemistry. The dolomite $\delta^{18}O$ signature is consistently heavier (by 0.4 to 3.8‰) than that of coexisting calcite as would be expected for precipitation of these minerals under equilibrium conditions (McKenzie, 1981).

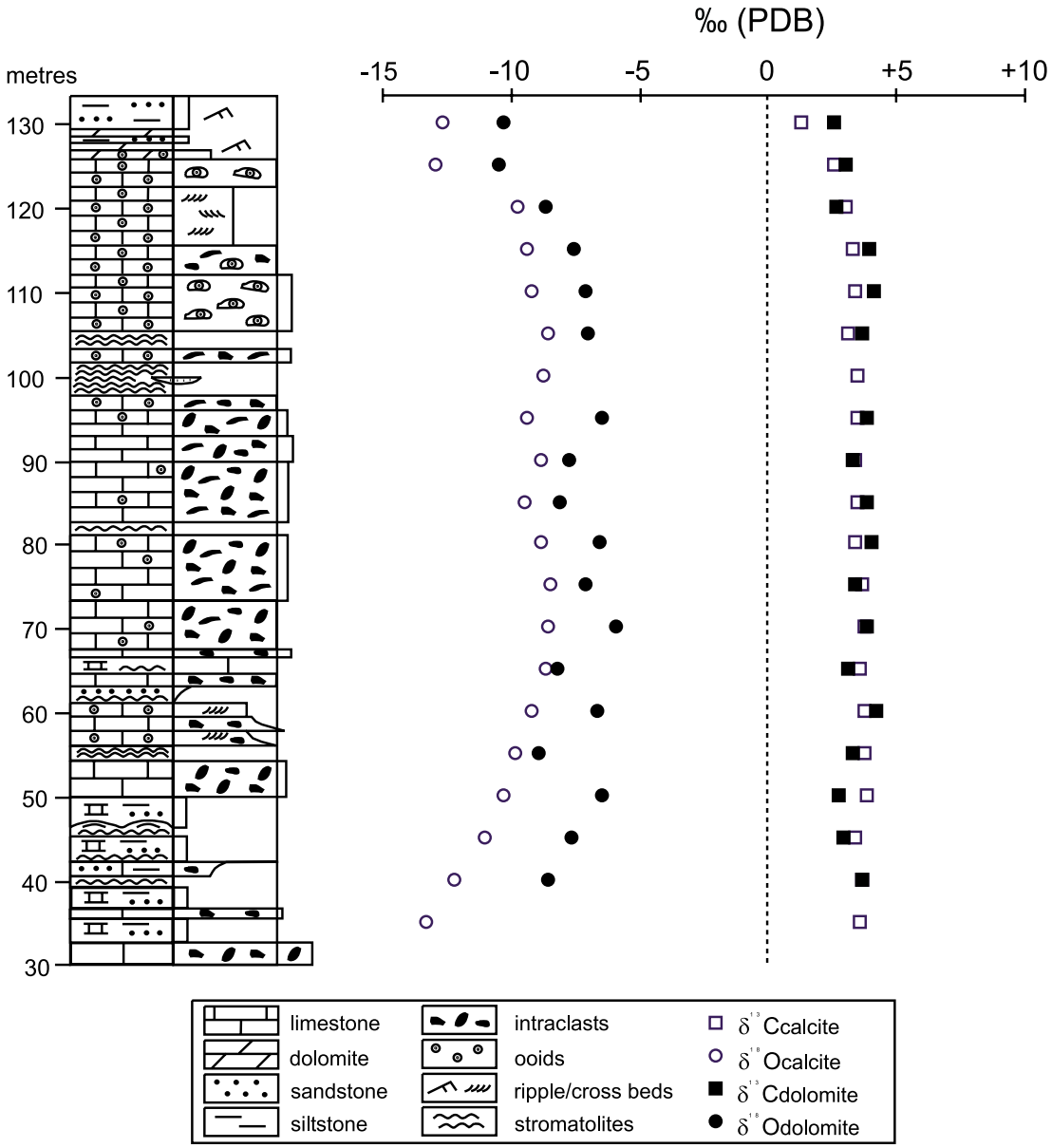

Figure 11. Brighton Limestone chemostratigraphy, Depot Flat.

At the very top of the section, there is the suggestion of diagenetic influence. Here the $\delta^{13}C$ of calcite drops back to +1.3‰, compared to +3 to +4‰ in the majority of the section, and the $\delta^{18}O$ also trails to more negative values of ~-13‰. This gradual negative trend occurring over

the upper 15 m is consistent with the meteoric alteration of some calcite phases.

Sample	δ^{13}Ccalc	δ^{18}Ocalc	δ^{13}Cdol	δ^{18}Odol
1041-19	+2.6‰	-12.9‰	+3.1‰	-10.4‰
1041-19x	+2.7‰	-11.4‰	+3.2‰	-9.3‰

Table 3. Carbon and oxygen isotopic compositions for groundmass of Brighton Limestone sample 1041-19, from 125 metres height in Depot Flat section and a reworked intraclast in the same sample (19x).

Comparison of the δ^{13}C and δ^{18}O values of *in situ* ooid limestone and a reworked ooid limestone intraclast drilled from within the same sample reveals negligible difference between the two specimens. The younger *in situ* carbonate is slightly more depleted in ^{18}O (Table 3), possibly attributable to diagenetic later-stage calcite that is not part of the intraclasts.

Another feature attributable to post-depositional alteration is the positive trend of δ^{18}O data at the bottom of the section which reflects an influence of post-burial dewatering of clay on the δ^{18}O of both carbonate phases formed during that time. Indeed, Lemon (1988) found that the dolomites at the base of this section are more iron rich, suggesting that they may have formed later in conjunction with clay dewatering.

The strontium isotopic ratios of three selected Brighton Limestone (Table 4) samples are relatively low and compare favourably with published end-Sturtian data (Derry et al., 1992). The chemostratigraphic significance of these and other strontium data will be discussed in more detail in Chapter 8.

Sample	section depth (m)	^{87}Sr/^{86}Sr
1041-17	115	0.707459
1041-12	90	0.707249
1041-9	75	0.707106

Table 4. Strontium isotopic compositions of selected Brighton Limestone samples.

4.5 Outcrop samples, top Tapley Hill Formation

The major stratigraphic sequence boundary at the top of the shelf-deposited Brighton Limestone may be mapped around the Blinman Diapir in the Central Flinders Ranges at the top of the Tapley Hill

Formation (Figure 7). Because of the undulating physiographic expression of the alternating shale-limestone lithology, it is most convenient to map bands of the outstanding lithologies in this region as opposed to mid-lithology sequence boundaries (Plate 4A, Figures 12 and 13).

The deposition of sediment directly to the north and south of the Blinman Diapir corresponds palaeogeographically to peripheral sinks adjacent the sporadically active diapir (Lemon, 1988). To the south of the Blinman Diapir, the Wockerawirra Dolomite can be clearly seen to comprise two distinct parasequences of shallow water dolomite that merge into one on the adjacent shelf to the east (Figure 12). The sequence boundary above this is also observed cutting down on to the shelf in this area.

Measurement of the Popes Paddock section, south of Blinman, began below the upper Wockerawirra Dolomite band and continued into the Etina Formation. At this location the upper paracycle of the Wockerawirra Dolomite comprises in excess of 20 metres of thinly bedded blue-green to grey fine sandy dolomitic limestone with occasional small-scale cross beds and cryptomicrobial lamination. The carbon isotopic composition of sample 1041-137 (Table 5, plotted in Figure 14) approaches that of the Wockerawirra Dolomite sampled at 95 metres depth in Blinman-2 ($\delta^{13}C_{dol}$ = +9.1‰). These values are not unexpected given a continuation of the post-glacial positive trend in $\delta^{13}C$.

sample	section.	δ^{13}Ccalc	δ^{18}Ocalc	δ^{13}Cdol	δ^{18}Odol
1041-137*	Popes Paddock	+8.4‰	-13.1‰	+6.0‰	-9.7‰
1041-138	Popes Paddock	+0.8‰	-4.5‰		
1041-69	Glass Gorge	+7.0‰	-13.1‰	+6.9‰	-2.7‰

Table 5. Carbon and oxygen isotopic compositions of upper Tapley Hill Formation outcrop samples. Asterisk indicates Wockerawirra Dolomite Member.

Since it occurs amid recessively outcropping siltstones and shales, the end-Sturtian unconformity is poorly outcropping and difficult to place in the Popes Paddock section (Plate 4A). A buff-yellow fine sandy calcareous siltstone (1041-138) was recovered in its approximate location. The C and O-isotopic composition of this siltstone (Table 5) would appear to have been altered by of meteoric water, confirming its proximity to the unconformity and its expected exposure during this hiatus.

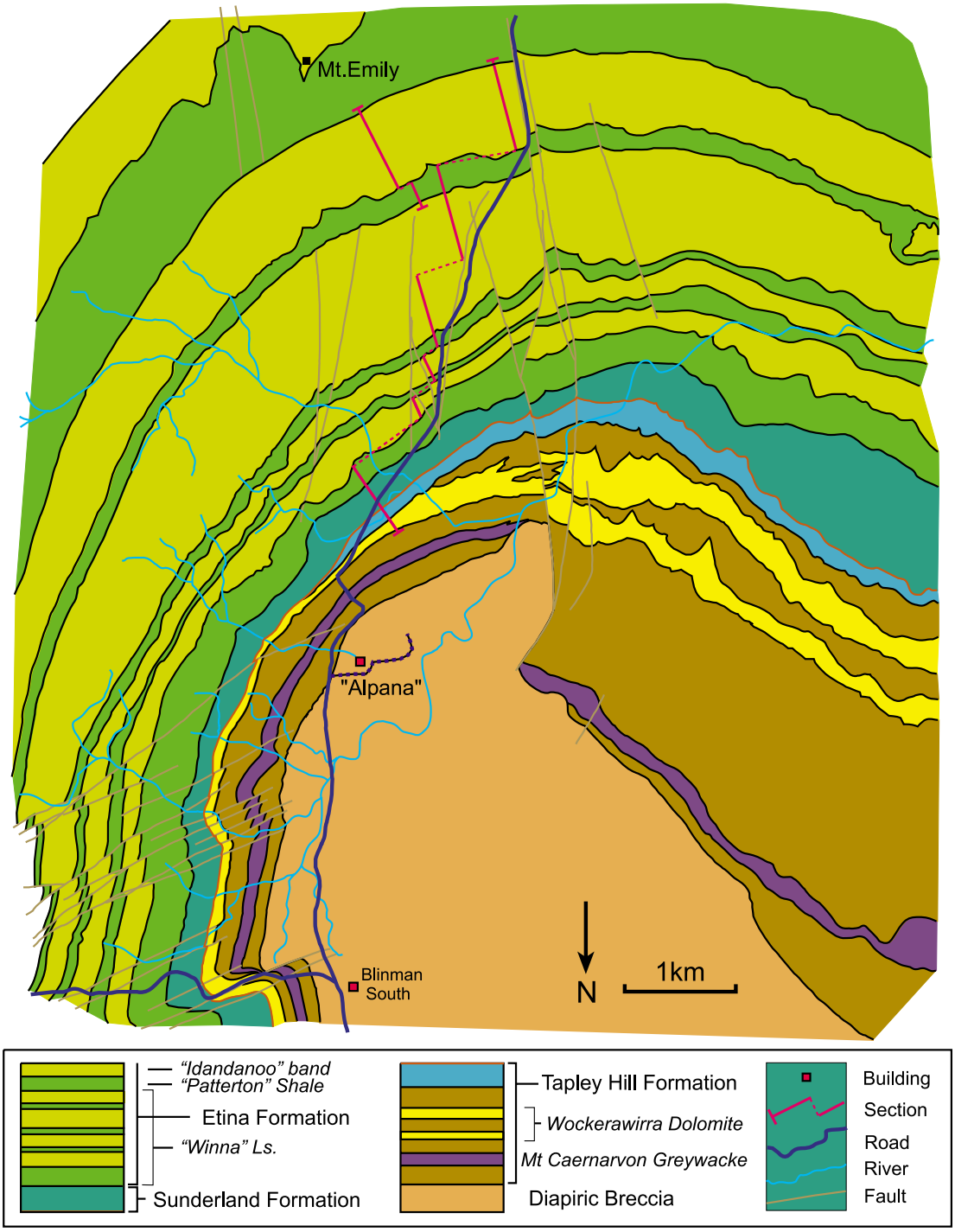

Figure 12. General geology, including several late-Sturtian paracycles converging to the east, south of the Blinman Diapir (after Lemon, 1988). "Popes Paddock" and smaller "Mt Emily" measured sections are indicated in pink.

Plate 4A. Physiographic expression of Wockerawirra Dolomite (foreground) looking across to the Etina Formation and Mt. Emily (central background), south of Blinman.

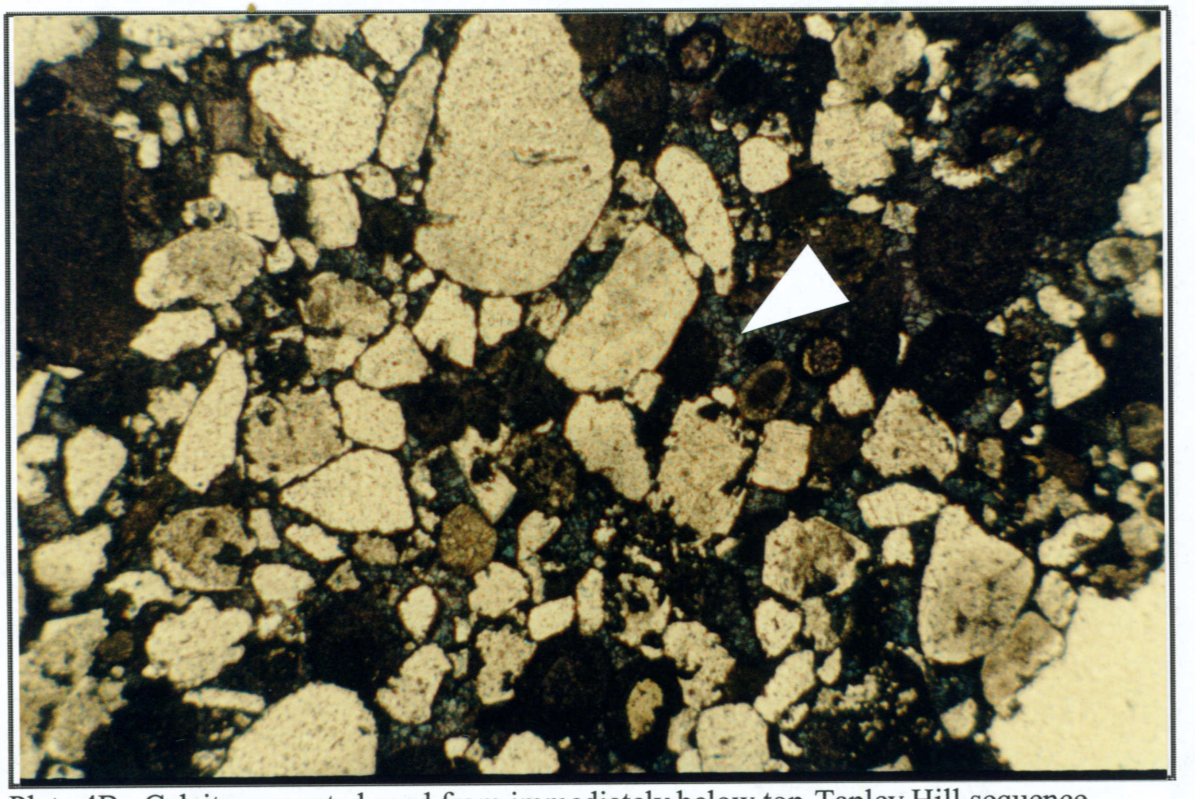

Plate 4B. Calcite cemented sand from immediately below top-Tapley Hill sequence boundary in Glass Gorge. Dark blue stain (arrow) shows interstitial ferroan calcite cement. 1041-69, δ^{13}Ccal +7.0‰, δ^{18}Ocal –13.1‰, δ^{13}Cdol +6.9‰, δ^{18}Odol –2.7‰ pl.pol., 10X mag.. Field of view is 2.3mm wide.

To the north of the Blinman Diapir through Glass Gorge, the same two paracycles within the Wockerawirra Dolomite were mapped (Figure 13). The uppermost Tapley Hill Formation sediments are also well exposed here. Grey siltstone coarsens up to medium grained, thinly ripple-cross-bedded calcareous sandstone and sandy limestone (Figure 14). Slumping and the clastic diversity of these sediments are indicative of the influence of the diapir to the south.

X-ray diffraction analysis of the sandy limestone sampled in this locality (1041-69) indicates that calcite is the dominant carbonate species, with minor amounts of dolomite. In thin section, staining highlights interstitial dark blue ferroan calcite cement (Plate 4B). Cathodoluminescence reveals a bright orange calcite cement coating most grains before a generally dull, pervasive interstitial calcite cement (Plate 5). Etching of silicic grains by carbonate cement is common, as well as alteration of a wide variety of feldspars. A diversity of carbonate intraclasts is also illustrated by their varying luminescence signatures. The generally high degree of rounding exhibited by grains suggests reworking of diapiric breccia by wave activity.

The $\delta^{13}C$ signatures of calcite and dolomite of this sample (Table 5) are close to that of the Wockerawirra Dolomite sampled in the Popes Paddock section to the south (Table 5). Although isotopically unlike the dolomite xenoclasts analysed in Chapter 3, it is likely that some of the dolomite contained in this rock is of detrital (diapiric) origin.

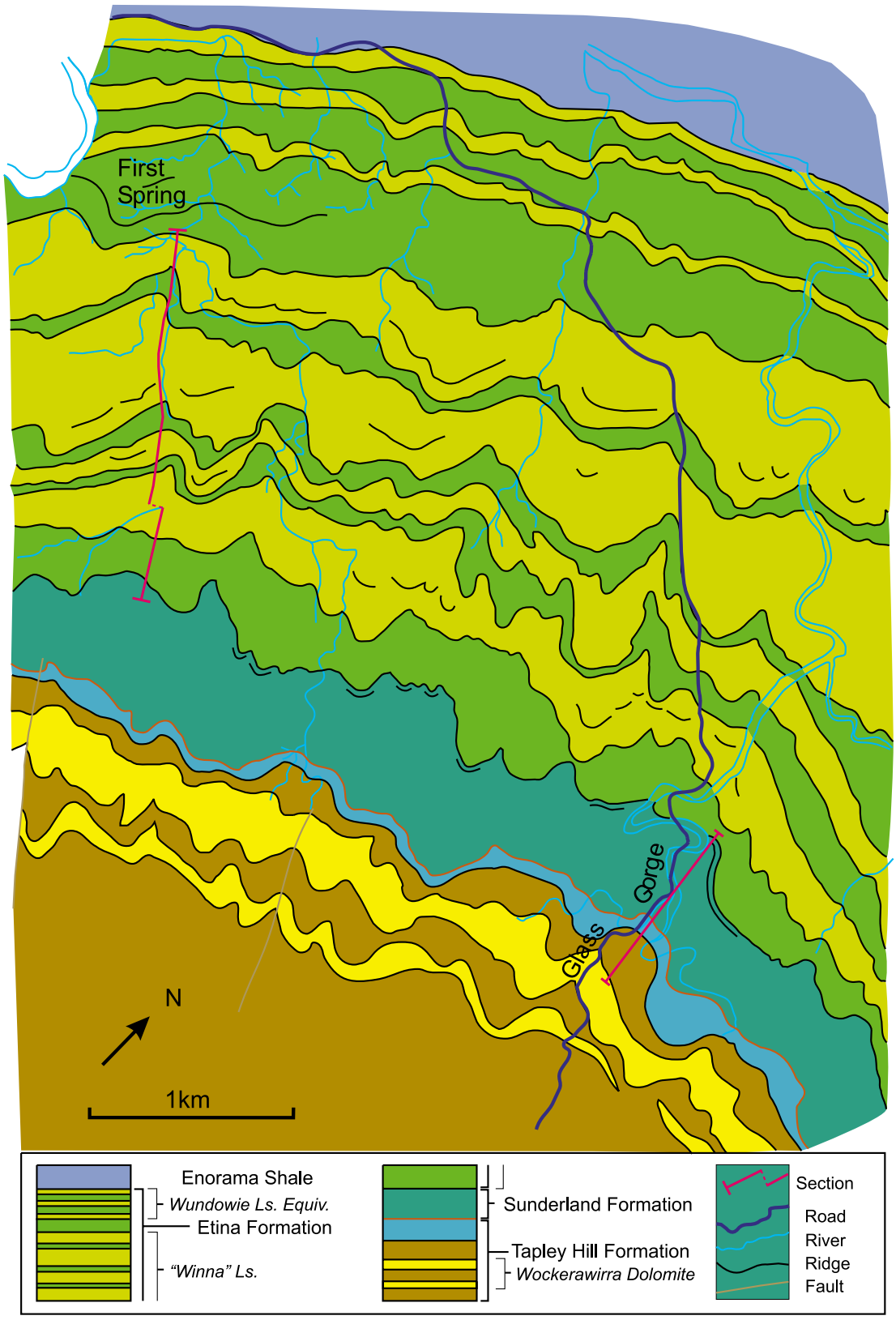

Figure 13. General geology, north of the Blinman Diapir. "First Spring" and smaller "Glass Gorge" measured sections as marked in pink.

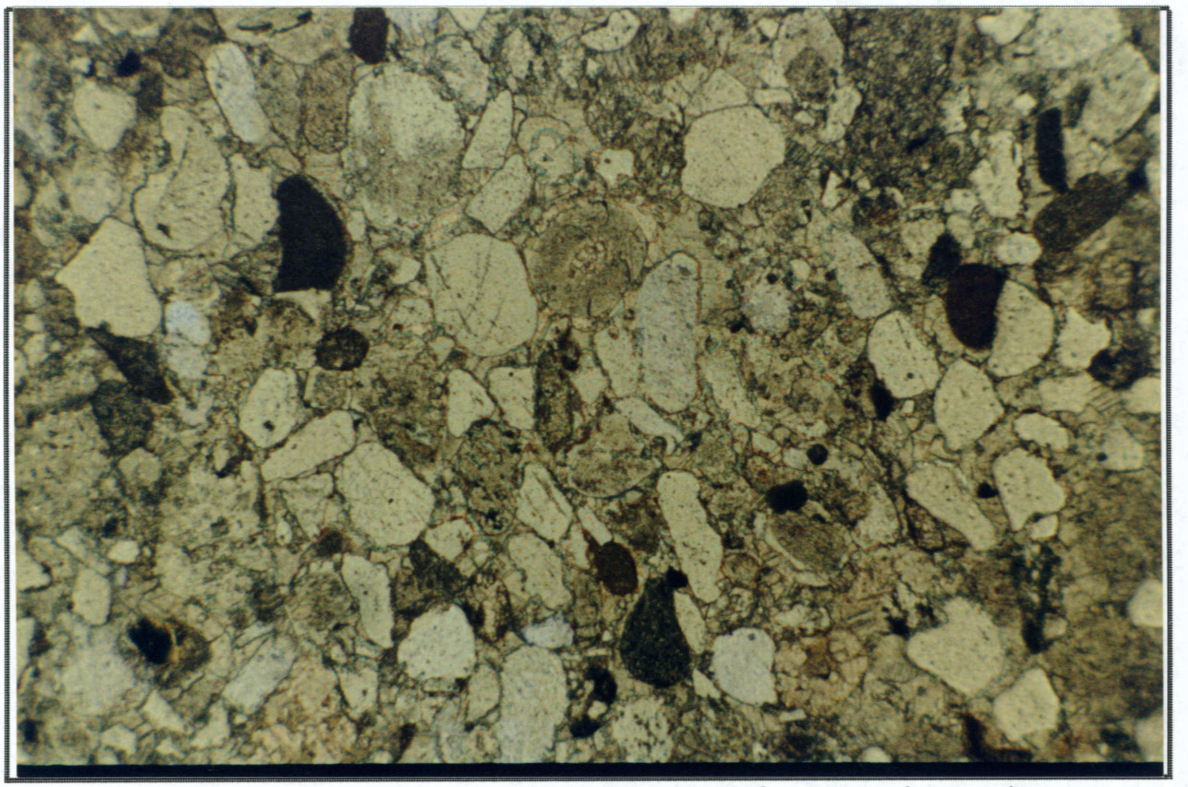

Plate 5A. Sub-rounded grains of quartz, feldspar and rock fragments characterise diapirically derived detritus. Top Tapley Hill Formation in Glass Gorge, sample 1041-69, pl.pol., 10X mag. Field of view is 2.3mm wide.

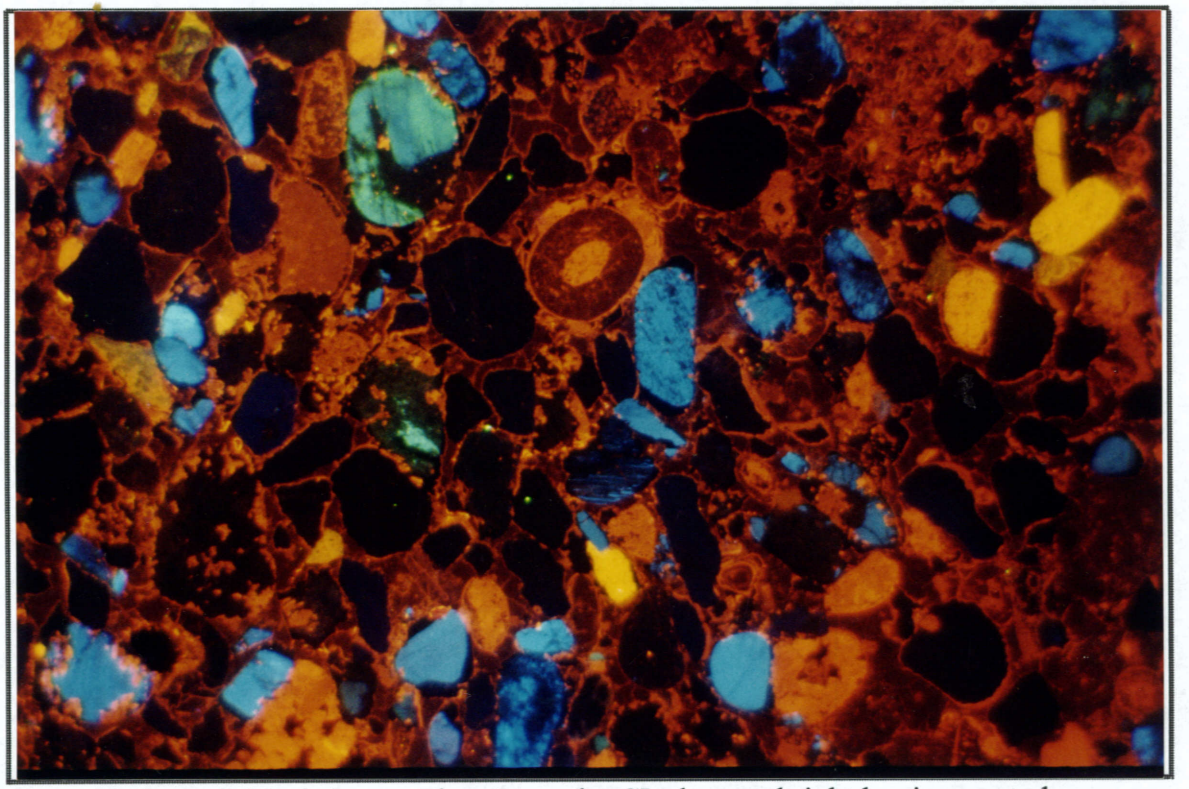

Plate 5B. Same field of view as Plate 5A under CL shows a bright luminescent phase of calcite cement around each framework grain. This phase deeply etches most grains, particularly the feldspars (bright blue under CL). Rare ooids are characteristic of the Wockerawirra Dolomite. 15kV, 215µA, 7 seconds.

4.6 Discussion

The overall carbon isotope stratigraphy of the Tapley Hill Formation and its subsidiary and equivalent units documented herein, delineates a typically post-glacial positive excursion. Covariation of the carbon isotopic composition of carbonate and organic matter in the Blinman-2 section confirms that these values are representative of post-Sturtian glacial seawater chemistry. Moreover, the high concentrations of organic matter in parts of the Tapley Hill Formation (TOC up to 1%) appears to have had no marked effect on the isotopic composition of the co-existing carbonate mineral phases (c.f. Kaufman and Knoll, 1995).

By the time sea level had fallen far enough from the post-glacial high stand level to deposit shallow water limestone on the Stuart Shelf, the $\delta^{13}C_{carb}$ of shallow ocean waters had increased to between +3 and +4‰ compared to immediately post-glacial values of -5‰. In the time it took the sea level to fall yet further so that shallow water carbonate was deposited adjacent to the Blinman Diapir, it had risen to give values in the vicinity of +7‰. Variation of the values at this level in the stratigraphy possibly arose due to a restricted depositional setting atop the diapir(s) or the influence of diapiric fluids and reworked diapiric xenoclasts.

In the absence of geochronological constraints, it is impossible to estimate the duration of the hiatuses associated with disconformity surfaces evident near the close of the Sturtian. Some diagenetic overprint is evident directly beneath the end-Sturtian unconformity (in sample 1041-138) and is perhaps to be expected, given the likely longer time break.

Data presented here for this end-Sturtian interval are in agreement with $\delta^{13}C$ values of +1 to +9‰ measured by Singh (1986) that were considered "primary and related to the marine water chemistry…during Sturtian times" in the Brighton-Wockerawirra equivalent Balcanoona Formation of the Northern Flinders Ranges.

The integrity of the $\delta^{13}C$ data presented herein is confirmed by its consistency over a wide geographic area. Given this finding, there is every reason to believe that $\delta^{13}C$ data from higher in the Umberatana Group will also be reflective of seawater chemistry at the time of deposition.

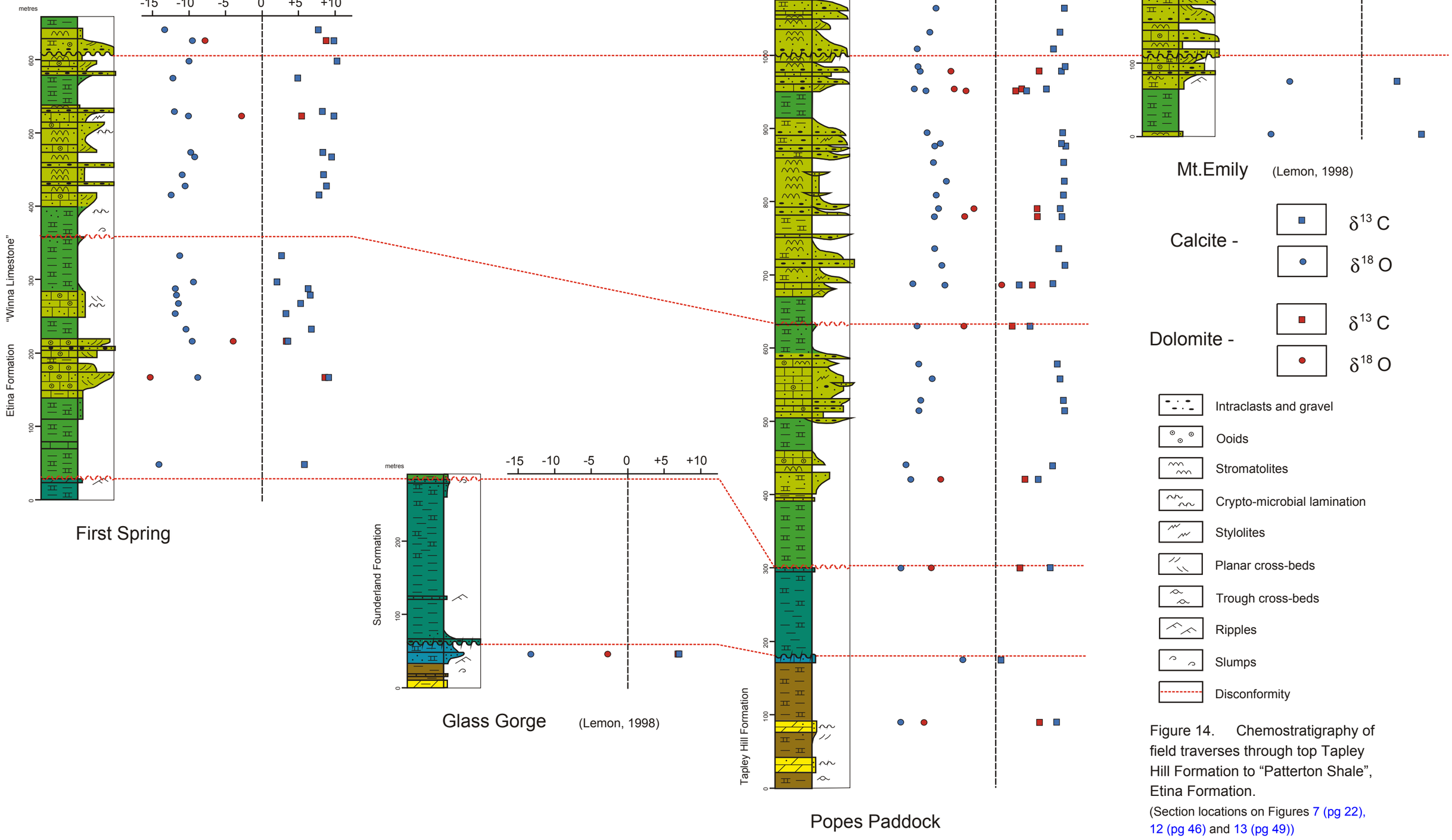

Figure 14. Chemostratigraphy of field traverses through top Tapley Hill Formation to “Patterton Shale”, Etina Formation.

(Section locations on Figures 7 (pg 22), 12 (pg 46) and 13 (pg 49))

5. SUNDERLAND AND ETINA FORMATIONS

5.1 Introduction

The unconformity marking the end of the Sturtian in the Adelaide Fold Belt has been recognised basin-wide (Preiss et al., 1998). The overall composition of sediments deposited above this unconformity generally reflects their palaeogeographic setting although fluctuation in sea level is evident throughout the sedimentary record. Units in the earliest-Marinoan Upalinna Subgroup include the Tarcowie and Waukaringa Siltstones of the Mid-North and Olary regions, Angepena and Wilmington Formations on the Stuart Shelf and in the South Flinders Zone, the Amberoona Formation in the North Flinders Zone and calcareous shale and shallow water limestones of the Sunderland and Etina Formations in the Central Flinders Zone (Preiss, 1987; Preiss et al., op. cit.).

The original type area for the Etina Formation was proposed by Dalgarno and Johnson (*in* Thomson et al., 1964) to be in Etina Creek to the west of the Oraparinna Diapir, although no section was measured or published. The Etina Formation is described therein as "sandy cross-bedded limestones and grey slabby shales" that correspond to Mawson's (1938) discrete lithological units 15 through 39. These include the three distinctive bands of the Wundowie Limestone Member in the upper Etina Formation. Dalgarno and Johnson (*in* Thomson et al., op. cit.) reported a thickness of 760 m for the Etina Formation, although Preiss (1987) suspected this estimate to be too low.

Lemon (1988) mapped the three limestone bands of the Wundowie Limestone Member throughout the Central Flinders Zone and noted that their lateral persistence indicated that sea-level fluctuation dominated over basin subsidence in creation of sediment accommodation space. The cyclical nature of sea-level fluctuation and its relative frequency are principally responsible for creating a series of disconformable sequence and parasequence boundaries that can be observed within the Etina Formation.

Revision of the stratigraphic classification of the Umberatana Group by Preiss et al. (1998) recognises a transitional sequence boundary in the Upalinna Subgroup within the shallow water limestones of the Etina Formation. This sequence boundary marks the shift in phase of depositional setting from largely regressive to transgressive. An informal nomenclature adopted by Lemon (1988) assigned the name

"Winna Limestone" to the limestone-dominated lower half of the Etina Formation with the "Patterton Shale" separating this from the three bands of the Wundowie Limestone Member (Coats *in* Coats and Blisset, 1971). The "Patterton Shale" and the Wundowie Limestone Member are paracycles of a transgressive-regressive package of the upper Etina Formation that overall deepens into the overlying Enorama Shale. Because of their calcareous nature, these upper units have historically been lithostratigraphically mapped as Etina Formation.

Although formerly variously included in the Etina Formation and the Tapley Hill Formation, Preiss et al. (1998) also reinstated the Sunderland Formation, as the initial Marinoan paracycle. In the Central Flinders Zone, the dominantly calcareous siltstone of the Sunderland Formation generally is recessively weathered and its outcrop poor. Excluding the Sunderland Formation, the dominantly calcareous Etina Formation attains a maximum thickness in excess of 1200 m and is well exposed around the Blinman Diapir.

5.2 "Winna Limestone" field traverses

The "Winna Limestone" or lower Etina Formation may be summarised as four distinct thick limestone bands separated by intervening bands of shale and calcareous siltstone (Figures 12, 13 and 14). Observation of the gradation of facies in the Brighton Limestone and Etina Formation has allowed for the identification of parasequences and their otherwise ambiguous boundaries.

5.2.1 First Spring

At First Spring, north of the Blinman Diapir (Figure 13), the Etina Formation begins with a transgressive green-grey calcareous siltstone overlying a yellow-brown, very fine, sandy dolostone of the top Sunderland Formation. This flaggy-outcropping, thinly bedded siltstone exhibits cryptomicrobial lamination in its lower 20 m and contains calcareous diagenetic nodules up to 1cm in diameter. Above this, the siltstone commonly contains more calcareous or sandy horizons. In sample 1041-38 at 50 metres in this section, micritic calcite is the dominant carbonate mineral phase. Very fine (<0.01 mm) rhombic crystals of dolomite are observed as inclusions in quartz overgrowths possibly indicating a moderately elevated salinity due to diapiric influence. A small amount (2%) of detrital dolomite is observed and the pervading calcite mud has a $\delta^{13}C$ of +5.9‰. This basal shaley siltstone

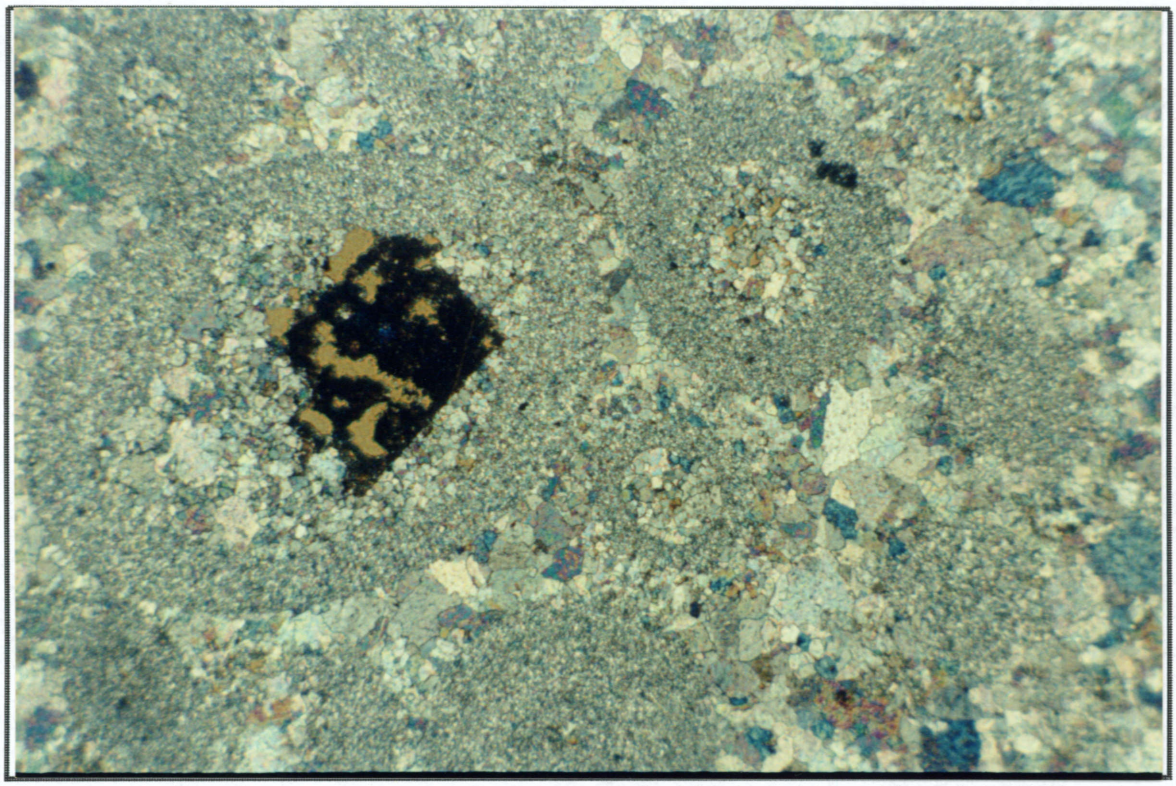

Plate 6A. Yellow-brown carbonate diapiric xenoclast included in ooid nuclei. 1041-39, Etina Formation First Spring,, 168m, δ^{13}Ccal +9.1‰, δ^{18}Ocal –8.8‰, δ^{13}Cdol +8.7‰, δ^{18}Odol –15.2‰, cross polars, 10X mag.. Field of view is 2.3mm.

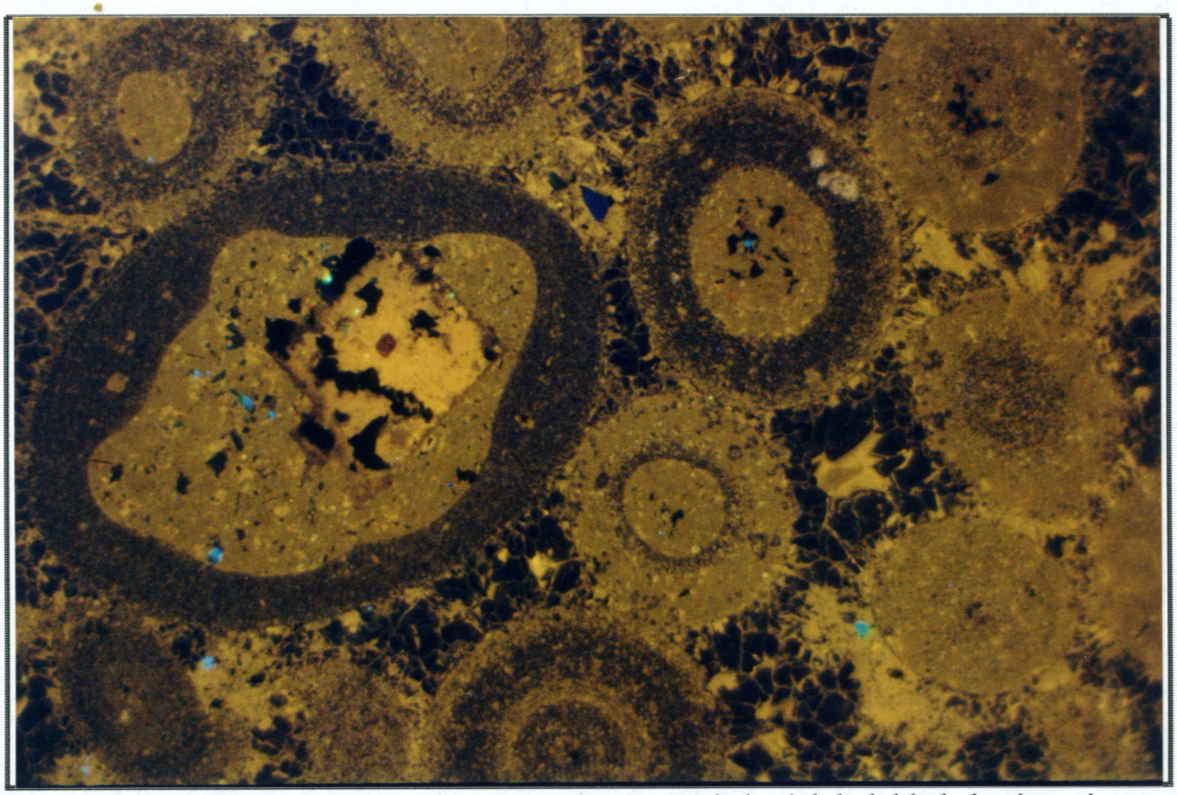

Plate 6B. Same field of view as Plate 6A under CL, early burial dark bladed-prismatic spar cement dominates inter-ooid spaces before last stage bright infill cement, 15kV, 200μA, 13.0 seconds.

extends up to 110 m height in the section where an overall increase in sand and calcareous content (Figure 14) indicates significant shallowing.

The first distinct limestone band of the Etina Formation grades upward over approximately 50 m through thinly-bedded, grey-green, silty to fine sandy limestone into a grey, planar cross-bedded, medium-grained, sandy oolitic limestone. Oolitic rims commonly coat a diverse range of diapirically-derived detritus which coarsens briefly to granule size in some beds and includes cyanobacterial flake intraclasts. Clasts of reworked limestone in ooid cores are observed at 168 metres in the section (sample 1041-39, Plate 6). The luminescent signature and thus elemental chemistry of these clasts appears to be the same as the ooidal micrite suggesting precipitation of the latter from sea water of similar chemistry. Dark luminescent, inter-ooid, bladed-prismatic calcite is characteristic of early burial diagenetic marine cements (Choquette and James, 1990). Despite high cement and detrital carbonate contents, the $\delta^{13}C$ of this rock remains very high at +9.1‰ for calcite and +8.7‰ for dolomite, continuing the positive trend evident throughout the Tapley Hill Formation.

Overlying a sharp break at 173 m (Figure 14), sedimentation of grey-green, medium-grained sandy oolitic limestone resumes and continues over the next 30 m in planar cross-bedded sets up to 15 cm thick, interbedded with grey-green silty and fine sandy limestone. Thinly interbedded granules and ooid-intraclastic limestones overlay a disconformity (sequence boundary). The carbon isotopic signatures of sample 1041-40 ($\delta^{13}C$ = +3.6‰ for calcite, +3.4‰ for dolomite) tend towards the low positive values observed for diapiric xenoclasts, which is not surprising given its intraclastic content.

Above this, transgression led to the deposition of cryptomicrobial laminated calcareous siltstone over the next 20 m. The blue-green, silty limestone (1041-131) at 234 m records a relatively high $\delta^{13}C$ of +6.8‰ for calcite.

The overlying interval of shale and siltstone extends upwards for 40 m before sand and calcareous content increases once again. This second limestone band exhibits the same characteristics documented by Mawson (1938) at Etina Creek, viz. thin interbeds (<10 cm) of green-grey, fine sandy, cryptomicrobially to shallow-planar cross-bedded limestone with silty horizons. Fine, ripple-like, cryptomicrobial lamination indicates that shallowing in this parasequence on the north side of the diapir was only into the lower photic zone (Plate 7A). Lamination is perpendicular

Plate 7A. Cryptomicrobial lamination in silty limestone in plan view, indicative of lower photic zone sedimentation. Sample 1041-135, Etina Formation, First Spring, 290 m, δ^{13}Ccal +6.3‰, δ^{18}Ocal –11.8‰.

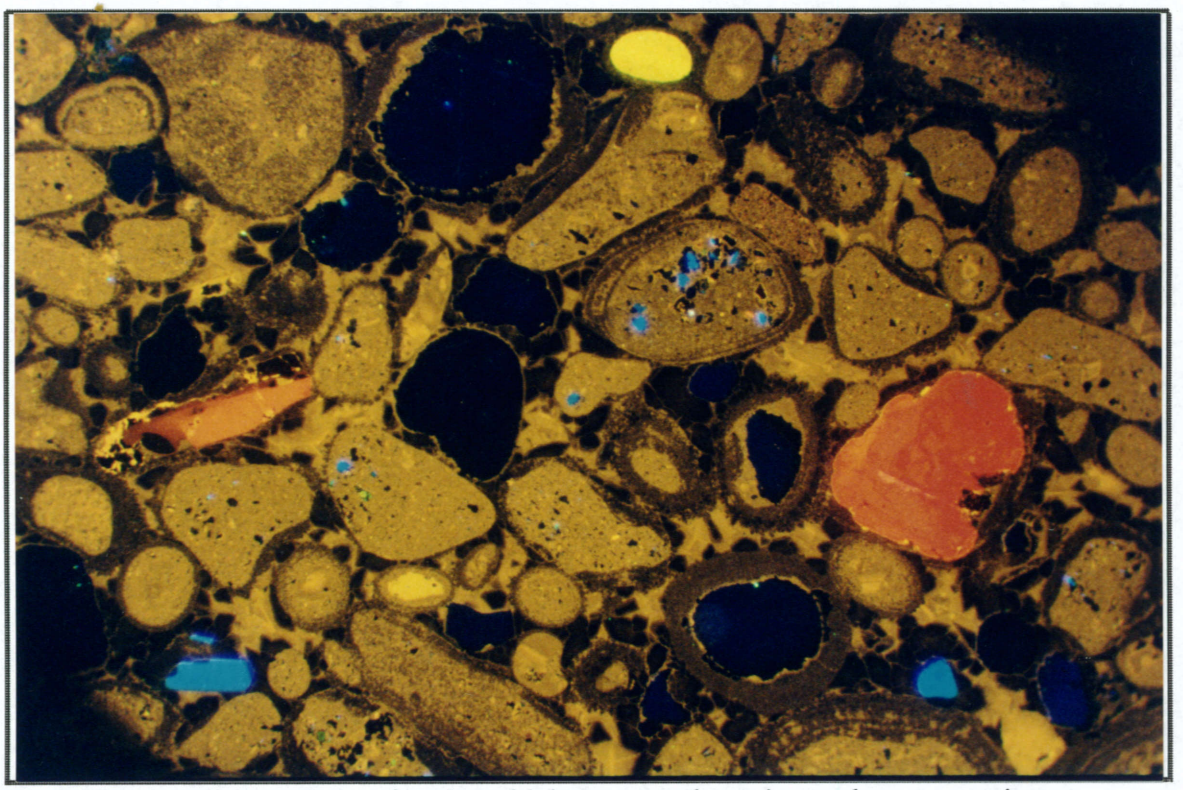

Plate 7B. Lamellar coatings of variant thicknesses and varying carbonate species including peloidal micrite, detrital calcite (bright yellow) and dolomite (red-orange). Sample 1041-53, Etina Formation, First Spring, 470 metres, δ^{13}Ccal +9.6‰, δ^{18}Ocal –9.2‰. 15kV, 200μA, 7.2 seconds, 4X mag.. Field of view is 4.2mm.

to strike possibly reflecting currents off the diapir-driven relief to the south. The carbon isotopic signatures of calcite through this second band record a minor positive excursion from +3.3‰ to +6.6‰ before trending negative towards the top (Figure 14).

The second limestone band grades quickly into fissile green calcareous siltstone and shale that is 100 m thick. Calcite in blue-green calcareous shale (1041-41) at 295 m records a low positive $\delta^{13}C$ of +2‰. Above this at 335 m, the same lithofacies (1041-42) records a slightly more positive $\delta^{13}C$ of +2.7‰. In the middle of this clastic interval, a brief shallowing event is evident. Increasing carbonate content parallels an upward gradation into a grey-green calcareous silty fine sandstone with shaley lamination, the sharp upper boundary of which is at 361 m height in the section (Figure 14).

The upper level of this fine-grained interval is again upward grading and notable for an increase in the size and occurrence of ripple lamination, as well as increasing amount of sand and carbonate. The third and thickest "Winna" limestone band includes numerous stromatolitic limestones, coarse oolitic and intraclastic sands, scouring gravels and flat pebble conglomerates that constitute numerous paracycles. This third band is 120 m thick at First Spring.

Shallowing culminates in deposition of large-scale (50 cm high), planar cross bedded, medium-grained, sandy-oolitic limestone with a calcite $\delta^{13}C$ of +7.8‰ at 418 m (1041-49). Above a sharp break, a sequence of digitate stromatolites with thin (10 cm thick) interbeds of green-grey siltstone is punctuated by occasional thin (<1 m thick) cyanobacterial-flake and intraclastic limestones over the next 53 m of section. Fine sandy, stromatolitic limestones over this interval record $\delta^{13}C$ values of +8.8‰ and +8.4‰ for calcite at 432 m and 446 m respectively.

Broad domal stromatolites briefly pass into white-grey calcareous siltstone before being overlain abruptly by a medium-grained, oolitic limestone with large-scale cross bedding at 470 m. Petrological investigation of this oolitic limestone reveals fine sandy-peloidal ooid nuclei with rims of varying thicknesses (Plate 7B). It also contains numerous detrital carbonates and although certainly present, early bladed-prismatic cement is less pervasive than late-stage mosaic spar. The calcite of this rock has a particularly high $\delta^{13}C$ of +9.6‰.

The ooid limestone is succeeded by blue-grey, fine sandy to silty, stromatolitic limestones. In thin section, minor pressure-dissolution

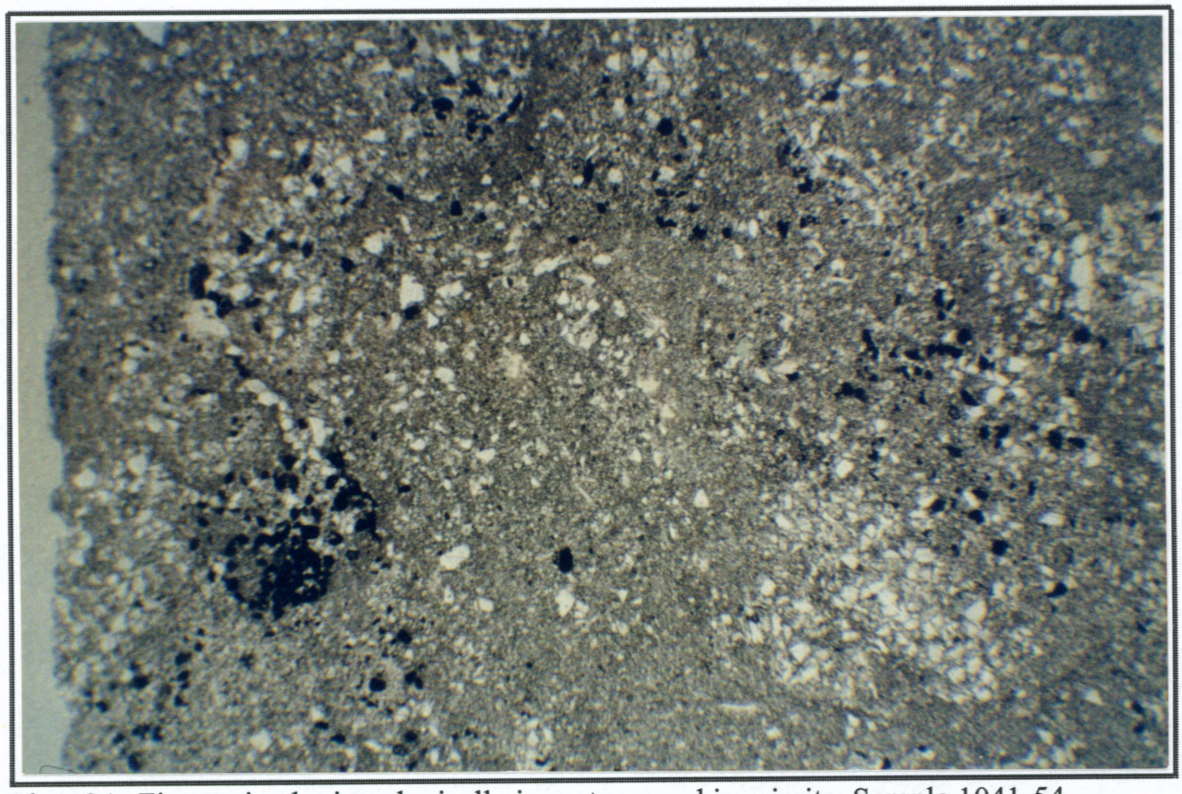

Plate 8A. Fine grained mineralogically immature sand in micrite. Sample 1041-54, Etina Formation, First Spring, 476 m, δ^{13}Ccal +8.4‰, δ^{18}Ocal –9.7‰, pl.pol., 4X mag.. Field of view is 4.2mm

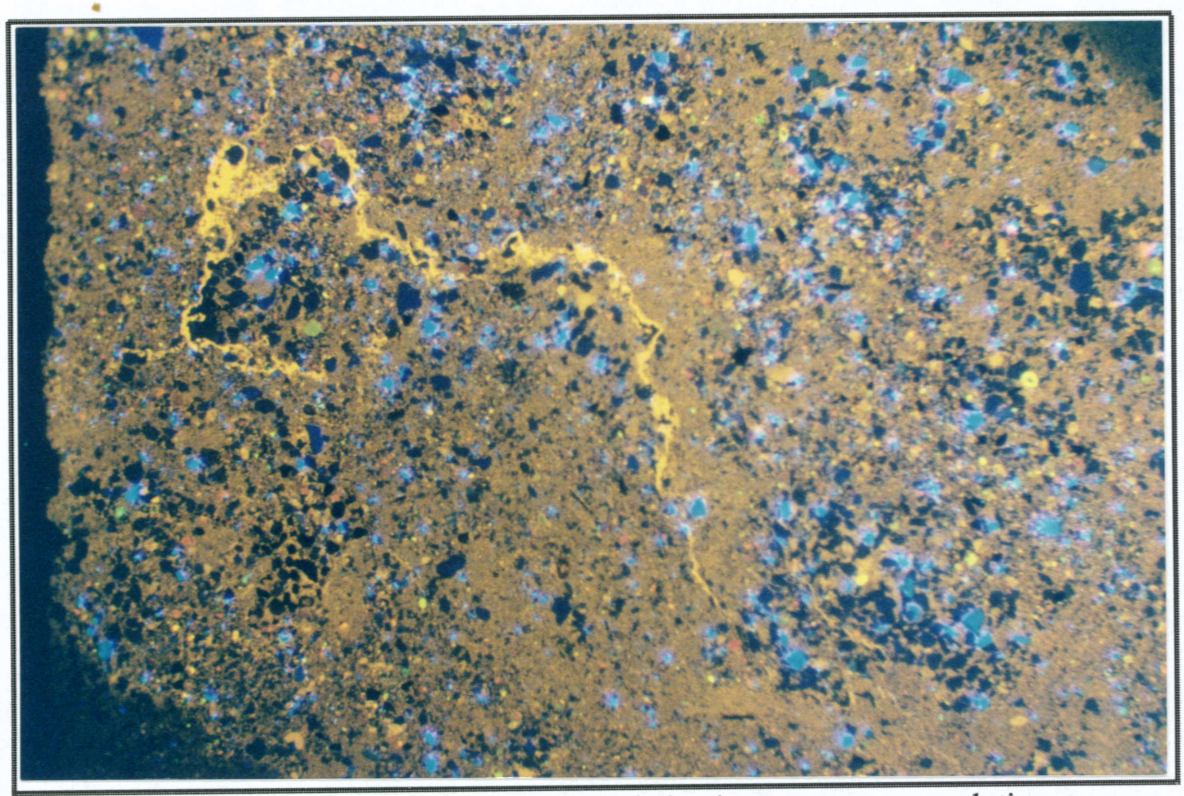

Plate 8B. Same field of view as Plate 8A. Brightly luminescent pressure solution seam as well as fine grained previously described detrital carbonates. 14kV, 190μA, 9.4 seconds.

seams have developed within these limestones from the dominant micrite carbonate phase (Plate 8). Once again, despite its content of detrital calcite and minor development of diagenetic phases, the whole-rock $\delta^{13}C$ of calcite records a high +8.4‰.

Shallowing is once again reflected by an increase in sand content and ripple lamination (Figure 14). Two distinct coarsening-upward cycles are evident in the overlying medium to thickly bedded, medium to coarse grained, sandy oolitic limestones that exhibit coarse stylo-lamination. They conclude at a 1 m-thick intraclastic, flat pebble conglomerate above a clearly erosive disconformable surface. Large pieces (~15 mm) of previously described oolitic limestone are reworked into a fine sandy micrite (Plate 9). Whole-rock $\delta^{13}C$ values are +9.8‰ for calcite and +5.4‰ for dolomite. It is apparent here that some inter-grain bladed-prismatic and mosaic spar cements pre-date reworking, thus confirming their early diagenetic marine origin.

At the top of the third limestone band, as the result of a transgression, rippled and stromatolitic fine sandy limestone recording calcite $\delta^{13}C$ of +8.3‰, passes quickly into 35 m of fissile, red-weathering green-grey shaley calcareous siltstone (Figure 14). Coarsening and thickening of beds towards the top of this siltstone interval indicates a repeat of the previously described shallowing event. Directly underlying limestones of the fourth band at 582m, laminar-bedded green calcareous siltstone records a relatively low $\delta^{13}C$ of +4.9‰.

Above a coarse gravel base overlying a disconformity surface, the fourth limestone band is initially dominated by medium to thick, coarsening-upward beds of blue-green medium to coarse sandy and oolitic limestone with characteristic large planar-cross bedding (Figure 14). Despite grain contacts and pressure solution indicating a high degree of compaction, this ooid limestone records a highly positive $\delta^{13}C$ value of 10.3‰ for calcite.

The succeeding 20 m of interbedded stomatolitic and medium to coarse sandy limestones is in turn disconformably overlain by 10 m of coarse sandy limestone and intraclastic granular conglomerate. This marks the sequence boundary into the “Patterton Shale” at First Spring (Figure 14). The blue, medium to coarse sandy intraclastic limestone above this disconformity records a $\delta^{13}C$ for calcite of +9.8‰ and +8.8‰ for dolomite.

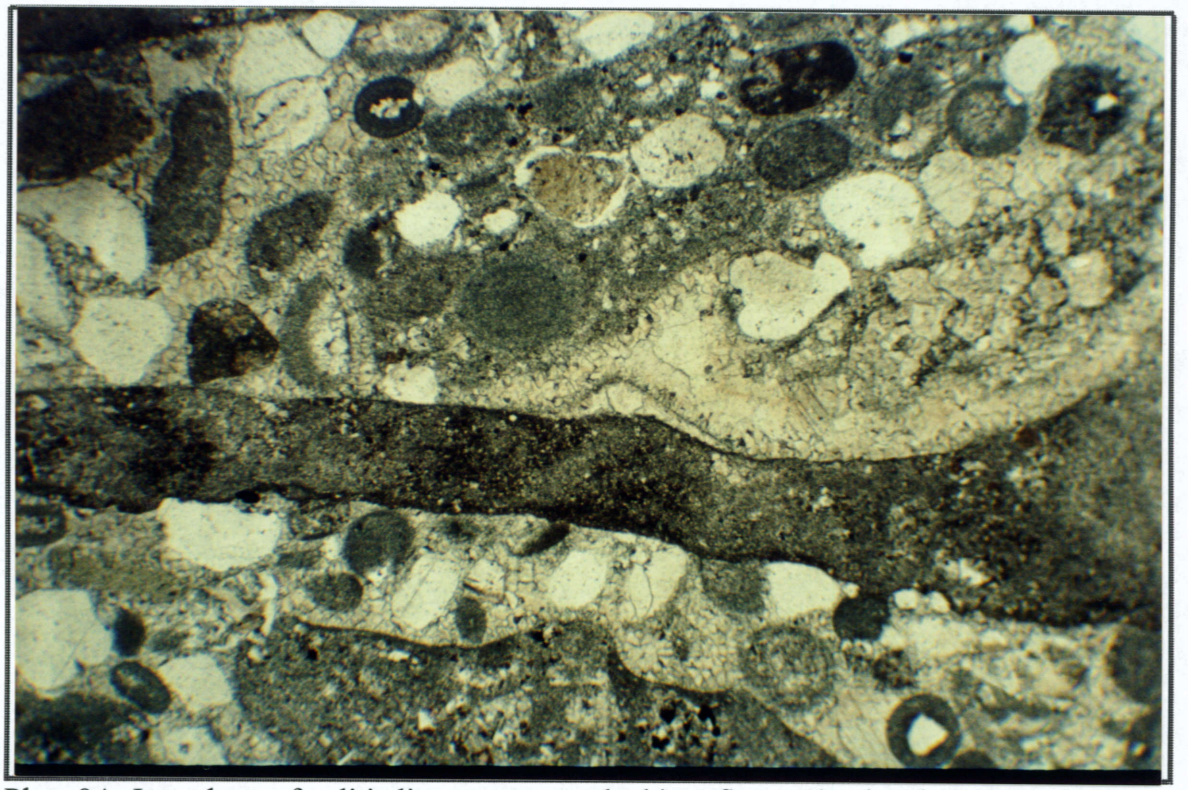

Plate 9A. Intraclasts of oolitic limestone reworked into fine-grained carbonate mud. Sample 1041-58, Etina Formation, First Spring, 528 m, δ^{13}Ccal +9.8‰, δ^{18}Ocal –10‰, δ^{13}Cdol +5.4‰, δ^{18}Odol –2.7‰, pl.pol., 4X mag.. Field of view is 4.2mm.

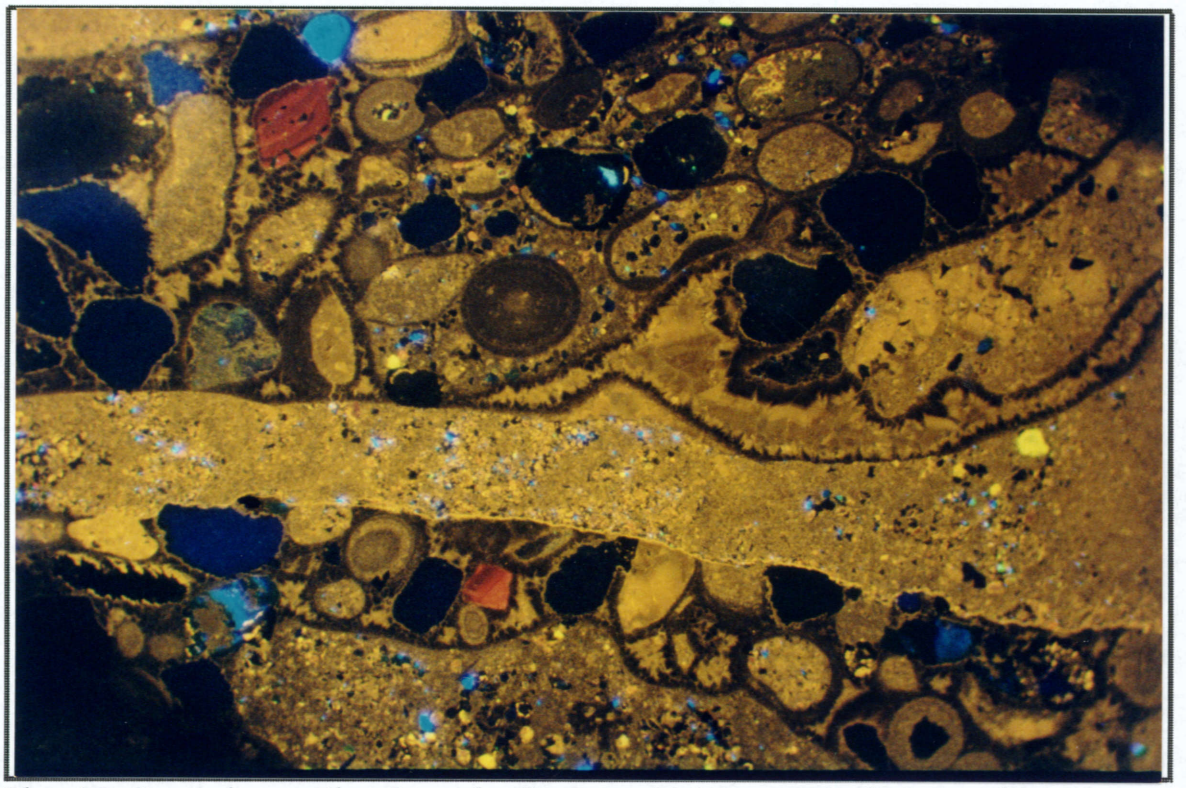

Plate 9B. Same view as Plate 9A under CL. Interstitial cements in the lower clast pre-date reworking, detrital dolomite (red-orange) evident within intraclasts. 15kV, 230μA, 7.2 seconds.

The ensuing transgression is characterised by thickening and fining upward, fine sandy stromatolitic bedsets. The $\delta^{13}C$ of a representative fine-grained limestone at this level is +7.7‰ at 643 m height in the section.

5.2.2 Popes Paddock and Mt Emily

A second complete section through the Etina Formation was measured where the unit is thickly developed to the south of the Blinman Diapir. The section through the "Winna Limestone" at Popes Paddock actually begins in the upper Tapley Hill Formation just south of Alpana Homestead near the Wilpena to Blinman road (Figure 12, Plate 4A). Like the Tapley Hill Formation in this area, the fine grained Sunderland Formation shows generally poor outcrop. A limited outcrop of blue-green fine sandy limestone was sampled (1041-139) for isotopic analysis. Given that the dolomite content is observed to increase up to parasequence exposure surfaces (Lemon, 1988), minor amounts of dolomite in this sample suggests it lies just beneath the Sunderland-Etina sequence boundary (Figure 14). The C-sotopic signatures of +7.4‰ for calcite and +3.3‰ for dolomite continues and amplifies the trend of moderately positive values observed at the top of the Tapley Hill Formation and through the Brighton Limestone. These values also herald a switch in the prevailing modality of the C-isotopic composition of calcite and dolomite, from $\delta^{13}C_{cal} \leq \delta^{13}C_{dol}$ through the preceding Sturtian succession, to $\delta^{13}C_{cal} > \delta^{13}C_{dol}$ in the first two units of the Marinoan sequence, viz. the Sunderland and Etina Formations (Figures 8 and 14).

In Popes Paddock, the Etina Formation begins much the same as it does at First Spring, with nearly 100 m of flaggy, fissile green-grey, calcareous siltstone. Whilst the upward increase in carbonate and grain size is again observed at the beginning of the first limestone band in this location, the band is thinner by some 40 m than it is at First Spring (Figure 14). Shallowing into massive blue-green, fine to medium, sandy limestone occurs between 395 and 415 m. This first limestone records modestly positive C-isotopic signatures of +5.7‰ for calcite and +4.0‰ for dolomite. Detrital carbonate is evident in sample 1041-140 but its fine-grained nature makes determination of the nature of any primary dolomite difficult.

The sharp upper contact of this sandy limestone is cut into by thin channel-scour sands before deepening through 40 m of fine sandy stromatolitic and oolitic limestone of decreasing bed thickness, grain size

Plate 10A. The base of 70 cm thick beds of medium to coarse sandy limestone can be seen scouring into finer grained grey silty limestone, Etina Formation, Popes Paddock section, 505-515 m.

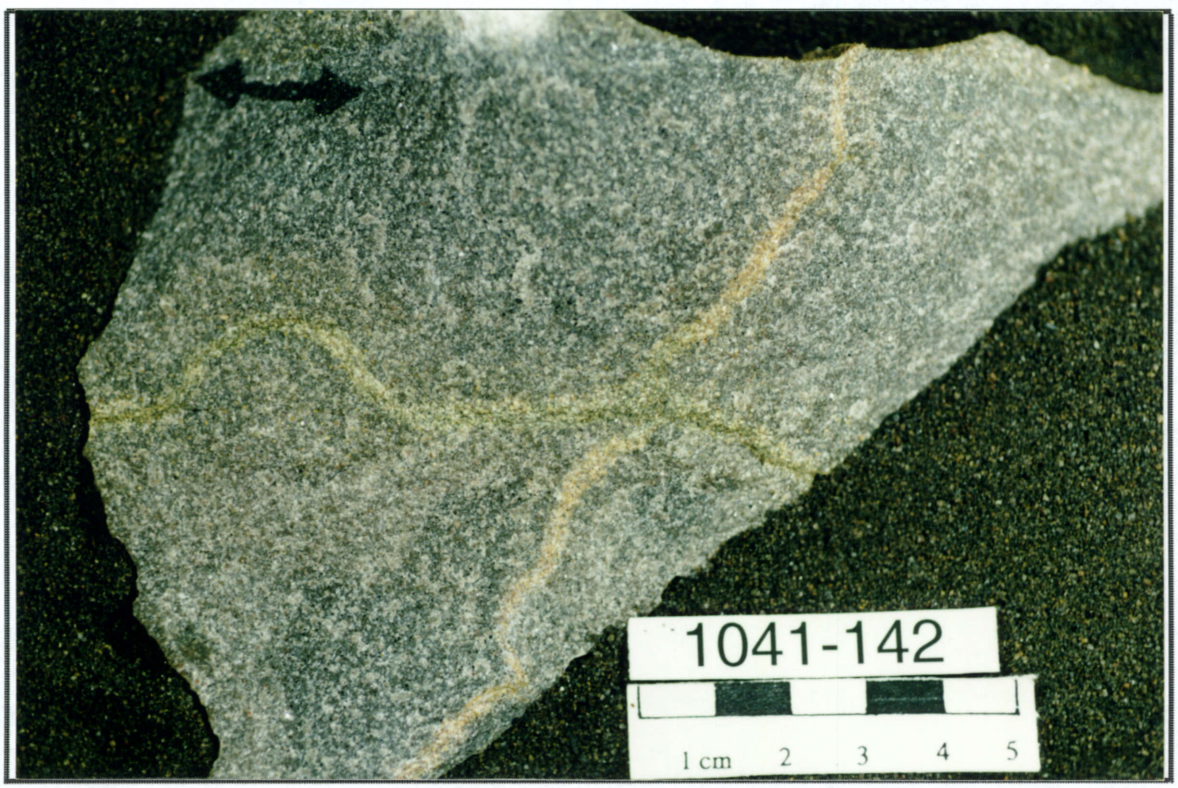

Plate 10B. Hand specimen showing two generations of bedding horizontal (green) and bedding oblique (orange) coarse stylo-laminae. Etina Formation, Popes Paddock section, 515 m, δ^{13}Ccal +9.4‰, δ^{18}Ocal –10.5‰.

and carbonate content. Oolitic limestone at 441 m has a calcite $\delta^{13}C$ value of +7.8‰.

The overlying red-weathering, (but grey-green when fresh) calcareous siltstone is 40 m thick and ends abruptly in a thin (~20 cm) sheet of gravel which marks the beginning of the second Etina limestone band at 505 metres. The top surface of medium to thickly laminar-bedded, fine sandy limestones is erosively truncated by channel-washed gravels that fine into medium to coarse grained sandy limestones with characteristic coarse (~5 mm) stylo-lamination (Plate 10).

The bedding-parallel green stylo-lamination appears to cross-cut the oblique orange stylo-lamination (Plate 10B). The latter is characterised by radiaxial fibrous calcite cement appearing to fill tension gashes and is also parallel to other microscopic pressure solution veins. Cathodoluminescence signatures of peloids, veinous and early diagenetic bladed cements are virtually identical indicating similar elemental chemistry and most likely recrystallisation in a closed system. Development of authigenic chlorite gives the compaction-driven, bedding parallel, laminae their characteristic green colour. Away from the pressure-solution features, the dominant carbonate forms of peloids and bladed cement record a highly positive whole rock $\delta^{13}C$ of +9.4‰.

Disconformably overlying this sandy limestone is a ~13 m thick, coarsening-upward parasequence that grades from laminar-bedded calcareous siltstone into medium-grained, stylo-laminated limestone with slumps and thin channel-fill gravels (Plate 11A). The lamination is in part stromatolitic as cyanobacteria have attempted to colonise the substrate between the higher-energy channel detritus (Plate 11B). The C-isotopic composition of the stromatolitic calcite (+9.2‰ at 528 m) continues the trend of highly positive $\delta^{13}C$ values.

Another thin (~10 m thick) coarsening-upward paracycle is followed by poorly-sorted, medium to coarse sandy, weakly stromatolitic limestones with common thin (<10 cm) gravel-filled channels up to 50 cm wide from 530 to 560 m. A thin bed of digitate stromatolites gives way to medium-sandy, oolitic and peloidal limestone that is in turn overlain by a final pebbly gravel which marks the onset of more significant transgression at 585 metres.

The moderately to well-rounded clastic detritus throughout this second limestone interval is dominated by silicic grains and lesser amounts of diapir-derived carbonate. Also present are significant amounts of fine

Plate 11A. A large (~30 cm) piece of fine micritic limestone reworked in sandy limestone, Etina Formation, Popes Paddock section, 525 m.

Plate 11B. Hand specimen at 528m showing stromatolite development and medium grained sandy influence. Etina Formation, Popes Paddock section, δ^{13}Ccal +9.2‰, δ^{18}Ocal –10.3‰.

sandy-peloidal detrital carbonate. Commonly exhibiting rhombic nucleii and varying thicknesses of ooid lamellae, these limestones provide strong evidence for the direct precipitation of carbonate in shallow marine to lagoonal environments. This carbonate is then swept into sediment sinks surrounding the diapirs in the manner discussed in Chapter 3.2. Despite the likelihood of diapiric salts influencing the salinity and facilitating precipitation of rhombic dolomite or high Mg calcite, the measured $\delta^{13}C$ of calcite in these limestones remains relatively high (+8.8‰ and +8.4‰ at 557 and 578 m respectively: Figure 14).

The overlying green calcareous siltstone interval is 90 m thick and at 620-630 m in the section displays the same brief shallowing event seen at First Spring (Figure 14). Two samples (1041-146s,c) were taken at 630 m just below the resultant sharp boundary. The sand-dominated sample has a calcite $\delta^{13}C$ of +4.8‰ whilst the more calcareous sample records values +4.6‰ for $\delta^{13}C$ of calcite and +2.2‰ for dolomite.

Increasing sand and carbonate once again define the shallowing upwards into the third "Winna" limestone band. This is the thickest of the Etina limestone bands and is well over 200 m thick at this locality. It is dominated by numerous oolitic and intraclastic, sandy stromatolitic limestone facies similar to those already described. It also includes several flat-pebble conglomerates above numerous disconformable parasequence boundaries. Where preserved, parasequences commonly show a gradation between blue-green, micritic and sandy, stromatolitic limestones and trough and planar-cross-bedded, oolitic, sandy limestones with coarse stylolitic lamination.

The stratigraphically anomalous isotopic values of calcite ($\delta^{13}C$ +3.2‰, $\delta^{18}O$ –7.0‰) and dolomite ($\delta^{13}C$ +5‰, $\delta^{18}O$ +0.8‰) in sample 1041-147 (686 m) reflect its likely altered nature. The unusual yellow-brown veined appearance of this sample would tend to indicate that it has been altered by fluid movement along fault planes (Plate 12A, Figures 7 and 12). Its isotopic values and appearance serve as an indicator of this type of alteration.

The adjacent, thin, wavy laminated beds of alternating fine sand and green micritic mud in sample 1041-148 at 688 m (Plate 12B) record a calcite $\delta^{13}C$ of +7.8‰. Rare thin, pressure-solution veinlets in this sample were not sampled for isotopic analysis.

Plate 12A. Whereas the predominant colour of Etina sediments is green-grey, this yellow-brown veinous limestone is most likely produced as a result of movement along faults. Popes Paddock section, 686 m, δ^{13}Ccal +3.2‰, δ^{18}Ocal –7.0‰, δ^{13}Cdol +5.0‰, δ^{18}Odol –0.8‰.

Plate 12B. Wavy bedding lamination of interbedded flows of fine sand and green micritic mud. Etina Formation, Popes Paddock section, 688 m, δ^{13}Ccal +7.8‰, δ^{18}Ocal –11.4‰.

Plate 13A. Sand influx (note scour base) hinders attempts by cyanobacteria to colonize substrate producing variable lamination. Etina Formation, Popes Paddock section, 710 m.

Plate 13B. Flat pebble conglomerate, including quartzite clasts and plastic oolitic-peloid muds (arrow) from which $\delta^{13}C$ was determined ($\delta^{13}C$cal +9.4‰, $\delta^{18}O$cal –7.4‰). Numbered label is ~3.5cm long. Etina Formation, Popes Paddock section, 712 m.

A 20 m-thick succession of sandy stromatolites occurs beneath a massively bedded, flat-pebble conglomerate that is 6 m thick at 710 m (Plate 13). Generally well-rounded clasts up to 9 cm long include heavy mineral-laminated quartzite and fine-grained, yellow dolomite of diapir xenoclast origin. Clasts of the latter are commonly elongate, some of them orthogonal to bedding indicating a high energy-debris flow type environment of deposition. Carbonate mud makes up a significant portion of this rock, both inside some clasts and between them. There are also large intraclasts (~7 cm) of dark blue, oolitic-peloidal limestone that are plastically deformed around more lithified clasts. C-isotopic analysis of one of these clasts returned a calcite $\delta^{13}C$ value of +9.4‰. There are also sets of very thin (<7 mm) microfractures in this sample. The largest of these fractures displaces clasts <1 mm in size in a reverse sense and is annealed with grey-brown calcite cement.

Sorting increases through the 40 m-thick, coarsely clastic sequence into 30 m of largely micritic stromatolites, ($\delta^{13}C$ of calcite +8.6‰ at 736 m). An ensuing transgression deposited 30 m of calcareous siltstone. Coarse sands and channels of gravel indicate shallowing once again at 780 m height in the section. The 20 m-thick, typically stylo-laminated sands grade into more than 60 m of dominantly blue-grey, sandy stromatolitic limestone punctuated by occasional channels and sheets of gravel. A return to clastic-dominated sedimentation above 860 m marks the last 40 m of shallow-water deposition before transgression into calcareous siltstone marks the top of the third Etina limestone band at this location.

Throughout this upper 120 m of clastic-stromatolitic-clastic deposition which comprise the third “Winna” limestone band at Popes Paddock, C-isotopic composition of calcite attains a definite plateau of ^{13}C enrichment. $\delta^{13}C$ values range from +9.0‰ to +8.8‰ in medium-sandy stromatolites at 780 and 791 m, through +9.4‰ in fine sandy stromatolites at 828 m and +9.6‰ in intraclastic limestone at 877 m, to +9.0‰ in sandy intraclastic limestone at 879 metres. The sandy stomatolites at 780 and 791 m also contain minor amounts of dolomite, both recording $\delta^{13}C$ values of +5.7‰.

Towards the top of the third band, grain-supported intraformational conglomerate (1041-158 at 895 m; Plate 14A) provides further evidence for periodic exposure and a high energy depositional environment. The sample includes a large clast (~5 cm) of digitate stromatolite deposited in poorly-sorted sand and calcareous mud. The $\delta^{13}C$ of calcite in the micritic stromatolite clast was +9.1‰ versus a whole-rock average value

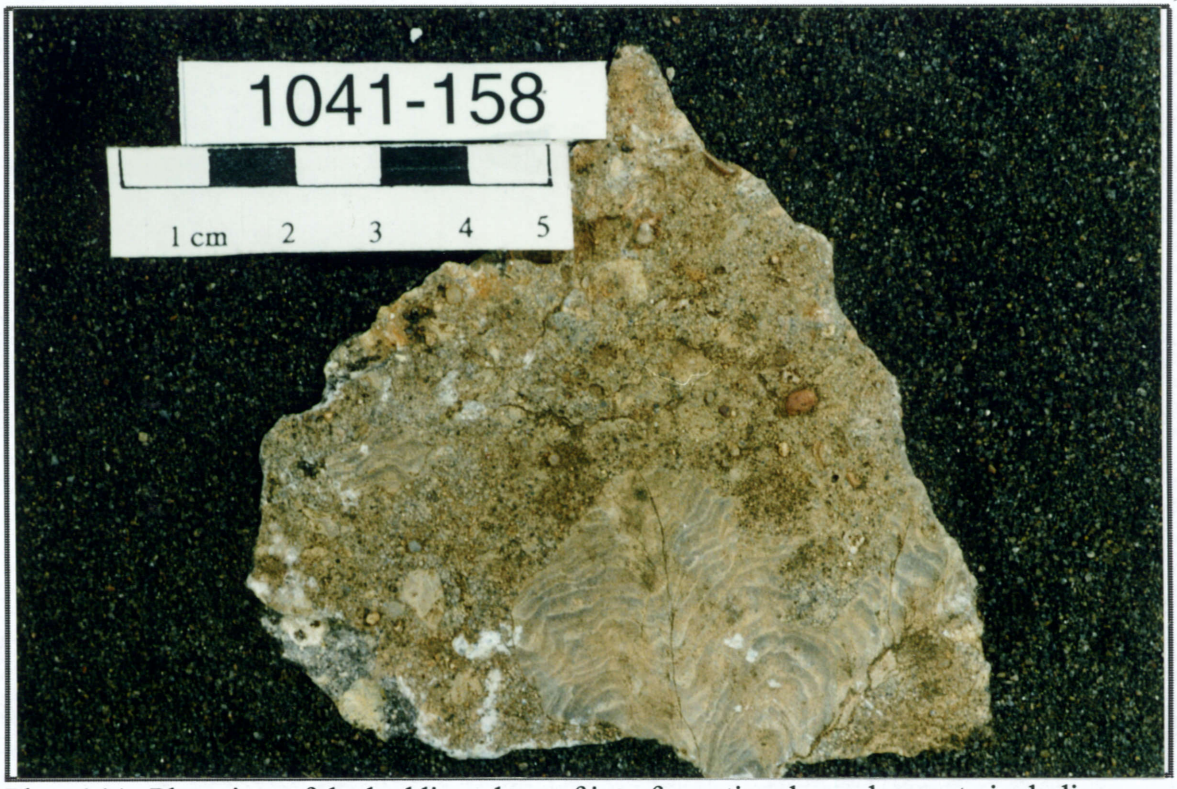

Plate 14A. Plan view of the bedding plane of intraformational conglomerate including clast of digitate stromatolite. Etina Formation, Popes Paddock section, 895 m. Strom clast δ^{13}Ccal +9.1‰, δ^{18}Ocal –9.4‰. Matrix, δ^{13}Ccal +9.3‰, δ^{18}Ocal –7.8‰.

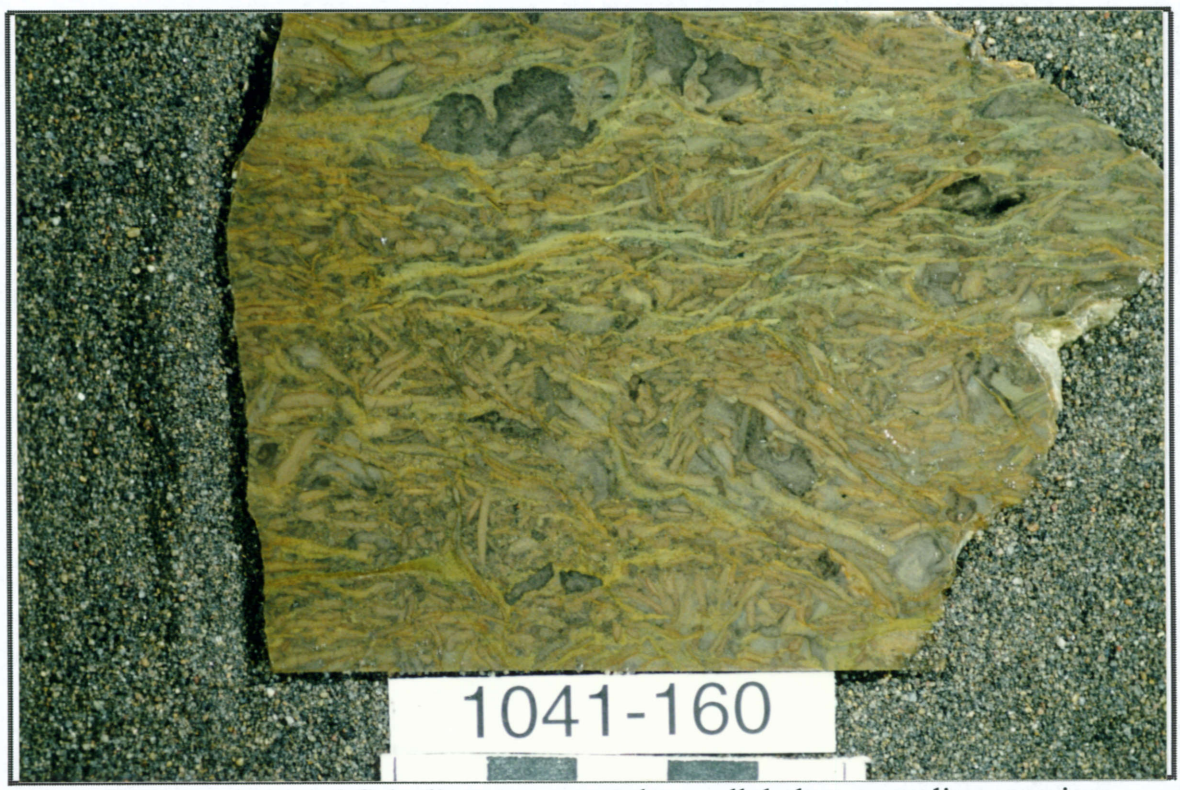

Plate 14B. Cyanobacterial-flake limestone, note the small dark stromatolites growing in the sediment at upper left. Etina Formation, Popes Paddock section, 954 m, δ^{13}Ccal +6.9‰, δ^{18}Ocal –11.1‰, δ^{13}Cdol +3.5‰, δ^{18}Odol –5.7‰.

of +9.3‰ indicating a negligible difference between the seawater chemistries of their respective depositional settings.

For the purposes of testing the validity of the chemostratigraphic data on the fourth "Winna" limestone band at Popes Paddock and detecting possible geochemical alteration on different regional scales, particularly due to local faulting, samples were collected along a reference section through the fourth limestone band and preceding siltstone, near Mt Emily (Lemon, 1998; Figures 12 and 14). This section began in fine-sandy stromatolites at the transgressive top of the third band where the $\delta^{13}C$ of calcite is +8.2‰.

The overlying siltstone coarsens upward into cryptomicrobial-laminated and cyanobacterial-flake limestone before being truncated by intraclastic limestones and flat pebble conglomerates. The green, fine-sandy, calcareous siltstones have closely comparable calcite $\delta^{13}C$ values of +4.2‰ at 952 m in the Popes Paddock section and +4.9‰ at 75 m in the Mt Emily section where a cryptomicrobial lamination is apparent. Minor amounts of dolomite are present in both samples, the former recording a dolomite $\delta^{13}C$ of +2.7‰.

Cyanobacterial-flake limestone at 954 m height in the Popes Paddock section is approximately 1 m thick and interbedded with fine-sandy limestone (Plate 14B). The internal flake-fabric of this rock resembles that of Mawson's (1938) "heiroglyphic limestone" description of the lower Trezona Formation, the flakes originating from the breakup of benthic microbial mats. The principal difference between this sample and the Trezona example is the oxidation state of the sediment. The Etina Formation is dominantly green-grey in colour reflecting suboxic environments of deposition compared to the Trezona's oxic red. In thin section, the flakes in Etina sample 1041-160 commonly exhibit brittle rupture annealed by early diagenetic cements (including minor dolomite). It also contains a considerable amount of carbonaceous material in stylolitic seams. The $\delta^{13}C$ values of this sample are +6.9‰ for calcite and +3.5‰ for dolomite.

Above its disconformable base marked by a coarse gravel, the fourth "Winna" limestone band in the southern sections is characterised by the same blue-green, large planar-cross bedded, medium to coarse-sandy and stromatolitic limestones as seen at First Spring. The fine to medium sandy ooid limestone at 978 m gives $\delta^{13}C$ values of +8.9‰ for calcite and +6.0‰ for its minor dolomite component. Blue-brown, fine-sandy,

Plate 15A. Large scale cross bedding in sandy limestone of the Etina Formation from 100 m in the Mt Emily section.

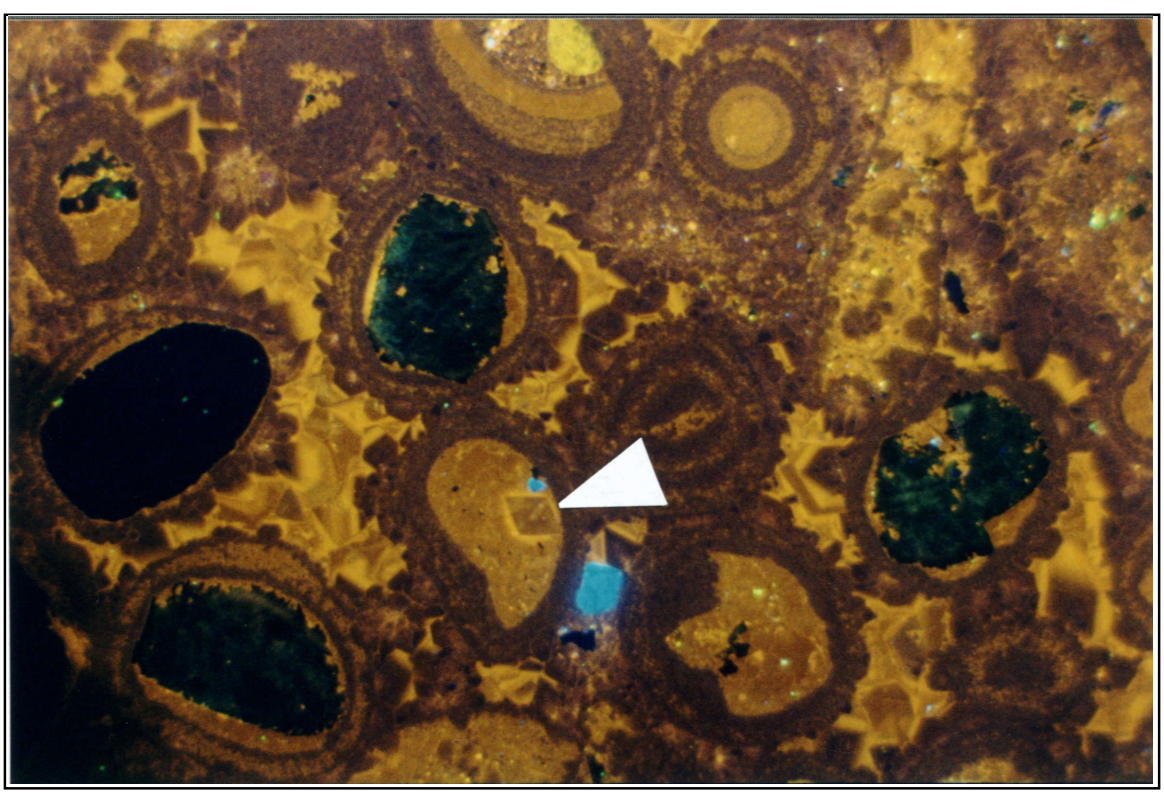

Plate 15B. Relic rhomboid (arrow) in peloidal ooid nuclei and extensive diagenetic cements. Sample 1041-165, Etina Formation, Popes Paddock section, 1065 m, d13Ccal +9.4‰, d18Ocal -8.2‰, 14kV, 195mA, 42.5 sec., 10X mag.. Field of view is 2.3mm.

domal-stromatolitic limestone at 985 m records a slightly higher value of +9.6‰ for calcite.

Coarse intraclastic gravels overlying a sharp break once again mark the sequence boundary within the fourth limestone band. The following succession of interbedded coarse-sandy-intraclastic and fine-sandy stromatolitic limestones is over 80 m thick. Dark blue, intraclastic cyanobacterial-flake limestone overlying the disconformity at 1009 m contains calcite with a $\delta^{13}C$ of +7.9‰. Fine to medium-sandy stromatolitic limestone at 1032 m records a slightly higher value of +8.8‰ for calcite.

The transgressive top of the fourth limestone band at Popes Paddock grades upward over 20 m from one last "burst" of coarse sand and intraclastic gravel through finer, cross-bedded, calcareous sands and stromatolites to calcareous silts and shales. Blue medium-sandy, oolitic limestone at 1065 m has a calcite $\delta^{13}C$ of +9.4‰ despite evidence of fairly extensive diagenesis, including relic rhomboid crystals in peloidal ooid nuclei and mosaic burial cements (Plate 15). Stratigraphically above this at 211 m in the Mt Emily section, a more micritic blue-brown, domal-stromatolite limestone records a calcite $\delta^{13}C$ of +8.1‰.

5.2.3 Discussion

Sedimentation throughout the "Winna Limestone" was strongly influenced by variation of sea level. Its shallow ooid and stromatolite limestone facies are indicative of marginal marine to marine platform/shelf environments particularly conducive to massive carbonate precipitation. Significant regression at different times throughout their deposition is likely to have given rise to locally restricted environments and debris-filled drainage channels leading away from an area of exposed diapir breccia.

Deposition of the upper Tapley Hill Formation in this area was controlled by secondary peripheral sinks to the north and south of the Blinman Diapir. It is likely that this relief continued to exist during sedimentation of the overlying units, although current directions measured by Lemon (1998) in the "Winna Limestone" to the south of the Blinman Diapir indicate a change in sediment input direction from towards the south-west into the peripheral sink, to towards the south-east during deposition of the third "Winna Limestone" band. Lemon's (1988) isopach mapping of the overlying Wundowie Limestone between the Blinman and Enorama Diapirs confirms that movement along the north-

south trending Patterton Fault had a large effect on the distribution of Etina Formation sediment in this area (Figure 7).

The thinner section and smaller grain size of the "Winna Limestone" to the north suggests an overall deeper environment of deposition than is evident to south of the diapir. The thinner first band in the Popes Paddock section (40 m versus 70 m at First Spring: Figure 14) is most probably due to exposure and a hiatus in this southern location. The contrast in relative water depth between the two locations is more obvious in the second band with thick, coarse sands preserved to the south and a sequence of relatively fine-grained silty limestones to the north.

Isotopically, the sections through the "Winna Limestone" display a fairly wide but systematic variation. The greatest amount of variation in calcite $\delta^{13}C$ occurs at First Spring where values range from +2.0‰ in calcareous siltstone to +10.2‰ in sandy ooid limestone. There is generally less variation evident in the Popes Paddock section, although a low value of +4.6‰ is obtained in a statigraphically similar position to that exhibiting low values at First Spring, namely in the siltstone separating limestone bands two and three.

Indeed the variation in the C-isotopic composition of calcite is as correlatable between the sections as the sedimentary paracycles themselves. There is a great similarity between the data from samples, at the same relative stratigraphic levels, at First Spring and Mt Emily. At the top of the third limestone band, digitate stromatolites 1041-59 and 1041-70 have $\delta^{13}C$ values of +8.3‰ and +8.2‰, respectively. In the regressive cycle shallowing-up to the fourth band, calcareous siltstones 1041-62 and 1041-74 both record a $\delta^{13}C$ of +4.9‰. And stromatolitic limestone samples 1041-68 and 1041-75, in the transgressive fourth band, give values of +7.7‰ and +8.1‰, respectively. The carbonate in all of these samples is mostly micritic calcite. Correlation of this kind is not only verification of the analytical technique employed in this study but it also confirms the viability of stable isotope chemostratigraphy in this region.

The overall consistency of calcite $\delta^{13}C$ through varying shallow carbonate lithologies, particularly through the Popes Paddock section, indicates no direct relation between carbon isotope data and the lithofacies. Indeed, on a metre scale through widely varying amounts of micrite and diagenetic cements, whole-rock $\delta^{13}C$ values have remained for the most part consistent. Apart from spatially confined and obviously

fault-related alteration (e.g. in sample 1041-147), there is no evidence to suggest that the cements observed throughout the "Winna Limestone" are related to anything other than early burial marine diagenesis. Through what limited micro-sampling was undertaken (samples 1041-146 and 1041-158), variance in $\delta^{13}C$ never amounted to more than 0.2‰.

The occurrence of dolomite in the "Winna Limestone" may be related to, but not solely reliant on, proximity to exposure surfaces within paracycles. Unlike that observed in the Brighton Limestone, the $\delta^{13}C$ of dolomite throughout the Etina Formation sections is consistently less positive than coexisting calcite, by amounts ranging from 0.2 to 4.4‰. Thin section analysis suggests that the origins of the minor amounts of dolomite within the "Winna Limestone" are unclear. Evidence would suggest that detrital forms may play as significant a part in the whole-rock geochemistry as primary forms that are the result of precipitation from sea water or interaction with saline pore fluids. With respect to the latter, it would be virtually impossible to discriminate between the influence of purely evaporitic-marine fluids and fluids influenced by diapiric salt. The presence of rhombic euhedra within peloids (eg. In samples 1041-144, 1041-165) indicates that minor amounts of primary dolomite have directly precipitated out of saline solution along with any carbonate "whitings" although the relation in $\delta^{13}C$ signatures is not clarified by the data presented here. Certainly through the lower part of the fourth band in the Popes section, the $\delta^{13}C$ values of coexisting calcite and dolomite both trend positive indicating a possible relationship between the two phases.

The sediment colour throughout the "Winna Limestone" is blue-green-grey indicating a prevailing suboxic environment of deposition. If we assume that the carbonaceous material observed in sample 1041-160 had some diagenetic effect on the C-isotopic composition of its coexisting carbonate, then it has reduced the $\delta^{13}C_{carb}$ of this sample by no more than 2-3‰. However, it is unlikely that interaction with organic matter has lowered $\delta^{13}C$ at this stratigraphic level in all three sections, leading to the probable conclusion that the carbonaceous material has had little or no effect on the coexisiting carbonate.

5.3 "Patterton Shale" and Wundowie Limestone

The "Patterton Shale" and Wundowie Limestone Members were extensively mapped throughout the Central Flinders Zone by Lemon (1988) and the reader is referred to this comprehensive work for a

detailed description of their lithofacies. The overall transgressive Patterton-Wundowie sequence is up to of 600 m thick and outcrops over a wide area in this region (Lemon, 1988; Figure 7).

The "Patterton Shale" thickens dramatically into the peripheral sink adjacent to the northern flank of the Enorama Diapir (Lemon, 1988). Apart from the two altered dolomicrite samples assessed in Chapter 3.2, no other isotopic data are available on this interval (Figure 15).

The three bands of the Wundowie Limestone (Figure 15) are in essence representatives of the aforementioned paracyclical sedimentation evident right the way through the Etina Formation. In a typical cycle, sediments coarsen and shallow up to an exposure surface disconformably overlain by conglomerate or gravel which is in turn succeeded by sandy oolitic and stromatolitic limestone before the ensuing transgression brings a return to shale deposition. Samples for chemostratigraphic purposes were taken from micritic stromatolite limestones above the disconformity in each of the limestone bands so as to minimise diagenetic alteration.

Lemon (1988) introduced further informal nomenclature for the three Wundowie Limestone bands. Blue-grey domal-stromatolitic limestone from the lower "Idandanoo Band" in Lemon's (op. cit.) Section No. 2 just west of Gum Creek gives $\delta^{13}C$ values of +7.3‰ and +5.9‰ for calcite and dolomite respectively. In thin section, this sample is seen to contain thin stylolitic-seams of both carbonate and carbonaceous matter but on the whole is predominantly micritic. There is a suggestion that most of the dolomite is mainly primary (as opposed to diagenetic), although diapiric-detrital forms are also evident.

From the middle "Aldoona Band" in Lemon's (1988) Section No. 2, a blue-grey, fine-sandy, digitate stromatolite comprises calcite with a $\delta^{13}C$ of +8.0‰. In thin section, micrite shows alteration to very fine diagenetic bladed burial cements. In the upper "Dedmans Band" from Lemon's (op. cit.) Section No. 3, a similar digitate stromatolitic limestone yields $\delta^{13}C$ values of +8.2 and +8.0‰ for calcite and dolomite, respectively. Minor amounts of darkly-luminescent bladed-euhedral calcite are indicative of early burial diagenesis of primary micrite. Despite evidence for diagenesis, all three samples record strongly positive C-isotopic compositions.

The onset of oxic environments of deposition for the first time in the interglacial Umberatana Group in the study area is observable in the top-Etina "Dedmans Band" near the Enorama Diapir at Dedmans Bore. This

change to a red-bed style of deposition was the basis of the original Farina (green) and Willochra (red) Subgroup stratigraphic subdivision first used by Thompson (1969) although the transition was acknowledged by earlier authors.

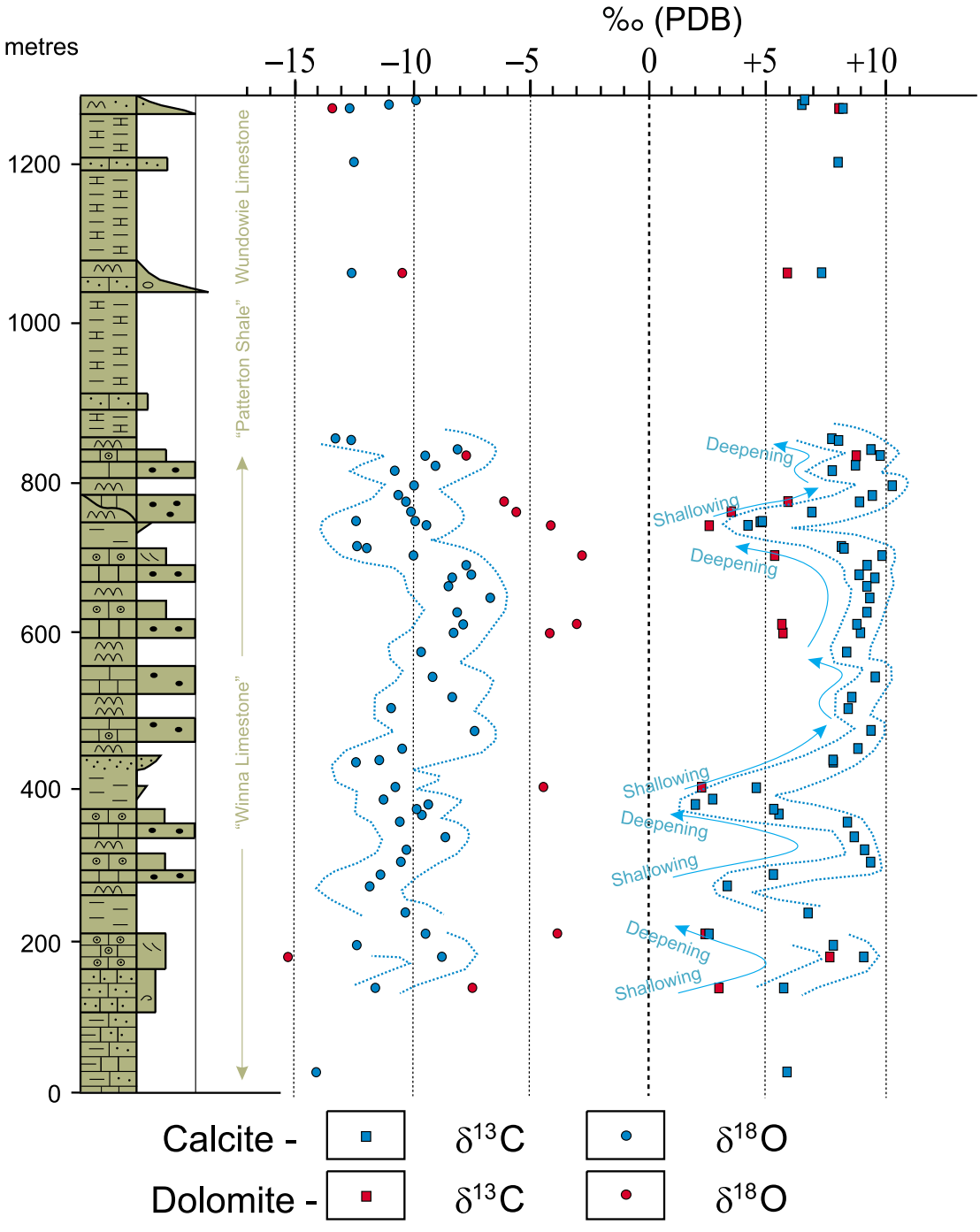

Figure 15. Composite chemostratigraphy of the Etina Formation.

Approximately in the middle of the "Dedmans Band", just to the north of the Enorama Diapir, dark red micritic limestone contains calcite with a $\delta^{13}C$ value of +6.5‰ (Figures 15 and 17). At the transgressive top of the

band, precipitation of shallow-water limestone continued around the diapir edge whilst deposition of the Enorama Shale took place in deeper parts of the basin. Dominantly micritic dark red, stromatolitic limestones at the top of and immediately above the "Dedmans Band" adjacent to the diapir continue the moderately high positive $\delta^{13}C$ of calcite at +6.6‰ and +7.0‰ (Figure 17), indicating no direct relationship between carbonate $\delta^{13}C$ and the oxidation state of the sediment.

5.4 Discussion

From a composite plot of the stable isotope chemostratigraphy of the Etina Formation (Figure 15), several things may be observed. The C-isotope profile of the Etina Formation continues the positive trend evident throughout the underlying Tapley Hill Formation and Brighton Limestone, reaching a plateau of highly positive values (+8 to +10‰), before a slight drop to +6 to +8‰ at the top. The reproducibility of data, both within and between sections sampled, confirms the primary nature of the data.

A high sampling density has allowed for very accurate correlation of the sections on the parasequence scale. This has revealed a strong link between $\delta^{13}C$ and water depth, with values trending out to +10‰ in shallow water platform carbonates and the intervening siltstone/shales having values in the range +2 to +5‰. This is perhaps best demonstrated in the second Winna Limestone band at First Spring where calcareous siltstones and cryptomicrobially laminated limestones outcrop between deep and shallow sediments. The $\delta^{13}C$ values in and surrounding this band range from +2 to +7‰ (Figure 14). This correlation with water depth is also very nearly mirrored by $\delta^{18}O$ data, although the greater susceptibility of oxygen to post-depositional alteration has somewhat obscured the correlation.

The Etina Formation data also exhibit no systematic difference between $\delta^{13}C$ values derived from micrite and cements in shallow water limestones. Whole-rock calcite data remained consistent through varying proportions of the two calcite forms, although most cements observed in thin section were likely to have originated from early burial diagenesis in the presence of pore fluids isotopically similar to the sea water from which the micrite precipitated. The abundance of intraclasts attests to the rapidity of cementation on the sea floor during sedimentation of the Etina Formation.

Carbon and oxygen data for dolomite largely mimics the trends observed for calcite through the Etina Formation, with the consistent difference that $\delta^{13}C$ is less positive and $\delta^{18}O$ less negative. This difference is to be expected for $\delta^{18}O$ (McKenzie, 1981), as was seen in data from the Brighton Limestone (Figure 11). The respective roles that small amounts of reworked detrital and diapirically-sourced carbonates (or even, perhaps, tainted saline fluids) play in producing the observed $\delta^{13}C$ values remain uncertain. However, it may be presumed at this stage that some as yet unconstrained diapiric influence causes this difference in dolomite $\delta^{13}C$.

Definite isotopic alteration exists in several samples that exhibit somewhat more obvious physical signs of recrystallisation. In these samples, the $\delta^{13}C$ of calcite was consistently less than that of coexisting dolomite, against the trend for other Etina Formation samples; and the $\delta^{18}O$ of dolomite is anomalously positive (up to +0.8‰). In the case of both carbon and oxygen, this may be explained by the preferential removal of lighter isotopes in the calcitization reaction, leaving the residual non-recrystallised dolomite relatively enriched in heavier isotopes.

Elsewhere, the Sturtian to Marinoan interglacial period is characterised by carbonates with heavy $\delta^{13}C$ signals, commonly up to +10‰ (Kaufman and Knoll, 1995). As yet there is no environment prescribed for the level of productivity that would be required to produce such anomalous $\delta^{13}C$ values. The oxidation state of Neoproterozoic marine sediments is not altogether unimportant in addressing this question.

Sample	section/depth (m)	$^{87}Sr/^{86}Sr$
1041-31	“Aldoona”	0.707693
1041-25	“Idandanoo”	0.707741
1041-66	First Spring/628	0.707714
1041-51	First Spring/446	0.707808
1041-39	First Spring/168	0.707608

Table 6. Strontium isotopic compositions for selected Etina Formation samples.

The new 87Sr/86Sr values from the Etina Formation (Table 6) are slightly higher than those for the Brighton Limestone, but still compare favourably with published interglacial values (Derry et al., 1992) and other unpublished attempts to document the Neoproterozoic strontium record in Australia (M. Corkeron, pers comm., 1998).

6. ENORAMA SHALE

6.1 Introduction

The Enorama Shale is the name introduced by Dalgarno and Johnson (*in* Thomson et al., 1964) for the recessively weathered shale between the limestone ridges of the Etina and Trezona Formations. The formation comprises fissile, finely laminated, grey-green and minor red shales, variously dolomitic and sandy (Preiss, 1987; Plate 16A).

Much of the evidence for syn-depositional diapirism in the Central Flinders Zone comes from Lemon's (1988) extensive study which included mapping thicknesses and observing widespread slumping and coarse debris flow adjacent the Enorama Diapir. He observed the top-Etina "Dedmans Band" grading upward into shales and siltstones of the Enorama Shale over a 10 m interval of red calcareous siltstone. The red siltstone in turn grades into interbedded red-brown and khaki siltstones, with occasional thin carbonate lenticles indicating weak current activity. The middle third of the Enorama Shale is a distinctive, well-laminated, green shale showing no evidence of current activity and indicative of deep water deposition. Lemon (op. cit.) observed the cessation of hummocky cross stratification at the lower contact of this green shale, and its return two-thirds of the way through the formation in more red-brown and khaki shales. On the basis of these observations, he interpreted the unit to be distinctly transgressive-regressive in character (Plate 16A). As much as the evidence of current activity, the deepening and shallowing are confirmed by the respective decrease and increase in carbonate content. The thickness of the Enorama Shale varies up to well in excess of 400 m depending on its relation to palaeotopography at the time of deposition.

6.2 Previous geochemical investigations

The Artipena Dolomite Member of the Enorama Shale is described by Dyson (1997) as two thin (0.1-0.4 m thick), buff dolostones separated by 5m of greyish red shale that are interpreted to represent a maximum flooding surface within the Enorama Shale. These dolostones are sharply overlain by grey-green shale. Outcropping 4 km southwest of "Artipena Hut" in the Central Flinders Zone, and nearly 60 km directly east of Wilpena, the Artipena Dolomite displays weakly undulose internal lamination and is similar to other thin dolostones of the Umberatana and Wilpena Groups. Its carbon and oxygen isotopic

Plate 16A. Fissile red-brown and khaki shales of the upper Enorama Shale at Mallee Water. Shallowing-up is indicated by incoming sand lenticles (arrow) which culminates in Trezona Fm. on the far side of the Wilpena-Blinman Road just out of shot at top.

Plate 16B. View looking north along the western margin of the Enorama Diapir at Mallee Water, vertically dipping Enorama Shale strikes into the diapir from left. The massive outcrop in the centre of the scene is the stromatolitic reef from which sample 1041-84 was collected (photo courtesy of N. Lemon).

compositions are reported to be -2.3‰ and -7.3‰ (PDB), respectively (Dyson, 1997). This member of the Enorama Shale is not developed in the vicinity of the Enorama Diapir.

6.3 Fringing stromatolite reefs

Stromatolite reefs that "grew" on the western edge of the Enorama Diapir are documented by Lemon (1988, 1999) and the reader is referred to these works for a comprehensive description of their lithological expression. The fortuitous continuation of shallow-water sedimentation adjacent the Enorama Diapir has allowed for chemostratigraphic study of carbonate through a shale interval where it would otherwise have been difficult.

Approaching the Enorama Diapir along strike from the southwest and northwest, Lemon (1988) documented a dramatic increase in dolomite content of the Enorama Shale over a distance of 2 km from its contact with the diapir. At Mallee Water (Figure 7), the Wundowie Limestone Member of the underlying Etina Formation grades into dolomite within 400 m of the diapir contact. Dolomite persists up section adjacent to the diapir where massive fenestral, cemented, stromatolitic limestones and intraformational dolomite breccias have developed into structures with over 40m of relief (Lemon, op. cit.; Figure 16; Plate 16B).

Investigation of the stromatolite reef facies itself revealed a distinctive clotted or globular texture resembling the reef-binding calcimicrobe *Renalcis* (James, 1983). Fenestral fabric is common throughout the reefs indicating periods of exposure, and dolomitization of these sediments has produced intercrystalline porosity and enhanced the fenestral and vuggy porosity. This dolomitization must have occurred early in the diagenetic history of the reefs to facilitate the inclusion of already dolomitized and cemented detritus in the surrounding sediments (Lemon, 1988).

Along the section at Mallee Water (Figures 16 and 17), the reef lithologies sampled for chemostratigraphic purposes differ little from the aforementioned description with generally only the clastic content varying. Their C-isotopic compositions are relatively consistent in the $\delta^{13}C$ range +6 to +7‰, except for three anomalously lighter values in the upper half of the section (Table 8).

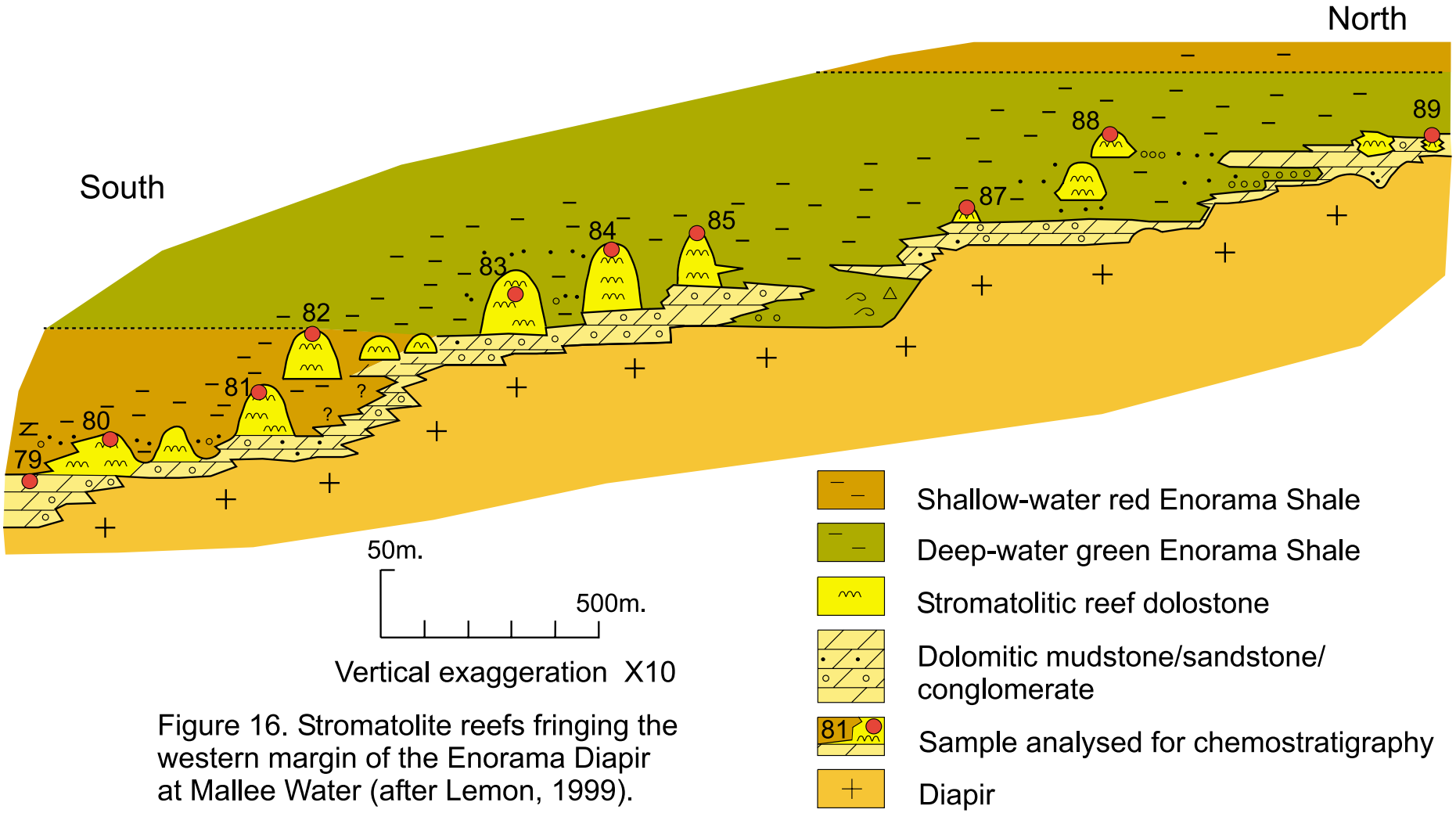

Figure 16. Stromatolite reefs fringing the western margin of the Enorama Diapir at Mallee Water (after Lemon, 1999).

sample	δ^{13}Cdol	δ^{18}Odol
1041-89	+7.0‰	-3.8‰
1041-88	+0.9‰	-2.8‰
1041-87	+2.0‰	-7.7‰
1041-85	+6.1‰	-5.3‰
1041-84	+1.8‰	-1.6‰
1041-83	+6.9‰	-2.1‰
1041-82	+7.0‰	-5.2‰
1041-81	+7.7‰	-3.4‰
1041-80	+6.2‰	-0.7‰
1041-79	+6.2‰	-2.6‰

Table 7. Carbon and oxygen isotopic compositions of dolomite in Enorama reefs (sample locations are shown schematically in Figure 16).

Petrographically, the pervasive dolomicrite in the reefs appears homogenous with respect to its characteristic red-orange cathodoluminescence signature and thus at least its iron and manganese trace element geochemistry. Small amounts of later-stage dolomite cement have a bright yellow-orange luminescence and commonly coat the walls of vugs. The ubiquitous dolomicrite is most likely responsible for the measured whole-rock dolomite δ^{13}C values of +6 to +7‰ lower in the section.

Disseminated carbonaceous material (almost certainly pyrobitumen) centred on vuggy porosity makes up more than 10% of sample 1041-84 and its diagenetic interaction with carbonate mineral phases may be the cause of the anomalously low δ^{13}C value of +1.8‰ in this sample. There is a minor clastic component, including detrital xenoclastic carbonate, which may also have had a slight effect on the δ^{13}C value.

Whilst less of the characteristic clotted or globular texture is evident in samples from reefs in the upper part of the section, there is an increase in intraclastic material of both xenoclastic and lagoonal mud origin. Coarser-grained clasts, including silica and carbonate with overgrowth cements, inhabit sample 1041-87 as well as discrete flakes of dolomicrite with variable mud contents that are probably of lagoonal derivation (Plate 17). Minor amounts of the previously described vug-lining dolomite cement are present but it is more likely a combination of the aforementioned clastics that causes the relatively low δ^{13}C value of +2‰.

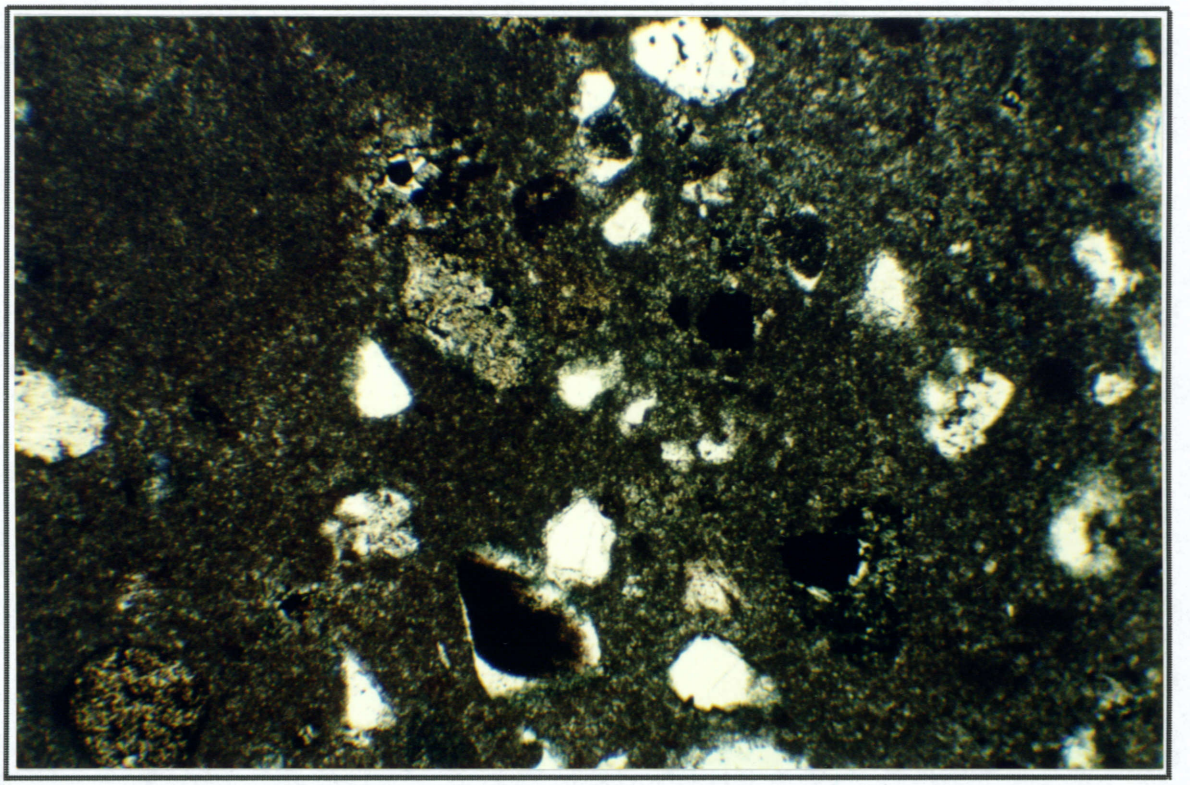

Plate 17A. Clasts in characteristic dolomicrite with varying (colour) mud content. Enorama Shale, Mallee Water, sample 1041-87, δ^{13}Ccal +0.7‰, δ^{18}Ocal –8.6‰, δ^{13}Cdol +2.0‰, δ^{18}Odol –7.7‰, pl.pol., 4X mag.. Field of view is 4.2mm wide.

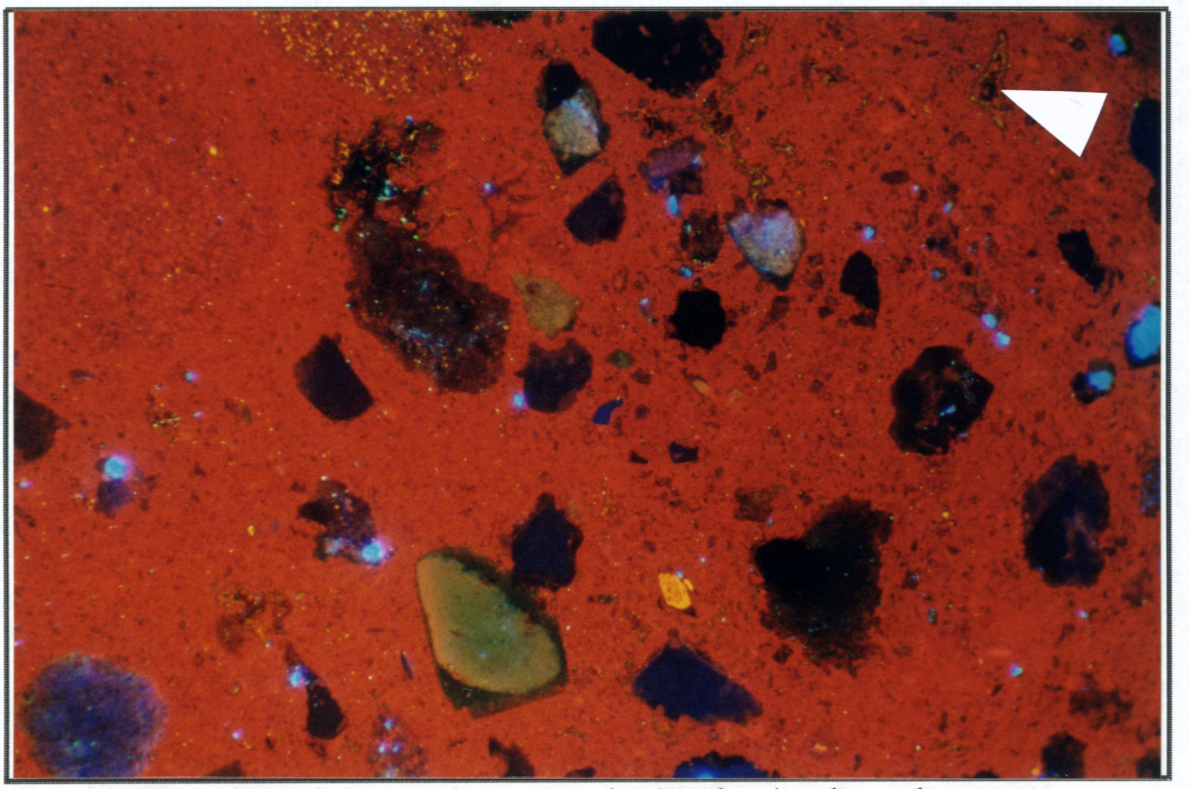

Plate 17B. Same field of view as Plate 17A under CL, showing that carbonate cement phases include epitaxial overgrowth on clasts and pore lining dolomite cement (arrow). 17kV, 190μA, 7.9 sec.

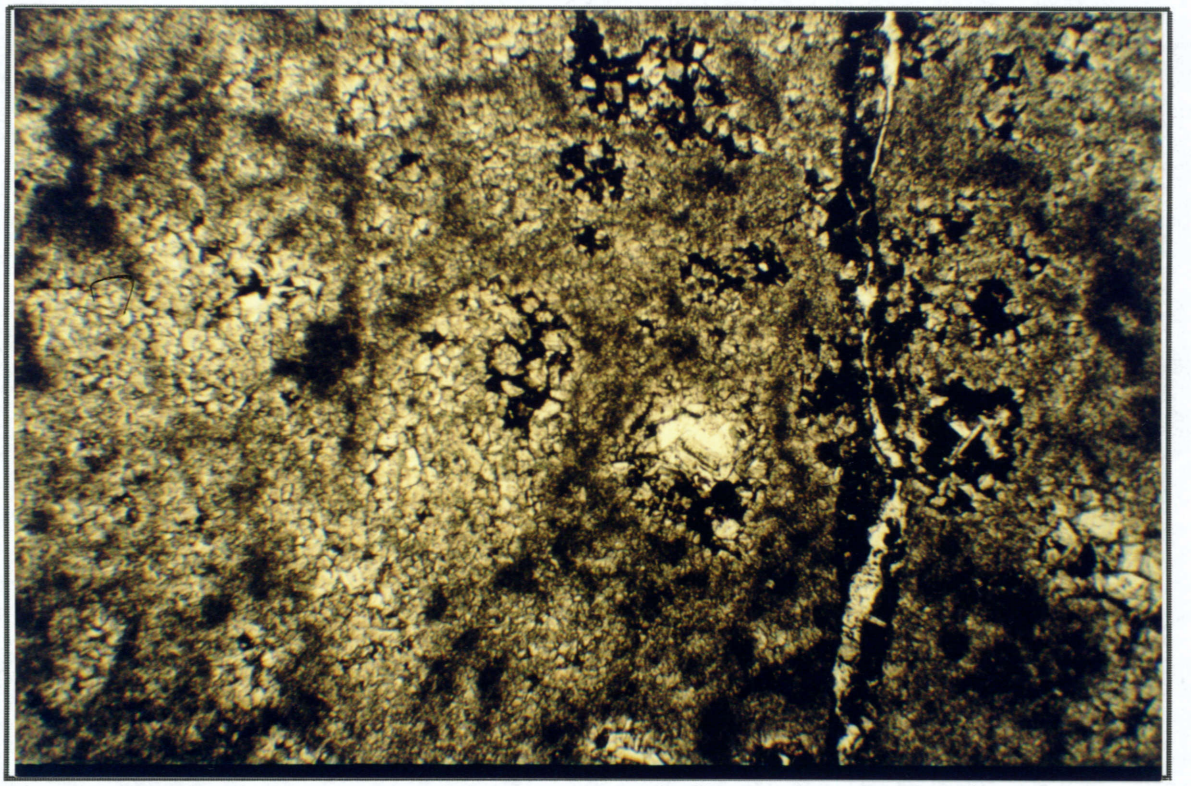

Plate 18A. Dolomicrite to coarse dolomite spar with dispersed mud and carbonaceous material. Enorama Shale, Mallee Water, sample 1041-89, δ^{13}Ccal +6.0‰, δ^{18}Ocal –3.4‰, δ^{13}Cdol +7.0‰, δ^{18}Odol –3.8‰, pl.pol., 4X mag.. Field of view is 4.2mm wide.

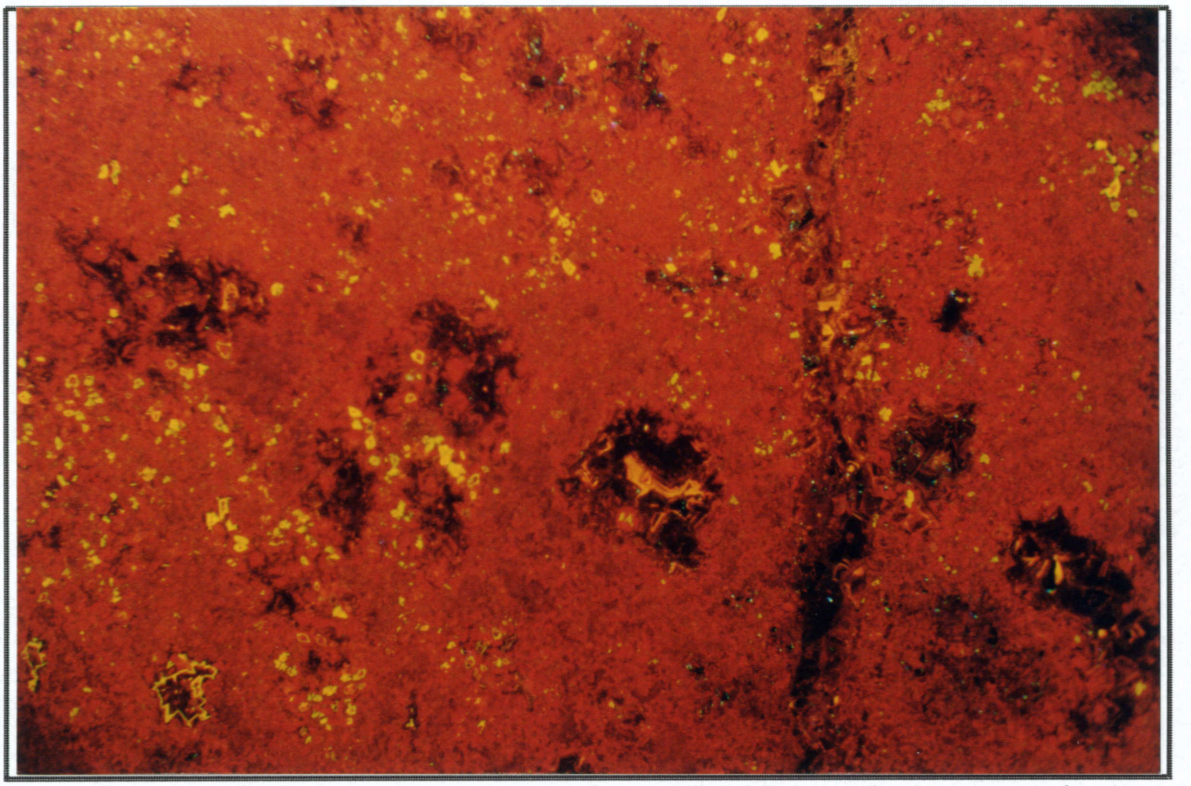

Plate 18B. Same field of view as Plate 18A, showing bright-rimmed microspar and more extensive diagenetic non-luminescent phases. 15kV, 192μA, 12.6 sec.

There is a high proportion of finer grained clastics in sample 1041-88 although they are combined in both the lagoonal and non-lagoonal dolomite muds. In this stratigraphic position, the previously homogenous background dolomicrite now appears to have developed into particulate microspar, irrespective of its lagoonal or other origin. Stylolitic-solution seams with carbonaceous material and authigenic quartz and dolomite phases are developed at a high angle to the fenestral-stromatolitic lamination.

Dolomicrospar has developed into pockets of coarsely-crystalline, idiotopic dolomite indicating greater recrystallization in sample 1041-89 (Plate 18). The brightly-luminescent, pore-lining cement phase observed in other samples is superseded herein by further orange-brown and non-luminescent crystalline phases. Stylolitic-solution seams are again associated with carbonaceous material and authigenic quartz and dolomite. In contrast to the other reef samples which are similarly carbonaceous and crystalline, this sample has a relatively high $\delta^{13}C$ value of +7‰ and is thus isotopically indistinguishable from those lower in the sequence.

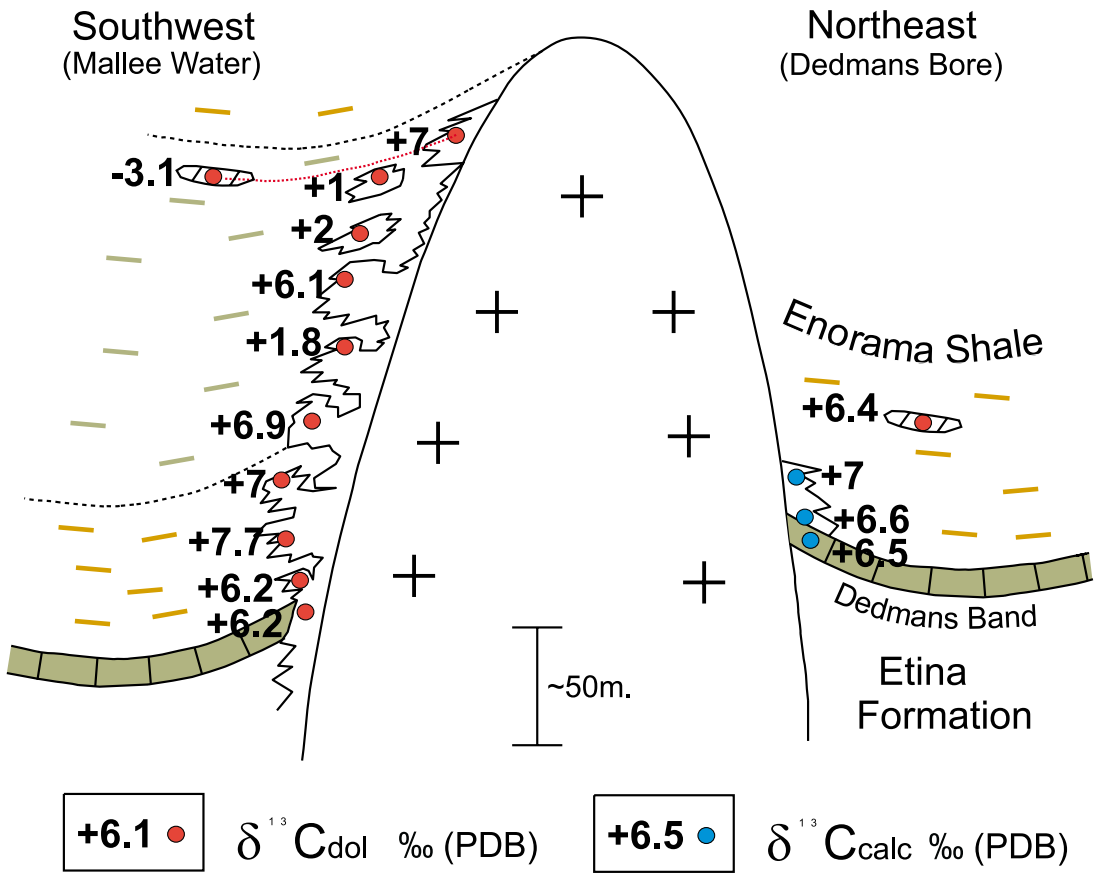

Figure 17. Composite chemostratigraphy of carbonates within the Enorama Shale against the Enorama Diapir.

6.4 Discussion

Despite not having been subjected to dolomitisation, the $\delta^{13}C$ values of the three calcitic Dedmans Band samples on the northeast flank of the diapir compare favourably with those of their dolomitised equivalents on the southwestern margin; and both trend slightly positive over several tens of metres (Figure 17). At and immediately above the Dedmans Band level, the $\delta^{13}C$ of dolomitised sediments to the southwest are several tenths of one permil less than the equivalent limestones to the north, aligning with the observations of dolomite in the Etina Formation (Chapter 5). The $\delta^{18}O$ values of the dolomitised samples at this level are once again less negative than their limestone equivalents.

While the development of fenestral fabric in the reef lithologies indicates some period of exposure, Lemon (1988) postulated that the main mechanisms for dolomitisation were the passage of brines through sediment adjacent the diapir or the supply of directly precipitated dolomite mud from a restricted local setting (see Chapter 3 for discussion of model). The elevated salinity of solutions and sediments surrounding diapirs in the Central Flinders Zone is evident from the microscopic observation of numerous rhombic dolomite euhedra in micrite and in silica overgrowth cements in both the Etina Formation and Enorama Shale. Reconstruction of the exact spatial sedimentological relationships around diapirs is difficult, and there is no obvious reason for the relative lack of dolomitisation of the Dedmans Band on the northern side of the Enorama Diapir.

There appears to be a polarity in the distribution of detritus from the Enorama Diapir, as is also evident around the Blinman Diapir during the time of Etina Formation deposition. This is perhaps an indication of asymmetrical diapir geometries as much as the translation of original sedimentary environments to present-day outcrop through tectonic deformation. Although present in varying amounts, the lagoonal dolomicrite washed into sediment to the north (sample 1041-37) appears to be lithologically analogous to that observed in the southwest (samples 1041-87, -88 and -114). In both instances these layers comprise mud and lagoonal-mud flakes of homogenous dolomicrite to dolomicrospar, with less common xenoclastic carbonate. Their C-isotopic composition varies widely from +6.4‰ on the northeast side (sample 1041-37), to +2‰ and +1‰ immediately adjacent the diapir (samples 1041-87 and -88) and -3.1‰ (sample 1041-114) further away from the diapir on its southwest flank. An overall negative trend up section is evident. This may be due

to the isotopic variation of the dolomite mud precipitated in the lagoon over time.

The involvement of carbonaceous material in lowering carbonate $\delta^{13}C$ values would seem less important since the latter varied widely between samples containing organic matter. It is possible that the interaction of carbonate and organic matter may be highly variable between samples with respect to its influence on carbonate C-isotopic composition.

Although of unspecified lateral extent, the Artipena Dolomite Member appears to persist around the Martins Well Dome but has not been officially recognised away from this area (Dyson, 1997). If palaeogeographic reconstructions of the succeeding regressive Trezona Formation prograding southeastward (Preiss, 1987; Lemon, 1988), are also applicable to the underlying Enorama Shale, then it is possible to assume that the Artipena area was marginally deeper at the time of Enorama Shale high stand than was the area around Blinman to the northwest. This may have provided the outer shelf, sediment-starved environment postulated as necessary for the precipitation of well-laminated dolostones such as those seen above Neoproterozoic glacial horizons (Dyson, 1992; Kennedy and Wallace, 1993). Certainly the C-isotope geochemistries of these dolostones (i.e. sample 1041-114 and the Artipena Dolomite sample analysed by Dyson, 1997) compare favourably and provide further evidence for the correlation of $\delta^{13}C$ with water depth. In the case of the Enorama Shale, a shallower water depth in the vicinity of the Enorama Diapir during the sea level high stand may explain the lateral impersistance of the Artipena Dolomite Member.

It is unclear to what degree the decrease of $\delta^{13}C$ with increasing depth may have affected the dolomites around the Enorama Diapir. It would not be expected to influence the shallow-water facies immediately fringing the diapir but precipitation of dolomite in deeper parts of the basin may have had an effect on the value of deeper water sample 1041-114. If this were the case, a plausible interpretation of the above data might be that the C-isotopic composition of dolomite precipitated in a restricted lagoon atop the diapir was relatively consistent and akin to that of much of the diapir's carbonate constituents (i.e. xenoclasts with low-positive $\delta^{13}C$). This would account for the three reef samples with $\delta^{13}C$ values of +1 to +2 (Figure 17).

The diagenetic history of the samples collected through the Enorama Shale is relatively well constrained and the whole-rock isotopic data are reflective of their respective environments of formation. Even in the

highly positive $\delta^{13}C$ range of the shallow-water stromatolite facies, there is a significant and unequivocal decline from +9‰ to +10‰ in the mid-Etina Formation down to +6‰ to +7‰ into the Enorama Shale. The cause of this negative trend and the overall variation in $\delta^{13}C$ data observed through this interval are not altogether clear. Whilst not directly correlatable, the change in oxidation state of shallow marine waters and the chemical stratification of ocean water evident through sediment colour changes through the Etina Formation-Enorama Shale interval considered to have significant biogeochemical implications.

7. TREZONA FORMATION

7.1 Introduction

The Trezona Formation was first defined by Dalgarno and Johnson (*in* Thomson et al., 1964) through the Trezona Range just southwest of the Enorama Diapir (Figure 7). Referred to in part as "heiroglyphic limestone" by Mawson (1938), it consists of pale red and grey, fine grained, stromatolitic, ooid and intraclast limestones interbedded with greenish grey calcareous shale and siltstone (Preiss, 1987). Attaining thicknesses of up to 400 m in the Central Flinders Zone, the Trezona Formation is the last major limestone sequence in the Umberatana Group.

The shallowing-upward Trezona Formation is a continuation of the overall regression expressed in the upper Enorama Shale. A marginal marine environment of deposition is postulated for this formation since it progrades southeastward and its distribution is restricted by the lowering of base level with the onset of Marinoan glaciation (Preiss 1987; Lemon 1988 and references cited therein). Despite containing obvious exposure surfaces and being interpreted as lagoonal and partly tidal in origin, the Trezona Formation is distinctly lacking in dolomite or evaporitic minerals. Diapirically-derived detritus is restricted to the uppermost parts of the formation (Lemon, 1988).

Yet further restricted in distribution are the tidal muds and sands of the Yaltipena Formation, disconformably overlying the Trezona Formation in the Central Flinders Zone. Another example of paracyclical sedimentation in the Umberatana Group, the Yaltipena Formation is over 100 m thick and comprises a basal red, sandy, ooid-intraclastic limestone, passing upward into calcareous siltstone and ripple laminated sandstone (Lemon and Reid, 1998).

7.2 Previous geochemical investigations

As part of his sedimentological and geochemical study of various Neoproterozoic limestones in the Adelaide Fold Belt, Singh (1986) measured the trace element chemistry (via microprobe analysis) and strontium, carbon and oxygen isotopic analyses of the Trezona Formation. Trace element analysis of more than 40 samples (including separately sub-sampled mineral phases) collected from the Trezona Range west of the Enorama Diapir, found that all but two had

concentrations of Sr in excess of 200 ppm and only 37% of the samples analysed had Mn/Sr ratios of 1.0 or greater. Stable C and O-isotope analyses of 39 samples yielded values that vary widely from -2.3 to -8.4‰ for $\delta^{13}C$ and from -6.0 to -13.9‰ for $\delta^{18}O$. Vein calcite was the only exception ($\delta^{13}C$ = +2.4‰ and $\delta^{18}O$ = -17.0‰). Strontium isotope determinations returned $^{87}Sr/^{86}Sr$ ratios ranging from 0.7072 to 0.7080 for micrites, and up to 0.7105 in fenestral cement.

7.3 Doodney's Well Hills section

Samples were collected along Lemon's (1988) reference section #30 in the Central Flinders Zone to the east of the Enorama Diapir (Figure 7). This location is away from the faulted Trezona Range to the west and in an area where there is a distinct lack of diapiric influence on sedimentation. Sampling through this section focussed on micritic stromatolite limestones and closely-interbedded ooid limestones in order to gauge their relative degrees of diagenetic alteration.

The Trezona Formation begins at this locality with two distinct bands of cyanobacterial-flake intraclast limestone (9 m and 2 m thick, respectively) separated by approximately 6 m of calcareous siltstone. A clean, dark red, domal-stromatolitic limestone in the lower band (sample 1041-90) records whole-rock $\delta^{13}C$ and $\delta^{18}O$ values for calcite of -8.2‰ and -13.1‰, respectively.

These two limestone bands are overlain by a 35 m-thick succession of green to brown-red, calcareous siltstone and interbedded fine sands with ripple marks. This is in turn overlain by what Lemon (1988) called a "dramatic deposit of intraclast granule conglomerate" or "intraclast complex". Over the next 100 m, cyanobacterial-flake limestones (similar to the lowermost two bands except that its flakes are smaller and have micritic envelopes suggestive of transport) are interbedded with stromatolitic limestones and red, fine sandy siltstones with characteristic ladder ripples. The cyanobacterial-flake intraclast limestones take the form of channel and spillover lobe deposits and have a characteristically lensoid outcrop pattern amongst recessively weathered siltstones (Lemon, 1988). Through the intraclast complex, stromatolitic and minor intraclastic limestones at 111 m (sample 1041-91), 130 m (-92), 154 m (-93), 172 m (-94) and 211 m (-95) record $\delta^{13}C$ values of -8.5, -8.6, -8.4, -9.0, and -9.5‰, respectively.

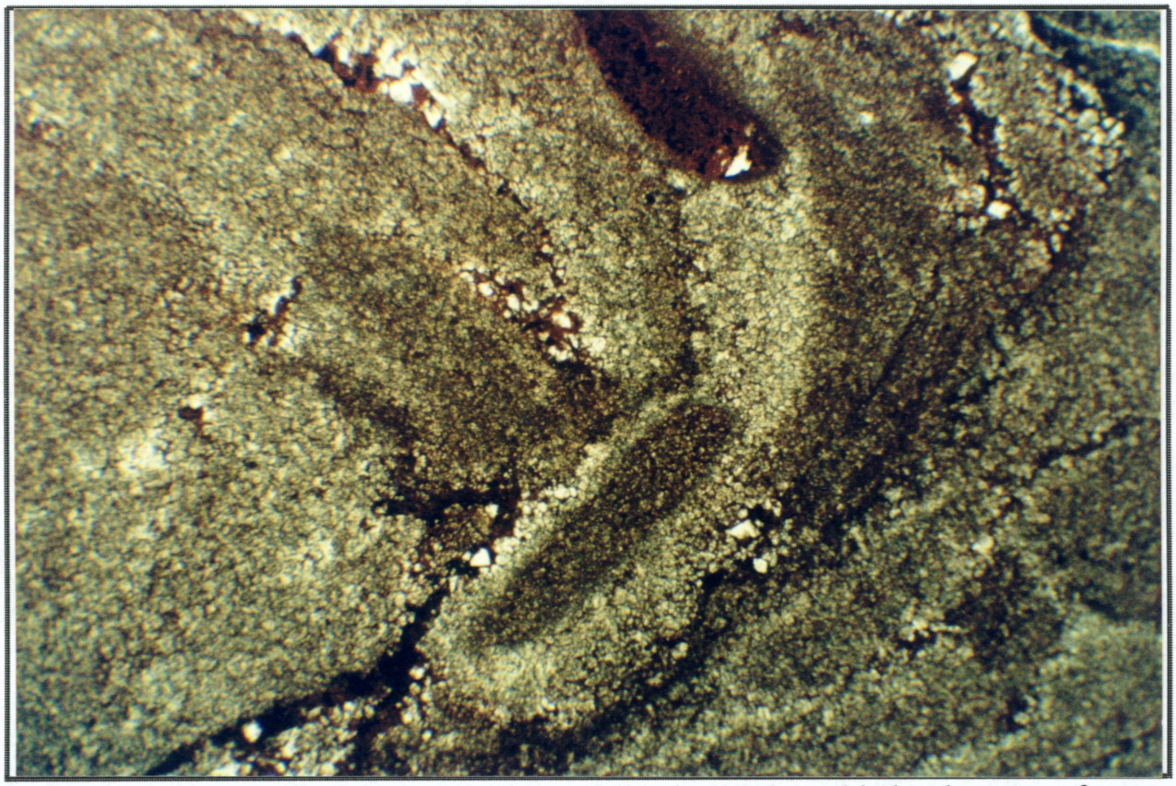

Plate 19A. Micritic intraclasts parallel stromatolitic lamination with development of interstitial spar. Sample 1041-93, Trezona Formation, Doodneys Well Hills, 134 m, δ^{13}Ccal -8.4‰, δ^{18}Ocal –12.2‰, pl.pol., 4X mag.. Field of view is 4.2mm wide.

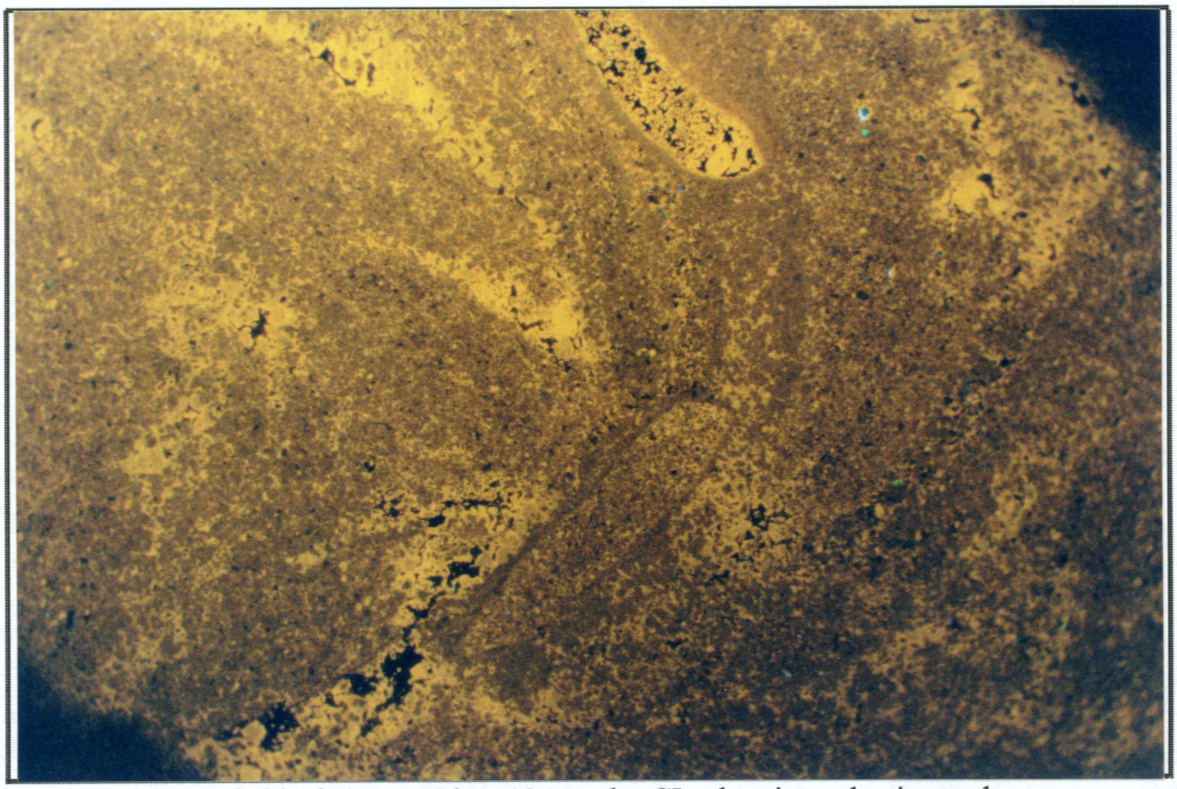

Plate 19B. Same field of view as Plate 19A under CL, showing selective early dissolution of intraclasts replaced by the same cement as interparticle cement phases. 15kV, 178μA, 7.6 sec.

Petrographic investigation of sample 1041-93 reveals the development of early-interstitial, blocky-calcite-spar cements in interparticle porosity (Plate 19). The dominant original micrite is generally retained with very minor recrystallisation to microspar on particle edges. Selective dissolution of intraclasts results in moulds filled with blocky microspar of the same interparticle composition, confirming the very early and relatively shallow burial diagenetic origin for the cements.

In sample 1041-95, characteristic cyanobacterial-stromatolitic lamination has developed into stylo-solution seams comprising drusy ferroan calcite and carbonaceous material. Areas of cleaner micrite have undergone slight recrystallisation to microspar, and blocky interstitial cements (such as those seen in sample 1041-93) are uncommon closing out remaining porosity. This sample also contains sets of thin (0.05 mm), parallel, calcite veinlets oblique to the bedding lamination.

An influx of red sandy silt, 30 m thick, separates the intraclast complex from an overlying 60 m-thick sequence of ooilitic limestone with occasional grey-green and khaki stromatolite interbeds. In close proximity, dark red stromatolitic (sample 1041-96) and buff-red ooid (sample 1041-97) limestones record $\delta^{13}C$ values of -7.9 and -7.6‰ at heights of 235 m and 237 m, respectively, in the section. Above this, at 253 and 255 m, blue-green stomatolite (sample 1041-98) and buff pink oolite (sample 1041-99) both have calcite $\delta^{13}C$ values of -9.4‰.

The aforementioned blue-green stromatolitic limestone (sample 1041-98) comprises homogenous and pervasive micritic calcite. Apart from minor development of thin calcite cements in carbonaceous stylo-solution seams, this sample contains no other cements of diagenetic origin (Plate 20). However it does contain a small proportion of fine sand that includes bright yellow and red-orange-luminescent detrital carbonate.

In contrast to the underlying stromatolitic limestone, the buff-pink oolitic limestone (sample 1041-99) demonstrates the typical range of diagenetic cements observed in the Trezona oolite facies. Development of blocky interstitial calcite cements predates the recrystallisation of micritic ooids and peloids from the inside out, as defined by relic micritic envelopes (Plate 21). Early dissolution has facilitated the crushing of ooids, developing thin zones of elephantine fabrics dominated by early-diagenetic blocky cements (Singh, 1987). Such early dissolution, fabric development and high Sr content may be indicative of aragonite being the primary precipitate in the Trezona Formation. Crushed ooids undergo the same selective recrystallisation as do uncrushed ooids.

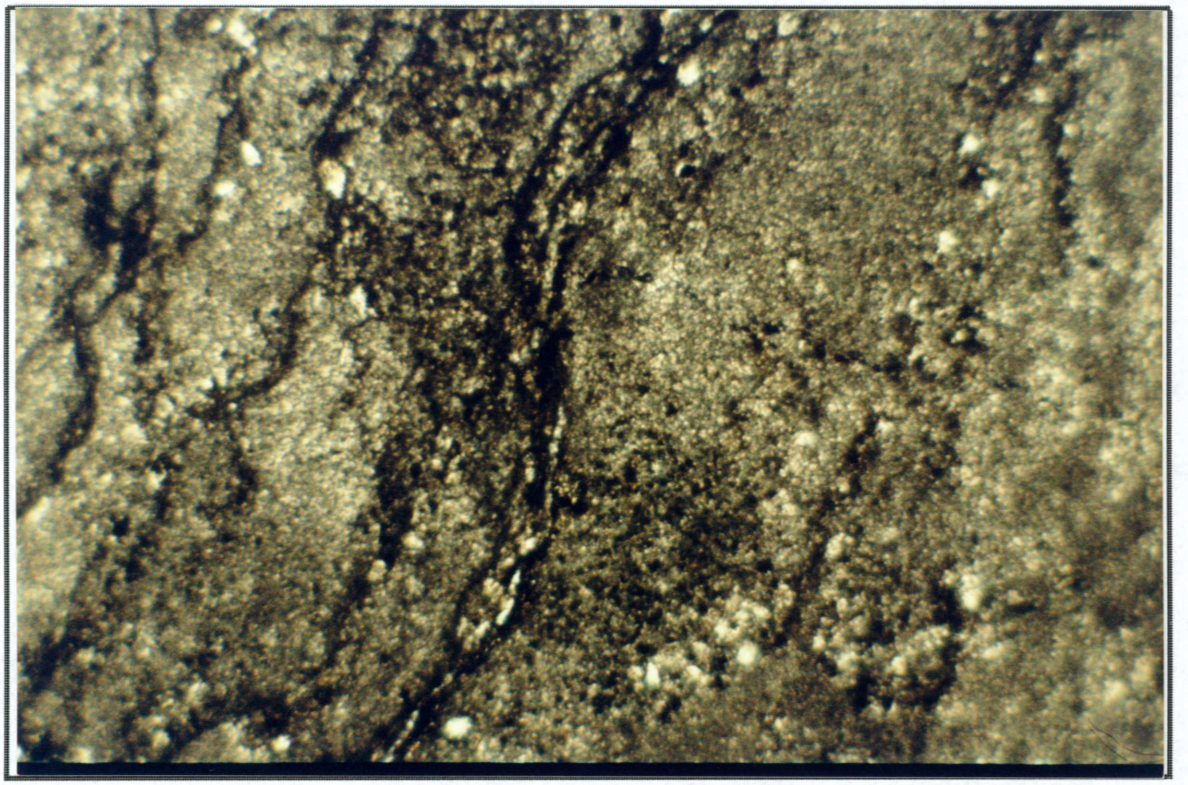

Plate 20A. Development of carbonaceous solution seams along stromatolitic bedding lamination. Sample 1041-98, Trezona Formation, Doodney's Well Hills, 253 m, δ^{13}Ccal -7.4‰, δ^{18}Ocal –9.3‰, pl.pol., 10X mag.. Field of view is 2.3mm wide.

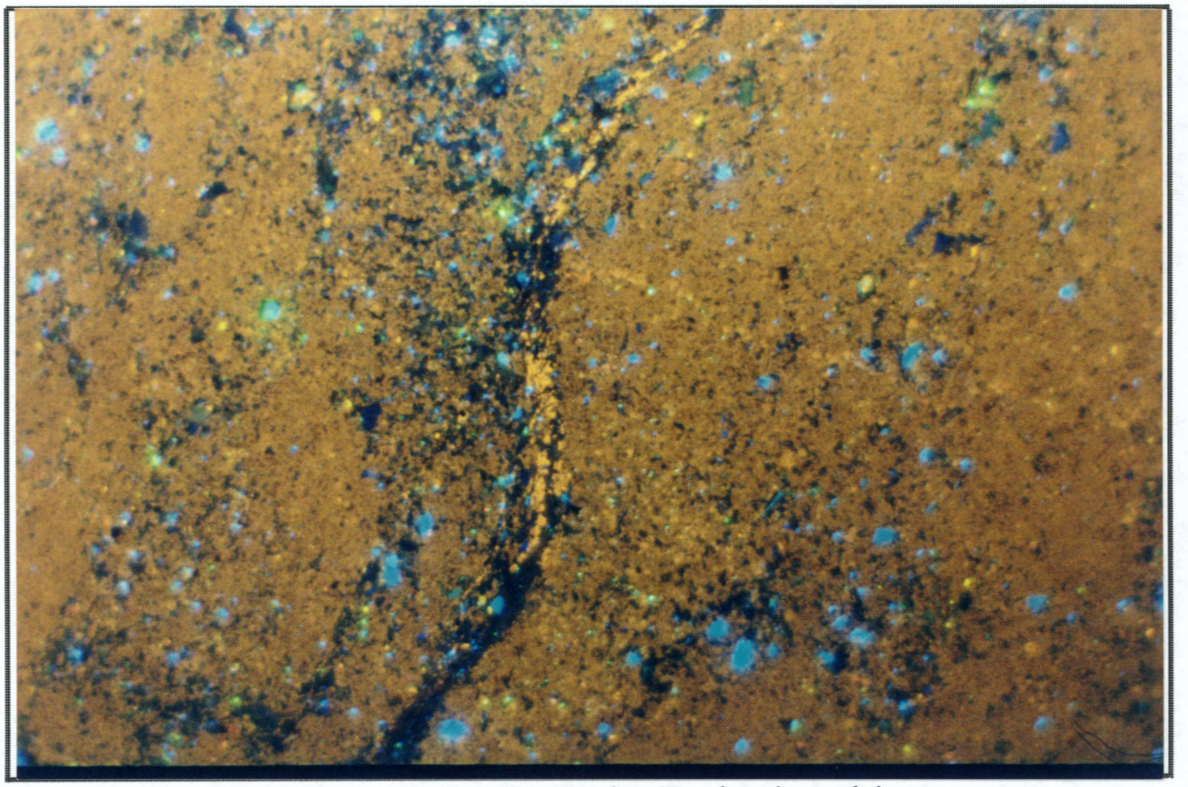

Plate 20B. Same field of view as Plate 20A under CL, showing calcite cement developed in the solution seam. The homogeneous micrite includes very fine, detrital carbonate. 15kV, 200μA, 26.9 sec.

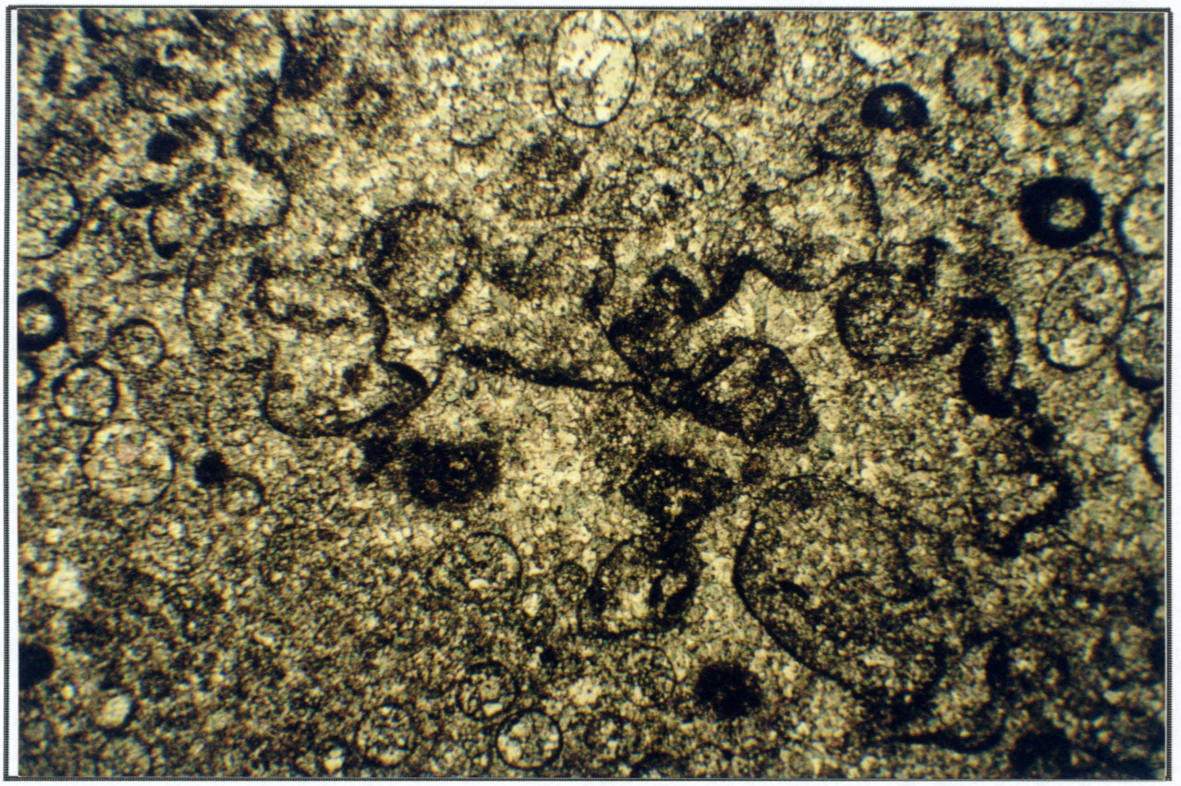

Plate 21A. The crushing of ooid fabric is facilitated by early dissolution. Sample 1041-99, Trezona Formation, Doodney's Well Hills, 255 m, δ^{13}Ccal -7.4‰, δ^{18}Ocal –8.2‰, cross pol., 10X mag.. Field of view is 2.3mm wide.

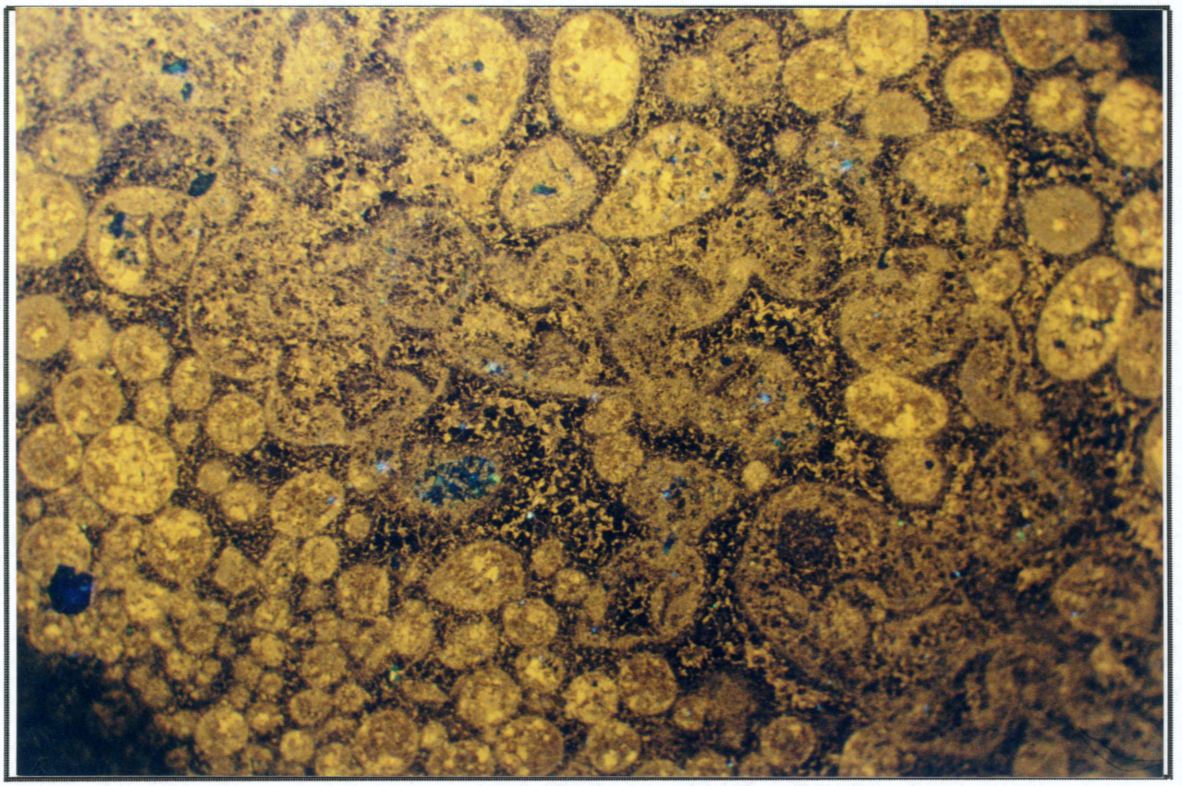

Plate 21B. Same view as Plate 21A, showing predominance of darkly-luminescing cements in areas of early dissolution. These ooids also show the same part-recrystallisation evident elsewhere. 15kV, 205µA, 41.8 sec.

Reworked intraclasts of the aforementioned recrystallised oolite indicate that the cements are the result of very early diagenesis under marine phreatic conditions. Latest stage interparticle cements and minor authigenic growth of silica minerals are indicative of further burial diagenesis.

Stromatolite occurrence increases towards the top of the ooid shoal deposits where blue-grey, stromatolitic limestone at 287 m height in the section has a calcite $\delta^{13}C$ of -6.5‰. The ooids are eventually overlain by a 50 m thick succession of brown-red stromatolites thought to be deposited in a back-barrier bar, near-shore lagoon setting (Lemon, 1988). At 315 m (sample 1041-102), dark red, stromatolitic limestone has a $\delta^{13}C$ of -5.5‰. Petrographically, this sample is dominated by micrite with minor development of microsparry calcite in zones that are relatively mud free. Carbonaceous stylolites are developed but lack any calcite cement. Rare calcite veinlets cross-cut bedding lamination at a low angle. At 332 m height in the section, dark red domal stromatolitic limestone (sample 1041-103) records a $\delta^{13}C$ of -3.8‰.

The preceding stromatolite interval is in turn overlain by 40 m of higher-energy intraclastic and oolitic limestones that are interbedded with brown-red stromatolites, before flat-pebble conglomerates above an erosive disconformity mark the beginning of the Yaltipena Formation. Blue-grey oolitic grainstone at 355 m (sample 1041-104) records $\delta^{13}C$ of -3.2‰. Petrographic investigation of this sample reveals a particularly complete, early interstitial, equant blocky calcite spar cement, with some ooids recrystallised to brightly luminescent blocky calcite spar (Plate 22). Recrystallisation is best developed along bedding planes, but can also be seen branching out dendritically leaving characteristic thin, remnant micritic envelopes. Thin zones of ruptured ooids are once again evident, predating recrystallisation. Rare, thin veinlets of brightly-luminescent calcite are also present, cross-cutting bedding lamination at a high angle.

A 3 m-thick band of light grey, medium-sandy, cross-bedded ooids sharply overlies stromatolitic limestone at 374 m in the section. It has a calcite $\delta^{13}C$ of -2.9‰ whereas calcite in the directly-overlying dark red stromatolitic limestone measures -3.5‰. Four metres of such stromatolites separates the ooid band from a slightly thicker ooid band that coarsens up over 6 m into the flat pebble conglomerates at the base of the Yaltipena Formation. The conglomerates are interbedded with buff coloured intraclastic, ooid limestone in which calcite has a $\delta^{13}C$ of -4.2‰ .

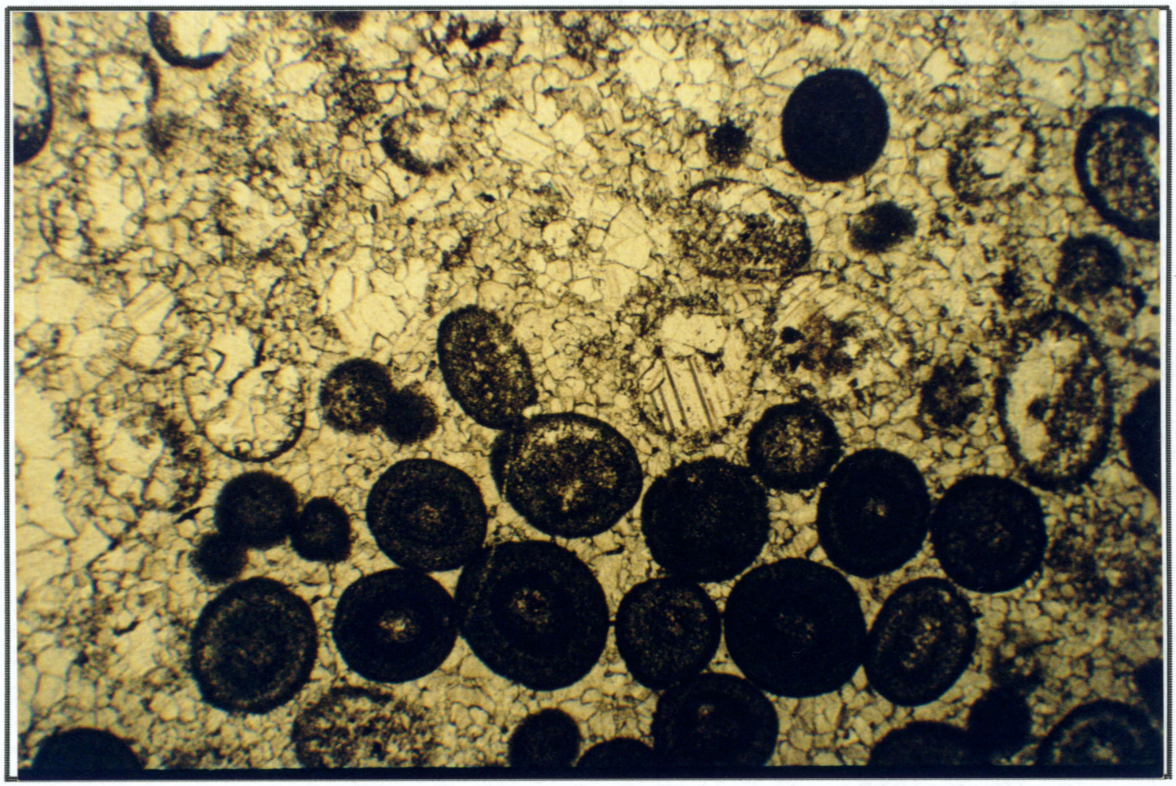

Plate 22A. Ooids recrystallise to blocky calcite spar with remnant micritic rims. Sample 1041-104, Trezona Formation, Doodney's Well Hills, 355 m, δ^{13}Ccal –3.2‰, δ^{18}Ocal –9.5‰, pl.pol., 4X mag.. Field of view is 4.2mm wide.

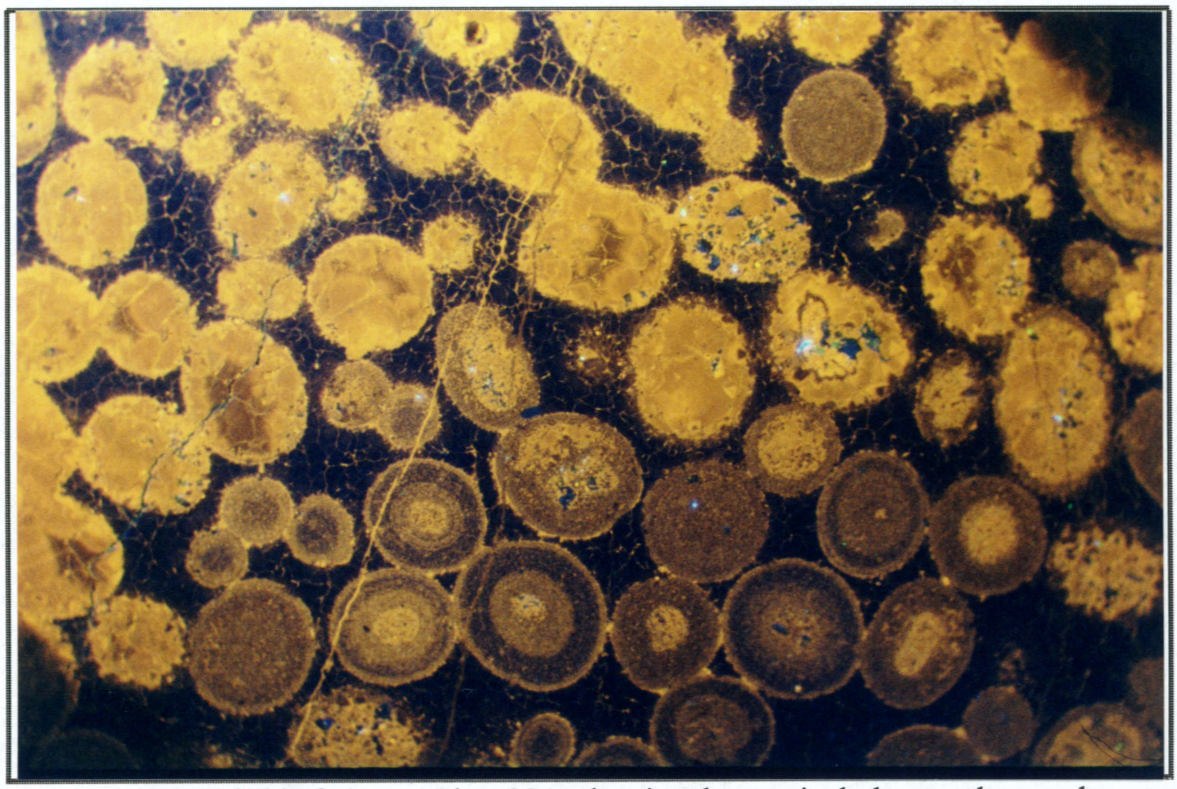

Plate 22B. Same field of view as Plate 22A, showing that particularly complete, early, darkly-luminescent interstitial cement predates brighter vein and ooid-replacing forms. 16kV, 210μA, 56.1 sec.

7.3.1 Discussion

The C-isotopic compositions of limestones in the Trezona Formation are particularly negative varying from –2.9‰ to –9.5‰ although the overall spread of 6.6‰ is somewhat less than the 8.3‰ variation evident in the primary calcite data of the shallow-water Etina Formation (Figure 18).

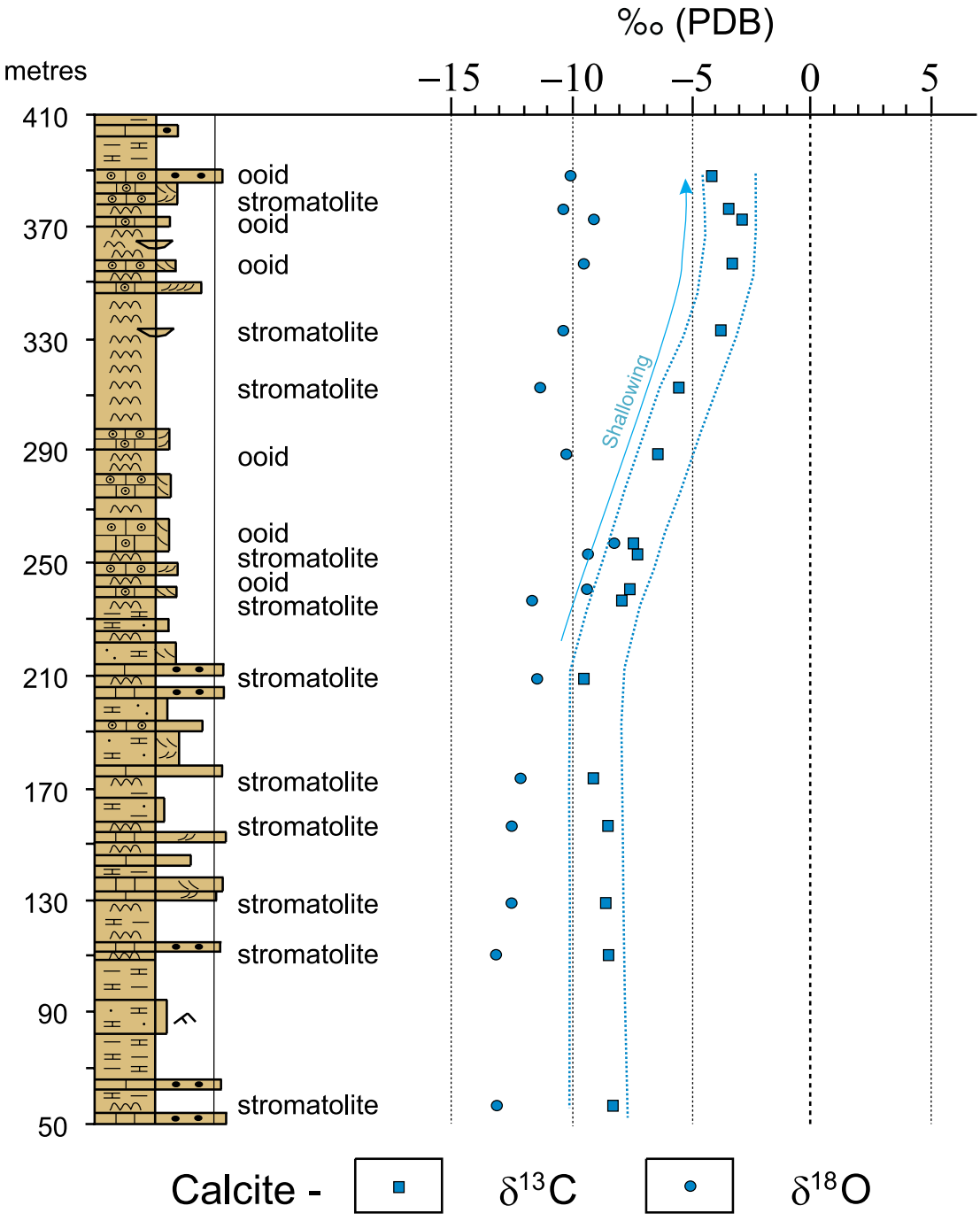

Figure 18. Chemostratigraphy of the Trezona Formation in the Doodney's Well Hills section.

The calcite $\delta^{18}O$ values range from –8.2 to –13.1‰ in the Trezona Formation, within the range of calcite $\delta^{18}O$ from the Etina Formation (viz. –6.7 to –14.1‰). This variation in whole-rock data from the eastern Central Flinders Zone compares similarly with micro-sampled and whole-rock data measured by Singh (1986) along the Trezona Range. Without a stratigraphic framework for Singh's samples, it is difficult to further compare with his dataset with that summarised in Figure 18. In terms of data variation with stratigraphic height, at 400 m thick, the Trezona Formation compares very favourably with the paracyclical isotopic variability (i.e. variation with water depth) of the Etina Formation (Figure 15).

The development of diagenetic cements in the Trezona Formation is restricted to ooid and intraclastic limestones. The former are isotopically indistinguishable from contiguous stromatolitic limestones (e.g. samples 1041-99, heavily cemented, and 1041-98, uncemented); and the latter do not contribute to the isotopic profile shown in Figure 18. Moreover, with the variation in whole-rock isotopic data from the eastern Central Flinders Zone comparing favourably with the micro-sample and whole-rock data obtained by Singh (1986) along the Trezona Range to the west of the Enorama Diapir, it would be unreasonable to expect any formation-wide alteration mechanism to displace $\delta^{13}C$ to more negative values while $\delta^{18}O$ remained relatively constant over such a wide area. Hence, one may conclude that diagenetic overprint has not significantly affected these data and that they are probably reflective of their respective waters of formation.

7.4 Palaeokarst surfaces

7.4.1 Mid-Trezona palaeokarst, Bulls Gap section

In his section 10 through Bulls Gap west of the Enorama Diapir (Figure 7), Lemon (1988) noted a mid-Trezona ooid shoal facies filling solution cavities of a karst surface. Extensive recrystallisation and iron and manganese enrichment occur 2-20 m below this irregular surface whilst red and grey pisoids, larger than those seen elsewhere, are deposited above it. Lemon (op. cit.) traced the karst surface south along strike for 6 km and postulated diapir uplift for its creation and local extent. This hypothesis is supported by the first incoming of diapiric detritus to the Trezona Formation in association with the pisoid limestone.

Plate 23A. View looking down section across the mid-Trezona karst surface at Bulls Gap. A clear change from dark red, karstic rocks to overlying light grey oolite is observable in the foreground (the change is also visible in vegetation).

Plate 23B. Sample from 3 m below karst surface at Bulls Gap, showing pyrolusite developed in fenestral vugs. δ^{13}Ccal –9.4‰, δ^{18}Ocal –5.8‰.

The physical appearance of the rocks is dramatically different in the first 3-4 m below this surface (Plate 23A). Their different mineralogy is also manifest in the local vegetation. Green shrubbery is developed below the karst in iron rich clays resulting from breakdown of the host lithology. Inspection of the hand specimen of sample 1041-118 from 3 m below the surface, shows the development of black pyrolusite and other, iron and manganese-rich minerals in fenestral porosity (Plate 23B). Petrographic inspection of the rock at the karst surface (sample 1041-120) reveals coarse, blocky, calcite spar, brecciated in part; development of solution seams filled with coarse sparite and veins and dendritic staining centred on fenestral vugs. The rock is too altered to detect any gravity-related diagenetic features typical of many other karsts.

Where present, dolomite comprises up to 80% of some samples in this section. Petrographic inspection of sample 1041-117, 5 m below the karst surface, reveals a coarse mosaic of idiotopic dolomite crystals. Calcite is largely dendritic and centred on dissolution seams and fenestral vugs (Plate 24). Although the presence of dolomite in this section is almost certainly related to the exposure surface, its abundance and coarsely crystalline nature is curious. Moreover its $\delta^{18}O$ values are distinctly more negative than most other Umberatana Group dolomites (Figure 19). The only other such $\delta^{18}O$-depleted dolomite occurs low in the Etina Formation at First Spring (sample 1041-39; $\delta^{18}O$ = -15.2‰). This mid-Trezona dolomite does, however, have $\delta^{13}C$ values close to those of the coexisting calcite indicating a genetic relation.

The $\delta^{13}C$ of both calcite and dolomite consistently hover around -4‰, above and below the mid-Trezona karst surface. In the most altered samples in the section, at and just below the exposure surface, an inversion of the calcite $\delta^{13}C$ and $\delta^{18}O$ profiles is observed. The trend in $\delta^{18}O$ is particularly pertinent, values trending positive from -13‰ to -6‰ approaching the karst surface. This trend is mirrored by $\delta^{13}C$, trending negative from -3.8‰ to -5.4‰ then jumping to -9‰ in more altered samples. The calcitisation reaction facilitated by influx of meteoric fluids, which is expected to decrease with depth, is inferred to cause this gradual shift in C and O-isotopic composition. This effect will be partly selective as tongues of meteoric alteration penetrate down from the exposure surface, causing some rocks nearer the karst surface to remain relatively unaltered, as is depicted in Figure 19.

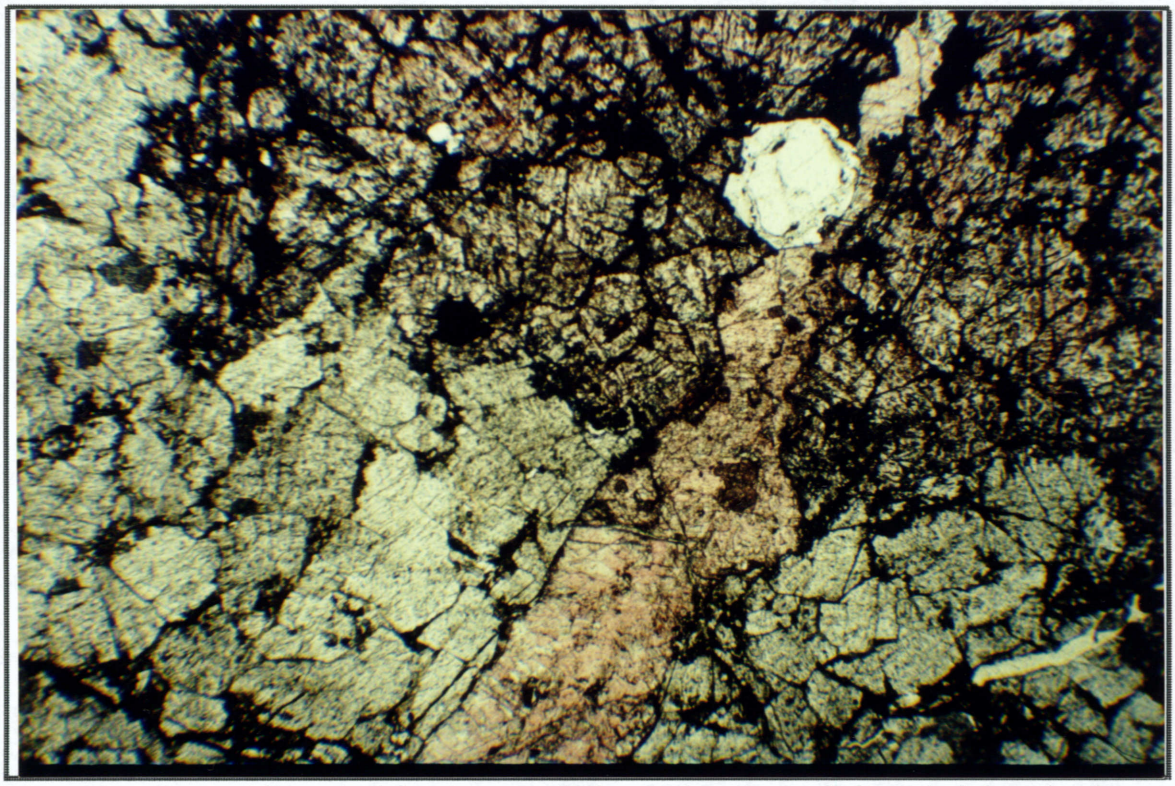

Plate 24A. Coarse idiotopic dolomite spar (lighter colour-lower left) and pink-stained blocky calcite. Sample 1041-117, Trezona Formation, Bulls Gap section, -5 m, δ^{13}Ccal -5.4‰, δ^{18}Ocal -7.0‰, δ^{13}Cdol -4.0‰, δ^{18}Odol –16.4‰, pl.pol., 4X mag.. Field of view is 4.2mm wide.

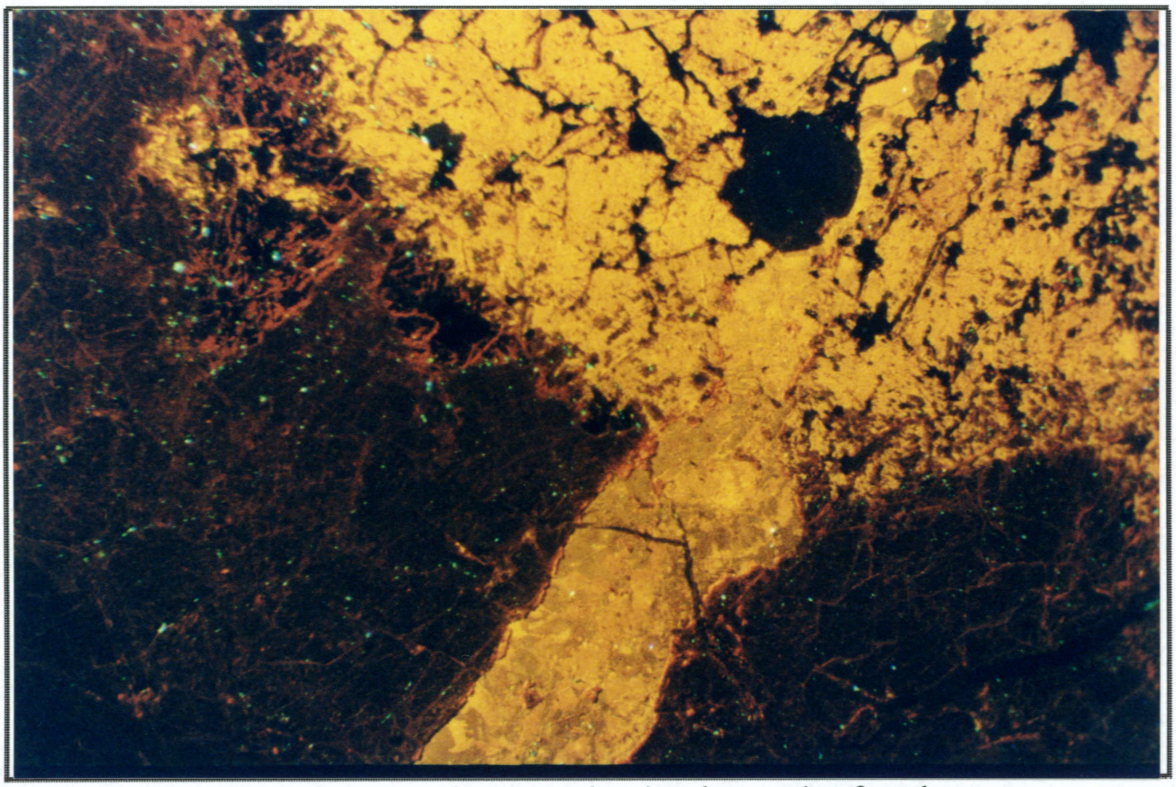

Plate 24B. Same field of view as Plate 24A, showing the reaction front between brightly luminescent calcite and dark dolomite, green speckling is diamond slide-polishing paste. 15kV, 195μA, 5.8 sec.

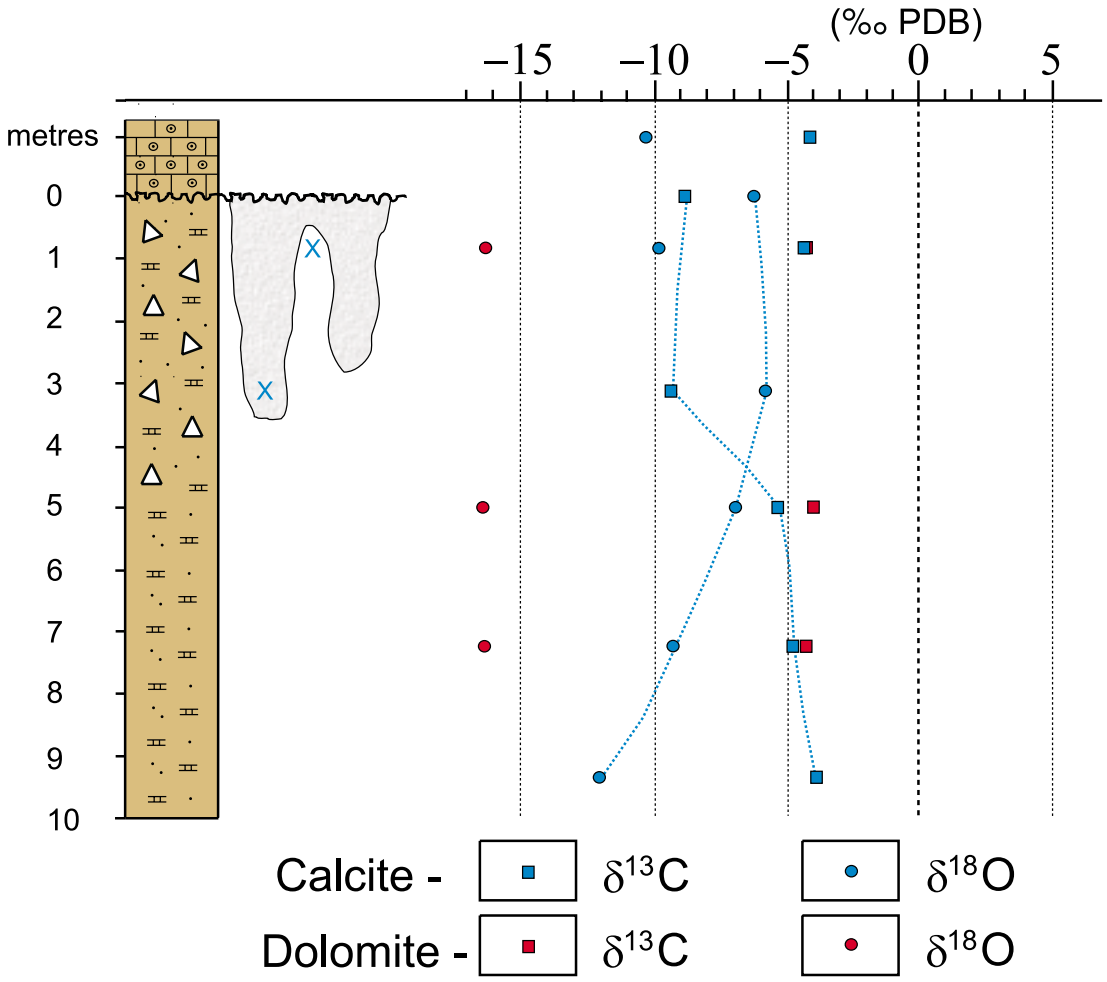

Figure 19. Chemostratigraphy surrounding mid-Trezona karst surface at Bulls Gap.

The apparently unaltered $\delta^{13}C$ and $\delta^{18}O$ values surrounding the Bulls Gap karst (-4‰ and -10‰, respectively) are almost coincident with rocks at equivalent stratigraphic height in the Doodney's Well Hills section (i.e. above 355 m: Figure 18).

7.4.2 Top-Trezona palaeokarst, Brachina Road section

The Trezona Formation is eroded and unconformably overlain by glacial deposits of the Elatina Formation. At the southern end of the Trezona Range near the Brachina Gorge road, southwest of the Enorama Diapir (Figure 7), a thin karst surface denoted by iron and manganese enrichment, is developed along the top of the Trezona Formation. The karst material itself is a brecciated pyrolusite after calcite and is commonly loosely consolidated due to further weathering (Plate 25). This visible iron and manganese enrichment is difficult to trace along strike, but it does not, in any position, extend more than 20 cm into the

Plate 25A. Looking back down section from top-Trezona palaeokarst indicated by black, iron and manganese enriched karstic lithology (arrow).

Plate 25B. Loosely consolidated pyrolusite and calcite of weathered karst lithology, Trezona Formation, Brachina Road section, δ^{13}Ccal -5.7‰, δ^{18}Ocal –1.8‰.

rocks below. The Yaltipena Member, which is preserved above the Trezona Formation elsewhere, has been completely eroded at this location. It is likely that the Trezona carbonates were well cemented before erosion took place, thus restricting alteration to the contact only.

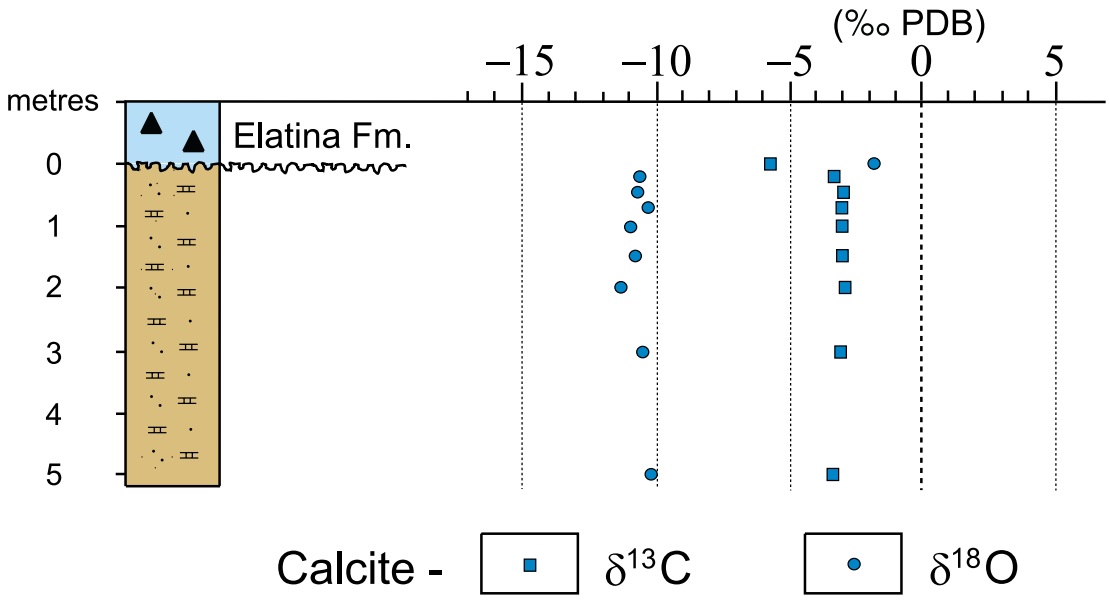

Figure 20. Chemostratigraphy surrounding top-Trezona karst surface.

The rocks immediately beneath the karst surface are typical upper-Trezona dark red, fine sandy and intraclastic limestones. Whole-rock calcite $\delta^{13}C$ and $\delta^{18}O$ values are consistent approaching the erosion surface (Figure 20). Within 50 cm of the karstic lithology, $\delta^{13}C$ trends negatively from previously uniform values of -3.0‰, through -4.3‰ at 20 cm to -5.7‰ in the karst material itself (sample 1041-129). The stable isotopes once again mirror each other in relation to the alteration as $\delta^{18}O$ increases from a consistent -10 to-11‰ below the karst surface to -1.8‰ at the surface.

The apparently unaltered $\delta^{13}C$ and $\delta^{18}O$ values below the Brachina Road karst (-3 to -4‰ and -10 to -11‰, respectively) are once again almost exactly coincident with rocks at equivalent stratigraphic height in the Doodney's Well Hills section (i.e. 380 - 390 m: Figure 18).

7.5 Trezona clast in Elatina Formation

The Marinoan glacial diamictite, the Elatina Formation, commonly includes clasts of the underlying Trezona Formation. In order to quantify any isotopic resetting effect glacial water may have had on such material, a clast of Trezona limestone was drilled from an Elatina Formation conglomerate (sample 1041-136) collected 20 m above the unconformity surface in the Brachina Gorge Road area.

The clast recorded calcite $\delta^{13}C$ and $\delta^{18}O$ values of -5.5‰ and -12.9‰, respectively. Both the separation and absolute values compare favourably with data acquired from the mid to upper Trezona Formation elsewhere, indicating no detectable influence of seasonal meltwater or the glacial ocean on its stable isotopic composition.

7.6 Discussion

The Trezona Formation appears to have undergone slightly more intense diagenetic alteration than was observed for carbonates of the Etina Formation lower in the sequence. Although erosive disconformity surfaces are observed in both formations, the Etina Formation was deposited in a less restricted marine setting and is not terminated by extensive basin-wide erosion. With the help of major and trace element chemistry, Singh (1986) was able to conclude that the ooid fabrics and cements, observed within the Trezona Formation, were neomorphic or the result of burial diagenesis under marine phreatic conditions. There is notable continuity in whole-rock isotopic data (away from erosive disconformity surfaces) between widely separated sections throughout the Central Flinders Zone. Furthermore, the Trezona Formation displays no difference between the $\delta^{13}C$ of inorganically-precipitated and microbially-trapped calcite, in ooids and stromatolites, respectively.

The exposure and erosion of Trezona Formation prior to and during the Marinoan Glaciation had the potential to impose a diagenetic overprint on its C and O-isotopic compositions. However, comparison of the isotopic signatures of a tillitic clast and the substrate beneath an exposure surface at the top of the Trezona Formation rules out any significant alteration of rocks in direct contact with glacial waters. Careful study of rocks immediately beneath exposure surfaces in the Trezona Formation, confirms the selected influence of meteoric fluids on their isotopic composition. Due to the observed iron and manganese enrichment at these karst surfaces, it is safely assumed that these

sediments were less consolidated and or lithified at mid-Trezona time, thereby allowing greater penetration by of meteoric fluids.

The possibility of a pervasive post-burial alteration process confined to the lower Trezona Formation, as suggested by Christie-Blick et al. (1999), is remote. It is possible that aragonite may have been the primary precipitate of the Trezona Formation (and calcite the primary precipitate of the Etina Formation), facilitating diagenetic alteration. However, consistent absolute isotope values and the same pattern of stratigraphic variation in the upper half of the Trezona Formation across the Central Flinders region argue against the possibility of this process having any more than a localised and minimal effect on data. This process may possibly explain the convergence of $\delta^{18}O$ with $\delta^{13}C$ values at 200 to 260 m height in the Doodney's Well Hills section (Figure 18) where such alteration is observed. But at least elsewhere in the section, the trend and separation of absolute isotope values never depart appreciably from what is logical and internally consistent. The $\delta^{13}C$ data summarised in Figure 18 are therefore considered to be primary and reflective of the ocean water chemistry of the time.

The whole of the Trezona Formation has never been interpreted to represent a totally restricted depositional setting. The positive trend in $\delta^{13}C$ in the upper half of the Doodney's Well Hills section (Figure 18) coincides with a regression and demonstrates the same relationship of C-isotopic composition with water depth as seen in the Etina Formation (Figure 15).

8. SECULAR C-ISOTOPIC VARIATION AND ITS BIOGEOCHEMICAL IMPLICATIONS

The isotopic data acquired in this study, when integrated with the lithostratigraphy of the Umberatana Group, yield what is arguably one of the most complete records of secular variation in the C-isotopic signature of the Late Cryogenian ocean between ~750 Ma and ~680 Ma. Five discrete segments of its composite curve (Figure 21) provide tie points for correlation with successions of comparable age in other basins. In order of decreasing age these segments are: 1) Sturtian glacial dolomicrite values between -5 and +2‰ (Wilerpa Formation); 2) a rapid initial drop from -2 to -5‰ before a sharp rise to +1.5‰ through a 'cap' dolomitic shale (Tindelpina Shale); 3) a steadily climbing trend from +1 to +4‰ through a shoaling-upward sequence of dolomitic and calcareous shale (Tapley Hill Formation) and stromatolitic, ooid and intraclastic carbonates (Brighton Limestone); 4) a further increase through similar shallow-water carbonates to a plateau of +8 to +10‰ (Etina Formation), declining to +6 to +7‰ in the stromatolite reef facies of the overlying Enorama Shale; and 5) a dramatic drop to -8 to -9.5‰, followed by a recovery to -3‰, in the youngest carbonate unit (Trezona Formation) beneath the Marinoan glacial diamictites (Elatina Formation).

This investigation of formation-scale, isotope chemostratigraphy through the Umberatana Group has revealed a definite, relationship between palaeowater-depth and $\delta^{13}C$ and, to a lesser extent $\delta^{18}O$, in Late Cryogenian marine carbonate. This relationship is not lithology specific, as illustrated by the interbedded stromatolitic and oolitic limestones of the Trezona Formation , nor is it an artefact of diagenetic or other alteration.

Positive trends in the carbonate $\delta^{13}C$ signal of about 4‰ that correspond to shoaling-upwards cycles are repeated throughout the interglacial sequence. Departures from the overall post-glacial positive trend recorded in the Tapley Hill Formation at Blinman-2 are attributable to local environmental perturbations die to rapid upward movement of the seafloor over the adjacent diapir. No such perturbations are evident further west on the Stuart Shelf. On the other hand, it would be diffiucult to obtain a C-isotope record for another deepwater siliciclastic unit, the Enorama Shale, if it was not for the growth of stromatolite reefs on the flanks of the of the ascending Enorama Diapir during its deposition. Conclusive evidence that sea level fluctuations, attributable to the interplay of eustasy and basin subsidence, can impart a second and third-order paracyclicity to the secular $\delta^{13}C$ record is provided by the

Etina Formation. Whilst displaying a massive and unpredicted shift to pre-glacial negative values, $\delta^{13}C$ data from the overall regressive Trezona Formation also trend positive in parallel with a fall in sea level.

One possible explanation calls for an exaggeration of the observed decrease in isotopic composition of dissolved inorganic carbon (DIC) with increasing water depth in present-day oceans (Kroopnick, 1985). The $\delta^{13}C$ of DIC decreases by more than 2‰ reaching a minimum at 1 km depth. This $\delta^{13}C$ minimum corresponds to an O_2 minimum in which remineralisation of organic matter, first by aerobic bacteria that consume oxygen and then by sulphate-reducing bacteria, results in the release of isotopically light CO_2 (Logan et al., 1995). As indicated by the Etina data, a late Cryogenian $\delta^{13}C$ minimum may have existed near the lower photic zone, possibly at a depth as shallow as 100 m.

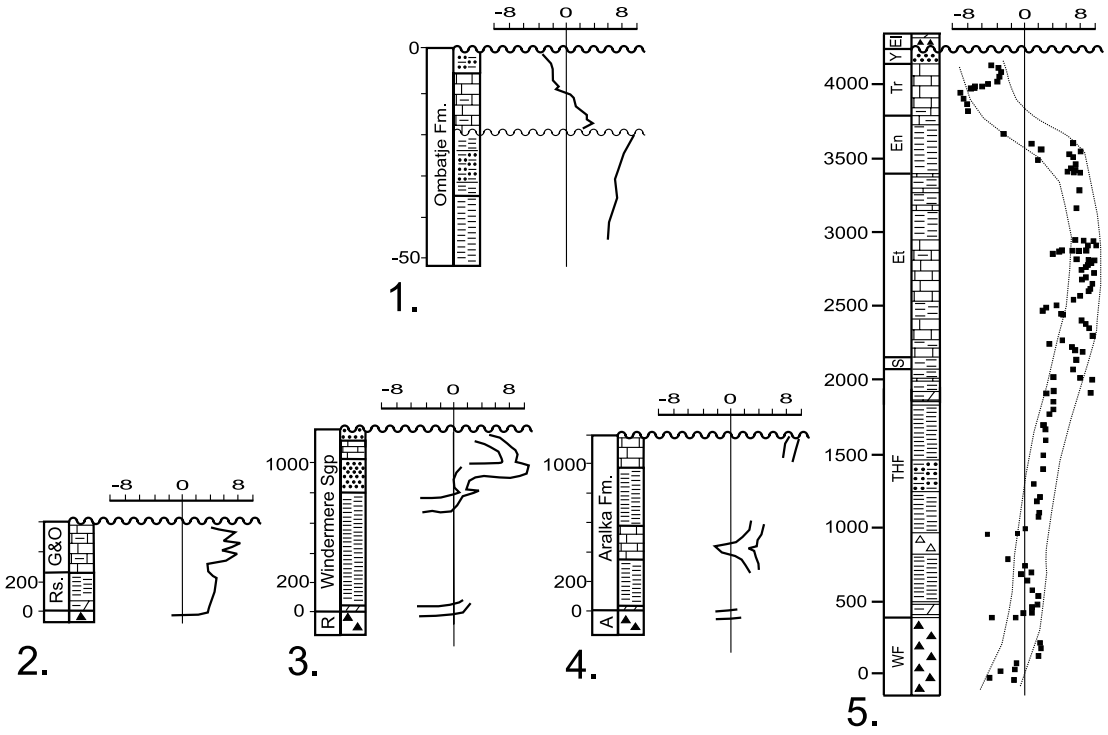

Figure 21. Late Cryogenian interglacial $\delta^{13}C$ record. Section 1., Southern Congo Craton, Africa (Hoffman et al., 1998); Section 2., 5-point running average of data from the western and southern Congo Craton, Africa (Kennedy et al., 1998; Rs.=Rasthoff Formation, G&O=Gruis and Ombaatjie Formations); Section 3., Mackenzie Mountains, Canada (Kennedy et al., 1998 after Kaufman et al., 1997; R=Rapitan glacials); Section 4., Amadeus Basin, Australia (Kennedy et al., 1998; A=Areyonga Formation); Section 5., this study. Section 1 is hung from the pre-Marinoan unconformity to illustrate the pre-glacial $\delta^{13}C$ negative trend. Sections 2-5 are tied to the top-Sturtian glacial unit as the datum and have the same vertical scale, thickness in metres.

The methodology hitherto employed by Neoproterozoic chemostratigraphers commonly recognises perturbations in $\delta^{13}C$ of 4‰ (or greater) to be of significance for inter-basinal correlation (Kaufman and Knoll, 1995; Hoffmann et al., 1998; Kennedy et al., 1998, and references therein). However, on the strength of the data presented herein, this would perhaps be akin to correlating cycles of sea level change after Haq et al. (1988). While also using peaks in $\delta^{13}C$ data, Kennedy et al. (1998) have employed other data manipulation techniques to help them interpret secular C-isotope curves. In an attempt to constrain secular variation, remove local variation and to assist in the correlation of interglacial sections measured in the western and southern Congo Craton, Kennedy et al. (1998) calculated a 5-point running average of $\delta^{13}C$ data (Figure 21, section 2). However, this technique reduces somewhat the resolution of the $\delta^{13}C$-sea level signal and does not recognise the significance of sea-level fluctuation as a cause of the data variation.

Correcting $\delta^{13}C$ data for sea level variation is difficult. From section 5 in Figure 21, one is able to observe several individual instances of paracyclical variation in $\delta^{13}C$. From the trend in the Wilyerpa Formation data, and assuming a post-Sturtian maximum flooding surface near the lowest Tapley Hill level, it is possible that ocean-surface waters may be enriched in ^{13}C immediately preceding the end of the Sturtian glaciation.

Interpreting secular $\delta^{13}C$ data thus becomes easiest at upper interglacial levels where shallow water marine depositional environments persist. Carbon isotope values trend back from +10‰ in the mid-Etina Formation to +7‰ and +6‰ in the overlying Enorama Shale. A directly measured segment of the secular curve linking these mid-positive values with negative values in the lower Trezona Formation (-8 to -9.5‰) is not observed but the $\delta^{13}C$ values of -2‰ in the Artipena Dolomite at or near the Enorama-high stand and -3‰ just above this level are a further confirmation of such an overall trend, reminiscent of that described by Hoffman et al. (1998) below the Ghaub glacials in Namibia (see Figure 21, section 1). It is likely that there are few other correlatives of the Trezona Formation; certainly none are recognised in Australia (Walter, et al., 1995). Therefore its geochemistry is as unique as it is unexpected.

Although sediment colour is perhaps an unreliable measure of environmental oxicity, as paralic equivalents of the Etina Formation are red and not grey-green, the role of oxygen in Late Cryogenian surface waters hitherto has possibly been understated. Under oxic conditions, iron in its 3+ valency state will not be included into the calcite lattice, in

exchange for the 2+ ions of magnesium and calcium, as it will in suboxic environments. It will instead be deposited as free iron oxides, imparting characteristic red colour to the host sediments (Lemon, 1988). Paralic sediments may alternatively be red due to inclusion of terrigenous material.

Growing evidence continues to strengthen the theory of a chemically stratified ocean during at least some stages of the Neoproterozoic (Knoll et al., 1996; see discussion Chapter 2). The Sturtian glaciation is associated with ironstone deposits worldwide and the oxidised state of the respective glacial-cap carbonates is readily recognised (Derry et al., 1992; Kennedy et al., 1998). The decline of stromatolites is another pivotal, but less well understood biogeochemical event (Grotzinger, 1990). Stromatolites, and indeed anoxic conditions, were never again dominant in the Adelaide Fold Belt after the interglacial Umberatana Group.

If chemical stratification of ocean waters may be reasonably assumed, given the observed change in sediment colour through the transgressive-regressive Enorama Shale, then perhaps a quantum jump in the degree of oxygenation of surface ocean waters sometime between the deposition of the Etina and Trezona Formations may also be assumed. Oxygenated surface waters would facilitate and perhaps explain the breakup of microbial mats necessary to crate the multitudinous amounts of cyanobacterial-flake intraclast limestones (i.e. “heiroglyphic limestone”) observed in the Trezona Formation (Walter, 1976).

Models of Neoproterozoic biogeochemistry have previously been constrained by the assumption that primary negative $\delta^{13}C$ values occur only in cap carbonates. The author favours an interglacial (and perhaps glacial) biogeochemical model not unlike that proposed by Knoll et al. (1996; Figure 1A). High organic productivity, most likely by photosynthetic autotrophs and a high proportional rate of burial of organic carbon relative to carbonate carbon (Hayes, 1983; Holser, 1997; Hayes et al., 1999), are necessary for the anomalously positive $\delta^{13}C$ values that characterise much of the Neoproterozoic. Chemical stratification of ocean waters would be as much a result of biological activity as a factor controlling it. Such photosynthetic activity would be restricted to surface waters, but matched by the ferocity of remineralisation of organic matter by sulphate-reducing bacteria lower in the water column, producing CO_2 enriched in the lighter isotope (Logan et al., 1995), so much indeed as to drive the formation of deep-sea chemical precipitates such as the Artipena Dolomite. It is likely that

biological drawdown of atmospheric CO_2, thought to trigger global glaciation (Kaufman, 1997), was matched by expiration of an equivalent amount of O_2, only in the first instance retained in the ocean surface, predisposing this ecological niche to invasion by respiring heterotrophs. Drawn by an abundance of fuel, the sulphate-reducing bacteria would have risen in the water column, thereby releasing lighter carbon into shallow waters, although the same trend of $\delta^{13}C$ versus depth continued. There are likely delays on such feedback mechanisms and a probable time lag between cause and effect.

Although largely beyond the scope of this thesis, the author finds the correlation of the Umberatana succession with other interglacial Neoproterozoic sequences in the manner proposed by Kennedy et al. (1998) relatively convincing (Figure 21). Even within the Adelaide Fold Belt, the whole Trezona Formation is only preserved in the Central Flinders Zone, in the more actively subsiding areas. It may well be that the Umberatana Group interglacial succession is more complete than anywhere else in the world. Indeed the sections shown in Figure 21 from the Congo Craton, Mackenzie Mountains and Amadeus Basin are less than one quarter as thick as the Adelaide Fold Belt succession. Clearly subsidence rates are less in these areas with potential for greater removal of section at the top of the succession. Strontium data presented in this thesis are in good agreement with the terminal Proterozoic $^{87}Sr/^{86}Sr$ ratio increase documented by Derry et al. (1992), Kaufman et al (1997), Kennedy et al. (1998) and Jacobsen and Kaufman (1999). Ratios steadily increase from 0.707106 to 0.707459 in the Brighton Limestone up to 0.707826 in the upper Etina Formation. Singh's (1986) data are also largely in agreement with this observation although ratios range from 0.7072 to 0.7080 in non-diagenetic components. Increase in strontium ratios is reflective of increased continental run-off, due to weathering reactions facilitated by a more oxygenated atmosphere as much as an active hydrological regime (c.f. Hoffman et al., 1998).

9. CONCLUSIONS

Geochemical criteria for identifying samples suitable for chemostratigraphic purposes, as elaborated by Kaufman and Knoll (1995) and relied upon by many chemostratigraphers, are only relative indicators of possible alteration and are not necessarily uniformly applicable from one succession to the next. Data quality has been evaluated throughout the interglacial Umberatana Group using a twofold approach: 1) by careful analysis of the isotopic signatures of selected samples known to have undergone diagenetic overprint by virtue of their proximity to exposure surfaces; and 2) by comparison of isotopic trends through widely separated correlative sections. Indeed, meteoric diagenesis has been shown to deplete ^{13}C and enrich ^{18}O in carbonates, throwing into doubt the use of Phanerozoic models for gauging Neoproterozoic meteoric alteration (Kaufman and Knoll, 1995 and references therein).

The reliance on geochemical parameters and cathodoluminescence to define unaltered samples suitable for isotope analysis appears to be unnecessarily restrictive. Cathodoluminescence certainly assists in the identification of cement phases but is not necessarily more definitive than standard petrology. Observations from outcrops can show the cements to be essentially of early sea floor origin when intraclasts are reworked. With regard to chemical selection criteria, a coherent $\delta^{13}C$-stratigraphic signal has been attained from the Trezona Formation where trace element chemistry was previously shown to vary considerably (Singh, 1986).

Dolomitisation by percolation of fluids down from exposure surfaces, as seen in the Brighton Limestone, commonly retains the $\delta^{13}C$ of the precursor calcite although, as expected, produces an enrichment in $\delta^{18}O$ of 1-4‰. The $\delta^{13}C$ of dolomite in the Central Flinders Zone is drawn to less positive values than for coexisting calcite because of the effect of emergent diapirs on local sea water chemistry. The C and O-isotope trends for calcite are broadly parallel through the Etina Formation.

There is an unequivocal relationship between the isotopic composition of carbonate and the water depth at which it precipitated. This has previously not been recognised in other terminal Proterozoic sequences. There is substantial difference in both depth, by an order of magnitude less, and in $\delta^{13}C$, by more than 2‰, relative to what is observed for present day ocean water (Kroopnick, 1985).

Accurate correlation of chemostratigraphic data must factor considerations sea level variation as dictated by local stratigraphy instead of relying on correlation of data variation and absolute values. One way to eliminate the variation induced by sea level fluctuation is to only select samples from a known water depth, i.e. only ooids interbedded with stromatolites or just stomatolites. If one does this, the secular trend can be plotted free from interference. This will be better than a 5-point moving average but requires careful attention to the exact lithofacies being sampled. This may be as, or indeed more important than selecting samples on a strictly geochemical basis. Provided the samples do not show any recrystallisation, one should be happy to accept the value measured.

Overall, the interglacial trend in $\delta^{13}C$ is from immediately post-glacial negative values of about -5‰ which plateau at +10‰ in shallow water carbonates before a pre-glacial decline to values in the range -3 to -9‰. The Sturtian to Marinoan interglacial succession of the Adelaide Fold Belt provides a useful reference for global chemostratigraphic correlation. By comparison the C-isotopic records obtained from pre-Varanger sequences in the Amadeus Basin, central Australia; the Mackenzie Mountains, northwestern Canada; the Otavi Mountainland, Namibia (as well as others elsewhere in East Greenland and Spitsbergen; Kaufman and Knoll, 1995) appear condensed and somewhat less complete, most notably in their upper part. A preglacial offset in $\delta^{13}C_{carb}$ values of such proportions (~14‰) is almost unprecedented, except for perhaps a major negative excursion recently documented in the upper Ombaatjie Formation beneath the Ghaub glacial facies of the Otavi Group, Namibia (Hoffman et al., 1998).

The upper Umberatana Group exhibits strong evidence for increased oxygenation of the shallow ocean during deposition of the Enorama Shale as indicated by the change from Fe^{2+} to Fe^{3+} in the iron minerals of its shallow water facies. Presently available models of Late Cryogenian biogeochemistry do not provide an adequate explanation for this proposed change in oxygenation. It is likely that elevated levels of activity by photosynthetic autotrophs have driven the drawdown of atmospheric CO_2 (acting as a trigger for the ensuing glaciation) and the rise in O_2 and carbonate $\delta^{13}C$, only to be followed by equivalent levels of remineralisation of organic matter by sulphate-reducing bacteria in shallow marine waters before the actual onset of the Marinoan Glaciation.

Negative $\delta^{13}C$ values preceding Neoproterozoic glaciations have largely gone unobserved because of lack of section or have been disregarded because of long held theories that this data occurs only in glacial-cap carbonates. It can now be shown that $\delta^{13}C$ signatures through this period of the Neoproterozoic are at least the sum of effects such as local conditions and water depth, as well as changes in the greater exogenic environment.

C-isotope signatures trend towards positve values through the glacial Wilyerpa Formation, indicating that the negative values in the post-glacial cap carbonate-Tindelpina Shale may indeed be the result of precipitation of this carbonate at significant water depth. A sluggish reaction time obviously exists in the feedback between changes in the global C reservoir (as reflected in $\delta^{13}C$ of ocean water) and glaciation and vice versa. The peak-negative values in the resultant secular curve that are reflective of global biogeochemical change, are thus offset to the preceding side of glaciation.

Increase in atmospheric oxygen over this interval may also assist continental weathering, as inferred through the strontium record, leading to clastic-dominated successions in the latest Neoproterozoic.

BIBLIOGRAPHY

Al-Aasm, I.S. and Veizer, J. (1986) Diagenetic stabilization of aragonite and low-Mg calcite, II. Stable isotopes in rudists. *Journal of Sed. Petrol*., **56**, No.6, 763-770.

Beukes, N.J. and Klein, C. (1992) Models for Iron-Formation Deposition. *In* Schopf, J.W. and Klein, C. (Eds) The Proterozoic Biosphere. (Princeton University Press).

Brasier, M.D., Shields, G., Kuleshov, V.N. and Zhegallo, E.A. (1996) Integrated chemo- and biostratigraphic calibration of early animal evolution: Neoproterozoic-early Cambrian of southwest Mongolia. *Geol. Mag.*, **133** (4), 445-485.

Choquette, P.W. and James, N.P. (1990) Limestones, the Burial Diagenetic Environment. *In* McIlreath, I.A. and Morrow, D.W. (Eds.) "Diagenesis" Geoscience Canada reprint series; 4.

Christie-Blick, N., Kennedy, M.J. and Sohl, L. (1999) Proposed location of Terminal Proterozoic GSSP, Nuccaleena Formation, Flinders Ranges, South Australia. IUGS Subcommission on the Terminal Proterozoic System, 12th Circular, 33–39.

Coats, R.P. and Blissett, A.H. (1971) Regional and Economic geology of the Mount Painter Province. Bulletin of the Geological Survey of South Australia., No. 43.

Coats, R.P. and Forbes B.G. (1977) Evidence for two Sturtian glaciations in South Australia - a reply. Quarterly Geol. Notes, Geol. Surv. of S.A., No. 64, 19-20.

Cooper, A.M. (1991) Late Proterozoic hydrocarbon potential and its association with diapirism in Blinman #2, Central Flinders Ranges, South Australia. Unpubl. Hons. thesis, University of Adelaide.

Crossing, A.R. and Gostin, V.A. (1994) Isotopic signatures of carbonates associated with Sturtian (Neoproterozoic) glacial facies, central Flinders Ranges, South Australia. In: M. Deynoux, J.M.G. Miller, E.W. Domack, N. Eyles, I.J. Fairchild and G.M. Young (Editors), Earth's Glacial Record. Cambridge Univ. Press, Cambridge, 165–175.

Derry, L.A., Kaufman, A.J. and Jacobsen, S.B. (1992) Sedimentary cycling and environmental change in the Late Proterozoic: Evidence from stable and radiogenic isotopes. *Geochimica et Cosmochimica Acta,* **56**, 1317-1329.

Des Marais, D.J., Strauss, H., Summons, R.E. and Hayes, J.M. (1992) Carbon isotope evidence for the stepwise oxidation of the Proterozoic environment. *Nature,* **359**, 605-609.

Dickson, J.A.D. (1965) A modified staining technique for carbonates in thin section. *Nature*, No. 4971, 587.

Dunham, R.J. (1962) Classification of carbonate rocks according to depositional texture. *In* Ham, W.E. (Ed.) Classification of Carbonate Rocks. American Assoc. Petroleum Geologists Memoir, **1**, 108-121.

Dyson, I.A. (1992) Stratigraphic nomenclature and sequence stratigraphy of the Lower Wilpena Group, Adelaide Geosyncline: the Sandison Subgroup. Geological Survey Of South Australia, Quarterly Geological Notes, **122**, 2-13.

Dyson, I. A. (1997) Definition of the Artipena Dolomite Member, Enorama Shale. *MESA Journal*, **6**, 43-45.

Fairchild, I.J. & Hambrey, M.J. (1995) Vendian basin evolution in East Greenland and NE Svalbard. *Precambrian Research,* **73**, 217-233.

Fairchild, I.J. and Spiro, B. (1987) Petrological and isotopic implications of some contrasting Late Precambrian carbonates, NE Spitsbergen. *Sedimentology*, **53**, 201-216.

Fairchild, T.R., Schopf, J.W., Shen-Miller, J., Guimarães, E.M., Edwards, M.D., Lagstein, A., Li, X., Pabst, M. and de Melo-Filho, L.S. (1996) Recent discoveries of Proterozoic microfossils in south-central Brazil. *Precambrian Research,* **80**, 125-152.

Fanning, C.M., Ludwig, K.R., Forbes, B.G. and Preiss, W.V. (1986) Single and multiple grain U-Pb zircon analyses for the early Adelaidean Rook Tuff, Willouran Ranges, South Australia. Geol Soc of Aust., 8th Aust. Geol. Convention, Abstracts #15.

Flöttmann, T, James, P.R., Rogers, J. and Johnson, T. (1994) Early Palaeozoic foreland thrusting and basin reactivation at the Palaeo-Pacific

margin of the southeastern Australian Precambrian margin: a re-appraisal of the structural evolution of the southern Adelaide Fold-Thrust Belt. *Tectonophysics*, **234**, 95–116.

Grotzinger, J.P. (1990) Geochemical model for Proterozoic stromatolite decline. *American Journal of Science,* **290-A**, 80-103.

Grotzinger, J.P., Bowring, S.A., Saylor, B.Z. & Kaufman, A. J. (1995) Biostratigraphic and Geochronologic Constraints on Early Animal Evolution. *Science,* **270**, 598-604.

Haines, P.W. (1987) Carbonate shelf and basin sedimentation, late Proterozoic Wonoka Formation, South Australia. Unpubl. PhD. thesis, University of Adelaide.

Hanor, J.S. (1994) Origin of saline fluids in sedimentary basins. *In* Parnell, J. (Ed) Geofluids: Origin, Migration and Evolution of Fluids in Sedimentary Basins. Geol. Soc. Spec. Publ. No.78, 151-174.

Haq, B.U., Hardenbol, J. and Vail, P.R. (1988) Mesozoic and Cenozoic chronostratigraphy and cycles of sea level change. *In* Wilgus, C.K. et al. (Eds) Sea Level Changes – an integrated approach. SEPM Special Publication No.42, 72-108.

Harland, W.B., Armstrong, R.L., Cox, A.V., Craig, L.E., Smith, A.G. & Smith, D.G. (1989) A Geological Time Scale 1989. (Cambridge University Press, Cambridge) 263pp.

Hayes, J.M., (1983) Geochemical evidence bearing on the origin of aerobiosis: a speculative hypothesis. In: J.W. Schopf (Editor), Earth's Earliest Biosphere: Its Origins and Evolution. Princeton Univ. Press, Princeton, N.J., 291–301.

Hayes, J.M., Kaplan, I.R. and Wedeking, K.W. (1983) Precambrian organic geochemistry: preservation of the record. In: J.W. Schopf (Editor), Earth's Earliest Biosphere: Its Origins and Evolution. Princeton Univ. Press, Princeton, N.J., 93–134.

Hayes, J.M., Strauss, H., and Kaufman, A.J. (1999) The abundance of ^{13}C in marine organic matter and isotopic fractionation in the global biogeochemical cycle of carbon during the past 800Ma. *Chemical Geology*, **161**, 103-125.

Hoffman, P.F., Kaufman, A.J., Halverson, G.P. and Schrag, D.P. (1998) A Neoproterozoic Snowball Earth. *Science,* **281**, 1342-1346.

Holser, W.T. (1984) Gradual and abrupt shifts in ocean chemistry during Phanerozoic time. *In* Holland and Trendall (Eds) Patterns of change in Earth Evolution. Springer-Verlag, Berlin, 123-144.

Holser, W.T., (1997) Geochemical events documented in inorganic carbon isotopes. *Palaeogeogr., Palaeoclimatol., Palaeoecol*., 132: 173–182.

Horodyski, R.J. and Knauth, L.P. (1994) Life on land in the Precambrian. *Science,* **263**, 494-498.

Howchin, W. (1922) A geological traverse of the Flinders Ranges from the Parachilna Gorge to the Lake Frome Plains. *Transactions of the Royal Society of S.A.*, **46**, 46-82.

Jacobsen, S.B. and Kaufman, A.J. (1999) The Sr, C and O isotopic evolution of Neoproterozoic seawater. *Chemical Geology*, **161**, 37-57.

James, N.P. (1983) Reef. *In* Scholle, P.A., Bedout, D.G. and Moore, C.H. (Eds) Carbonate Depositional Environments. AAPG Memoir No.8, 345-462.

Jenkins, R.J.F. (1990) The Adelaide Fold Belt: Tectonic reappraisal. In: J.B. Jago and P.S. Moore (Editors), The Evolution of a Late Precambrian–Early Palaeozoic Rift Complex: The Adelaide Geosyncline. Geol. Soc. Aust., Spec. Publ., 16, 396–420.

Jenkins, R.J.F and Nedin, C. (1998) The Ediacaran question: north and south. Inaugrual Sprigg Symposium, Geol. Soc. Aus., Abstracts No.51.

Kaufman, A.J. (1997) An ice age in the tropics. *Nature*, **386**, 227-228.

Kaufman, A.J. & Knoll, A.H. (1995) Neoproterozoic variations in the C-isotopic composition of seawater: stratigraphic and biogeochemical implications. *Precambrian Research,* **73**, 27-49.

Kaufman, A.J., Hayes, J.M. and Klein, C. (1990) Primary and diagenetic controls of isotopic composition of iron formation carbonates. *Geochimica et Cosmochimica Acta,* **54**, 3461-3473.

Kaufman, A.J., Knoll, A.H. and Narbonne, G.M. (1997) Isotopes, ice ages and terminal Proterozoic earth history: Proceedings of the National Academy of Sciences. **95**, 6600-6605.

Kay, M. (1947) Geosynclinal nomenclature and the craton. *Am. Assoc. Petrol. Geol. Bull*., **31**, 1289–1293.

Kennedy, M.J. and Wallace, M.W. (1993) The stratigraphy and significance of post-glacial carbonate horizons in the Amadeus Basin. *In* Alexander, A.M. and Gravestock, D.I. (Eds) Central Australian Basins Workshop. Programme and Abstracts, 75-76.

Kennedy, M.J., Runnegar, B., Prave, A.R., Hoffmann, K.H. and Arthur, M.A. (1998) Two or four Neoproterozoic glaciations? *Geology*, **26**, No.12, 1059-1063.

Knoll, A.H., Hayes, J.M., Kaufman, A.J., Swett, K. & Lambert, I.B. (1986) Secular variation in carbon isotope ratios from Upper Proterozoic successions of Svalbard and East Greenland. *Nature,* **321**, 832-838.

Knoll, A.H., Bambach, R.K., Canfield, D.E. & Grotzinger, J.P. (1996) Comparative Earth history and Late Permian mass extinction. *Science*, **273**, 452-457.

Krapez, B. (1996) Sequence stratigraphic concepts applied to the identification of basin-filling rhythms in Precambrian successions. *Australian Journal of Earth Sciences*, **43**, 355-380.

Kroopnick, P.M. (1985) The distribution of ^{13}C of CO_2 in the worlds oceans. *Geology*, **32**, No.1, 57-84

Lambert, I.B., Donnelly, T.H. and Rowlands, N.J. (1980) Genesis of Upper Proterozoic Stratabound Copper Mineralization, Kapunda, South Australia. *Mineralium Deposita*, **15**, 1-18.

Lambert, I.B., Knutson, J., Donnelly, T.H., Etminan, H., and Mason, M.G. (1984) Genesis of Copper Creek Mineralisation, Myall Creek Prospect, South Australia. *Mineralium Deposita*, **19**, 266-273.

Lemon, N.M. (1988) Diapir recognition and modelling. Unpubl. PhD. thesis, University of Adelaide.

Lemon, N.M. (1996) Geology. *In* Davies, M., Twidale, C.R. and Tyler, M.J. (Eds) Natural History of the Flinders Ranges. Royal Society of South Australia Inc.

Lemon, N.M. (1998) Unpublished personal data collection.

Lemon, N.M. (1999) Fringing stromatolite reefs, Enorama Diapir, Central Flinders Ranges. *Precambrian Research*, in press.

Lemon, N.M., Cooper, A.M. and McKirdy, D.M. (1992) Proterozoic source rocks associated with diapirs in the Central Flinders Ranges, South Australia. AAPG International Conference and Exhibition, Sydney, Program and Abstracts, p.61.

Lemon, N.M. and Reid, P.W. (1998) The Yaltipena Formation of the central Flinders Ranges. *MESA Journal*, **8**, 37-39.

Li, Z. X., Zhang, L., and Powell, C. McA. (1995) South China in Rodinia: Part of the missing link between Australia-East Antarctica and Laurentia? *Geology*, **23**, No.5, 407-410.

Logan, G.A., Hayes, J.M., Hieshima, G.B. & Summons, R.E. (1995) Terminal Proterozoic reorganization of biogeochemical cycles. *Letters to Nature, Nature,* **376**, 53-56.

Mawson, D (1938) Cambrian and sub-Cambrian formations at Parachilna Gorge. *Transactions of the R oyal Society of S.A.,* **62**, 255-262.

Mawson, D. (1949) The Elatina Glaciation. A third recurrence of glaciation evidenced in the Adelaide System. *Transactions of the Royal Society of S.A.,* **73**, 117-121.

Mawson, D. and Sprigg, R. (1950) Subdivision of the Adelaide System. *Australian Journal of Science*, **13**, 69-72.

McBriar, E.M. (1949) Petrological examination of rocks from the Oraparinna asbestos deposit at Oraparinna. *Miner. Review*, Adelaide, **87**, 179-180.

McClune, W.F. and Macguire, T.M. (1980) Mineral powder diffraction file - Data book. JCPDS - International center for Diffraction Data.

McKenzie, J.A. (1981) Holocene dolomitisation of calcium carbonate sediments from the coastal sabkhas of Abu Dhabi, U.A.E.; a stable isotope study. *Journal of Geology,* **89**, No.2, 185-198.

McKirdy, D.M. and Powell, T.G. (1974) Metamorphic alteration of carbon isotopic composition in ancient sedimentary organic matter: new evidence from Australia and South Africa. *Geology*, **2**, No.12, 591-595.

McKirdy, D.M., Sumartojo, J., Tucker, D.H. and Gostin, V.A. (1975) Organic, mineralogic and magnetic indicators of metamorphism in the Tapley Hill Formation, Adelaide Geosyncline. *Precambrian Research,* **2**, 345-373.

McKirdy, D.M., Lemon, N.M., Yu, X., Burgess, J.M., Cooper, A.M., Ayliffe, D.J., Michaelson, B.H., Jenkins, R.J.F. & Strauss H. (1995) Carbon isotope stratigraphy of the Neoproterozoic interglacial Tapley Hill Formation, Adelaide Fold Belt. Proceedings for the 5th AOGC, Adelaide, South Australia.

McKirdy, D.M., Jenkins, R.J.F. and Gostin, V.A. (1997) Neoproterozoic carbon budget of the Officer Basin and Adelaide Fold Belt. Large Research Grant Final Report submitted to University of Adelaide Research Branch.

Mendelson, C.V. and Schopf, J.W. (1992) Summary and Conclusions: the current status of Proterozoic Micropaleontology. *In* Schopf, J.W. and Klein, C. (Eds) The Proterozoic Biosphere. (Princeton University Press).

Mount, T.J. (1975) Diapirs and Diapirism in the Adelaide Geosyncline, South Australia. Unpubl. PhD. thesis, University of Adelaide.

Narbonne, G.M., Kaufman, A.J. and Knoll, A.H. (1994) Integrated chemostratigraphy and biostratigraphy of the Windermere Supergroup, northwestern Canada: Implications for Neoproterozoic correlations and the early evolution of animals. Geol. Soc. Am. Bull., **106**, 1281–1292.

Paeche, H. (1995) Cathodoluminescence signatures of selected South Australian minerals. Unpubl. Hons. thesis, University of Adelaide.

Pelechaty, S.M., (1998) Integrated chronostratigraphy of the Vendian System of Siberia: implications for a global stratigraphy. *J.Geol. Soc. London*, **155**, 957–973.

Powell, C.McA., Preiss, W.V., Gatehouse, C.G., Krapez, B. and Li, Z.X. (1994) South Australian record of a Rodinian epicontinental basin and its mid-Neoproterozoic breakup (~700Ma) to form the Palaeo-Pacific Ocean. *Tectonophysics,* **237**, 113-140.

Preiss, W.V. (1983) Depositional and tectonic contrasts between Burra Group and Umberatana Group sedimentation. In Dalgarno, C.R. (convenor), Adelaide Geosyncline sedimentary environments and tectonic settings: Symposium. Geol. Soc. Aus., Abstracts No.10.

Preiss, W.V. (Ed.)(1985) Stratigraphy and Tectonics of the Worumba Anticline and Associated Intrusive Breccias. Bulletin of the Geological Survey of South Australia., No. 52.

Preiss, W.V. (Ed.)(1987) The Adelaide Geosyncline-late Proterozoic stratigraphy, sedimentation, palaeontology and tectonics. Bulletin of the Geological Survey of South Australia., No. 53.

Preiss, W.V. (1996) New members of the Waukaringa Siltsone - early Marinoan sequence boundaries in the Nackara Arc and their implications for gold mineralisation. *MESA Journal*, **1**, 40-45.

Preiss, W.V., Dyson, I.A., Reid, P.W. and Cowley, W.M. (1998) Revision of lithostratigraphic classification of the Umberatana Group. *MESA Journal*, **9**, 36-43.

Rutland, R.W.R.R., Parker, A.J., Pitt, G.M., Preiss, W.V. and Murrell, B. (1981) The Precambrian of the South Australia. *In* Hunter, D.R. (Ed) Precambrian of the Southern Hemisphere. (Elsevier, Amsterdam) 309-360.

Schmidt, P.W. and Williams, G.E. (1995) The Neoproterozoic climatic paradox: Equatorial palaeolatitude for Marinoan glaciation near sea level in South Australia. *Earth and Planetary Science Letters*, **134**, 107-124.

Scoffin, T.P. (1987) An introduction to carbonate sediments and rocks. Blackie and Son Ltd., Glasgow.

Shieh, Y.N. and Taylor, H.P. (1969) Oxygen and carbon isotope studies of contact metamorphism of carbonate rocks. *Journal of P etrology*, 10, 307-331.

Shixing, Z. and Huineng, C. (1995) Megascopic Multicellular organisms from the 1700-Million-year-old Tuanshanzi Formation in the Jixian Area, North China. *Science*, **270**, 620-622.

Singh, U. (1986) Late Precambrian and Cambrian carbonates of the Adelaidean, South Australia. Unpubl. PhD. thesis, University of Adelaide.

Singh, U. (1987) Ooids and cements from the Late Precambrian of the Flinders Ranges, South Australia. *Journal of Sed. Petrol.*, **57**, No. 1, 117-127.

Strauss, H. (1997) The isotopic composition of sedimentary sulfur through time. *Palaeogeogr., Palaeoclimatol., Palaeoecol*., **132**, 97–118.

Strauss, H., Des Marais, D.J., Hayes, J.M. and Summons, R.E. (1992) Concentrations of organic carbon and maturities and elemental composition of kerogens. *In* Schopf, J.W. and Klein, C. (Eds) The Proterozoic Biosphere. (Princeton University Press).

Sumartojo, J. (1974) A study of the mineralogy and geochemistry of the Tindelpina Shale (Upper Proterozoic) Adelaide Geosyncline, South Australia. Unpubl. PhD. thesis, University of Adelaide.

Summons, R.E. and Hayes, J.M. (1992) Principles of Molecular and Isotopic Biogeochemistry. *In* Schopf, J.W. and Klein, C. (Eds) The Proterozoic Biosphere. (Princeton University Press).

Tennant, C.B. and Berger, R.W. (1957) X-ray determination of calcite-dolomite ratio of a carbonate rock. *American Mineralogist*, **42**, 23-29.

Thomson, B.P., Coats, R.P., Mirams, R.C., Forbes, B.G., Dalgarno, C.R. and Johnson, J.E. (1964) Precambrian rock groups in the Adelaide Geosyncline: a new subdivision. *Quarterly Geol. Notes*, Geol. Surv. of South Australia, **9**, 1-19.

Veizer, J. and Hoefs, J. (1976) The nature of $^{18}O/^{16}O$ and $^{13}C/^{12}C$ secular trends in sedimentary carbonate rocks. *Geochimica et Cosm ochimica Acta,* **40**, 1387-1395.

Walter, M.R. (Ed.)(1976) Stromatolites. Developments in Sedimentology, 20 (Elsevier Scientific Publishing Co.), 790pp.

Walter, M.R., Veever, J.J., Calver, C.R. and Grey, K. (1995) Neoproterozoic stratigraphy of the Centralian Superbasin, Australia. *Precambrian Research,* **73**, 173-195.

Wickham, S.M. and Peters, M.T. (1993) High $\delta^{13}C$ Neoproterozoic carbonate rocks in western North America. *Geology*, **21**, 165-168.

Williams, G.E. (1979) Sedimentology, stable-isotope geochemistry and palaeoenvironment of dolostones capping late Precambrian glacial sequences in Australia. *J. Geol. Soc. Aust*., **26**, 377–386.

Winter, B.L. and Knauth, L.P. (1992) Stable isotope geochemistry of cherts and carbonates from the 2.0Ga Gunflint Iron Formation: implications for the depositional setting and the effects of diagenesis and metamorphism. *Precambrian Research,* **59**, 283-313.

Wymond, A.P. and Wilson, B. (1951) An occurrence of crocidolite near Robertstown, South Australia. *Transactions of the Royal Society of S.A.,* **74**, 44-48.

Young, G.M. and Gostin, V.A. (1988) Stratigraphy and sedimentology of Sturtian glacigenic deposits in the western part of the North Flinders Basin, South Australia. *Precambrian Research,* **39**, 151-170

APPENDIX 1: ANALYTICAL METHODS AND RAW DATA

A1.1 Stable C and O-isotope analyses

The rock samples in this study varied greatly in carbonate content, from limestone to slightly calcareous shale and siltstone. Their mineralogy was determined by X-ray diffractometry. Representative limestones were screened petrographically (including by staining and cathodoluminescence microscopy of polished thin sections) for evidence of meteoric or metamorphic alteration. Those selected for isotopic analysis are generally micrites that show no signs of recrystallisation. In certain cases a dental drill was employed to selectively micro-sample desired mineral phases. For the most part, however, whole-rock powders were used since manual separation of discrete carbonate phases was not possible. Instead, for samples containing more than one carbonate species, an acid digestion procedure was employed whereby separate aliquots of CO_2 were collected from coexisting calcite and dolomite.

Whilst sampling of discrete carbonate mineral phases was not directly possible, manual separation of expired CO_2 representative of coexisiting mineral species was possible on the basis of trials conducted. Based on the reactive nature of calcite and dolomite, a strategy was devised to accurately extract mineral species-representative CO_2 once a sample containing both these minerals was digested in 100% phosphoric acid (After methods of Al-Aasm and Veizer, 1986; Brasier et al., 1996). Geological Survey of Japan dolomite standard (JDo-1; containing mostly dolomite and a small amount of calcite) and UNIVAR analytical calcite were mixed in varying proportions (Table A1) and reacted in phosphoric acid. Expired CO_2 was collected at regular intervals thus; 0-0.5hrs @ 25°C, 0.5-4hrs @ 25°C, 4-9.5hrs @ 50°C, and 9.5-24hrs @ 50°C. Yields of expired CO_2 were calculated, as a percent of total expected from mass of material digested, to monitor amounts of periodic expulsion (Table A2). Results showed that $\delta^{13}C$ representative of calcite phases was ideally collected at the 0.5hr mark with minimal influence of $\delta^{13}C$ from other minor phases (Figure A1). Samples with more evenly proportioned mixes of mineral phases predictably gave values that reflected a inexact sum of constituent phases. Coincident data collected at 9.5 and 24hrs indicates total expulsion of CO_2 representing calcite after 4hrs at 25°C.

Whole-rock powder (30–100 mg, depending on carbonate content) was digested off-line under vacuum in 100% phosphoric acid. Expired CO_2 was collected at regular intervals, thus: 0–0.5 hrs at 25°C (calcite); 0.5–4

Analytical standards; dolomite JDo-1 Geological Survey of Japan standard, UNIVAR analytical calcite

Table A1 mixtures (mg)

sample	1	2	3	4	5	6
calcite	100	-	90	80	70	50
JDo-1	-	100	10	20	30	50

Table A2

sample		0.5 hour	4 hour	9.5 hour	24 hour	total Y%
1	δ13C	-36.97	-37.14	not	not	
1	δ18O	-21.13	-17.88	meas.	meas.	
	%YIELD	97.0	2.9	-	-	99.9
2	δ13C	3.36	4.86	5.02	4.99	
2	δ18O	-7.53	-3.87	-3.99	-4.24	
	%YIELD	19.5	25.0	49.0	5.2	98.7
3	δ13C	-36.18	-20.9	4.52	4.63	
3	δ18O	-20.94	-11.85	-4.04	-4.03	
	%YIELD	88.3	4.5	4.9	0.7	98.4
4	δ13C	-34.59	-7.15	4.98	4.92	
4	δ18O	-20.37	-7.62	-4.02	-4.06	
	%YIELD	78.5	7	11.7	1.4	98.6
5	δ13C	-33.69	-6.8	4.95	5.08	
5	δ18O	-20.2	-7.76	-4.08	-3.39	
	%YIELD	71.6	9.2	15.2	2.4	98.4
6	δ13C	-31.48	-1.34	5.01	4.88	
6	δ18O	-18.91	-5.82	-3.95	-4.22	
	%YIELD	63.4	11.7	21.6	1.7	98.4

Figure A1

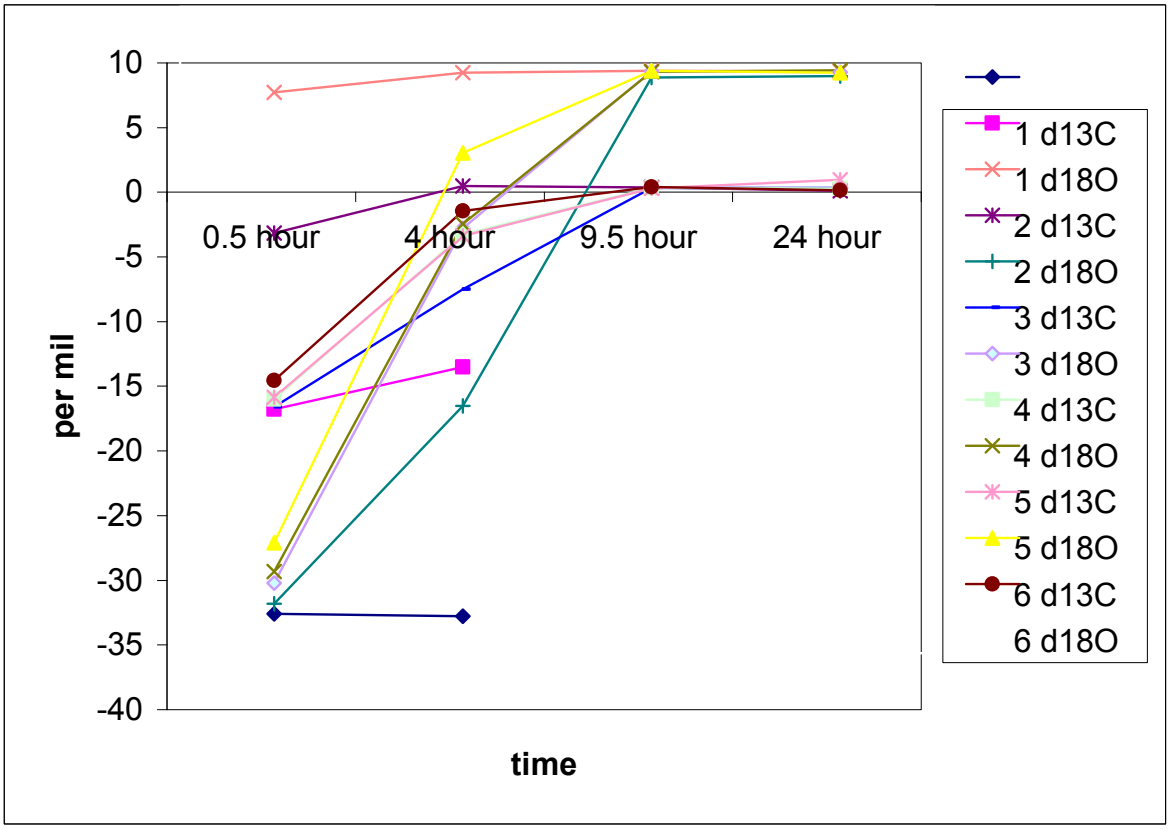

yield % = $\frac{\text{gas volume } (cm^3)}{\text{mass digested (mg)}}$

where gas volume = (Pi - Po) * 0.0795 (glasswr const.)
Pi=intitial pressure, Po= value at zero pressure

Results show almost coincident 3rd and 4th fraction values indicating total expulsion of calcite derived CO_2 after a period of 4 hours.

hrs at 25°C (mixed, discarded); and 4–24 hrs at 50°C (dolomite). After separation of the co-produced H_2O on a vacuum line, the CO_2 was collected for introduction to the mass spectrometer. $^{13}C/^{12}C$ and $^{18}O/^{16}O$ ratios were measured on a Micromass 602E instrument. Late in the study a Fisons Optima isotope mass spectrometer, incorporating a carbonate self-preparation facility, became available and was used for the analysis of a few calcite-only samples. Results are reported relative to the PDB standard. Replicate analyses of laboratory standards (commonly JDo-1) typically showed a precision equal to, or better than, ± 0.1‰ for $\delta^{13}C$ and ± 0.2‰ for $\delta^{18}O$.

Isotopic analysis of organic carbon in the Tapley Hill Formation was performed on either kerogen concentrates or carbonate-free residues. The former were obtained by serial acid digestion in HCl (32% v/v) and HF (50% v/v) followed by reaction with sodium borohydride to remove pyrite (McKirdy et al., 1974); and the latter by treatment of powdered rock with HCl (50% v/v). In both cases the residues were washed in distilled water until neutral. Aliquots of dried kerogen or decarbonated shale (20–100 mg), together with CuO and Ag wire, were sealed in evacuated silica tubes and heated at 900°C for 8 hrs. The resulting CO_2 was purified and collected as above, and its $^{13}C/^{12}C$ ratio measured on the Micromass 602E instrument. Total organic carbon (TOC) values were determined at AMDEL Limited using a Leco IR-12 carbon analyser.

A1.2 Strontium isotope analysis

Eight samples were selected for strontium isotope analysis. Approximately 1g. of powdered sample was weighed into a clean teflon beaker and dissolved in 20ml. of 1N HCl. Three samples were taken up in 0.5M acetic acid as well to test if HCl was overly harsh on clastic components in samples as per analytical procedures used by Derry et al. (1992). The samples were then decanted and centrifuged twice. They were then dried then taken up into HCl and loaded onto resin ion exchange columns to separate the strontium. The resultant fluid was concentrated onto filaments and measured in a Finnigan 261 Mass spectrometer. The strontium isotopic ratios of samples digested in acetic acid are only marginally, but consistently, higher by up to 0.00013 than for the same sample digested in hydrochloric acid, exactly opposite to behaviour observed by Derry et al. (1992).

Samples analysed for strontium isotope ratios in this study were generally upwards of 70-80% whole rock carbonate (commonly micrite,

typical Umberatana Group carbonates and thus assumed Sr content >200ppm after Singh (1986)) and the effect of silica components esp. clays, on resultant data is assumed to be minimal. External replicate TPB's (Total procedural blanks) over the course of this study averaged 1.7ng, and represent a contribution of <0.001% to measured ratios. Through the duration of the study, NBS SRM 987 standard Sr yielded a value of 0.710177 ± 0.000055. A value of 0.710248 is accepted for this standard. All Sr data reported in this study have had a correction applied (multiplied by 1.000099975) so as to be comparable with published Sr ratios.

A1.3 Tabulated isotopic and other geochemical data.

The following tabulated geochemical data have been cited in the text without reference to their location in Appendix 1.

Isotopic compositions, $\delta^{13}C$ and $\delta^{18}O$ are reported in ‰ relative to PDB. TOC is reported as weight %. The strontium data are reported as the ratio $^{87}Sr/^{86}Sr$ along with the run precision on the measurement.

Table 1: C and O-isotope and TOC data on Wilyerpa and Tapley Hill Formations

Unit	Depth (m)	$\delta^{13}C_{calc}$	$\delta^{18}O_{calc}$	$\delta^{13}C_{dol}$	$\delta^{18}O_{dol}$	$\delta^{13}C_{org}$	$\Delta^{13}C$	TOC (%)
FRONTIER BLINMAN-2								
Tapley Hill Formation	35.0			2.2	–11.4			
	95.0W			9.1	–9.6			
	200.0	3.8	–14.6	3.5	–10.9	–26.3	29.8	
	300.0	2.0	–17.0	2.6	–13.0	–26.1	28.7	
	400.0	2.6	–14.8	2.8	–11.4	–26.3	29.0	
	500.0	2.0	–15.8	2.2	–11.3	–26.7	28.9	
	600.0			2.2	–10.7	–27.0	29.2	
	710.0M	–0.2	–17.3	0.5	–12.0	–26.2	26.7	0.30
	800.0	1.0	–16.2	1.4	–10.0	–28.0	29.4	0.60
	900.0	1.4	–15.1	1.6	–9.7	–27.5	29.1	0.75
	1010.5	–2.3	–13.1	–0.5	–7.6	–30.1	29.6	0.99
	1022.3			–1.4	–6.9	–30.2*	28.8	0.61
	1032.0			–5.5	–12.7			0.09
	1211.7			–2.9	–10.5	–26.1*	23.2	0.08
	1216.9			–2.2	–10.4	–27.1	24.9	0.11
	1234.6			–1.6	–10.5			0.14
	1261.0	–1.3	–13.7	–0.2	–9.8			0.15
	1297.2	–0.7	–13.6	0.2	–9.5	–27.4	28.6	0.28
	1315.7	–0.7	–13.5	0.3	–9.6			0.11
	1316.7	–0.4	–12.5	0.5	–8.5	–27.5	28.1	0.29
	1348.1	–0.5	–14.7	0.5	–9.1	–26.7	27.2	0.20
	1366.8	–1.4	–13.8	–0.3	–9.8			0.20
	1367.0	–1.0	–13.2	0.2	–9.2			0.23
	1380.5	–1.0	–13.0	0.3	–8.6	–27.5	27.8	0.25
	1426.1	0.3	–13.6	1.0	–9.2			0.23
	1447.6	0.4	–14.1	1.1	–10.0			0.22
	1467.0	0.8	–13.6	1.4	–8.7	–25.9	27.3	0.26
	1475.2	0.8	–13.7	1.4	–8.4			
	1485.2	0.9	–13.6	1.4	–8.6			0.23
	1488.9	0.9	–13.8	1.5	–7.5			
Tindelpina Shale Mbr	1509.5	1.0	–14.0	1.5	–8.2			
	1522.8	0.6	–14.1	1.4	–8.6	–26.2	27.6	0.31
	1528.6	1.4	–14.5	1.2	–10.2	–27.4	28.6	
	1531.7	0.4	–14.0	1.2	–8.6			
	1551.7	0.2	–13.9	1.2	–8.3	–26.5	27.7	0.40
	1563.0	–0.3	–13.7	0.8	–8.4			0.50
	1584.0			–0.8	–8.4	–28.1	27.3	0.83
	1601.8			–1.6	–10.3	–28.9	27.3	0.61
	1608.1			–5.0	–10.7			
	1610.0			–1.7	–12.5			1.10
Wilyerpa Formation	1630.6			–3.0	–12.2	–27.0*	23.9	0.05
	1782.0			1.5	–7.6			
	1804.6			2.0	–7.3			

Table 1 continued

Unit	Depth (m)	δ^{13}Ccalc	δ^{18}Ocalc	δ^{13}Cdol	δ^{18}Odol	δ^{13}Corg	Δ^{13}C	TOC (%)
FRONTIER BLINMAN-2								
Wilyerpa Formation	1832.1			1.8	–7.4			
	1866.5			1.5	–8.1			
	1934.8			–1.6	–11.7	–28.5	26.9	0.06
	1954.6			–1.9	–10.1			
	1962.3			–1.8	–9.6	–29.5	27.7	0.17
	1974.7			–3.9	–10.9			
	2006.0			–1.9	–11.2			
	2009.0			–5.3	–13.4	–30.1	24.8	0.13
	2024.8			–2.2	–9.2			
AMOCO SCYW-1A								
Brighton Limestone	1184.8					–27.8		0.13
	1192.0					–27.3		0.11
Tapley Hill Formation	1206.3					–29.6		0.19
	1230.4					–28.3		0.20
	1238.8					–28.5		0.22
	1250.1					–28.4		0.19
	1263.8					–28.9		0.23
	1278.9					–28.9		0.24
	1289.9					–28.6		0.25
	1308.1					–29.0		0.29
	1322.1					–29.2		0.29
	1332.9					–29.3		0.34
	1345.1					–30.2		0.38
Tindelpina Shale Mbr	1354.6					–31.0		0.51
	1368.0					–33.8		0.67
	1372.5					–31.5		0.14
SADME BUTE-3								
Brighton Limestone	55.0							0.21
	60.9					–28.7		0.21
Tapley Hill Formation	70.2					–28.7		0.32
	80.4					–29.0		0.30
	89.9					–28.9		0.25
	99.4					–29.3		0.33
	106.1					–29.5		0.30
Woocalla Dol Mbr	117.8					–29.8		0.40

$\Delta^{13}C = \delta^{13}Cdol - \delta^{13}Corg$ * H. Strauss, pers. comm. (1991) W = Wockerawirra Dolomite Member

M = Mt Caernarvon Greywacke Member

Table 2: C, O and Sr-isotope data on Brighton Limestone

Measured section	Sample 1041-	Height (m)	$\delta^{13}C_{calc}$	$\delta^{18}O_{calc}$	$\delta^{13}C_{dol}$	$\delta^{18}O_{dol}$	$^{87}Sr/^{86}Sr$
Depot Flat	20	130	1.3	–12.6	2.7	–10.3	
	19	125	2.6	–12.9	3.1	–10.5	
	18	120	3.0	–9.7	2.7	–8.7	
	17	115	3.3	–9.3	4.0	–7.5	0.707459 ±0.000081
	16	110	3.4	–9.2	4.2	–7.1	
	15	105	3.1	–8.6	3.7	–6.9	
	14	100	3.5	–8.7			
	13	95	3.5	–9.3	3.9	–6.4	
	12	90	3.4	–8.8	3.3	–7.7	0.707249 ±0.000111
	11	85	3.5	–9.4	3.9	–8.1	
	10	80	3.4	–8.8	4.1	–6.5	
	9	75	3.7	–8.4	3.5	–7.1	0.707106* ±0.000129
	8	70	3.8	–8.5	3.9	–5.9	
	7	65	3.6	–8.6	3.2	–8.2	
	6	60	3.8	–9.2	4.3	–6.6	
	5	55	3.8	–9.8	3.3	–8.9	
	4	50	3.9	–10.2	2.8	–6.4	
	3	45	3.4	–11.0	3.0	–7.6	
	2	40	3.7	–12.2	3.7	–8.5	
	1	35	3.6	–13.3			

* Acetic acid treatment gave value of 0.707052 ± 0.000098

Table 3: C, O and Sr-isotope data on Etina Formation

Measured section	Sample 1041-	Height (m)	δ^{13}Ccalc	δ^{18}Ocalc	δ^{13}Cdol	δ^{18}Odol	$^{87}Sr/^{86}Sr$
First Spring	68	643	7.7	–13.3			
	66	628	9.8	–9.5	8.8	–7.8	0.707714 ±0.000047
	64	599	10.3	–10.0			
	62	577	4.9	–12.1			
	59	532	8.3	–12.0			
	58	528	9.8	–10.0	5.4	–2.7	
	54	476	8.4	–9.7			
	53	470	9.6	–9.2			
	51	446	8.4	–10.9			0.707808 ±0.000037
	50	432	8.8	–10.5			
	49	418	7.8	–12.4			
	42	335	2.7	–11.2			
	41	295	2.0	–9.3			
	135	290	6.3	–11.8			
	134	282	6.6	–11.7			
	133	270	5.3	–11.4			
	132	255	3.3	–11.8			
	131	234	6.8	–10.3			
	40	217	3.6	–9.5	3.4	–3.8	
	39	168	9.1	–8.8	8.7	–15.2	0.707608** ±0.000083
	38	50	5.9	–14.1			
Glass Gorge	69	52	7.0	–13.1	6.9	–2.7	
Mount Emily	75	211	8.1	–12.6			
	74	75	4.9	–9.9			
	70	0	8.2	–12.4			
Gum Creek	35 WU	–	8.2	–12.7	8.0	–13.4	
	31 WU	–	8.0	–12.5			0.707693* 0.000119
	25 WU	–	7.3	–12.6	5.9	–10.5	0.707741 0.000119
Dedmans Bore	76 WU	–	6.5	–11.0			
	112	150(N)	1.3	–3.5	4.7	–2.7	
	111	50(N)	–0.5	–10.0	1.2	–6.4	

Table 3 continued

Measured section	Sample 1041-	Height (m)	$\delta^{13}C_{calc}$	$\delta^{18}O_{calc}$	$\delta^{13}C_{dol}$	$\delta^{18}O_{dol}$	$^{87}Sr/^{86}Sr$
Popes Paddock	165	1065	9.4	–8.2			
	164	1032	8.8	–9.0			
	163	1009	7.9	–10.8			
	162	985	9.5	–10.7			
	161	978	8.9	–10.3	6.0	–6.2	
	160	954	6.9	–11.1	3.5	–5.7	
	159	952	4.2	–9.5	2.7	–4.1	
	158 mat	895	9.3	–7.8			
	158 str	895	9.1	–9.4			
	157	879	9.0	–7.6			
	156	877	9.6	–8.3			
	155	854	9.3	–8.5			
	154	828	9.4	–6.7			
	153	809	9.2	–8.1			
	152	791	8.9	–7.9	5.7	–3.0	
	151	780	9.0	–8.3	5.6	–4.2	
	150	763	8.6	–8.4			
	149	712	9.4	–7.4			
	148	688	7.8	–11.4			
	147	686	3.2	–7.0	5.0	0.8	
	146 ls	630	4.6	–10.7	2.2	–4.4	
	146 sd	630	4.8	–11.4			
	145	578	8.4	–10.5			
	144	557	8.8	–8.6			
	143	528	9.2	–10.3			
	142	515	9.4	–10.5			
	141	441	7.8	–12.3			
	140	419	5.7	–11.6	4.0	–7.5	
	139 S	300	7.4	–12.9	3.3	–8.8	
	138 T	171	0.8	–4.5			
	137 WO	85	8.4	–13.1	6.0	–9.7	

mat = micrite matrix str = stromatolitic clast ls = limestone sd = sandy limestone

Acetic acid treatment gave $^{87}Sr/^{86}Sr$ values of 0.707826 ± 0.000106 (*) and 0.707705 ± 0.000070 (**)

WU = Wundowie Limestone Member S = Sunderland Formation T = Tapley Hill Formation

W = Wockerawirra Dolomite Member

Table 4: C and O-isotope data on Enorama Shale

Measured section	Facies	Sample 1041-	δ^{13}Ccal	δ^{18}Ocal	δ^{13}Cdol	δ^{18}Odol
Mallee Water	dolomicrite	114			–3.1	–4.7
	fringing reefs	89 (E11)	6.0	3.4	7.0	–3.8
		88 (E10)	0.5	–3.2	0.9	–2.8
		87 (E9)	0.7	–8.6	2.0	–7.7
		85 (E7)	5.3	–4.7	6.1	–5.3
		84 (E6)	–0.6	–1.0	1.8	–1.6
		83 (E5)	4.9	–2.6	6.9	–2.1
		82 (E4)	5.4	–4.2	7.0	–5.2
		81 (E3)	5.7	–4.5	7.7	–3.4
		80 (E2)			6.2	–0.7
		79 (E1)	4.1	–2.0	6.2	–2.6
Dedmans Bore	dolomicrite	37	4.0	–5.9	6.4	–6.1
	fringing reefs	78	7.0	–11.8		
		77	6.6	–9.7		

Table 5: C and O-isotope data on Trezona Formation

Measured section	Sample 1041-	Height (m)	δ^{13}Ccalc	δ^{18}Ocalc	δ^{13}Cdol	δ^{18}Odol
Doodney's Well Hills	107	384	–4.2	–10.1		
	106	377	–3.5	–10.3		
	105	375	–2.9	–9.0		
	104	355	–3.2	–9.5		
	103	332	–3.8	–10.4		
	102	315	–5.5	–11.3		
	100	287	–6.5	–10.2		
	99	255	–7.4	–8.2		
	98	253	–7.4	–9.3		
	97	237	–7.6	–9.4		
	96	235	–7.9	–11.6		
	95	211	–9.5	–11.5		
	94	172	–9.0	–12.2		
	93	134	–8.4	–12.2		
	92	130	–8.7	–12.5		
	91	111	–8.5	–13.2		
	90	53	–8.2	–13.1		
Bulls Gap palaeokarst	121	1.00	–4.2	–10.3		
	120	0	–8.8	–6.3		
	119	–0.83	–4.4	–9.9	–4.3	–16.3
	118	–3.12	–9.4	–5.8		
	117	–4.99	–5.4	–7.0	–4.0	–16.4
	116	–7.28	–4.8	–9.3	–4.3	–16.3
	115	–9.36	–3.9	–13.1		
Brachina Rd palaeokarst	136cl	20.00	–5.5	–12.9		
	129	0	–5.7	–1.8		
	128	–0.20	–4.3	–10.6		
	127	–0.45	–3.0	–10.7		
	126	–0.70	–3.1	–10.3		
	125	–1.00	–3.0	–10.9		
	124	–1.50	–3.0	–10.8		
	123	–2.00	–2.9	–11.3		
	122	–3.00	–3.1	–10.5		
	130	–5.00	–3.3	–10.2		

cl = diamictite clast (Trezona) from overlying Elatina Formation

APPENDIX 2: SAMPLE INDEX

Including locations, abbreviated hand specimen description, and analysis data - mineralogy and geochemistry.

Location: AMG coordinates
Analysis conducted: hs = hand specimen only (XRD on all samples with the obvious exception of conglomerates and diamictites), 13C = Carbon and Oxygen stable isotope analyses, TS = reported thin section description, Sr = Strontium isotopic analysis.
Major mineralogies (via XRD): (D)=Dominant (1200+ counts), (S)=Subsidiary (1200>counts>800), (m)=minor (800>counts>400), (tr)=trace (400>counts) and (?)=indication
Q=quartz, Calc=Calcite, Dol=Dolomite, Plg=Plagioclase, Chl=Chlorite, Oth=Orthoclase, Pyrol=Pyrolusite

Lithologies: Classification of limestones after Dunham (1962).
Mud-supported <10% grains = Limestone, mud-supported >10% grains = Wackestone, grain supported = Packestone, lacks mud and grain supported = Grainstone.

Abbreviations used;
Colour; dk = dark, lt = light; bl = blue, gn = green, gr = grey, orang. = orange, brn = brown
Lamination; dig.= digitate stromatolite, cr-cy. = crypto-cyanobacterial lamination, intclst = intraclastic,

Sample #	colln. date	Formation.	Area	Easting	Northing	Dominant mineralogy	analysis	rock type/descr
1041-1	06/01/1994	Brighton Ls.	Depot Ck.	778662	6426888	Calc(D)Q(m)Dol(m)	13C	lt-blue digitate strom. Limestone
1041-2	06/01/1994	Brighton Ls.	Depot Ck.	778669	6426886	Calc(D)Q(tr)Dol(tr)Plg(tr)	13C	lt-blue digitate strom. Limestone
1041-3	06/01/1994	Brighton Ls.	Depot Ck.	778676	6426884	Calc(D)Q(m)Dol(tr)Chl(S)	13C	lt-blue intra-flake-strom Limestone
1041-4	06/01/1994	Brighton Ls.	Depot Ck.	778683	6426883	Calc(D)Q(S)Dol(m)Plg(tr)	13C	blue-grey flake-intraclast Wackestone
1041-5	06/01/1994	Brighton Ls.	Depot Ck.	778690	6426881	Calc(D)Q(m)Dol(tr)Plg(tr)	13C	blue-grey flake-intraclast Wackestone
1041-6	06/01/1994	Brighton Ls.	Depot Ck.	778697	6426879	Calc(D)Q(m)Dol(m)Chl(tr)	13C	blue-grey-pink intraclast Wackestone
1041-7	06/01/1994	Brighton Ls.	Depot Ck.	778704	6426877	Calc(D)Q(m)Chl(tr)	13C	blue-grey intraclast Wackestone
1041-8	06/01/1994	Brighton Ls.	Depot Ck.	778710	6426875	Calc(D)Q(m)Dol(?)Chl(m)	13C	blue-grey intraclast Wackestone
1041-9	06/01/1994	Brighton Ls.	Depot Ck.	778718	6425873	Calc(D)Q(m)Dol(?)Plg(tr)	13C,Sr	blue-grey intraclast Wackestone
1041-10	06/01/1994	Brighton Ls.	Depot Ck.	778724	6426871	Calc(D)Q(tr)Dol(tr)Chl(?)	13C	blue-grey intraclast Limestone
1041-11	06/01/1994	Brighton Ls.	Depot Ck.	778732	6426869	Calc(D)Q(tr)Dol(tr)Chl(?)	13C	blue-grey-orang. intraclast Wackestone
1041-12	06/01/1994	Brighton Ls.	Depot Ck.	778738	6426865	Calc(D)Q(m)Dol(tr)	13C,Sr	blue-grey-orang. intraclast Wackestone
1041-13	06/01/1994	Brighton Ls.	Depot Ck.	778746	6426863	Calc(D)Q(tr)Dol(tr)Chl(tr)	13C	blue-grey flake-intraclast Limestone
1041-14	06/01/1994	Brighton Ls.	Depot Ck.	778752	6426861	Calc(D)Q(m)Dol(tr)Plg(tr)	13C	blue-grey digitate strom. Limestone
1041-15	06/01/1994	Brighton Ls.	Depot Ck.	778760	6426860	Calc(D)Q(m)Dol(?)Chl(?)	13C	blue ooid-intraclastic Packestone
1041-16	06/01/1994	Brighton Ls.	Depot Ck.	778766	6426858	Calc(D)Q(tr)Dol(tr)	13C	blue ooid-intraclastic Packestone
1041-17	06/01/1994	Brighton Ls.	Depot Ck.	778774	6426856	Calc(D)Dol(tr)	13C,TS,Sr	blue intraclastic Packestone
1041-18	06/01/1994	Brighton Ls.	Depot Ck.	778780	6426854	Calc(D)Q(m)Dol(tr)Plg(?)	13C	blue intraclastic Packestone
1041-19	06/01/1994	Brighton Ls.	Depot Ck.	778788	6426852	Calc(D)Q(tr)Dol(m)	13C,TS	blue intraclastic Packestone
1041-20	06/01/1994	Brighton Ls.	Depot Ck.	778794	6426852	Calc(D)Q(tr)Dol(S)Plg(?)	13C	buff-pink fn.sandy-clastic Dolostone
1041-21	07/11/1994	Etina Fm.	Gum Ck.	274650	6547160	Calc(S)Q(D)Dol(m)Chl(S)	hs	blue-green fn.sandy Wackestone
1041-22	07/11/1994	Etina Fm.	Gum Ck.	274640	6547150	Calc(D)Q(tr)Plg(tr)	hs	blue-grey digitate strom. Limestone
1041-23	07/11/1994	Etina Fm.	Gum Ck.	274630	6547140	Calc(D)Q(tr)Plg(tr)	hs	blue fn-med. sandy Wackestone
1041-24	07/11/1994	Etina Fm.	Gum Ck.	274620	6547140	Calc(D)Q(m)Dol(tr)Plg(tr)	hs	blue med-cs. intraclastic Packestone
1041-25	07/11/1994	Etina Fm.	Gum Ck.	274600	6547080	Calc(D)Q(S)Plg(tr)	13C,TS, Sr	blue-grey small-broad strom. Limestone
1041-26	07/11/1994	Etina Fm.	Gum Ck.	274590	6547050	Calc(D)Q(S)Dol(tr)Plg(m)	hs	green-blue fn.sandy cr-cy. Wackestone
1041-27	07/11/1994	Etina Fm.	Gum Ck.	275300	6546150	Calc(S)Q(D)Dol(tr)Chl(m)	hs	green-blue fn.sandy cr-cy. Wackestone
1041-28	07/11/1994	Etina Fm.	Gum Ck.	275300	6546130	Calc(D)Q(S)Dol(tr)Plg(m)	hs	green-blue fn.sandy broad-strom Wack.
1041-29	07/11/1994	Etina Fm.	Gum Ck.	277920	6544720	Calc(D)Q(D)Plag(tr)	hs	blue-grey med.sandy Packestone
1041-30	07/11/1994	Etina Fm.	Gum Ck.	277900	6544700	Calc(D)Q(m)Dol(tr)Plg(tr)	hs	blue broad-strom Limestone
1041-31	07/11/1994	Etina Fm.	Gum Ck.	275250	6546100	Calc(D)Q(S)Dol(tr)Plg(m)	13C,TS, Sr	blue-gr fn.sandy dig.-strom Limestone
1041-32	07/11/1994	Etina Fm.	Gum Ck.	275200	6546090	Calc(D)Q(D)Dol(m)Plg(S)	hs	blue-gn rippled fn.sandy calc Siltstone
1041-33	07/11/1994	Etina Fm.	Gum Ck.	273240	6546890	Calc(S)Q(D)Dol(m)Chl(S)	hs	blue-gn cr-cy. fn.sandy calc Siltstone
1041-34	07/11/1994	Etina Fm.	Gum Ck.	273230	6546850	Calc(D)Q(S)Dol(tr)Plg(m)	hs	green-grey intraclastic Packestone

Sample #	colln. date	Formation.	Area	Easting	Northing	Dominant mineralogy	analysis	rock type/descr
1041-35	07/11/1994	Etina Fm.	Gum Ck.	273210	6546830	Calc(D)Q(S)Dol(tr)Plg(m)	13C,TS	blue-green digitate strom. Limestone
1041-36	07/11/1994	Etina Fm.	Gum Ck.	273200	6546800	Calc(D)Q(S)Dol(tr)Chl(m)	hs	blue-gn fn.sandy/silty Limestone
1041-37	08/06/1994	Enorama Sh.	Dedmans B.	277720	6541650	Dol(D)Q(S)Orth(S)Plg(S)	13C,TS	red massive dolomicrite
1041-38	10/12/1994	Etina Fm.	First Spring	269850	6561550	Calc(S)Q(D)Dol(?)Plg(S)	13C,TS	blue-gn fn.sandy Wackestone
1041-39	10/12/1994	Etina Fm.	First Spring	269600	6561750	Calc(D)Q(tr)Dol(tr)Plg(tr)	13C,TS,Sr	bl-gr med.intrclastic/ooid Packestone
1041-40	10/12/1994	Etina Fm.	First Spring	269550	6561850	Calc(S)Q(D)Dol(S)Chl(m)	13C	green calcareous Shale
1041-41	10/12/1994	Etina Fm.	First Spring	269270	6562040	Calc(D)Q(D)Dol(tr)Chl(m)	13C	blue-green calcareous Shale
1041-42	10/12/1994	Etina Fm.	First Spring	269250	6562050	Calc(D)Q(D)Dol(tr)Chl(m)	13C	blue-green calcareous Shale
1041-43	10/12/1994	Etina Fm.	First Spring	269290	6562140	Calc(D)Q(D)Plg(m)Chl(tr)	hs	blue-green calcareous Shale
1041-44	10/12/1994	Etina Fm.	First Spring	269200	6562080	Calc(D)Q(D)Plg(m)Chl(tr)	hs	blue-green calcareous Shale
1041-45	10/12/1994	Etina Fm.	First Spring	269190	6562190	Calc(D)Q(D)Plg(m)Chl(tr)	hs	blue-green calcareous Shale
1041-46	10/12/1994	Etina Fm.	First Spring	269170	6562190	Calc(D)Q(D)Plg(m)Chl(m)	hs	blue-gn fn.sandy calcareous Shale
1041-47	10/12/1994	Etina Fm.	First Spring	269170	6562180	Calc(D)Q(D)Plg(m)Chl(m)	hs	blue-gn fn.sandy Wackestone
1041-48	13/10/94	Etina Fm.	First Spring	269150	6562170	Calc(D)Q(D)Dol(tr)Plg(S)	hs	blue-green calcareous Shale
1041-49	13/10/94	Etina Fm.	First Spring	269150	6562170	Calc(D)Q(D)Dol(?)Plg(m)	13C	blue-green fn.sandy Limestone
1041-50	13/10/94	Etina Fm.	First Spring	269140	6562150	Calc(D)Q(tr)Plg(m)	13C	blue-gn fn.sandy dig. strom Limestone
1041-51	13/10/94	Etina Fm.	First Spring	269100	6562240	Calc(D)Q(S)Dol(tr)Plg(tr)	13C,Sr	blue-green digitate strom Limestone
1041-52	13/10/94	Etina Fm.	First Spring	269090	6562270	Calc(D)Q(S)Dol(tr)Plg(tr)	hs	blue-green digitate strom Limestone
1041-53	13/10/94	Etina Fm.	First Spring	269090	6562290	Calc(D)Q(tr)Dol(?)Plg(tr)	13C,TS	blue-gr med.intraclastic Packestone
1041-54	13/10/94	Etina Fm.	First Spring	269080	6562290	Calc(D)Q(tr)Dol(m)Plg(tr)	13C,TS	gn-bl-gr fn.sandy dig.strom Wackestone
1041-55	13/10/94	Etina Fm.	First Spring	269070	6562300	Calc(D)Q(D)Dol(m)Plg(S)	hs	gn-pink fn.sandy/intclst Packestone
1041-56	13/10/94	Etina Fm.	First Spring	269070	6562310	Calc(D)Q(S)Dol(tr)Plg(tr)	hs	bl-gn-gr fn.sandy dig.strom Wackestone
1041-57	13/10/94	Etina Fm.	First Spring	269050	6562330	Calc(D)Q(D)Dol(m)Plg(m)	hs	bl-gn fn.sandy Limestone
1041-58	13/10/94	Etina Fm.	First Spring	269030	6562350	Calc(D)Q(S)Dol(tr)Plg(tr)	13C,TS	bl-gr flake cs.sand/intclst Packestone
1041-59	13/10/94	Etina Fm.	First Spring	269020	6562360	Calc(D)Q(S)Dol(tr)Plg(m)	13C	blue-green digitate strom Limestone
1041-60	13/10/94	Etina Fm.	First Spring	268950	6562390	Calc(D)Q(D)Plg(m)	hs	brown-green calcareous Shale
1041-61	13/10/94	Etina Fm.	First Spring	268900	6562430	Calc(S)Q(D)Plg(m)	hs	green calcareous Shale
1041-62	13/10/94	Etina Fm.	First Spring	268800	6562550	Calc(S)Q(D)Dol(tr)Chl(m)	13C	green calcareous Shale
1041-63	13/10/94	Etina Fm.	First Spring	268740	6562700	Calc(D)Q(S)Dol(m)Plg(tr)	hs	bl-gr flake intraclast Wackestone
1041-64	14/10/94	Etina Fm.	First Spring	268700	6562740	Calc(D)Q(S)Dol(?)Plg(m)	13C,TS	blue cs.sandy ooid Packestone
1041-65	14/10/94	Etina Fm.	First Spring	268670	6562760	Calc(D)Q(S)Dol(m)Plg(m)	hs	blue-grey digitate strom Limestone
1041-66	14/10/94	Etina Fm.	First Spring	268600	6562800	Calc(D)Q(S)Dol(tr)Plg(tr)	13C,TS,Sr	blue intraclastic Wackestone
1041-67	14/10/94	Etina Fm.	First Spring	268570	6562840	Calc(D)Q(S)Dol(tr)Plg(tr)	hs	blue-green digitate strom Limestone
1041-68	14/10/94	Etina Fm.	First Spring	268590	6562860	Calc(D)Q(S)Dol(m)Plg(m)	13C,TS	blue-green digitate strom Limestone
1041-69	14/10/94	Tapley H.F.	Glass Gorge	272800	6562120	Calc(D)Q(S)Dol(m)Plg(m)	13C,TS	blue intraclastic Packestone

Sample #	colln. date	Formation.	Area	Easting	Northing	Dominant mineralogy	analysis	rock type/descr
1041-70	10/04/1995	Etina Fm.	Popes	278860	6548520	Calc(D)Q(m)Dol(?)	13C	blue digitate stromatolite Limestone
1041-71	10/04/1995	Etina Fm.	Popes	278960	6548400	Calc(?)Q(D)Plg(m)	hs	red-weathering green Shale
1041-72	10/04/1995	Etina Fm.	Popes	279000	6548330	Calc(tr)Q(D)Dol(tr)Plg(m)	hs	red-weathering green Shale
1041-73	10/04/1995	Etina Fm.	Popes	278940	6548250	Calc(S)Q(D)Dol(m)Chl(m)	hs	blue green v.fn.-sandy Shale
1041-74	10/04/1995	Etina Fm.	Popes	278980	6548190	Calc(S)Q(D)Dol(m)Chl(m)	13C	gn fn.sandy strom calc Siltstone
1041-75	10/04/1995	Etina Fm.	Popes	279360	6547810	Calc(D)Q(tr)Dol(tr)Plg(tr)	13C	blue-brown broad strom Limestone
1041-76	16/12/95	Etina Fm.	Dedmans B.	277740	6541400	Calc(D)Q(S)Dol(?)Plg(tr)	13C	dk-red micritic Limestone
1041-77	16/12/95	Enorama Sh.	Dedmans B.	277690	6541450	Calc(D)Q(S)Dol(m)Plg(m)	13C	dk-red micritic broad strom Limestone
1041-78	16/12/95	Enorama Sh.	Dedmans B.	277650	6541590	Calc(D)Q(S)Dol(tr)Plg(?)	13C	dk-red micritic broad strom Limestone
1041-79	16/12/95	Enorama Sh.	Mallee Water	280300	6536250	Q(m)Dol(D)Plg(tr)	13C	orang-brn fn.sandy strom Limestone
1041-80	16/12/95	Enorama Sh.	Mallee Water	280120	6536350	Q(tr)Dol(D)	13C,TS	orange-brown stromatolitic Limestone
1041-81	16/12/95	Enorama Sh.	Mallee Water	279890	6536730	Calc(tr)Q(?)Dol(D)	13C	buff-brn broad strom Limestone
1041-82	16/12/95	Enorama Sh.	Mallee Water	279800	6536850	Q(tr)Dol(D)	13C	orange-brown lithic strom Limestone
1041-83	16/12/95	Enorama Sh.	Mallee Water	279660	6537050	Calc(tr)Q(tr)Dol(D)	13C,TS	buff-brn lithic-sandy strom Limestone
1041-84	16/12/95	Enorama Sh.	Mallee Water	279580	6537160	Q(m)Dol(D)Plg(tr)	13C,TS	orange-brown strom Limestone
1041-85	16/12/95	Enorama Sh.	Mallee Water	279450	6537300	Q(tr)Dol(D)Orth(tr)	13C	blue-brown stromatolitic Limestone
1041-86	16/12/95	Enorama Sh.	Mallee Water	279300	6537550	Calc(?)Q(tr)Dol(D)Plg(tr)	hs	blue-grey stromatolitic Limestone
1041-87	16/12/95	Enorama Sh.	Mallee Water	279000	6537950	Q(S)Dol(D)Plg(tr)	13C,TS	red intraclastic strom Limestone
1041-88	16/12/95	Enorama Sh.	Mallee Water	278940	6538100	Q(tr)Dol(D)Plg(tr)	13C,TS	red-brown stromatolitic Limestone
1041-89	16/12/95	Enorama Sh.	Mallee Water	278690	6538550	Q(tr)Dol(D)Plg(?)	13C,TS	pink-grey stromatolitic Limestone
1041-90	17/12/95	Trezona Fm.	Doodney's	286210	6544605	Calc(D)Q(S)Plg(tr)	13C	dk red broad-strom. Limestone
1041-91	17/12/95	Trezona Fm.	Doodney's	286530	6544670	Calc(D)Q(m)Plg(tr)	13C	dk red broad-strom. Limestone
1041-92	17/12/95	Trezona Fm.	Doodney's	286640	6544690	Calc(D)Q(m)Plg(tr)Chl(tr)	13C	dk red strom-flake Limestone
1041-93	17/12/95	Trezona Fm.	Doodney's	286770	6544720	Calc(D)Q(m)Plg(tr)	13C,TS	dk red stromatolitic Limestone
1041-94	17/12/95	Trezona Fm.	Doodney's	286870	6544740	Calc(D)Q(S)Plg(tr)	13C	dk red fn.sandy strom Limestone
1041-95	17/12/95	Trezona Fm.	Doodney's	287080	6544790	Calc(D)Q(m)Plg(tr)Chl(?)	13C,TS	dk red digitate strom. Limestone
1041-96	17/12/95	Trezona Fm.	Doodney's	287220	6544820	Calc(D)Q(tr)Plg(tr)	13C	dk red stromatolitic Limestone
1041-97	17/12/95	Trezona Fm.	Doodney's	287220	6544820	Calc(D)Q(tr)	13C	buff red fn.sandy ooid Packestone
1041-98	17/12/95	Trezona Fm.	Doodney's	287320	6544840	Calc(D)Q(S)Plg(tr)	13C,TS	blue-green stromatolitic Limestone
1041-99	17/12/95	Trezona Fm.	Doodney's	287320	6544840	Calc(D)Q(tr)	13C,TS	buff-grey-pink fn.ooid Packestone
1041-100	17/12/95	Trezona Fm.	Doodney's	287510	6544880	Calc(D)Q(tr)Plg(?)	13C	blue-grey broad strom. Limestone
1041-101	17/12/95	Trezona Fm.	Doodney's	287510	6544880	Calc(D)Q(tr)Plg(tr)	hs	buff fine ooid Packestone
1041-102	17/12/95	Trezona Fm.	Doodney's	287620	6544910	Calc(D)Q(m)Plg(tr)	13C,TS	dk red stromatolitic Limestone
1041-103	17/12/95	Trezona Fm.	Doodney's	287740	6544930	Calc(D)Q(m)Plg(tr)	13C	dk red domal stromatolitic Limestone
1041-104	17/12/95	Trezona Fm.	Doodney's	287860	6544960	Calc(D)	13C,TS	blue-grey fn-med ooid Packestone

Sample #	colln. date	Formation.	Area	Easting	Northing	Dominant mineralogy	analysis	rock type/descr
1041-105	17/12/95	Trezona Fm.	Doodney's	287980	6544980	Calc(D)Q(?)	13C	buff-grey med.sandy ooid Packestone
1041-106	17/12/95	Trezona Fm.	Doodney's	287980	6544980	Calc(D)Q(tr)Plg(tr)	13C	dk red stromatolitic Limestone
1041-107	17/12/95	Trezona Fm.	Doodney's	288040	6544990	Calc(D)	13C	buff flake-intclst med.ooid Packestone
1041-108	15/5/97	Diap. xenocl.	Dedmans B.	277544	6541567	Q(D)Dol(D)	13C	buff fenestral Dolostone
1041-109	15/5/97	Diap. xenocl.	Dedmans B.	277551	6541567	Q(D)Dol(D)	13C	buff fenestral Dolostone
1041-110	15/5/97	Diap. xenocl.	Dedmans B.	277604	6541511	Calc(D)Q(m)Dol(m)	13C	yellow dolomitic Wackestone
1041-111	15/5/97	Etina Fm.	Dedmans B.	278300	6541293	Calc(D)Q(S)Dol(tr)	13C,TS	yell-brown chloritic Marble
1041-112	15/5/97	Etina Fm.	Dedmans B.	278177	6541179	Calc(S)Q(D)Dol(D)	13C	yell-brown chloritic Marble
1041-113	15/5/97	Diap. xenocl.	Mallee Water	278400	6539090	Q(S)Dol(D)	13C,TS	buff-yell rippled dolomitic Wackestone
1041-114	15/5/97	Enorama Sh.	Mallee Water	278380	6539070	Q(S)Dol(D)	13C,TS	dk red dolomitic Wackestone
1041-115	15/5/97	Trezona Fm.	Bulls Gap	275150	6540880	Calc(S)Q(m)	13C	buff-grey med.sandy Packestone
1041-116	15/5/97	Trezona Fm.	Bulls Gap	275130	6540870	Calc(S)Q(S)Dol(D)	13C	buff-orang. med.sandy dolo-Packestone
1041-117	15/5/97	Trezona Fm.	Bulls Gap	275100	6540860	Calc(D)Q(m)Dol(D)	13C,TS	buff-orange crystalline limestone
1041-118	15/5/97	Trezona Fm.	Bulls Gap	275080	6540850	Calc(D)Q(tr)	13C	orange-brown recrystallised Limestone
1041-119	15/5/97	Trezona Fm.	Bulls Gap	275070	6540840	Calc(m)Q(tr)Dol(D)	13C	orange-brown recrystallised Limestone
1041-120	15/5/97	Trezona Fm.	Bulls Gap	275060	6540830	Calc(D)Q(tr)	13C,TS	brown-orange recrystallised Limestone
1041-121	15/5/97	Trezona Fm.	Bulls Gap	275050	6540820	Calc(D)Q(?)	13C	buff-grey pisolitic Grainstone
1041-122	16/5/97	Trezona Fm.	Brachina Rd.	274850	6530196	Calc(D)Q(S)Plg(tr)Chl(tr)	13C	dk red stromatolitic Limestone
1041-123	16/5/97	Trezona Fm.	Brachina Rd.	274845	6530197	Calc(D)Q(tr)	13C	dk red fn.sandy Wackestone
1041-124	16/5/97	Trezona Fm.	Brachina Rd.	274840	6530198	Calc(D)Q(m)	13C	dk red fn.sandy intraclastic Wackestone
1041-125	16/5/97	Trezona Fm.	Brachina Rd.	274837	6530199	Calc(D)Q(tr)	13C	dk red fn.sandy Wackestone
1041-126	16/5/97	Trezona Fm.	Brachina Rd.	274835	6530199	Calc(D)Q(tr)	13C	dk red fn.sandy Wackestone
1041-127	16/5/97	Trezona Fm.	Brachina Rd.	274833	6530200	Calc(D)Q(m)	13C	dk red fn.sandy intraclastic Wackestone
1041-128	16/5/97	Trezona Fm.	Brachina Rd.	274831	6530200	Calc(D)Q(m)	13C	buff-red fn.sandy Wackestone
1041-129	16/5/97	Trezona Fm.	Brachina Rd.	274830	6530200	Calc(D)Q(m)Pyrol(tr)	13C	black brecciated limestone
1041-130	16/5/97	Trezona Fm.	Brachina Rd.	274860	6530195	Calc(D)Q(S)Dol(tr)	13C	dk red fn-med sandy Wackestone
1041-131	16/5/97	Etina Fm.	First Spring	279440	6561870	Calc(D)Q(S)Dol(?)	13C	blue-green silty Limestone
1041-132	16/5/97	Etina Fm.	First Spring	279400	6561900	Calc(S)Q(D)Dol(tr)	13C	blue-green calcareous Siltstone
1041-133	16/5/97	Etina Fm.	First Spring	279380	6561920	Calc(S)Q(D)Dol(tr)	13C	blue-green stromatolitic Limestone
1041-134	16/5/97	Etina Fm.	First Spring	279350	6561950	Calc(D)Q(D)Plg(m)Chl(m)	13C	green cryptmicrobial calc. Siltstone
1041-135	16/5/97	Etina Fm.	First Spring	279300	6562000	Calc(D)Q(D)Plg(m)Chl(m)	13C	green cryptmicrobial silty Limestone
1041-136	16/5/97	Elatina Fm.	Brachina Rd.	274800	6530600	-	13C	glacial diamictite
1041-137	17/5/97	Tapley H.F.	Popes	278900	6551110	Calc(D)Q(D)Dol(S)Plg(S)	13C	blue-green fn.sandy Limestone
1041-138	17/5/97	Tapley H.F.	Popes	279000	6550950	Calc(m)Q(D)Dol(m)Plg(m)	13C	buff-yellow calc. Siltstone
1041-139	17/5/97	Sunderland Fm	Popes	279200	6550800	Calc(D)Q(S)Dol(m)Plg(m)	13C	blue-green fn.sandy Limestone

Sample #	colln. date	Formation.	Area	Easting	Northing	Dominant mineralogy	analysis	rock type/descr
1041-140	17/5/97	Etina Fm.	Popes	279300	6550670	Calc(D)Q(D)Dol(m)Plg(m)	13C,TS	blue-green fn.sandy Limestone
1041-141	17/5/97	Etina Fm.	Popes	278800	6550240	Calc(D)Q(S)Plg(tr)	13C,TS	blue fn-med sandy ooid Packestone
1041-142	17/5/97	Etina Fm.	Popes	278850	6550150	Calc(D)Q(S)Plg(tr)	13C,TS	blue med-cs sandy Packestone
1041-143	17/5/97	Etina Fm.	Popes	278900	6550050	Calc(D)Q(m)Plg(tr)	13C	blue-grey sandy-strom Wackestone
1041-144	17/5/97	Etina Fm.	Popes	278950	6549950	Calc(D)Q(m)Plg(tr)	13C	blue sandy-strom Wackestone
1041-145	17/5/97	Etina Fm.	Popes	279000	6549900	Calc(D)Q(m)Plg(?)	13C,TS	dk.blue sandy oolitic Packestone
1041-146	18/5/97	Etina Fm.	Popes	278800	6549600	Calc(S)Q(D)Dol(tr)Plg(tr)	13C	blue-green calcareous Siltstone
1041-147	18/5/97	Etina Fm.	Popes	278850	6549410	Calc(S)Q(S)Dol(D)Plg(tr)	13C	yellow-brown fn.sandy Dolostone
1041-148	18/5/97	Etina Fm.	Popes	278800	6549500	Calc(D)Q(S)Plg(tr)Chl(tr)	13C,TS	blue-grn ripple fn.sandy Wackestone
1041-149	18/5/97	Etina Fm.	Popes	278850	6549400	-	13C	blue flat pebble conglomerate
1041-150	18/5/97	Etina Fm.	Popes	278900	6549300	Calc(D)Q(tr)Plg(?)	13C	blue digitate stromatolite Limestone
1041-151	18/5/97	Etina Fm.	Popes	278450	6549000	Calc(D)Q(S)Dol(m)Plg(tr)	13C	blue-gn rippled fn.sandy Wackestone
1041-152	18/5/97	Etina Fm.	Popes	278500	6548900	Calc(D)Q(S)Dol(m)Chl(tr)	13C	blue-green cryptmicrobial Limestone
1041-153	18/5/97	Etina Fm.	Popes	278550	6548800	Calc(D)Q(m)Plg(?)	13C	blue-gn fn-med ooid Wackestone
1041-154	18/5/97	Etina Fm.	Popes	278590	6548700	Calc(D)Q(S)Dol(?)Chl(m)	13C	dk.blue-brn fn.sandy Limestone
1041-155	18/5/97	Etina Fm.	Popes	278600	6548650	Calc(D)Q(S)Dol(?)Chl(tr)	13C	dk.blue-brn flake-intraclast Limestone
1041-156	18/5/97	Etina Fm.	Popes	278640	6548600	Calc(D)Q(S)Dol(?)Plg(tr)	13C	blue-grn flake-intraclast Limestone
1041-157	18/5/97	Etina Fm.	Popes	278650	6548500	Calc(D)Q(m)Plg(?)	13C	blue-grey sandy intraclast Packestone
1041-158	18/5/97	Etina Fm.	Popes	278700	6548400	-	13C	blue-grn calc. intraclast Conglomerate
1041-159	18/5/97	Etina Fm.	Popes	278800	6548100	Calc(S)Q(D)Dol(m)Chl(m)	13C	green fn.lam. calc. Siltstone
1041-160	18/5/97	Etina Fm.	Popes	278050	6547950	Calc(D)Q(S)Dol(tr)Plg(m)	13C,TS	blue-grn-brn intraclast Packestone
1041-161	18/5/97	Etina Fm.	Popes	278100	6547800	Calc(D)Q(S)Dol(m)Chl(tr)	13C	buff-grey fn.sandy ooid Wackestone
1041-162	18/5/97	Etina Fm.	Popes	278120	6447700	Calc(D)Q(S)Dol(tr)Chl(tr)	13C	blue-brn broad strom Limestone
1041-163	18/5/97	Etina Fm.	Popes	278150	6547600	Calc(D)Q(m)Dol(tr)Plg(tr)	13C	dk.blue flake intraclast Limestone
1041-164	18/5/97	Etina Fm.	Popes	278200	6547450	Calc(D)Q(S)Dol(tr)Plg(tr)	13C	blue-grey med.sandy Wackestone
1041-165	18/5/97	Etina Fm.	Popes	278250	6547300	Calc(D)Q(S)Dol(?)Plg(?)	13C,TS	blue med/sandy Packestone

APPENDIX 3: REPORTED PETROLOGICAL INVESTIGATIONS

A3.1 Staining of thin sections.

Staining of polished thin sections was carried out where carbonate species determination was difficult. The method used (after Dickson, 1965) involved -

(1) Alizarin Red S (0.2g.) dissolved in 100ml. of 1.5% HCl.
(2) Potassium Ferricyanide (2.0gm) dissolved in 100ml. of 1.5% HCl.
(3) These solutions were mixed in a ratio of 3 parts Alizarin Red S to 2 parts Potassium Ferricyanide.
(4) Half of each polished section was dipped in 1.5% HCl for 15 seconds for slight etching then rinsed in deionised water.
(5) They were then half submersed in the mixed staining solution for 30 seconds then rinsed with deionised water.

The resultant colours exhibited by minerals is reflective also of their iron content. Calcite will exhibit pale pink-red colour, ferroan calcite mauve-purple-royal blue whilst dolomite will exhibit no colur and ferroan dolomite will exhibit pale-deep turquoise colour depending on ferrous content.

A3.2 Cathodoluminescence.

Polished thin sections were analysed for carbonate cement stratigraphy and for any obvious carbonate alteration textures using a Technosyn Cold Cathode Luminoscope Model 8200 attached to a Leitz microscope. Although actual carbonate mineral species can not be conclusively determined using this microscopic technique, deductions can be made about mineral history given that luminescence is brought about by the elemental chemistry (amount of Mn versus Fe) of the mineral (Paeche, 1995).

A3.3 X-ray Diffraction.

Descriptions are accompanied by an XRD trace that plots degrees 2ϑ against total counts. Smears of crushed whole rock sample powders were analysed in a Siemens X-Ray Diffractometer to determine minerals present. Relative quantities of minerals were determined using peak height measurement plotted on correction curves (after Lemon, 1988, Tennant and Berger, 1957). Semi-quantitative dolomite iron content was measured via the d-spacing of the primary dolomite peak at approximately 36.1˚ 2Ø using a dolomite-ankerite correction curve (after McClune and Macguire, 1980).

Abbreviated macro rock descriptions follow no strict convention, as samples collected in this study were often small, but big enough to suit the geochemical purposes. Greater macro-description accompanied sections measured.

SAMPLE: 1041-17
FORMATION: Brighton Limestone LOCATION: Depot Flat

MACRO: Blue intraclastic packestone. Dominantly oolitic and micritic, moderately crystalline with a yellow/orange stylolitic after clastic fabric.

MICRO: quartz grain ave. 0.1mm, intraclasts to 10mm long.
Composition: 5% Quartz, 2% Plagioclase, 40% Calcitic micrite, 15% Dolomitic micrite, 12% micaceous hematite muds, 26% Poikilotopic interstitial spar.
Dolomite d-spacing: 2.889 - $Ca_{(1.0)}Mg_{(0.91)}Fe_{(0.01)}(CO_3)_2$

Comments: Dark micritc dolomite early stage cement binding ooids in reworked intraclasts. Same luminescent signature as early calcite cements indicates precipitation from similar sea water chemistry. Early cement stages include micaceous hematite muds. Late stage calcite spar cements pore space as opposed to recrystallisation cement. Three separate stages of interstitial spar may be indentified from crystal growth, beginning with a thin iron-rich black stage, followed by a thick brightly luminescent stage and a final pore occluding moderately luminescent stage. Rare fabric-cutting calcite veins are brightly luminescent.

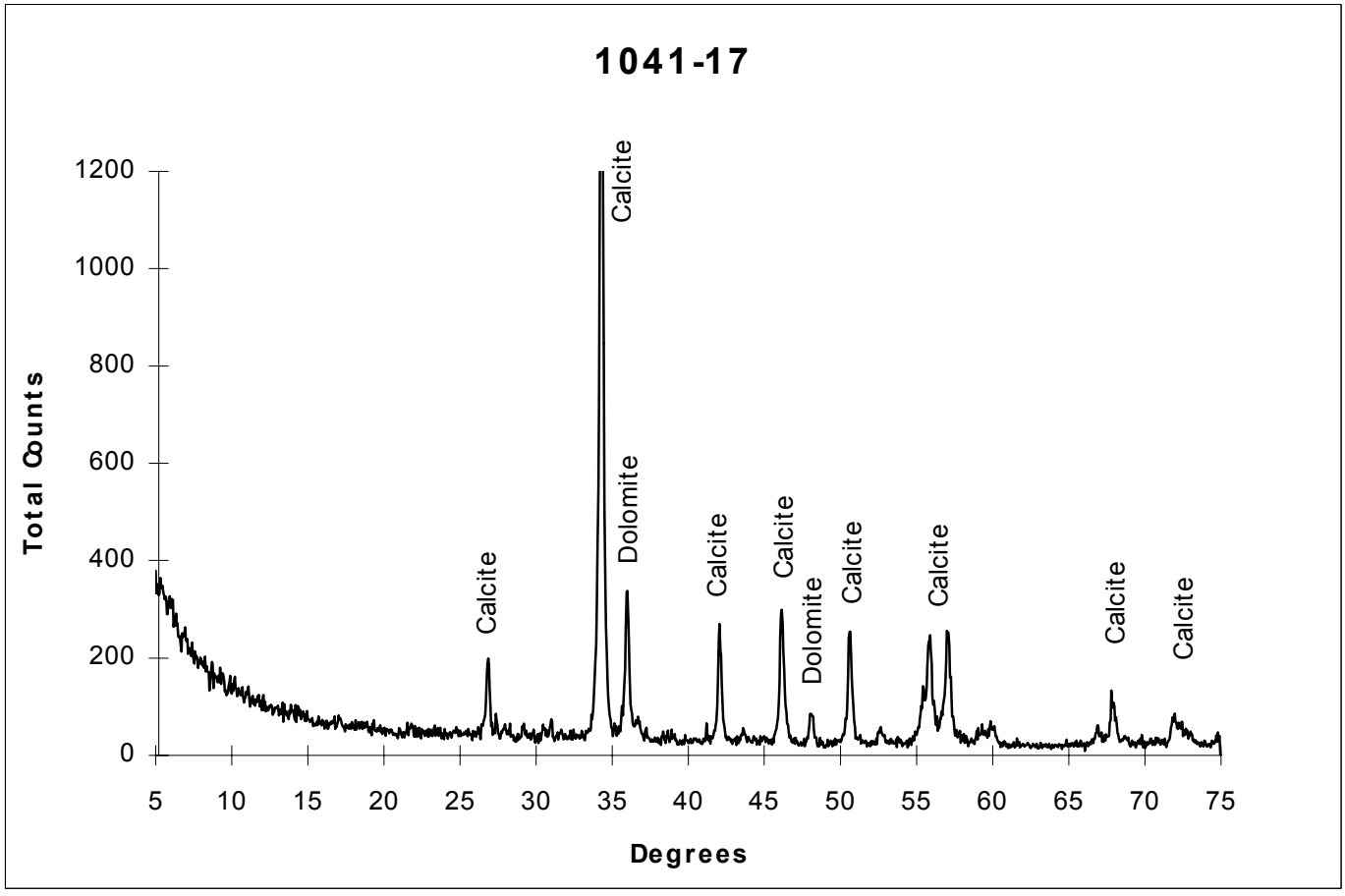

SAMPLE: 1041-19
FORMATION: Brighton Limestone LOCATION: Depot Flat

MACRO: Blue intraclastic packestone. Dominantly oolitic and micritc, moderately crystalline with a yellow/orange fenestral to stylolitic fabric.

MICRO: rare quartz 0.01-0.05mm grains, intraclast size 10-50mm across
Composition: 5% Quartz, 2% Plagioclase, 40% micritc Calcite, 28% dolomitic micrite, 4% hematitic mud, 21% Blocky interstitial calcite spar.
Dolomite d-spacing: 2.885 - $Ca_{(1.0)}Mg_{(0.98)}Fe_{(0.02)}(CO_3)_2$

Comments: Ooids medium to coarse sand size with minor crystalline cores. Micritc dolomite commonly early ooid-rim cement with some rare recrystallised xenotopic forms in reworked intraclasts. Dolomite is dull luminescent but no colour under stain. Early stage micritc calcite stains purple - relatively iron rich whereas blocky pore filling late stage calcite spar stains pink. This latest stage calcite spar has characteristic bright orange luminescence. Minor calcite veins luminesce dull orange in continuity with the majority of this limestone.

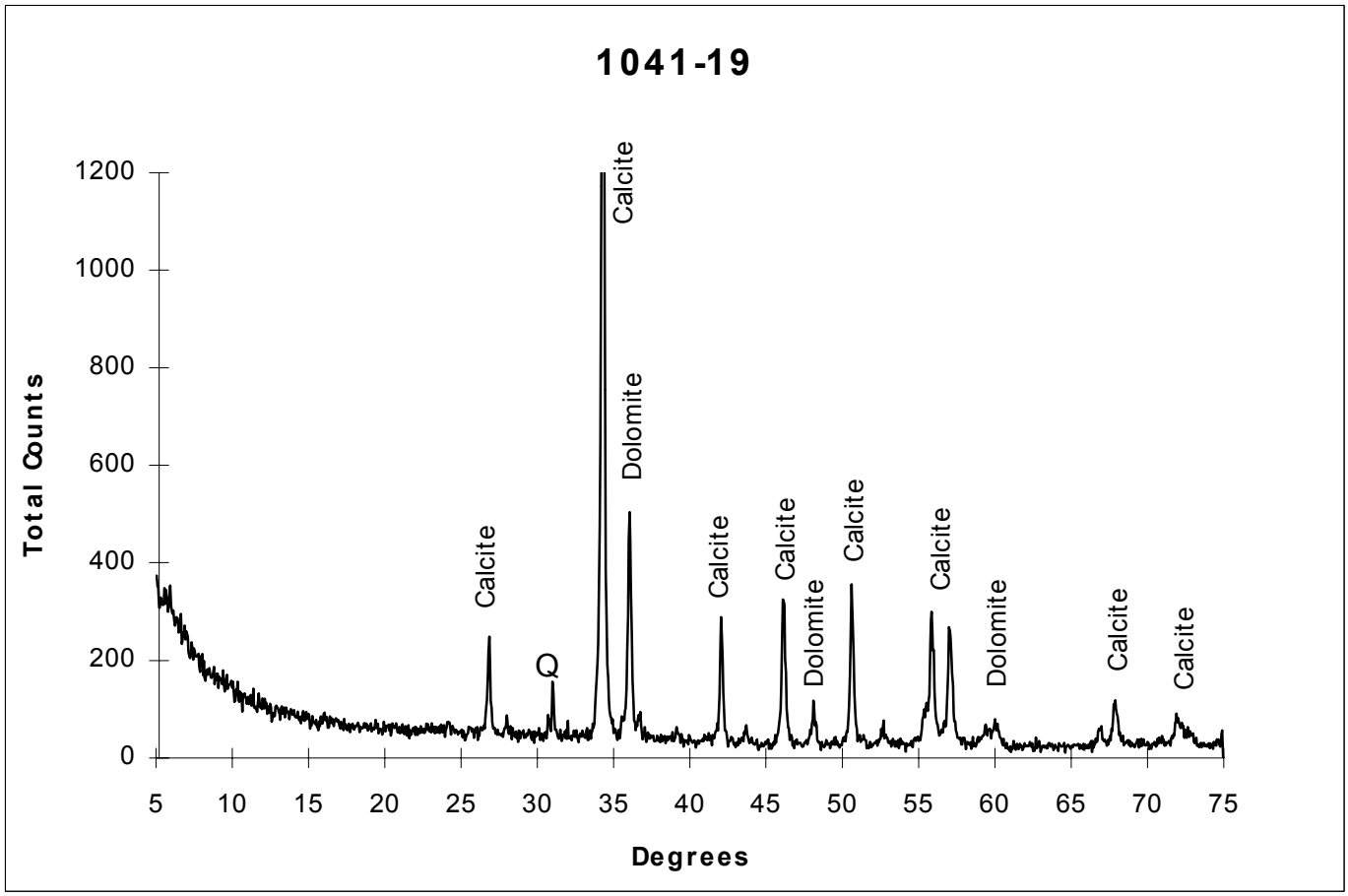

SAMPLE: 1041-25
FORMATION: Etina Formation LOCATION: Gum Creek

MACRO: Blue-grey broad-stomatolitic limestone.

MICRO: moderate-poorly sorted, angular grains size average 0.05mm (max.=0.1mm)
Composition: 19% Quartz, 8% Plagioclase, 4% Orthoclase (commonly microcline), 58% micritic Calcite (2% vein spar), 4% Hematite/heavy minerals, 3% Lithic fragments, 2% mud, 2% Chlorite.

Comments: Quartz is generally mono-crystalline, lacking overgrowth cements and slightly etched by carbonate cements. Grains retain original angularity and the mineralogic immaturity suggests minimal sediment transport. Feldspars show slight indication of alteration to carbonate. Authigenic chlorite after muds defining cyanobacterial laminae. Cathodoluminescence defines dark rhombic forms in clastic parts of this rock, perhaps original Fe-rich dolomite recrystallized to fine calcite early diagenesis. Cement stratigraphy belies the carbonate's biogenically acquired origin.

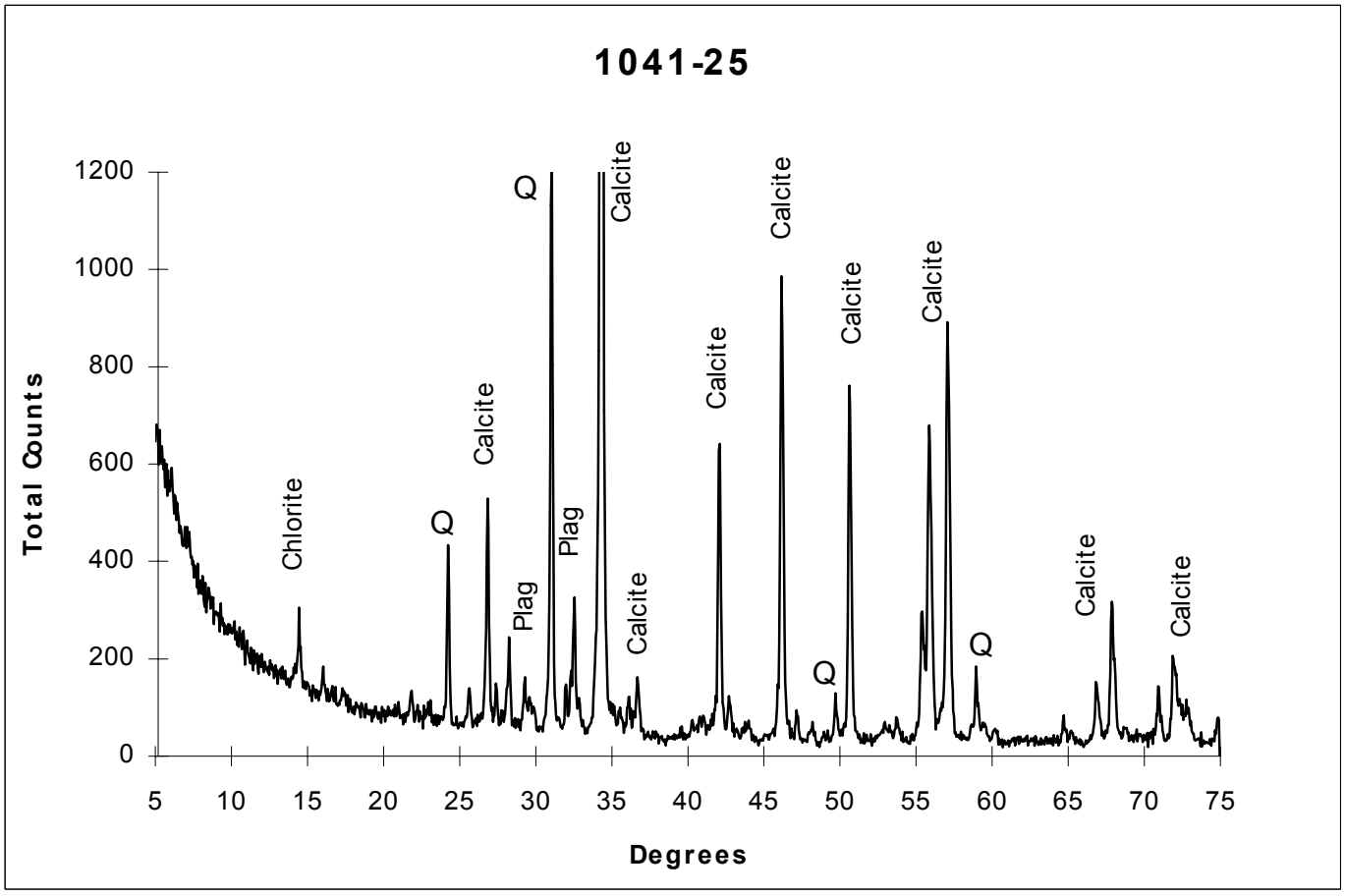

SAMPLE: 1041-31
FORMATION: Etina Formation LOCATION: Gum Creek

MACRO: Blue-grey fine sandy digitate stromatolitic Limestone.

MICRO: poorly sorted, moderate to well rounded grain size 0.05-2mm
Composition: Quartz 38% (of that 18% chert), 12% Plagioclase, 14% Orthoclase (commonly microcline), 19% Calcite, 4% Hematite, 13% Dolomite.
Dolomite d-spacing: 2.885 - $Ca_{(1.0)}Mg_{(0.98)}Fe_{(0.02)}(CO_3)_2$

Comments: Mineralogically very immature. Many feldspars, including microcline, at various stages of alteration to carbonate. All grains, including chert and calcareous lithic grains, are moderatly to well rounded, commonly have inclusions and a weathered-exposed-diapiric origin is suggested. A brightly birefringent thin carbonate phase coats all grains. Purple-stained Fe-rich calcite as well as non-coloured dolomite common in variety of carbonate clasts. Late stage porosity occluding dolomite cement stains blue and is thus iron-rich. Sutured grain contacts, as well as altering feldspar and etching of silica grains indicates moderate degree of compaction.

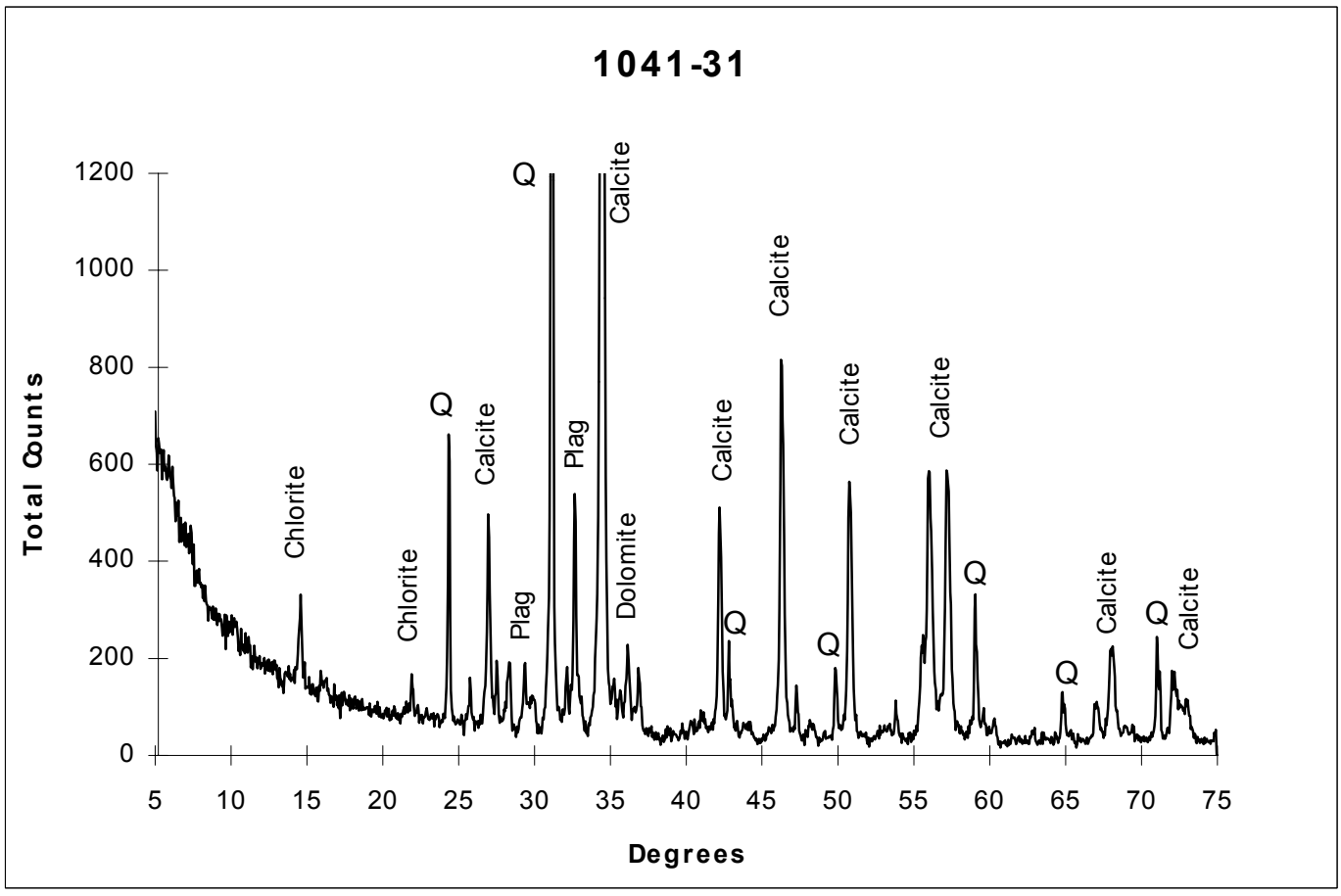

SAMPLE: 1041-35
FORMATION: Etina Formation LOCATION: Gum Creek

MACRO: Orange weathering, dark blue-grey calcareous/dolomitic lithic feldsarenite. Slightly bedded, medium grained, poorly sorted

MICRO: poorly sorted, moderate to well rounded grain size 0.05-2mm
Composition: Quartz 38% (of that 18% chert), 12% Plagioclase, 14% Orthoclase (commonly microcline), 19% Calcite, 4% Hematite, 13% Dolomite.
Dolomite d-spacing: 2.881 - $Ca_{(1.0)}Mg_{(1.0)}(CO_3)_2$

Comments: Mineralogically very immature. Many feldspars, including microcline, at various stages of alteration to carbonate. All grains, including chert and calcareous lithic grains, are moderatly to well rounded, commonly have inclusions and a weathered-exposed-diapiric origin is suggested. A brightly birefringent thin carbonate phase coats all grains. Purple-stained Fe-rich calcite as well as non-coloured dolomite common in variety of carbonate clasts. Late stage porosity occluding dolomite cement stains blue and is thus iron-rich. Sutured grain contacts, as well as altering feldspar and etching of silica grains indicates moderate degree of compaction.

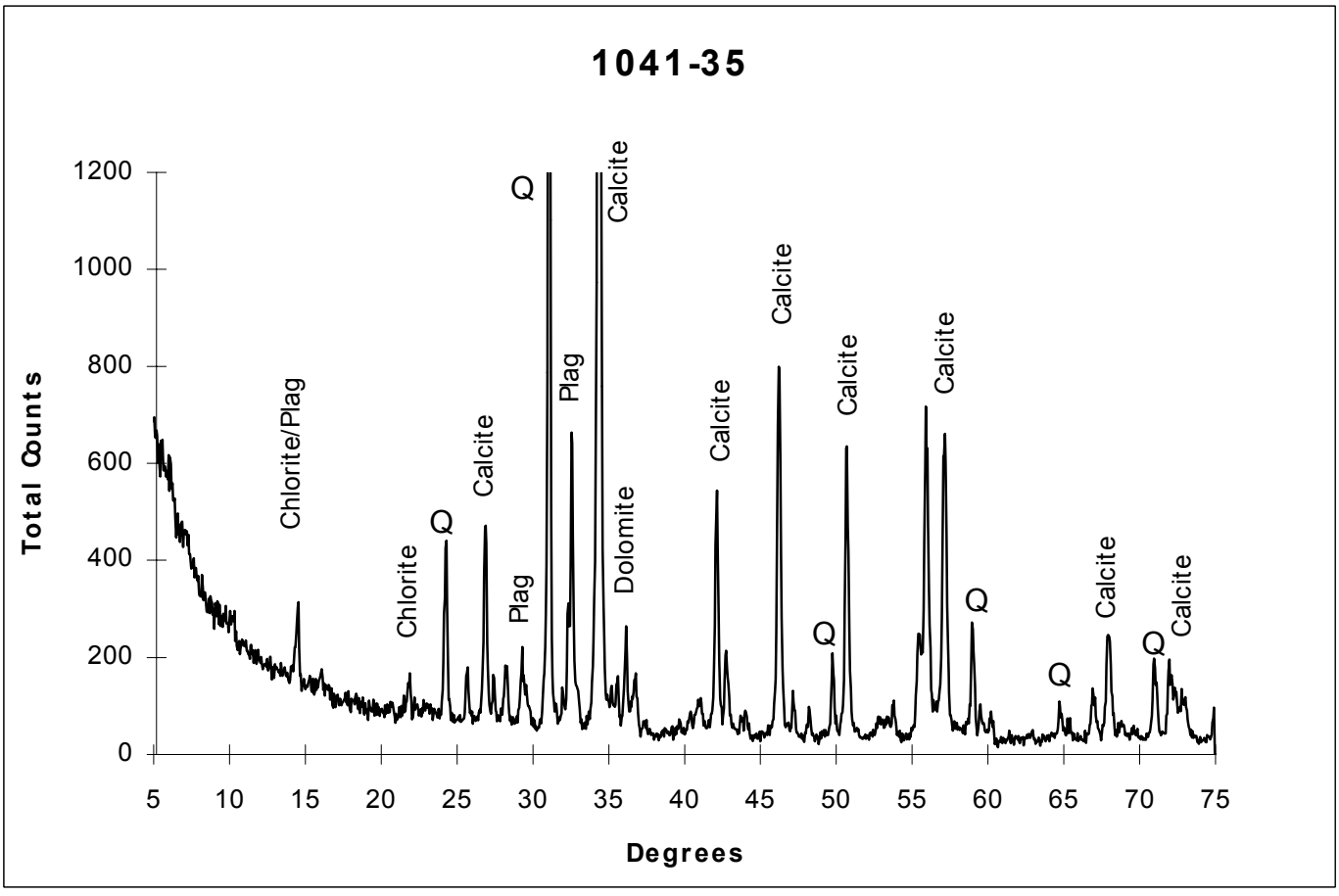

SAMPLE: 1041-37
FORMATION: Enorama Shale LOCATION: Dedmans Bore

MACRO: red massive slightly arenacous dolomicrite, rare (5-10%) visible detrital grains-poorly sorted fine sand, hummock-ripple current texture.

MICRO: poorly sorted, grain size 0.5-0.05mm
Composition: Quartz 21% (of that 15% chert), 5% Plagioclase, 2% lithic fragments, 2% heavy mineral (hematite), 2% detrital organics, 66% Dolomite as micrite and microspar.
Dolomite d-spacing: 2.885 - $Ca_{(1.0)}Mg_{(0.98)}Fe_{(0.02)}(CO_3)_2$

Comments: Recrystallizing quartz cements regularly include micro-dolomite rhombs. A solution seam veinlet cross cuts coarse plag. grains and is seen to facilitate recrystallisation of micrite to microspar and development of silica cements. High degree of siliciclastic etching indicates considerable post-burial compaction. Detrital cyanobacterial flake-like carbonaceous mud clasts are common.

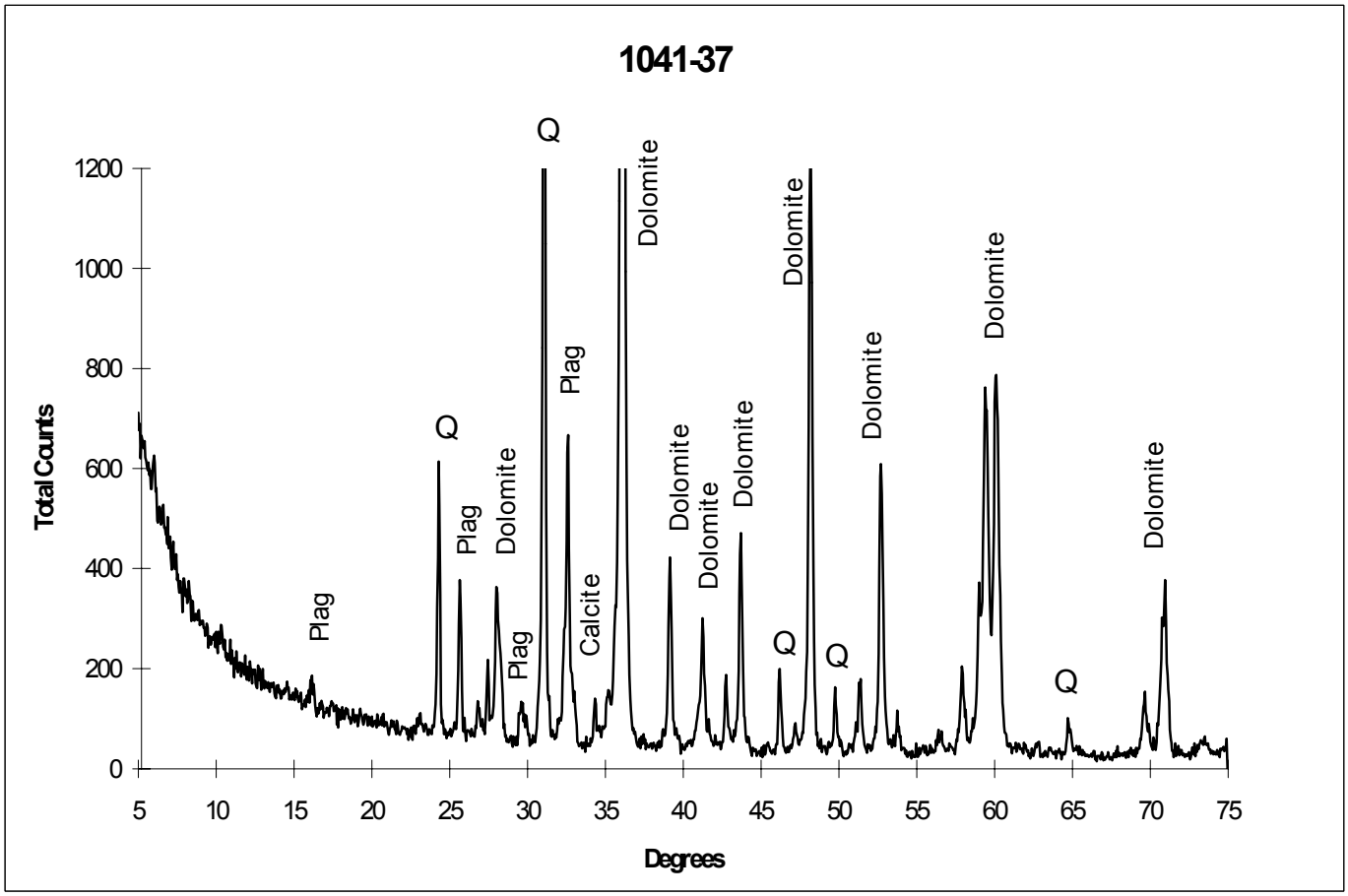

SAMPLE: 1041-38
FORMATION: Etina Formation LOCATION: First Spring

MACRO: Blue-green fine sandy limestone.

MICRO: poorly sorted, sub-angular grains size average 0.07mm (max.=0.4mm)
Composition: 41% Quartz, 12% Plagioclase, 6% Orthoclase, 23% micritic Calcite, 10% Micaceous Haematite/heavy minerals, 6% mud/chlorite clays, 2% Dolomite.
Dolomite d-spacing: 2.889 - $Ca_{(1.0)}Mg_{(0.91)}Fe_{(0.09)}(CO_3)_2$

Comments: Quartz is generally mono-crystalline but some minor chert, has occasional thin overgrowth cements and slightly etched by carbonate cements. Quartz overgrowths include silt sized (<0.01mm) rhombic dolomite inclusions. Grains exhibit little rounding or signs of weathering and the mineralogic immaturity suggests minimal sediment transport. Feldspars also have occasional overgrowth cement and show slight indication of alteration to carbonate. Red micaceous haematite exhibits euhedral form. Chloritic muds are generally incorporated in fine micritc interstitial mass. Very little difference in geochemistry and cathodoluminescence signature between original micrite and calcite alteration cements.

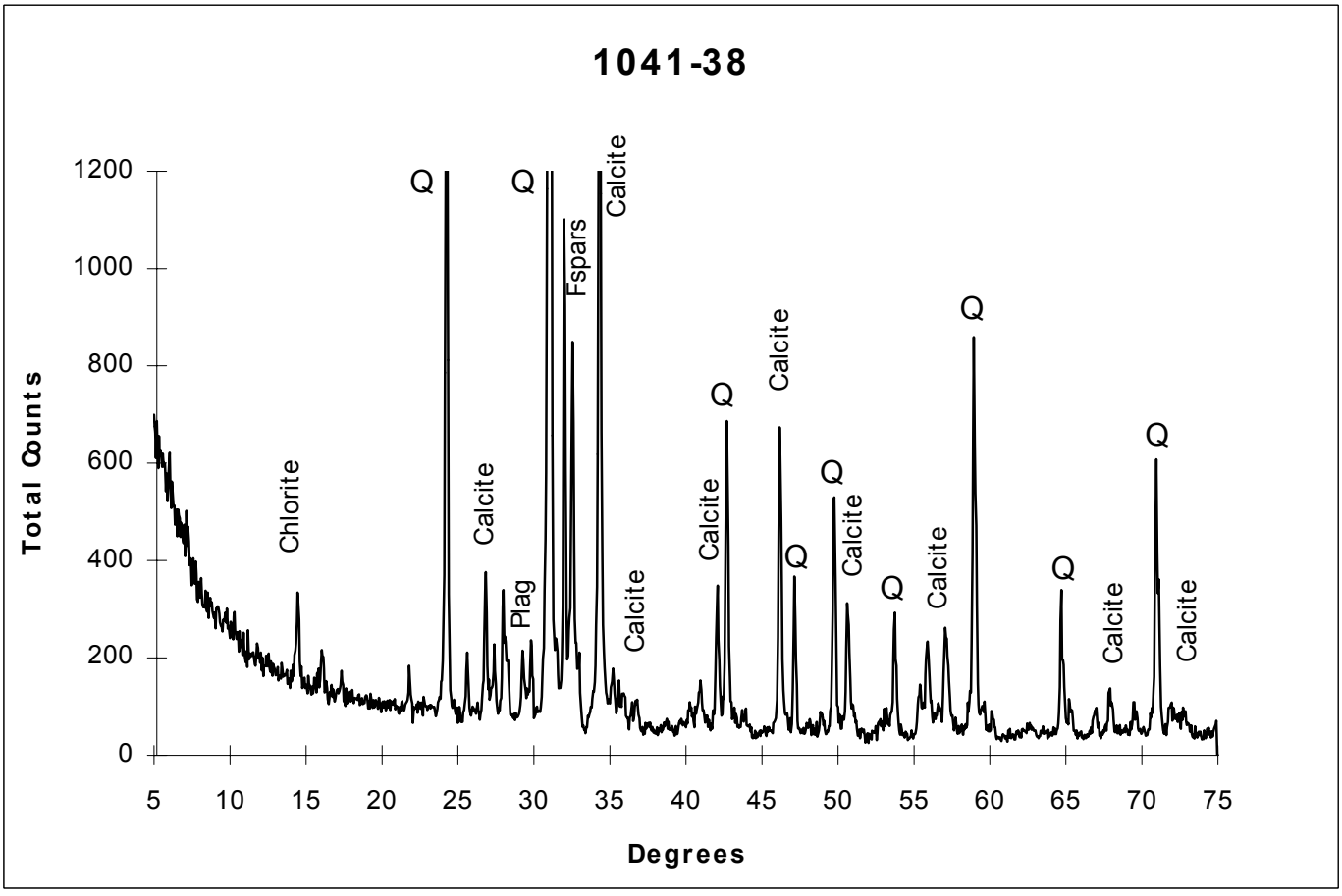

SAMPLE: 1041-39
FORMATION: Etina Formation LOCATION: First Spring

MACRO: Blue-green fine to medium sandy oolitic limestone.

MICRO: moderate-well sorted, sub-well rounded grains size average 0.2mm (max.=0.7mm)
Composition: 10% Quartz, 3% Plagioclase, 27% micritic Calcite (ooid), 46% interstitial cement Calcite, 3% Hematite/heavy minerals/muds, 9% Lithic fragments, 2% Dolomite (in clasts).
Dolomite d-spacing: 2.889 - $Ca_{(1.0)}Mg_{(0.91)}Fe_{(0.09)}(CO_3)_2$

Comments: Lithoclasts common in ooid cores, they include occasional dolomite. Silica ooid cores exhibit common euhedral overgrowth cement which breaches rim cement then is etched by the carbonate. Despite silica overgrowth cements, neither ooid nuclei or rims are recrystallised. Mud-defined bedding lamination generally micritic precluding ooids. Blocky interstitial spar exhibits generally dark/no luminescence, typical bladed-prismatic-like appearance of Mg-calcite cement of marine origin. Less common pore occluding brightly luminescing cement.

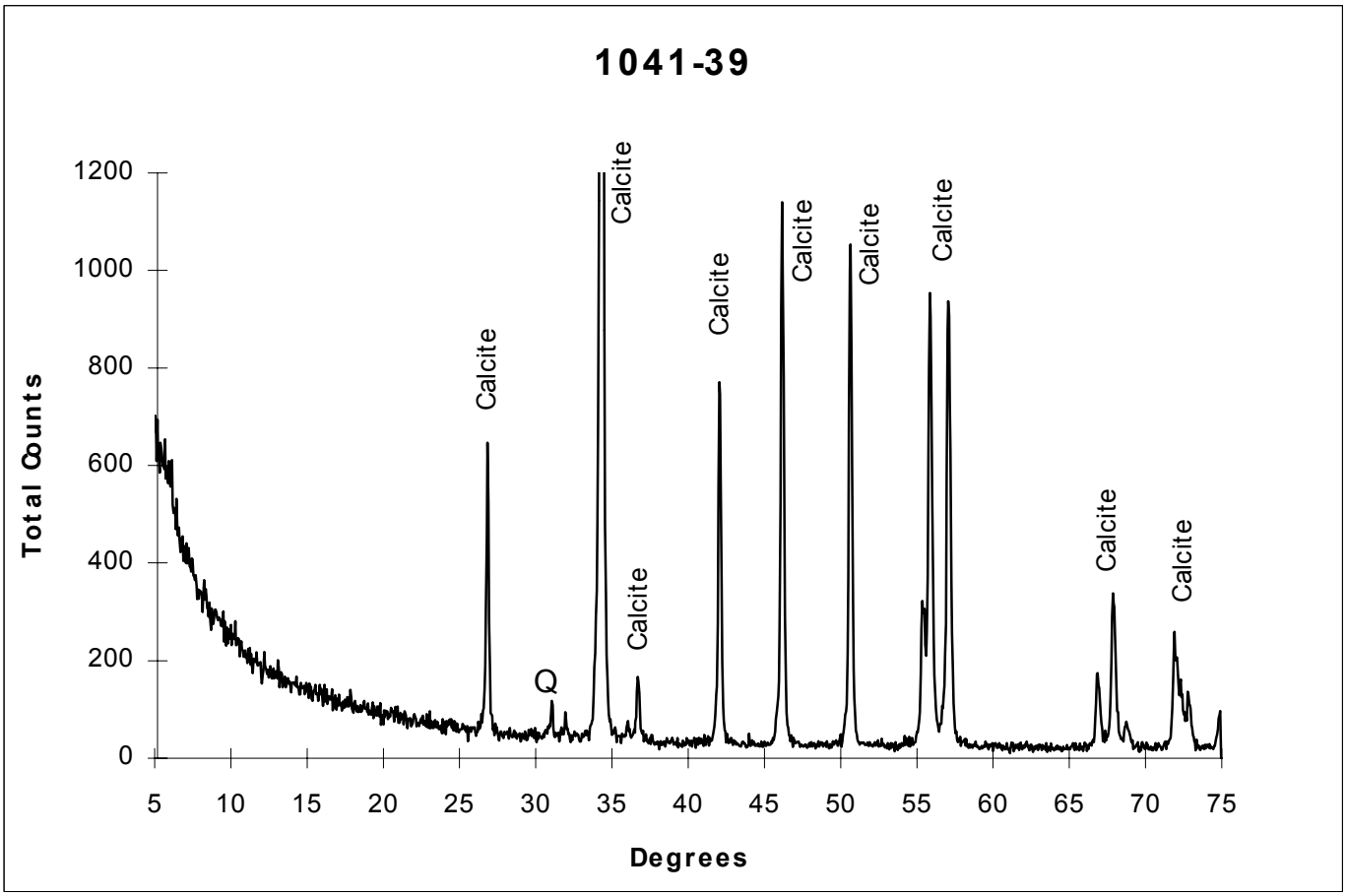

SAMPLE: 1041-53
FORMATION: Etina Formation LOCATION: First Spring

MACRO: Blue-grey medium sandy intraclastic limestone.

MICRO: moderately sorted, sub-well rounded ooids/grains size average 0.5mm (max.=1mm)
Composition: 20% Quartz, 7% Feldspar (commonly Orthoclase), 67% Calcite (41% ooid cores (lithic) and rims, 26% cements), 2% heavy minerals/opaques, 2% mud/clay, 2% Dolomite (also in lithic ooid cores).

Comments: Silicic ooid nuclei are well rounded, have minor overgrowth cements and are generally etching-encroached by carbonate. Quartz variety is both chert and mono-crystalline. Feldspars, mainly plagioclase, also with minor overgrowths, show slight indication of alteration. Peloidal to fine sandy lithic ooid nuclei are common and contain rhombic forms and varied carbonate mineral species. Cathodoluminescence once again defines restricted dark bladed-prismatic forms extra-ooids before lighter coloured interstitial mosaic calcspar. Very little compaction or dissolution evident, cement development primarily early burial.

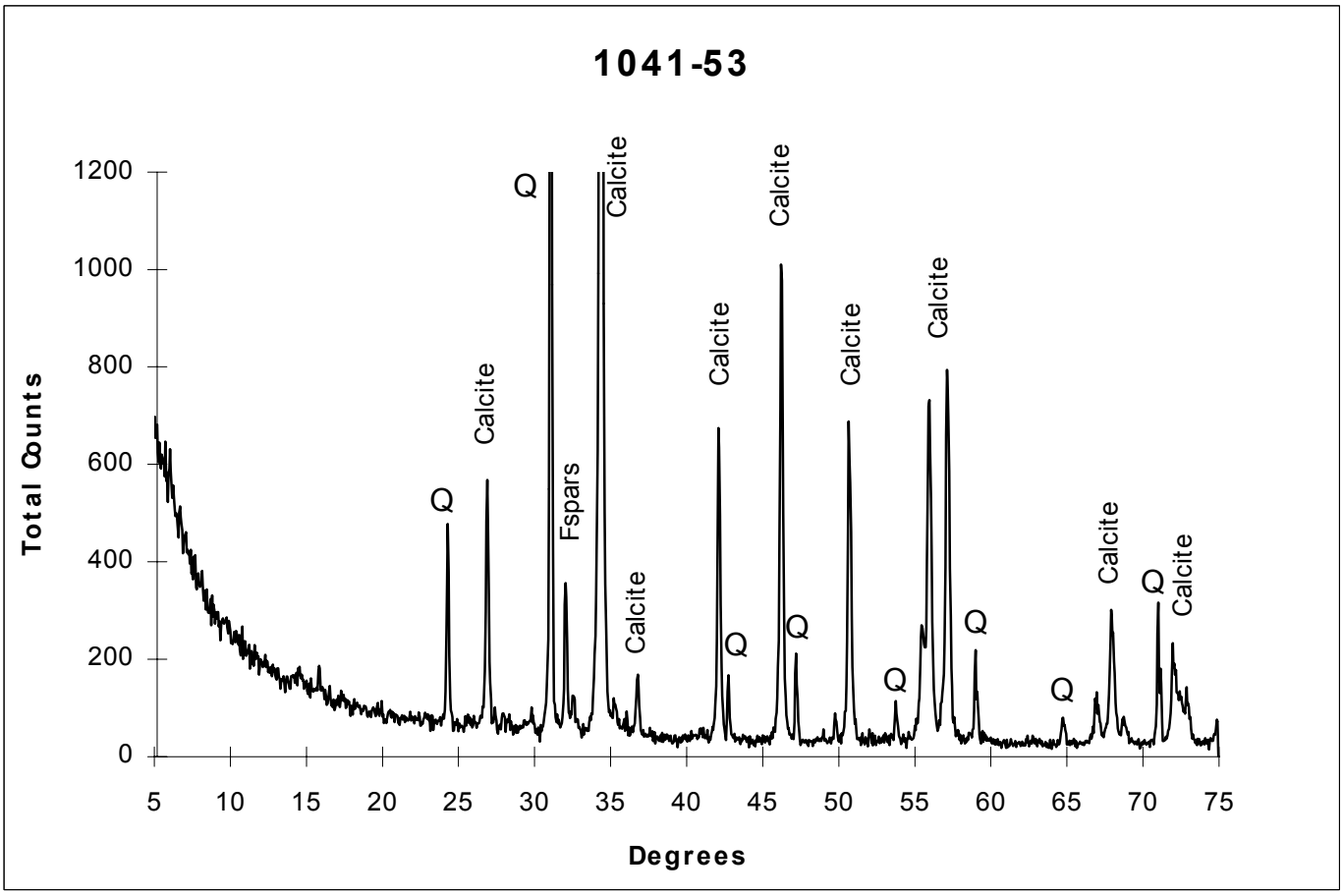

SAMPLE: 1041-54
FORMATION: Etina Formation LOCATION: First Spring

MACRO: Green-blue-grey fine sandy digitate-stomatolitic limestone.

MICRO: moderate-well sorted, sub-angular to sub-rounded grains, size average 0.07mm (max.=0.15mm)
Composition: 24% Quartz, 10% Feldspars (plagioclase and orthoclase), 48% Calcite (38% micrite, 14% detrital forms), 4% Dolomite, 8% heavy minerals/opaques, 6% mud/clays.
Dolomite d-spacing: 2.889 - $Ca_{(1.0)}Mg_{(0.91)}Fe_{(0.09)}(CO_3)_2$

Comments: Quartz, generally mono-crystalline, and feldspar exhibit minor overgrowth cements. Alternating dominantly clastic-dominantly micritic layers define a thin (1mm) bedding lamination. Cathodoluminescence delineates a diverse range of detrital carbonate species. Rare fine stylo-laminae are evident in the more micritic areas by a brightly luminescent signature.

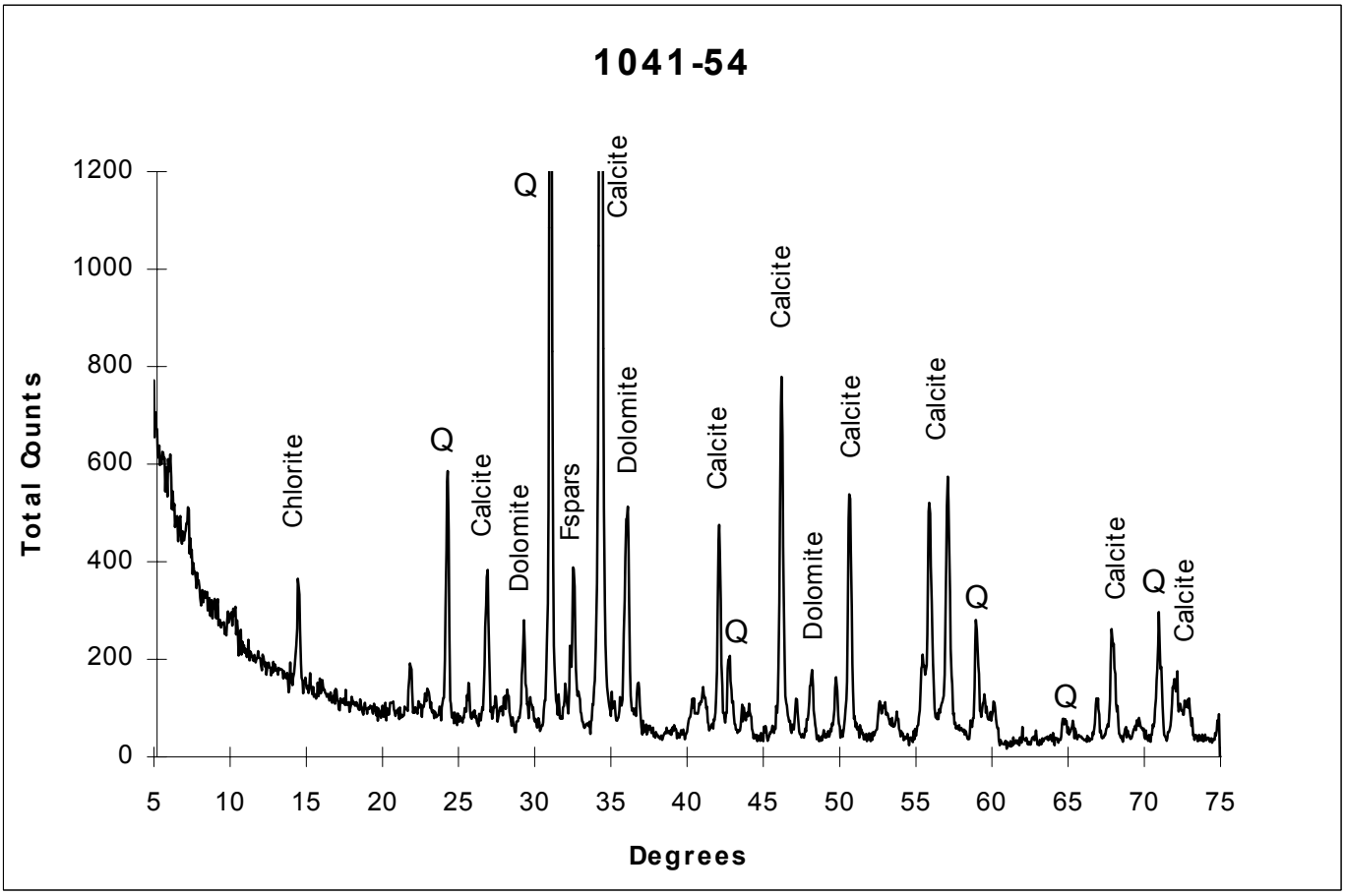

SAMPLE: 1041-58
FORMATION: Etina Formation LOCATION: First Spring

MACRO: Blue-grey coarse sandy intraclastic limestone.

MICRO: moderate-poorly sorted, sub-rounded grains size average 0.5mm (max.=20mm)
Composition: 12% Quartz, 6% Feldspars (commonly orthoclase), 67% Calcite (42% micrite (incl. intraclasts and ooids), 25% cements), 3% Dolomite, 3% heavy minerals/opaques, 9% Chlorite/mud/clays.
Dolomite d-spacing: 2.881 - $Ca_{(1.0)}Mg_{(1.00)}Fe_{(0.00)}(CO_3)_2$

Comments: Large reworked intraclasts of both fine grained stromatolitic and medium grained ooilitic limestone are mixed in with ooids that are indistinguishable in composition from those in reworked intraclasts. Quartz is generally mono-crystalline, well rounded, minorly etched and lacking overgrowth cements and feldspars show slight indication of alteration. Diverse range of ooid cores and variety of ooid rim thickness. Detrital dolomite has characteristic dark red luminescence. Thin, brightly luminescent stylo-laminae are rare in more-micritic areas. Dark bladed-prismatic cements sometimes coat ooids before lighter mosaic interstitial spar. General pervading calcite orange colour indicates micrite and cements of similar chemical composition.

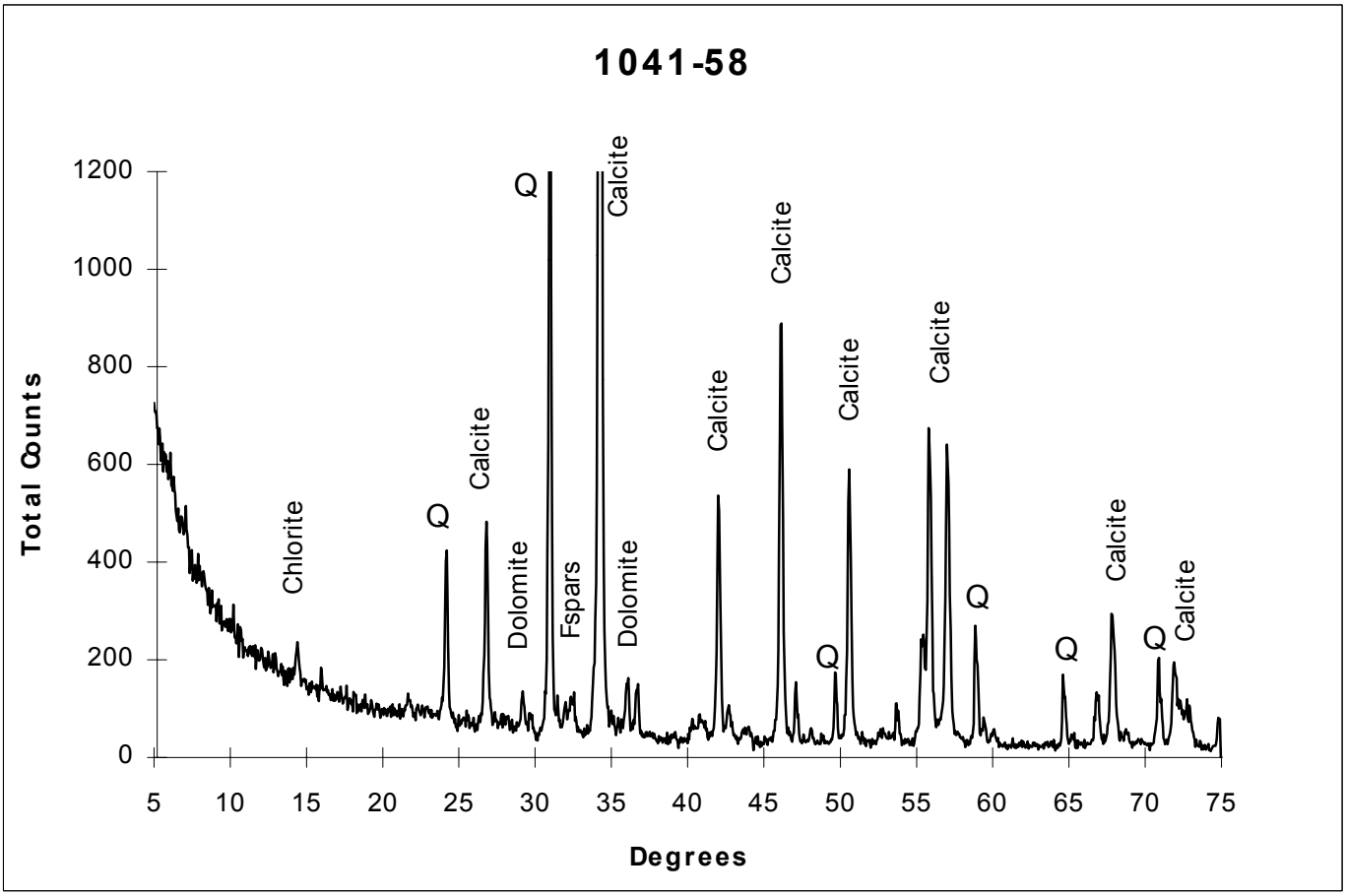

SAMPLE: 1041-64
FORMATION: Etina Formation LOCATION: First Spring

MACRO: Blue coarse sandy ooid limestone.

MICRO: moderate-well sorted, sub-rounded grains size average 0.7mm (max.=1.2mm)
Composition: 15% Quartz, 11% Feldspars (orthoclase and plagioclase), 69% Calcite (22% micritic ooids, 47% spar/cements), 2% heavy minerals/opaques, 3% mud/clay.

Comments: Silicic ooid cores exhibit common euhedral overgrowth forms but commonly have been etched/encroahced or altered. Quartz is generally mono-crystalline. Feldspars commonly exhibit alteration to carbonate. Cathodoluminescence defines rare bright rhombic forms included in ooid nuclei, along with a wide range of other lithic-carbonate components. Darkly luminescent blade-prismatic cement not strictly isopachous as seen before. More cements overall (silicic and carbonate) than other samples in this section. High degree of compaction increasing alteration and recrystallisation of calcite retaining luminescent signature.

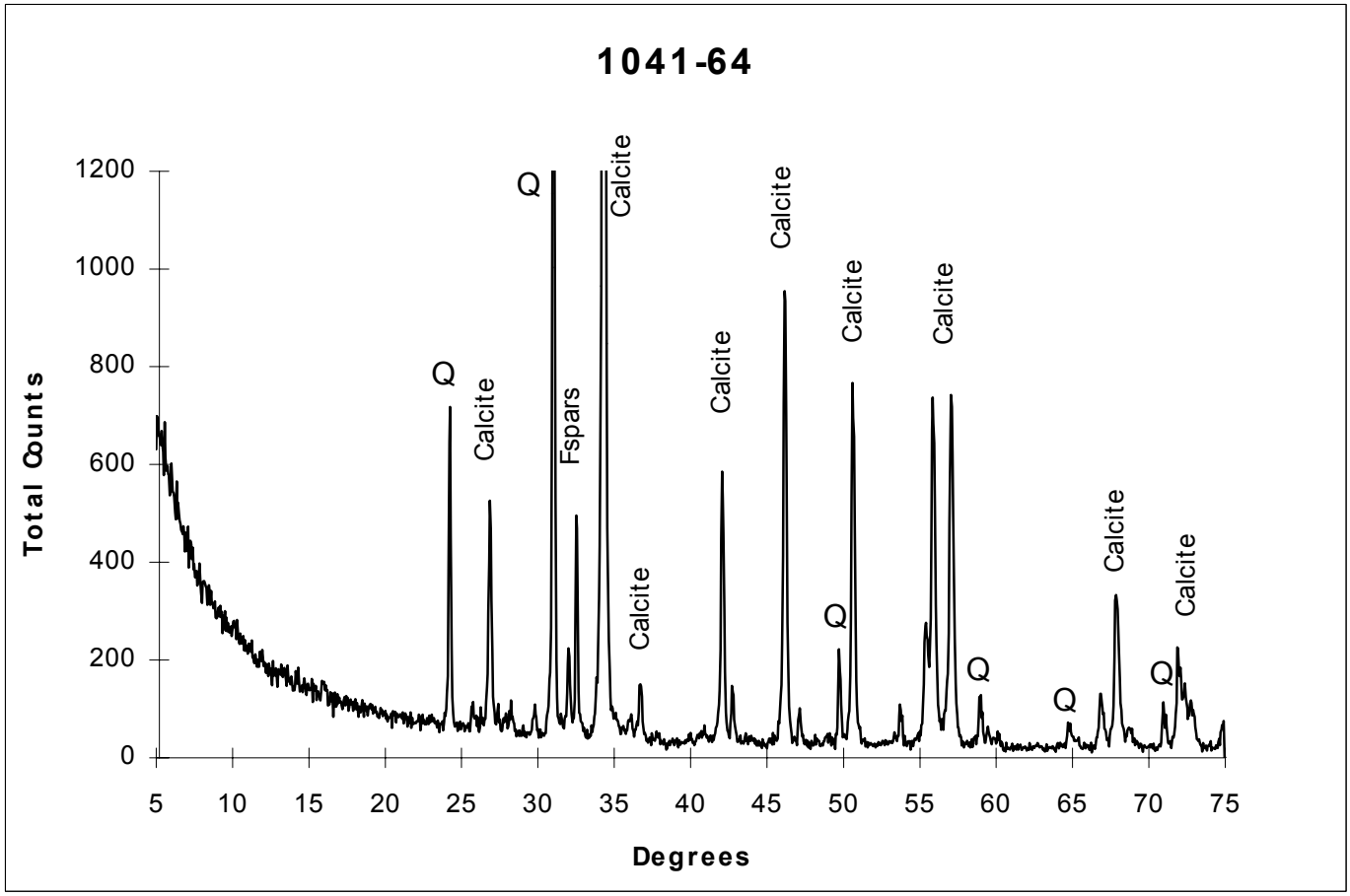

SAMPLE: 1041-66
FORMATION: Etina Formation LOCATION: First Spring

MACRO: Blue medium to coarse sandy intraclastic limestone.

MICRO: moderate-well sorted, rounded grains size average 0.5mm (max.=1.0mm)
Composition: 37% Quartz, 11% Feldspars (orthoclase and plagioclase), 41% Calcite (7% micrite, 11% detrital clasts, 23% cements), 4% Dolomite (detrital), 2% heavy mineral/opaques, 5% mud/alteration clays.
Dolomite d-spacing: 2.885 - $Ca_{(1.0)}Mg_{(0.98)}Fe_{(0.02)}(CO_3)_2$

Comments: Quartz is generally mono-crystalline, well rounded with very few overgrowth cements evident and etched by carbonate cements. A high degree of compaction is evident given common sutured and even concavo-convex grain contacts. Some rare euhedral overgrowth forms on orthoclase grains, little alteration but etching and encroachment by calcite cement common. Lithic and carbonate clasts of varied mineral species include a dark red dolomite rhomb also altering under compaction. Bladed early calcite cement forms are common before ubiquitous mosaic spar.

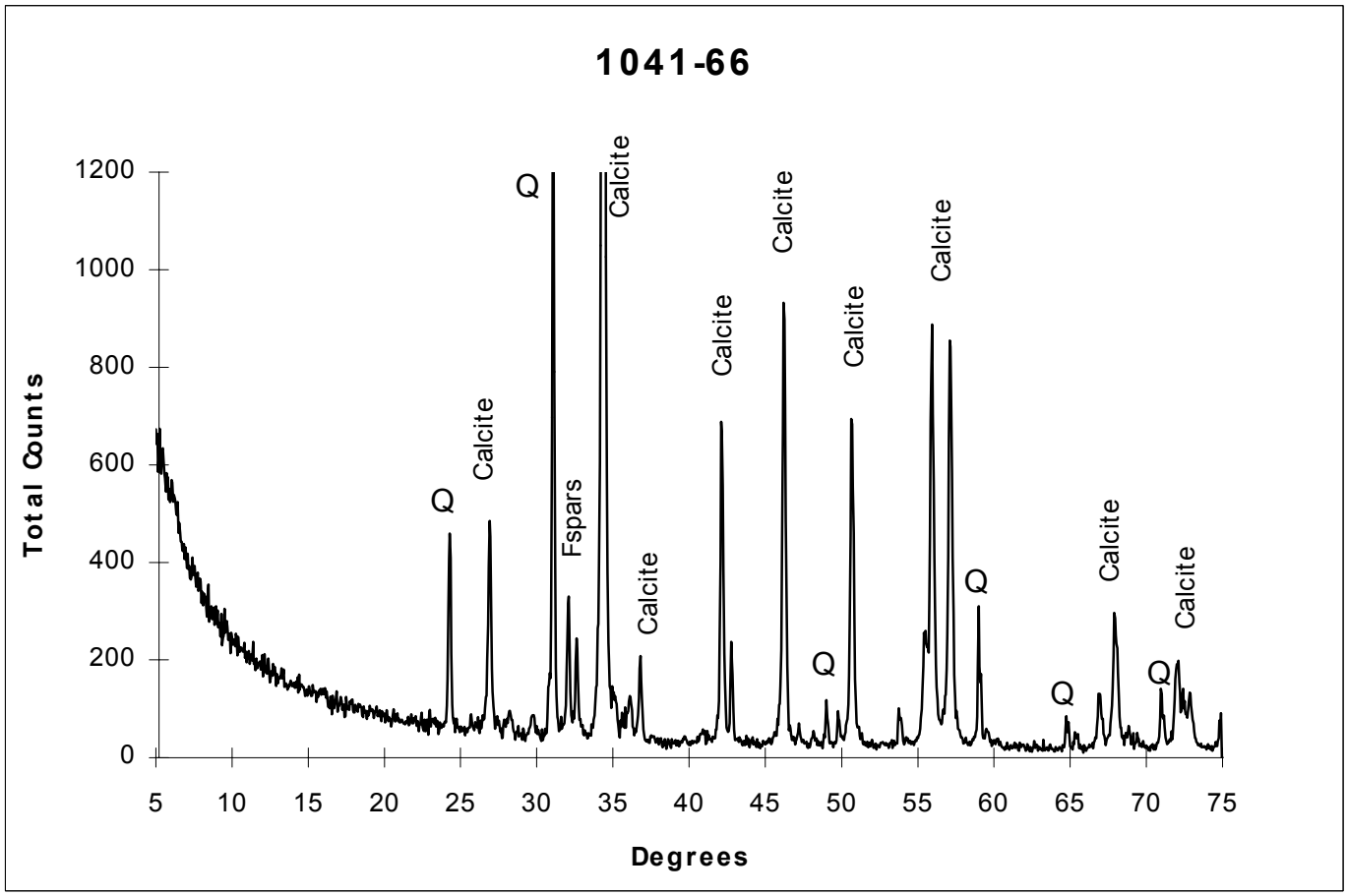

SAMPLE: 1041-68
FORMATION: Etina Formation LOCATION: First Spring

MACRO: Blue-green fine sandy digitate-stomatolitic limestone.

MICRO: poorly sorted, sub-angular grains size average 0.05mm (max.=0.1mm)
Composition: 21% Quartz, 9% Feldspars (orthoclase and plagioclase), 51% Calcite (37% micrite, 14% cements), 12% Dolomite (detrital), 3% heavy mineral/opaques, 4% mud/clays.
Dolomite d-spacing: 2.885 - $Ca_{(1.0)}Mg_{(0.98)}Fe_{(0.02)}(CO_3)_2$

Comments: Fine grained quartz is generally mono-crystalline with minor overgrowth cements. Feldspars also exhibit minor overgrowth cements and etching. Dominantly micritic calcite cement. Detrital dolomite is common, less common in fine rhombic form. Bladed-prismatic calcite cement among micrite indicative of early burial marine-influence diagenesis.

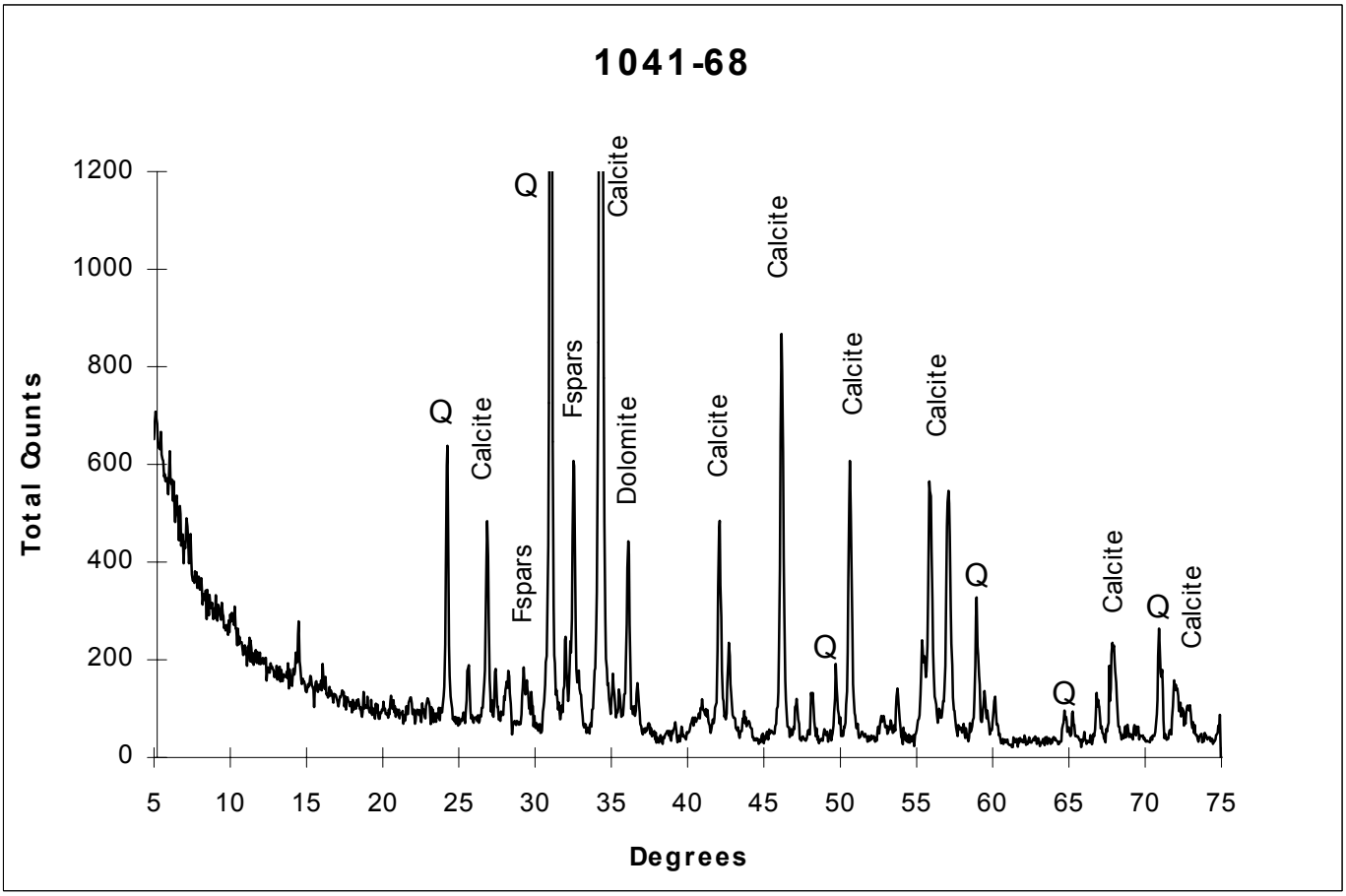

SAMPLE: 1041-69
FORMATION: Tapley Hill Formation LOCATION: Glass Gorge

MACRO: Orange weathering, dark blue-grey calcareous/dolomitic lithic feldsarenite. Slightly bedded, medium grained, poorly sorted

MICRO: poorly sorted, moderate to well rounded grain size 0.05-2mm
Composition: Quartz 38% (of that 18% chert), 12% Plagioclase, 14% Orthoclase (commonly microcline), 19% Calcite, 4% Hematite, 13% Dolomite.
Dolomite d-spacing: 2.885 - $Ca_{(1.0)}Mg_{(0.98)}Fe_{(0.02)}(CO_3)_2$

Comments: Mineralogically very immature. Many feldspars, including microcline, at various stages of alteration to carbonate. All grains, including chert and calcareous lithic grains, are moderatly to well rounded, commonly have inclusions and a weathered-exposed-diapiric origin is suggested. A brightly birefringent thin carbonate phase coats all grains. Purple-stained Fe-rich calcite as well as non-coloured dolomite common in variety of carbonate clasts. Late stage porosity occluding dolomite cement stains blue and is thus iron-rich. Sutured grain contacts, as well as altering feldspar and etching of silica grains indicates moderate degree of compaction.

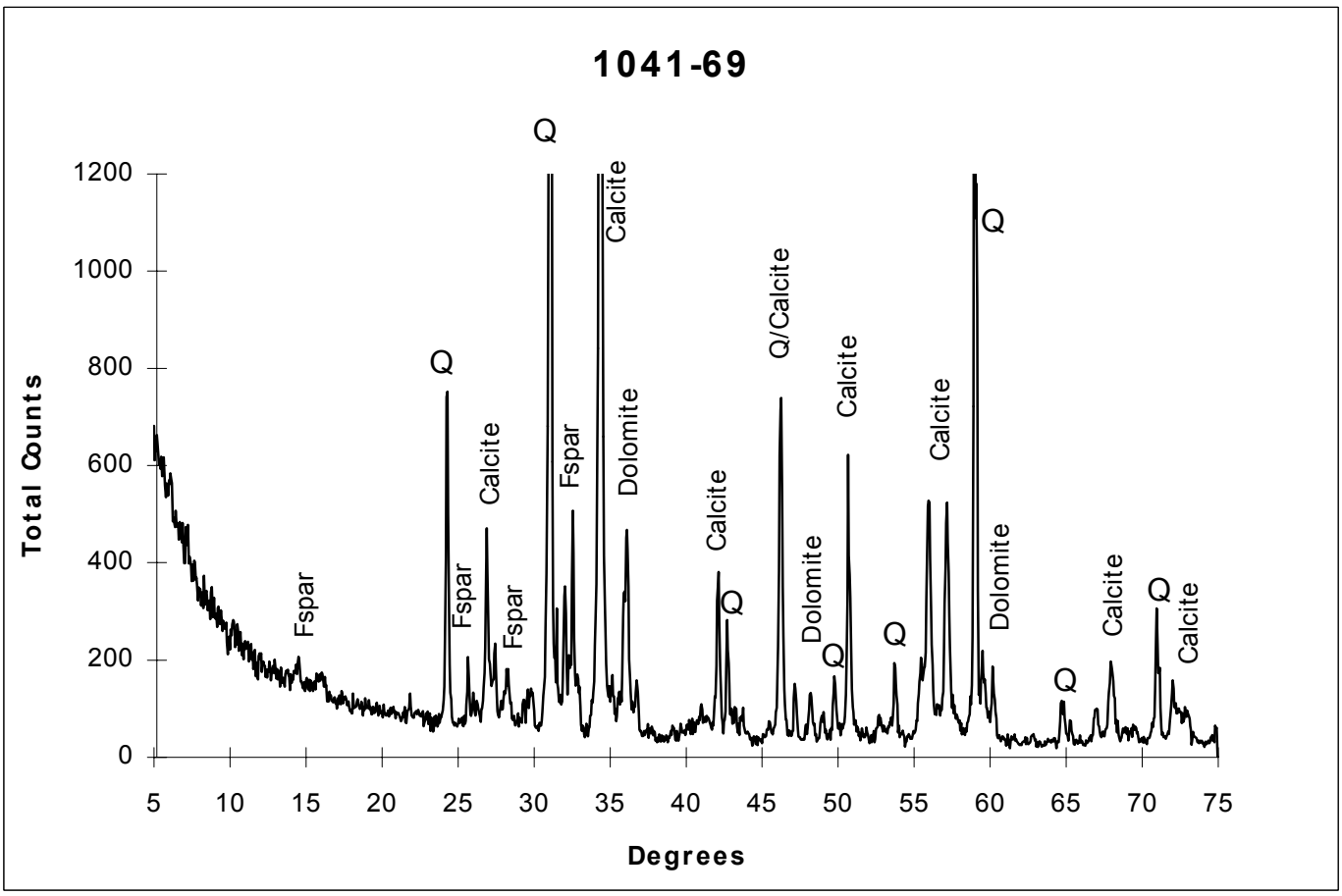

SAMPLE: 1041-80
FORMATION: Enorama Shale LOCATION: Mallee Water

MACRO: Orange-brown stomatolitic limestone.

MICRO: moderate-poorly sorted, dispersed minor clastic content, grains size average 0.05mm (max.=0.2mm)
Composition: 5% Quartz, 91% Dolomite, 4% Carbonaceous/mud/heavy mineral.
Dolomite d-spacing: 2.885 - $Ca_{(1.0)}Mg_{(0.98)}Fe_{(0.02)}(CO_3)_2$

Comments: Dominant orange-brown dolomitic micrite to microspar with globular or clotted texture. Slight carbonaceous material collected in cryptomicrobial to fenestral laminae. Cathodoluminescence discerns minor bright yellow-orange dolomite phase coating and sometimes filling vugs from dominant orange-brown microsparite. Authigenic quartz phases fill out remaining vug porosity.

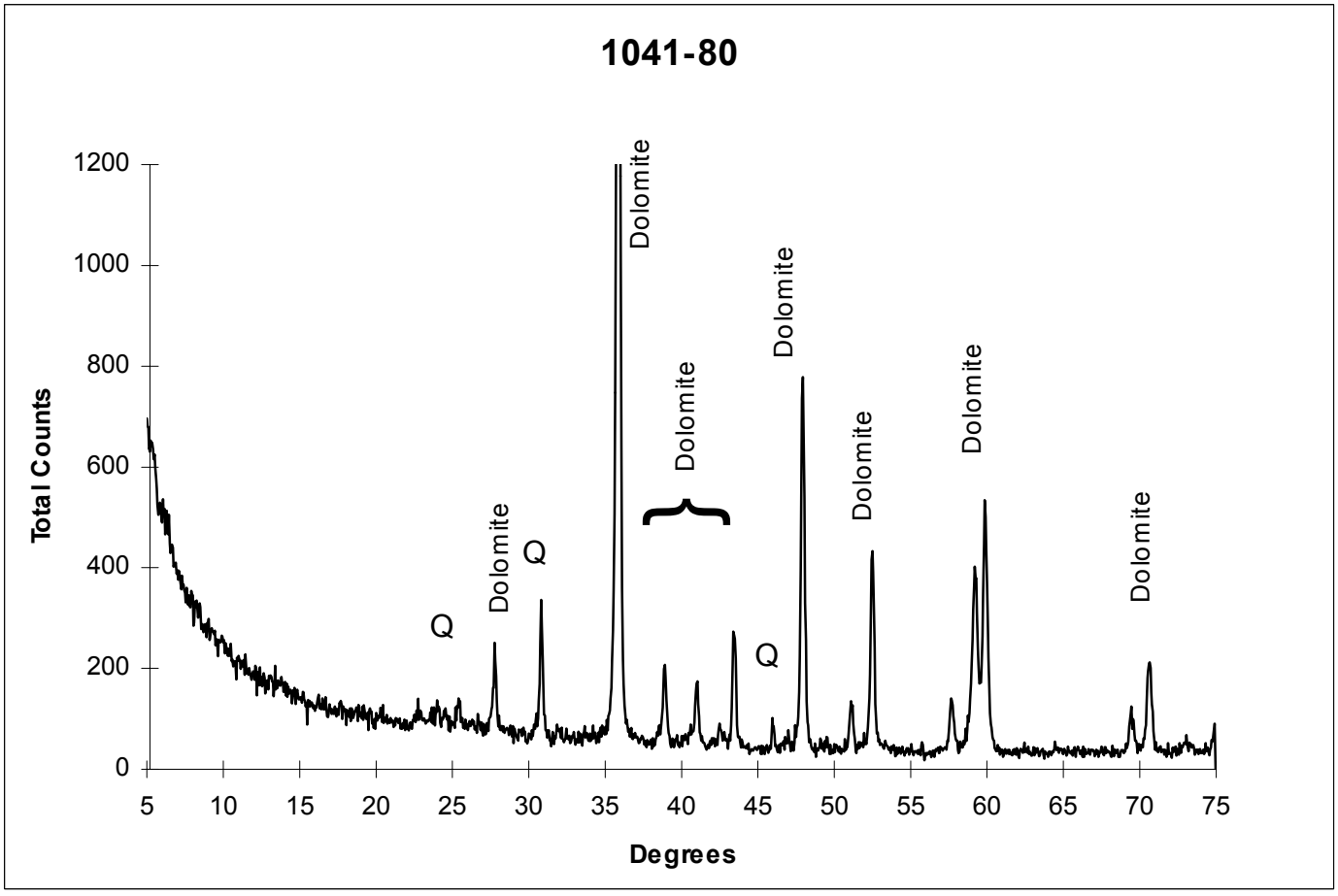

SAMPLE: 1041-83
FORMATION: Enorama Shale LOCATION: Mallee Water

MACRO: Buff brown fine sandy stomatolitic limestone.

MICRO: moderate-poorly sorted, dispersed minor clastic content, grains size average 0.05mm (max.=0.2mm)
Composition: 8% Quartz, 2% Orthoclase (commonly microcline), 87% Dolomite, 3% mud/heavy minerals.
Dolomite d-spacing: 2.885 - $Ca_{(1.0)}Mg_{(0.98)}Fe_{(0.02)}(CO_3)_2$

Comments: Dominant dolomicrosparite with globular texture. Early diagenetic thin quartz filled stylo-laminae low angle oblique to stromatolitic lamination. Cathodoluminescence defines thin, brighter orange dolomite cement coating shrinkage vugs and bright yelllow patches, possibly included acquiescent carbonate xenoclasts but more likely restricted pore occluding late diagenetic cement. Authigenic quartz and minor orthoclase phases fill out vug porosity.

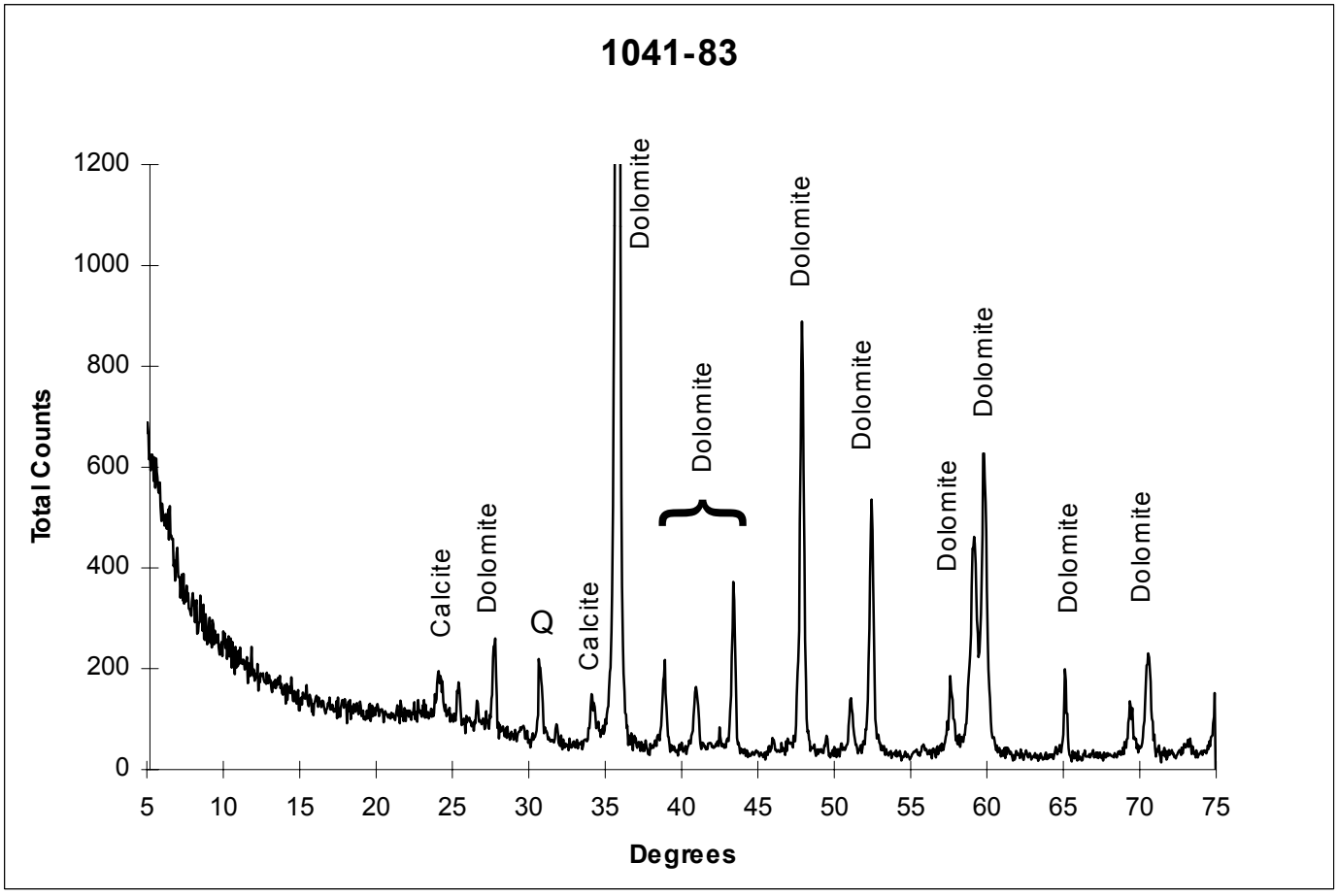

SAMPLE: 1041-84
FORMATION: Enorama Shale LOCATION: Mallee Water

MACRO: Orange-brown stomatolitic limestone.

MICRO: moderate-poorly sorted, sub-angular grains size average 0.05mm (max.=0.3mm)
Composition: 7% Quartz, 5% Feldspars (commonly Orthoclase), 72% Dolomite, 12% Carbonaceous muds, 3% Lithic fragments.
Dolomite d-spacing: 2.885 - $Ca_{(1.0)}Mg_{(0.98)}Fe_{(0.02)}(CO_3)_2$

Comments: Dominant orange-brown dolomitic micrite to microspar with globular or clotted texture. Carbonaceous material at times centred on vugs and dispersed into micrite creating dark stain. More, predominantly fine grained, detrital input indicated by higher feldspar content and inclusion of detrital, dark orange luminescent, carbonate. Green specks are as much, if not more, the diamond polishing paste used in thin sectioning as very fine grained plagioclase. Late stage yellow orange dolomite developed into vugs, sometimes in rhombic form.

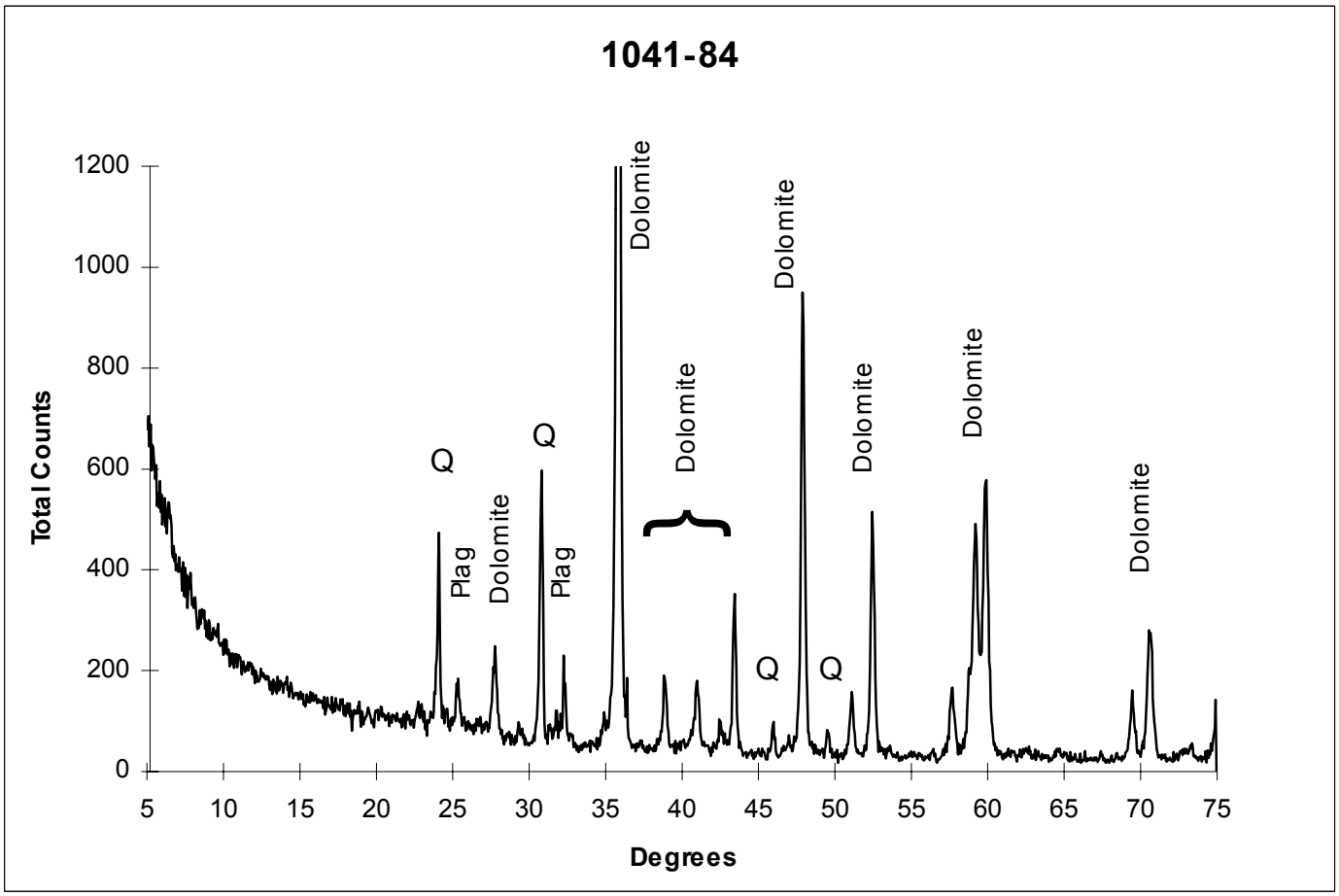

SAMPLE: 1041-87
FORMATION: Enorama Shale LOCATION: Mallee Water

MACRO: Red fine sandy and intraclastic limestone.

MICRO: poorly sorted, sub-angular grains size average 0.2mm (max.=10mm)
Composition: 10% Quartz, 6% Feldspar (commonly Orthoclase), 63% Dolomite, 6% Carbonaceus mud/heavy minerals (including pyrite), 15% Lithic fragments.
Dolomite d-spacing: 2.885 - $Ca_{(1.0)}Mg_{(0.99)}Fe_{(0.01)}(CO_3)_2$

Comments: Dominant dolomicrite has not developed the characteristic clotted texture of previous reef stones, instead this rock is influenced by intraclasts including dolomicrite-mud flakes. Small amounts of interstitial vug porosity has been filled with previously described brightly luminescent isopachous dolomite cement and authigenic quartz. Lithoclasts are of typical xenoclastic diversity. Small amounts of carbonaceous mud with characteristic adjacent micrite staining are reworked. One thin (~1mm) microfracture is filled with authigenic quartz.

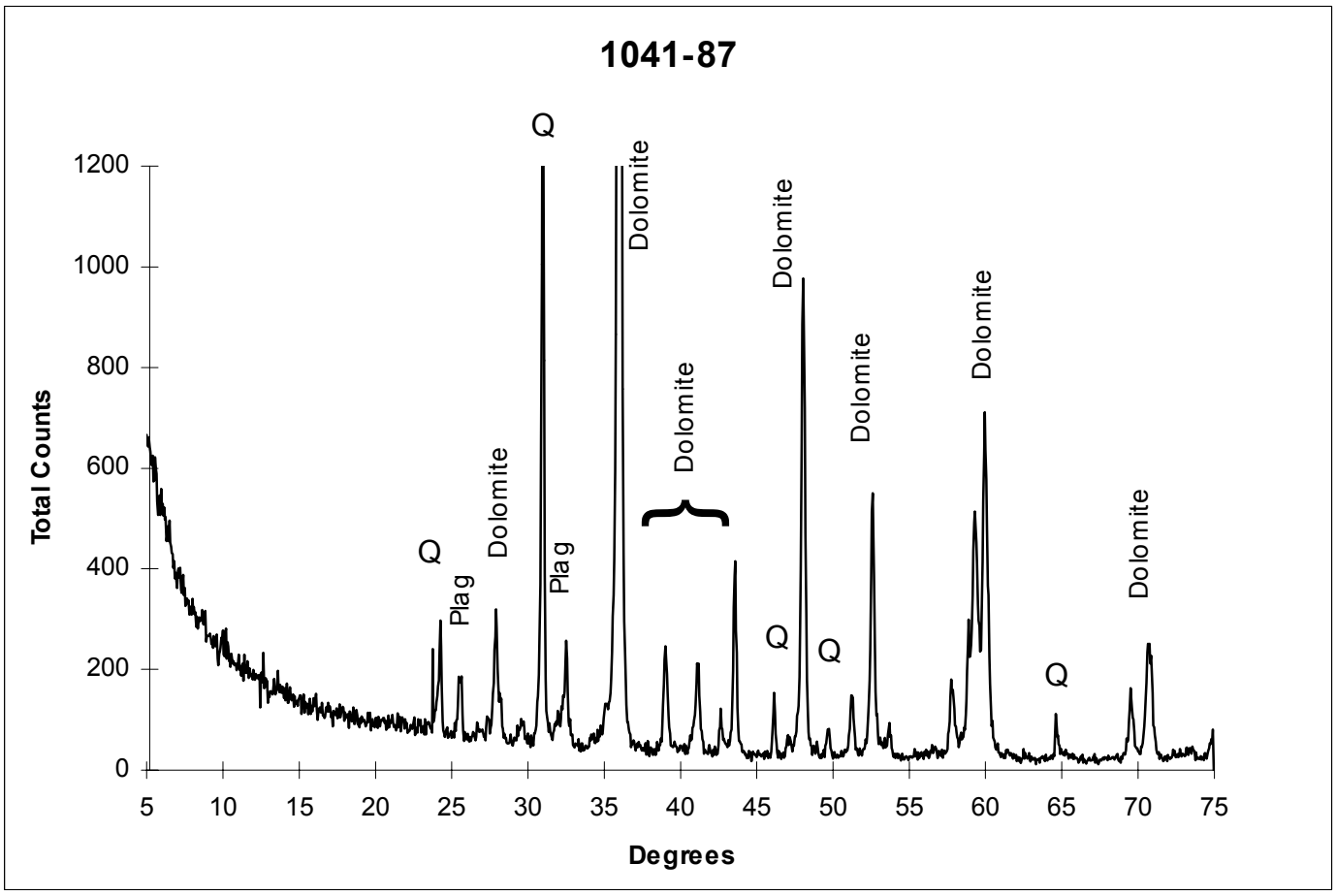

SAMPLE: 1041-88
FORMATION: Enorama Shale LOCATION: Mallee Water

MACRO: Red-brown fine sandy stomatolitic limestone.

MICRO: moderately sorted, angular grains size average 0.05mm (max.=0.07mm)
Composition: 8% Quartz, 9% Feldspars (Plagioclase and Orthoclase), 79% Dolomite, 4% Carbonaceous mud/heavy minerals.
Dolomite d-spacing: 2.885 - $Ca_{(1.0)}Mg_{(0.99)}Fe_{(0.01)}(CO_3)_2$

Comments: Dominant dolomicrite again lacks clotted texture but looks more like mud-flake intraclastic with stromatolitic lamination. Mud flakes distinguishable through varying amounts of included red mud. Several stylo-solution seams with associated disseminating carbonaceous mud, authigenic quartz and brightly luminescent dolomite cement, cut the bedding lamination at a high angle. Fine grained detritus includes diverse silicics and common xenoclstic carbonate.

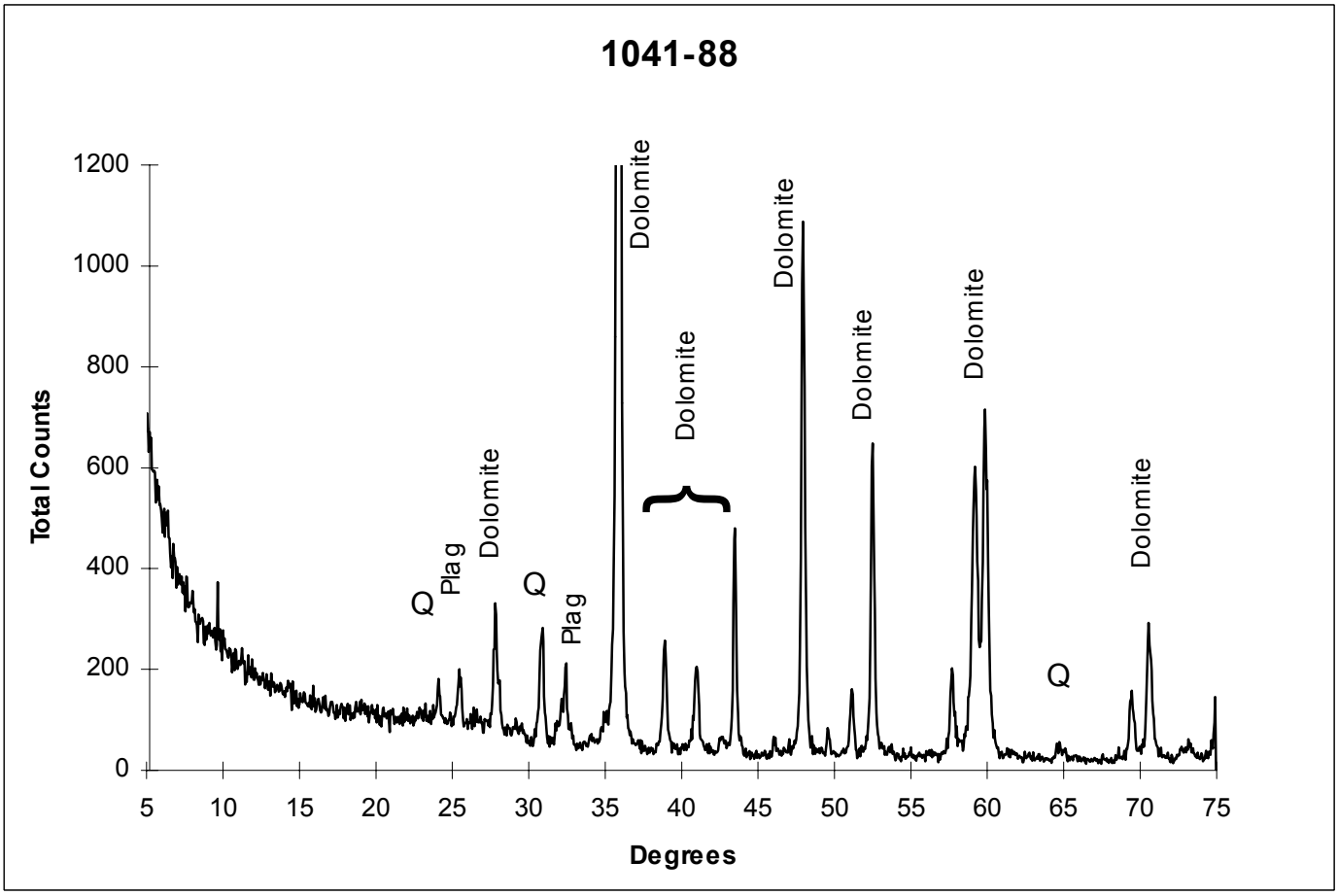

SAMPLE: 1041-89
FORMATION: Enorama Shale LOCATION: Mallee Water

MACRO: Pink-grey stomatolitic limestone.

MICRO: moderately sorted, dispersed minor clastic content, grains size average 0.05mm (max.=0.1mm)
Composition: 5% Quartz, 2% Feldpspar, 85% Dolomite, 8% Carbonaceous mud/heavy minerals.
Dolomite d-spacing: 2.885 - $Ca_{(1.0)}Mg_{(0.99)}Fe_{(0.01)}(CO_3)_2$

Comments: Dominant dolomite ranges from micrite to sparite. Again largely lacking clotted texture but recrystallisation developed around dolomitization vugs defined by anastomosing muddy micritic rims. Same bright yellow-orange luminescent vug coating cement is present and developed around rhombic dolospar euhedra. Coarser crystalline carbonate does not luminesce. Common high angle stylo-solution seams are generally associated with small amounts of dolomite and quartz cements and more carbonaceous material that disseminates into the surrounding dolomicrite. Includes rare "pockets" of locally abundant sub-rounded quartz grains and intraclasts.

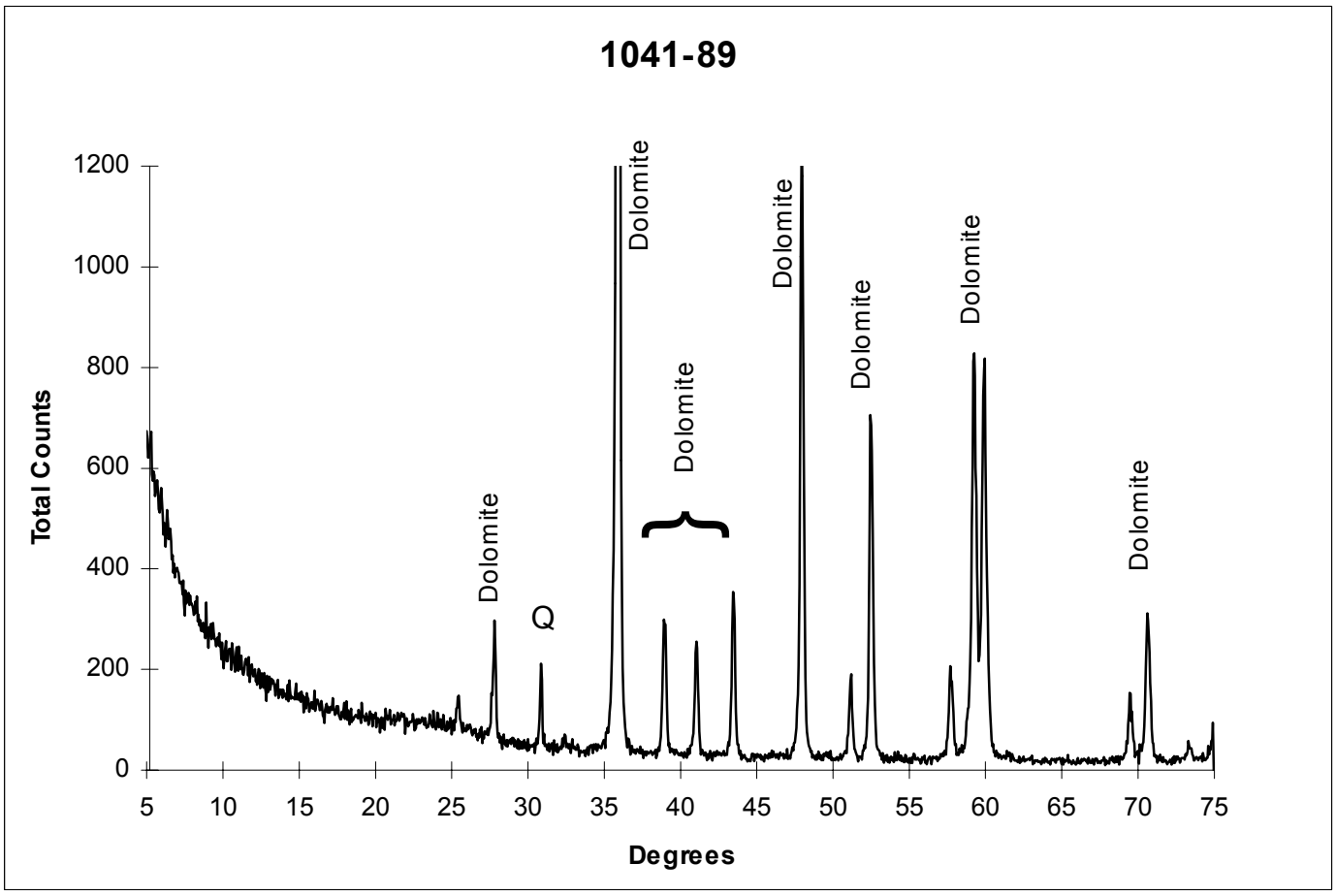

SAMPLE: 1041-93
FORMATION: Trezona Formation LOCATION: Doodney Hills

MACRO: Dark red stomatolitic limestone.

MICRO: moderate-well sorted, uncommon angular grains size average 0.05mm (max.=0.05mm)
Composition: 4% Quartz, 2% Feldspar, 88% Calcite, 1% Hematite/heavy minerals, 5% Carbonaceous mud.

Comments: Predominantly micrite to microspar, containing sparry molds of ripped-up cyanobacterial flakes with in situ stromatolitic carbonate mud. Well developed early diagenetic coarser subequant drusy calcite spar and carbonaceous mud provide cavity fill for a large proportion of this rock. Original inter-flake/granular porosity quite significant in parts. Rare stylo-veinlets are developed cross-cutting anastomosing cyanobacterial lamination. Small pockets of very fine silica minerals are uncommon.

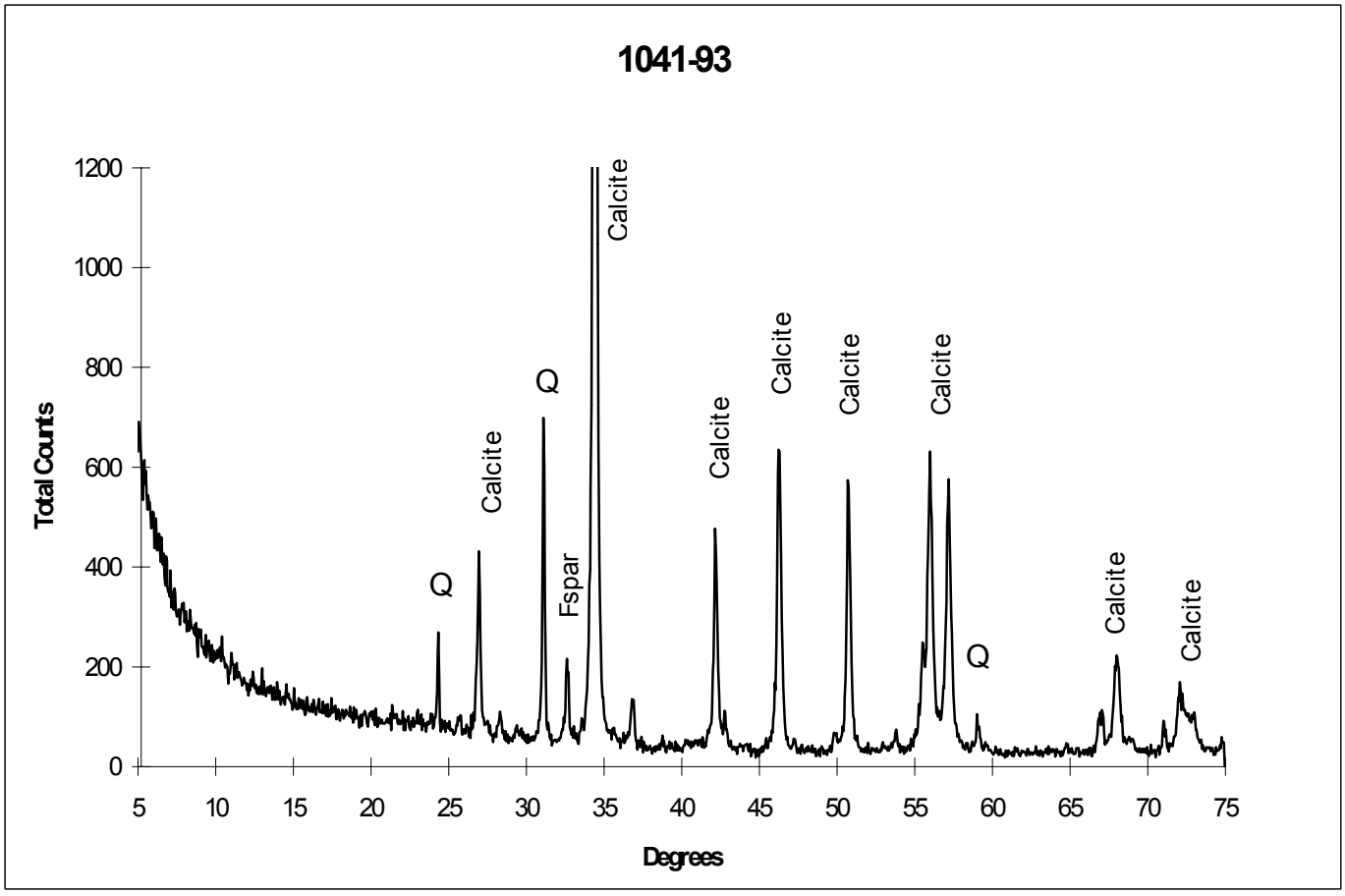

SAMPLE: 1041-95
FORMATION: Trezona Formation LOCATION: Doodney Hills

MACRO: dark red digitate stomatolitic limestone.

MICRO: moderate-well sorted, sub-angular grains size average 0.05mm (max.=0.07mm)
Composition: 3% Quartz, 2% Feldspar, 87% Calcite, 1% Hematite/heavy minerals, 7% Carbonaceous mud.

Comments: Carbonaceous mud and ferroan non-luminescent calcite populates poorly developed stylo-lamination parallel to original cyanobacterial-bedding. Micrite and microspar separate along bedding lamination. Development of small amounts of burial diagenetic mosaic spar in various porosity. Diagenetic history includes calcite solution seam developed at a low angle to bedding and several sets of thin (<0.05mm) long veinlets cross-cut the cyanobacterial-bedding lamination at a high angle. Relatively rare fine silica grains are dispersed amongst carbonate.

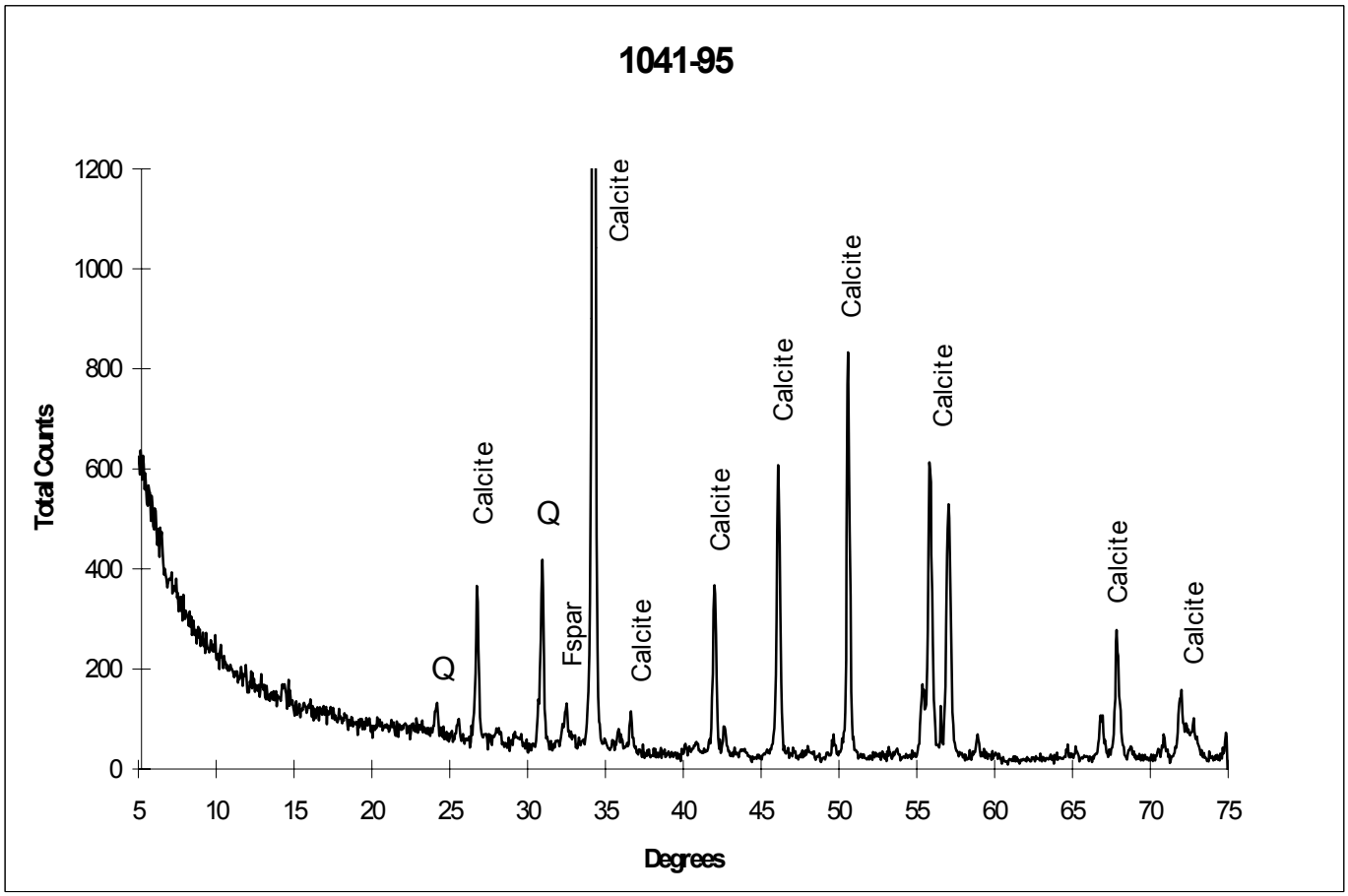

SAMPLE: 1041-98
FORMATION: Trezona Formation LOCATION: Doodney Hills

MACRO: Blue-green stomatolitic limestone.

MICRO: moderate-poorly sorted, angular grains size average 0.02mm (max.=0.05mm)
Composition: 8% Quartz, 7% Feldspar (commonly Orthoclase), 76% Calcite, 9% Carbonaceous muds/heavy minerals.

Comments: Pervasive micrite. Carbonaceous stylo-laminae including development of small amounts of brightly luminescent calcite cement. Dispersed and bedded fine grained clastics include large proportion (~5%) of both brightly yellow and dull orange luminescing detrital carbonates. Wholly consolidated stromatolitic limestone with less original porosity through turbidity/breakup and thus virtually no cement.

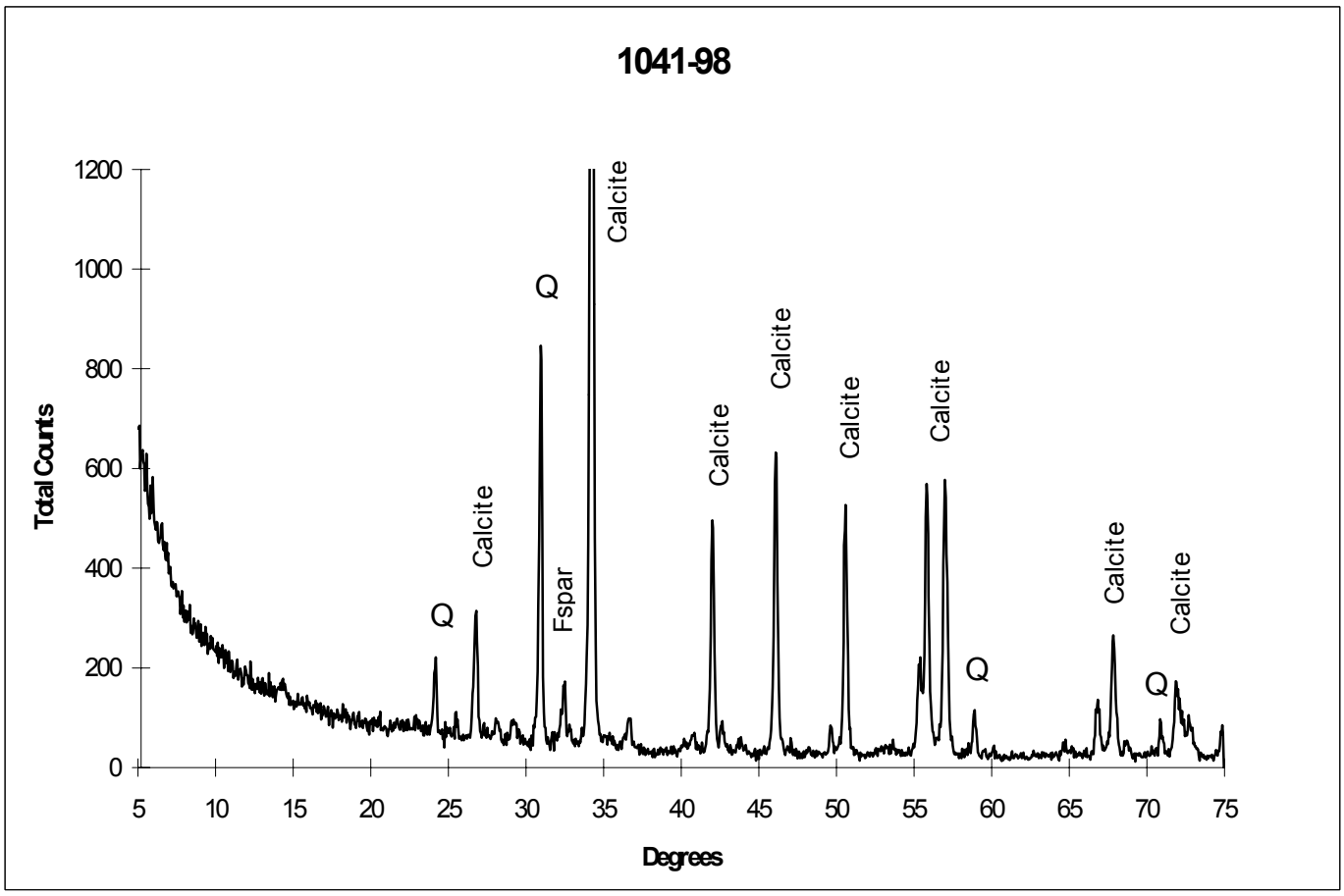

SAMPLE: 1041-99
FORMATION: Trezona Formation LOCATION: Doodney Hills

MACRO: Buff-grey pink ooid grainstone.

MICRO: moderate-well sorted, relatively equant sized ooids average 0.2mm (max.=0.5mm)
Composition: 3% Quartz, 4% Feldspar, 86% Calcite, 1% Micaceous hematite/heavy minerals, 6% Carbonaceous muds/clay.

Comments: Nearly homogenous ooid grainstone but for the top corner of this slide indicating reworking of ooid and micritic limestones. Ooids in general have peloidal nuclei that has commonly recrystallised into microsparry cement and include authigenic growths of silica minerals. Soft sediment deformation breaks ooids along micro-lineaments and pre-dates recrystallisation as it involves the dark bladed early burial isopachous cement like that seen in the Etina Formation. Ghosted ooid molds nearly disappear in plane polarised light due to recrystallisation. Minor late stage drusy mosaic spar developed in reworked inter-particle porosity. Rare very thin veinlets also developed.

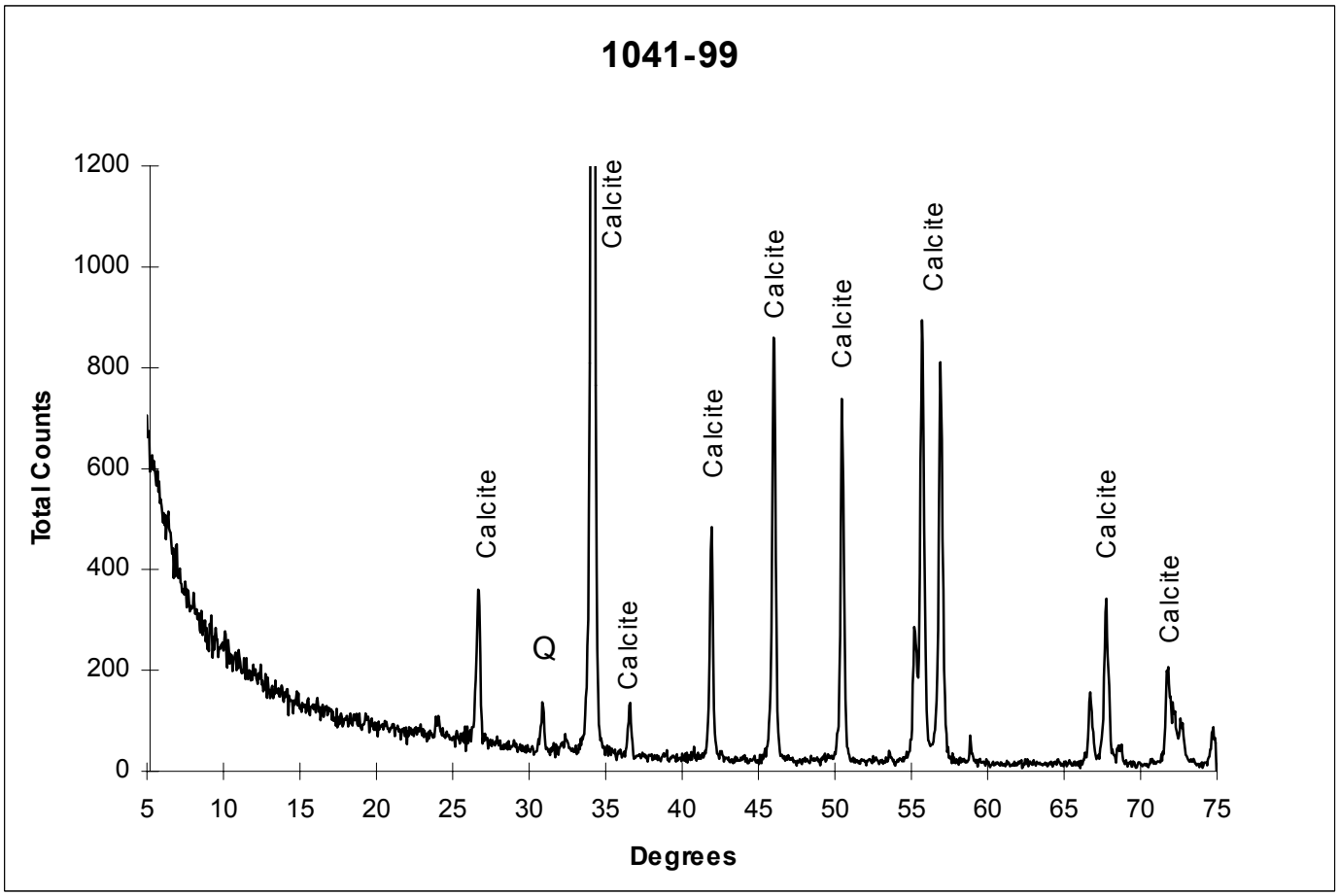

SAMPLE: 1041-102
FORMATION: Trezona Formation LOCATION: Doodney Hills

MACRO: Dark red stomatolitic limestone.

MICRO: moderate-well sorted, very fine sub-angular grains size <0.01mm (max.=0.01mm)
Composition: 4% Quartz, 6% Feldspar (commonly Orthoclase), 78% Calcite, 2% Hematite/heavy minerals, 10% Carbonaceous mud/clay.

Comments: Predominantly micrite to diagenetic microspar developed in cleaner/mud free bedding. Carbonaceous mud populates poorly developed stylo-lamination parallel to original cyanobacterial-bedding. Very rare early diagenetic solution veinlet oblique to bedding and in luminescent continuity with background recrystallisation. Dispersed and very fine silica grains are common in small amounts but perhaps more common in occurrence with carbonaceous material.

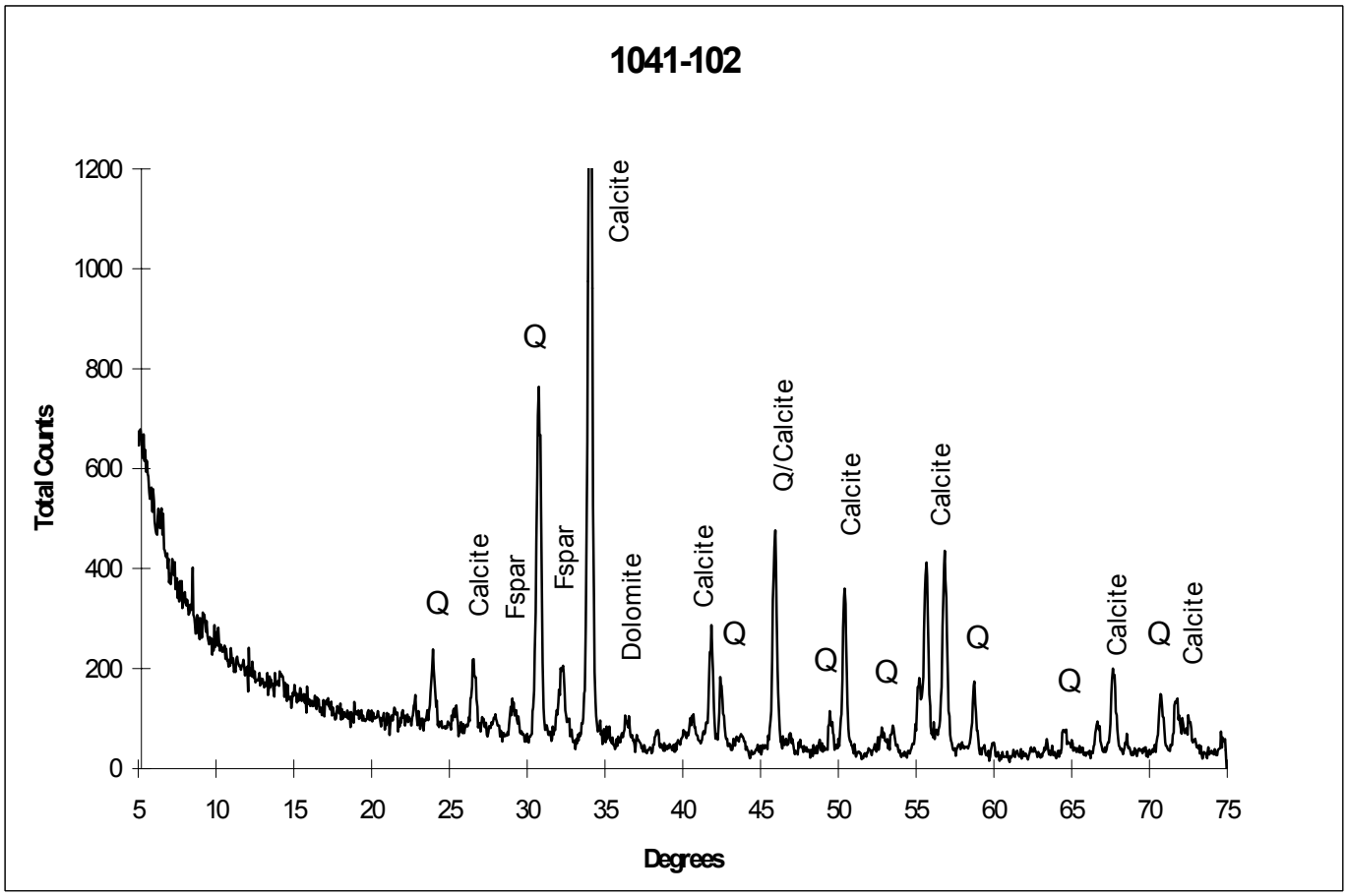

SAMPLE: 1041-104
FORMATION: Trezona Formation LOCATION: Doodney Hills

MACRO: Blue-grey fine-medium ooid grainstone.

MICRO: moderate-well sorted, relatively equant sized ooids average 0.2mm (max.=0.3mm)
Composition: 2% Quartz, 1% Feldspar, 95% Calcite, 2% Carbonaceous mud/heavy minerals.

Comments: Generally bedding parallel but also in a wide dendritic pattern, recrystallisation of ooid fabric leaving minor relic rim-defining muds that are nearly undecipherable in plane light but clearly separated under cathodoluminescence. Inter-ooid early marine burial dark bladed cement is nearly complete in occluding pores before generation of a brightly luminescent ooid recrystallisation phase. Soft sediment deformation/compaction features once again include linear features of crushed ooids and development of both dark and lighter phases therein. Rare development of two distinct generations of thin calcite cement veinlets.

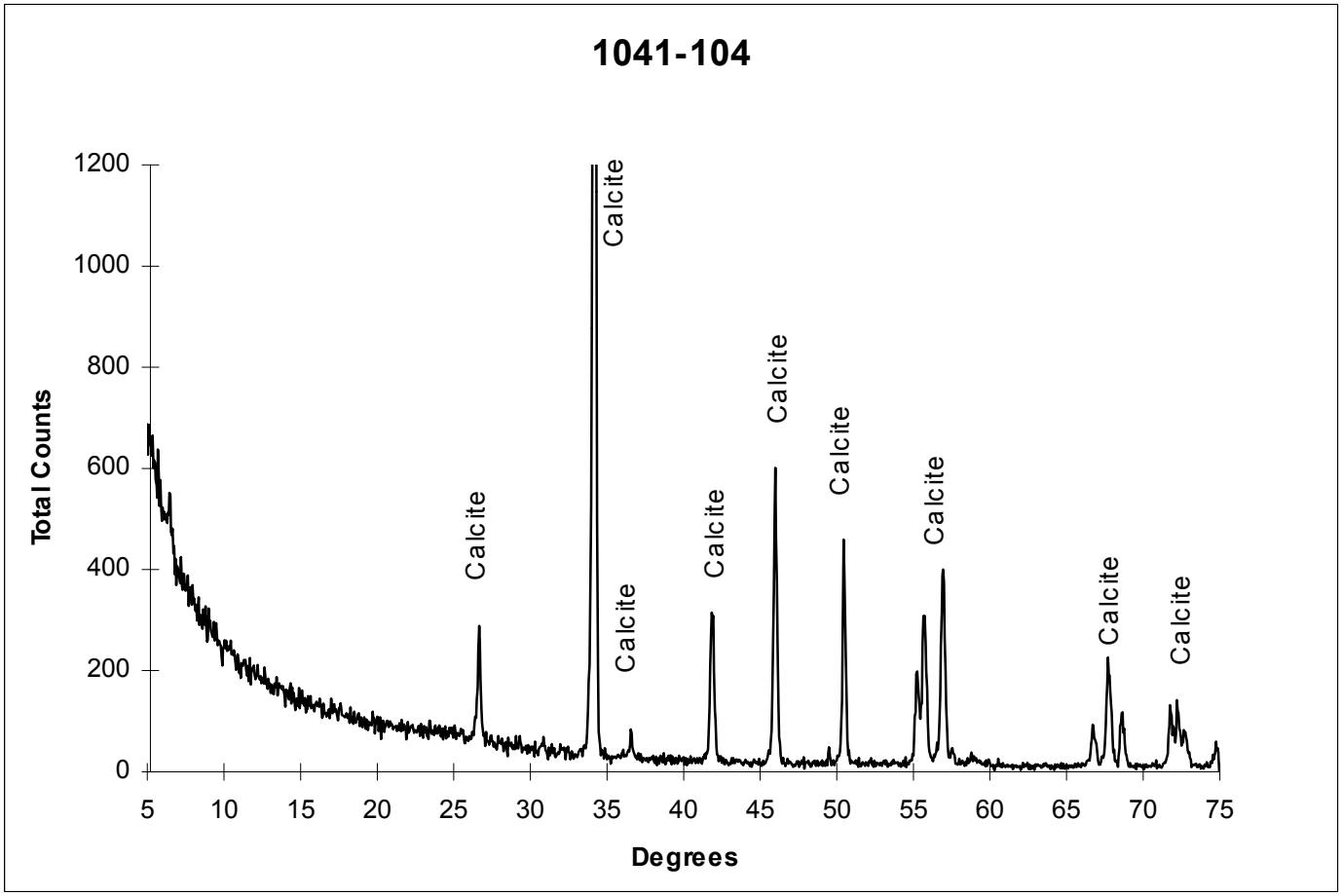

SAMPLE: 1041-111
FORMATION: Etina Formation LOCATION: Dedmans Bore

MACRO: yellow-brown coarsly crystalline (1-2mm) marble, occasional calcite vein in hand sample.

MICRO: poorly sorted, crystal-grain size 2-0.05mm,
Composition: Quartz 28% (of that 15% chert), 8% Plagioclase, 38% Calcite spar, 22% calc-micritc matrix (2% micritic Limestone intraclasts), 4% dolomicrite.
Dolomite d-spacing: 2.885 - $Ca_{(1.0)}Mg_{(0.98)}Fe_{(0.02)}(CO_3)_2$

Comments: Relic intraclast rims and a fabric of solution seams observable before widespread recrystalization of this rock topoikilotopic calcite spar. Very fine (0.05mm) euhedral quartz grains often include micro-crystalline carbonate minerals. Rare larger crystalline quartz grains exhibit fractured habit with etched grain boundaries indicating a high degree of post-burial compaction.

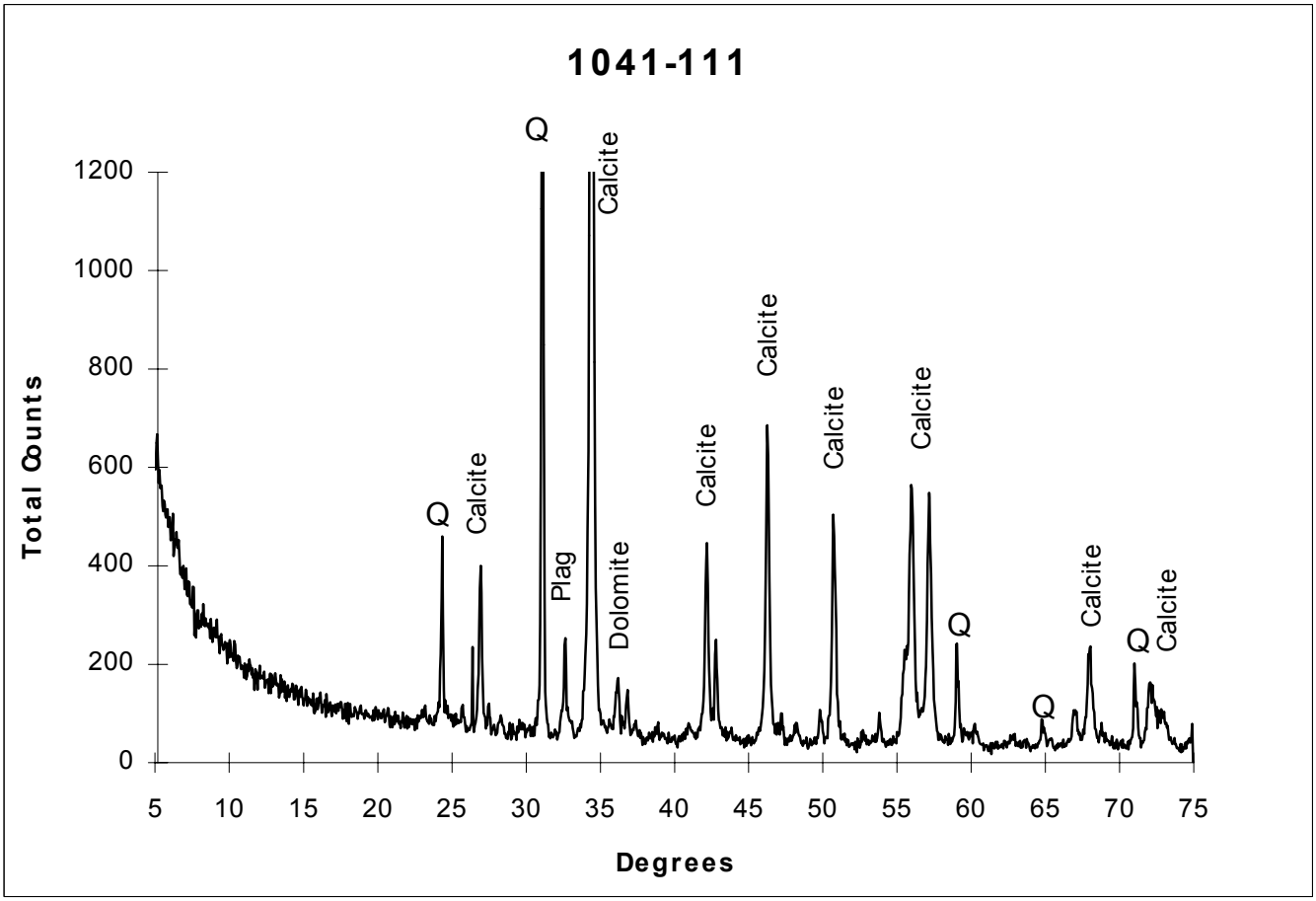

SAMPLE: 1041-113
FORMATION: Diapiric xenoclast LOCATION: Mallee Water

MACRO: yellow sandy ripple-bedded dolostone, rare (5%) visible scattered heavy minerals, occasional fine fracture.

MICRO: moderate-poorly sorted, grain size 0.1-0.01mm
Composition: Quartz 21% (of that 22% chert), 7% Plagioclase, 6% Chlorite, 2% Micaceous Hematite, 5% Talc, 59% Dolomite as microcrystalline micritc cement.
Dolomite d-spacing: 2.885 - $Ca_{(1.0)}Mg_{(0.98)}Fe_{(0.02)}(CO_3)_2$

Comments: Graded bedding defines separate mineral fabrics. More coarsely grained (0.1mm) areas are dominated by siliciclastic cements. Fibrous-elongate chlorite defines laterally inconsistent solution seams in micritc layers. Talc laths up to 2mm long that replace anhydrite after gypsum are produced by decarbonation of dolomite reacting with chert. Rosettes resembling original gypsum precipitation can be observed. Red-rimmed euhedral micaceous hematite was probably detrital in origin. Late stage fractures are for the most part spar-healed.

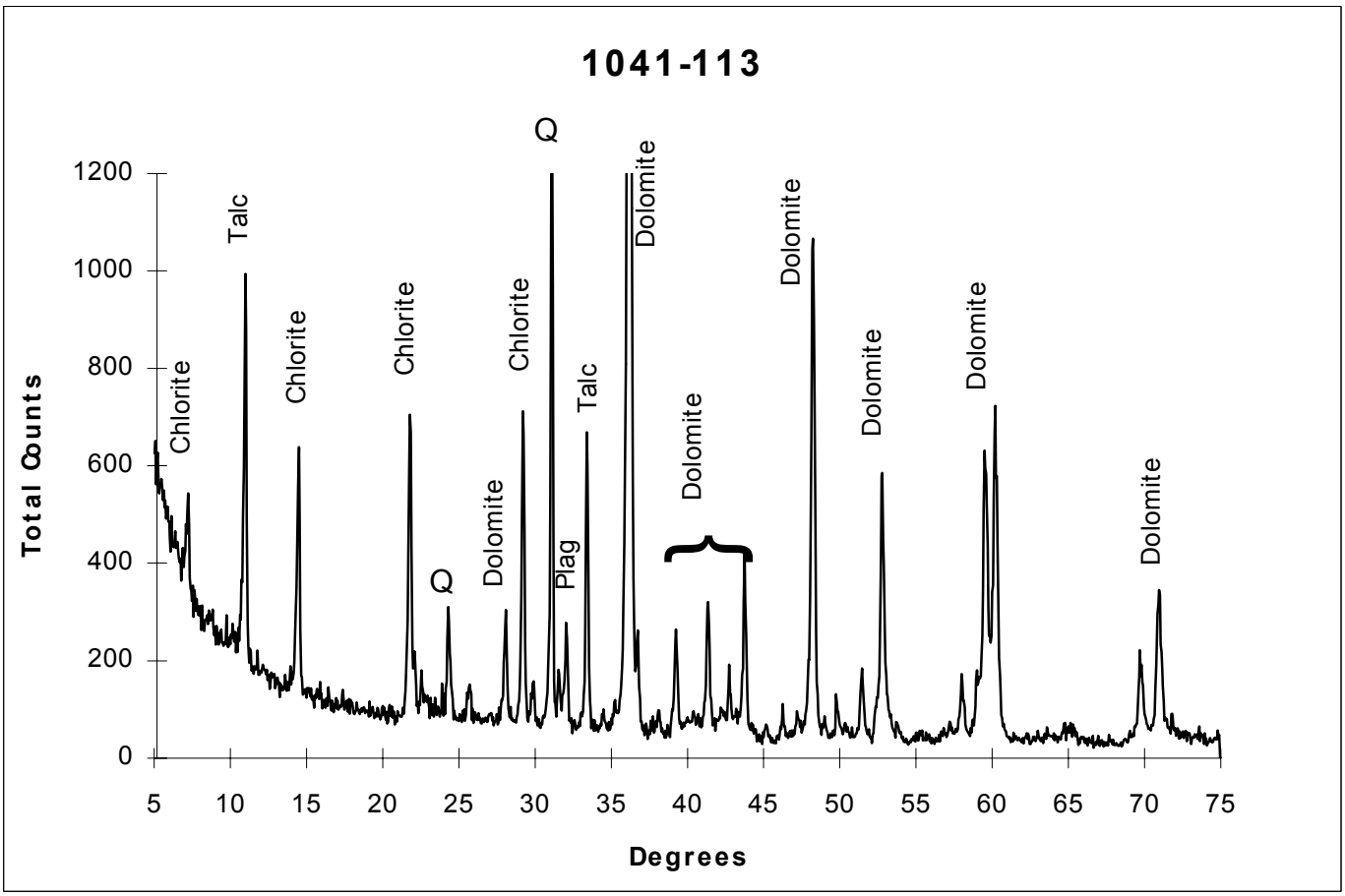

SAMPLE: 1041-114
FORMATION: Enorama Shale LOCATION: Mallee Water

MACRO: dark red arenacous ripple-bedded dolostone, rare stylolitic-type solution seam texture.

MICRO: poorly sorted, grain size 0.1-0.01mm
Composition: Quartz 18% (of that 10% detrital chert), 9% Plagioclase, 3% Heavy Minerals, 63% Dolomite, 7% Fe-mud matrix.
Dolomite d-spacing: 2.885 - $Ca_{(1.0)}Mg_{(0.98)}Fe_{(0.02)}(CO_3)_2$

Comments: Quartz overgrowths visible on larger grains are defined by inclusion of micrite. Slight elongate bedding parallel solution seam textures provide impetus for rare recrystallization of siliciclastic grains. An iron rich mud makes up a finely dispersed portion of the matrix which gives this rock its characteristic colour. The rock is characterised by inclusion of light coloured mud clasts that do not have the dark red matrix, yet under CL. they are in luminescence-continuity with the rest of the rock. They are most likely pure dolomicrite intraclasts from the lagoon atop the Enorama Diapir.

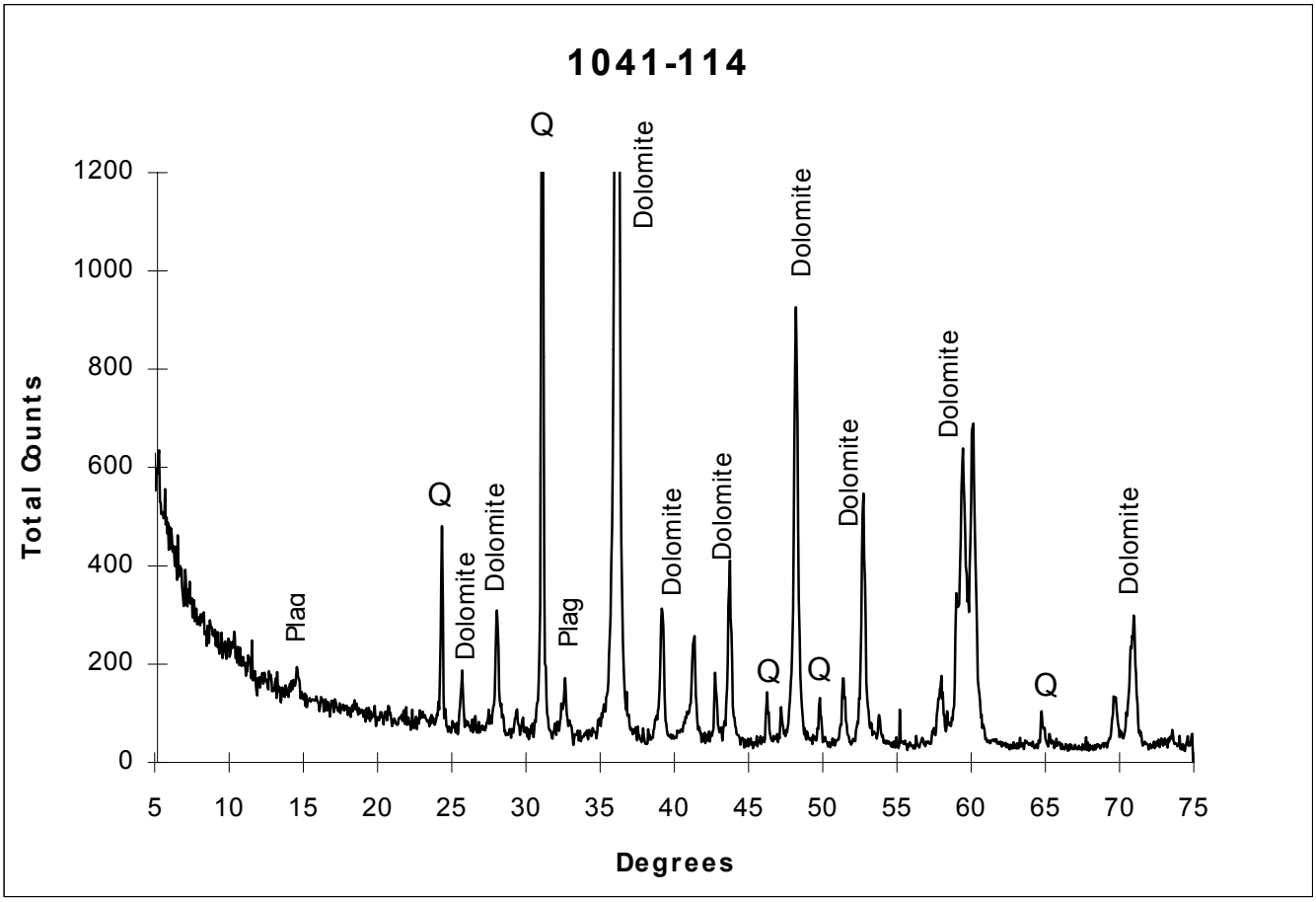

SAMPLE: 1041-117
FORMATION: Trezona Formation LOCATION: Bulls Gap

MACRO: Buff crystalline limestone.

MICRO: sub-equant (ave.=0.5mm) coarse crystalline mosaic
Composition: 1% Quartz, 15% Calcite, 77% Dolomite, 4% Pyrolucite/heavy minerals, 3% Limonite/mud.
Dolomite d-spacing: 2.885 - $Ca_{(1.0)}Mg_{(0.98)}Fe_{(0.02)}(CO_3)_2$

Comments: Dominated by the idiotopic coarse dolomite spar, this sample contains smaller amounts of interstitial limonite/calcite cements, heavy mineral opaques and occasional quartz grains with well developed overgrowth cement. Blocky anhedral calcite cements are focussed on fenestrae and larger dissolution porosity that is distributed in a dendritic pattern. There are both solution seams and veins at a high angle to bedding filled with blocky calcite cement, the latter the coarser and cleaner of the two.

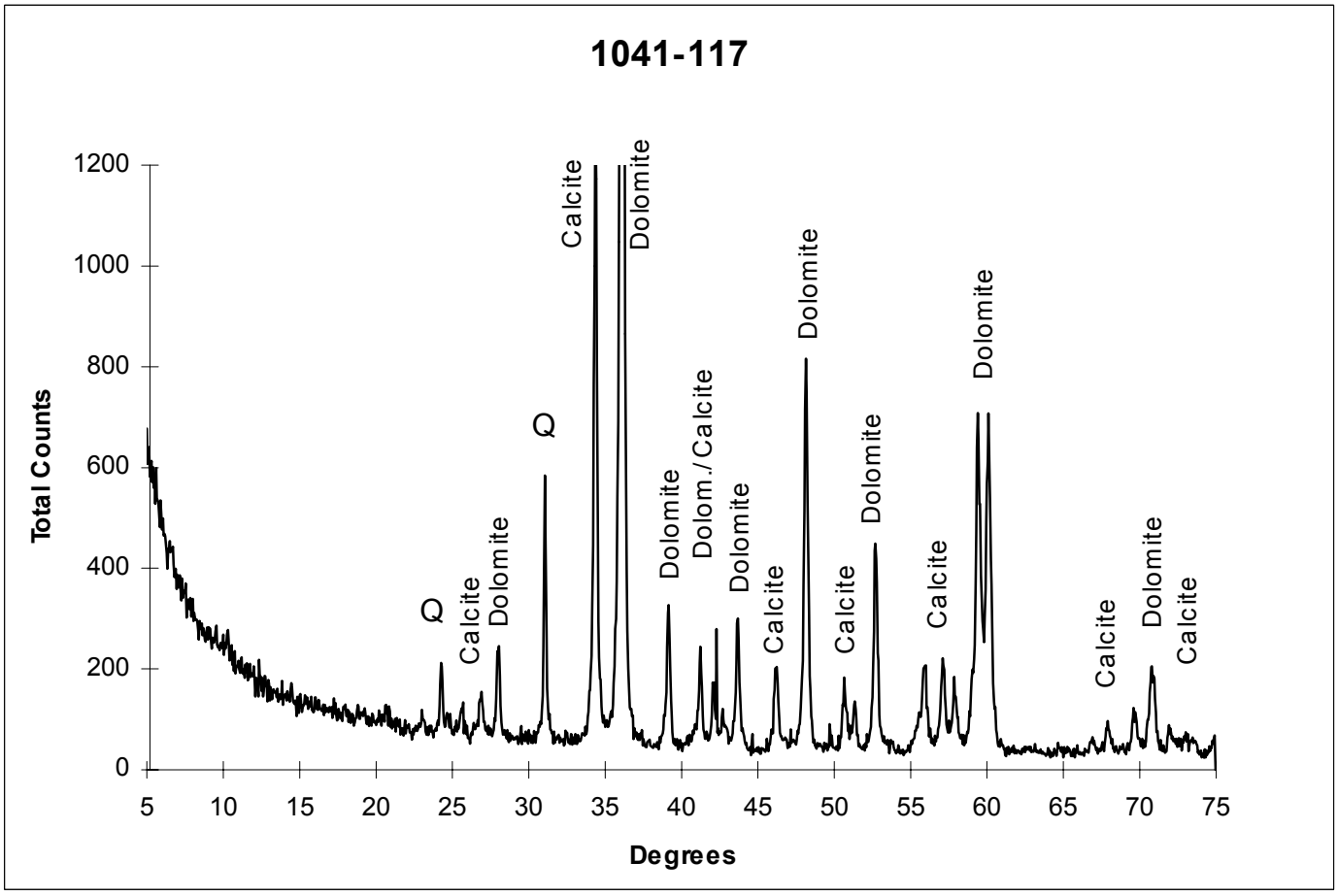

SAMPLE: 1041-120
FORMATION: Trezona Formation LOCATION: Bulls Gap

MACRO: Orange-brown recrystallised limestone.

MICRO: coarse crystalline mosaic
Composition: 2% Quartz, 92% Calcite, 2% Pyrolucite/heavy minerals, 4% Limonite/mud.

Comments: Irregular anhedral mosaic of calcite cements dominated by drusy orange calcite and puncuated by dissolution cavities filled with further generations of spar. Orange-brown ferroan calcite spread in semi-dendritic pattern focussing on developed fenestral porosity. Several generations of stylolites and veins are filled with individual calcite cements. Rare intercrystalline quartz commonly has authigenic growth cements. Any primary fabric is indistinguishable.

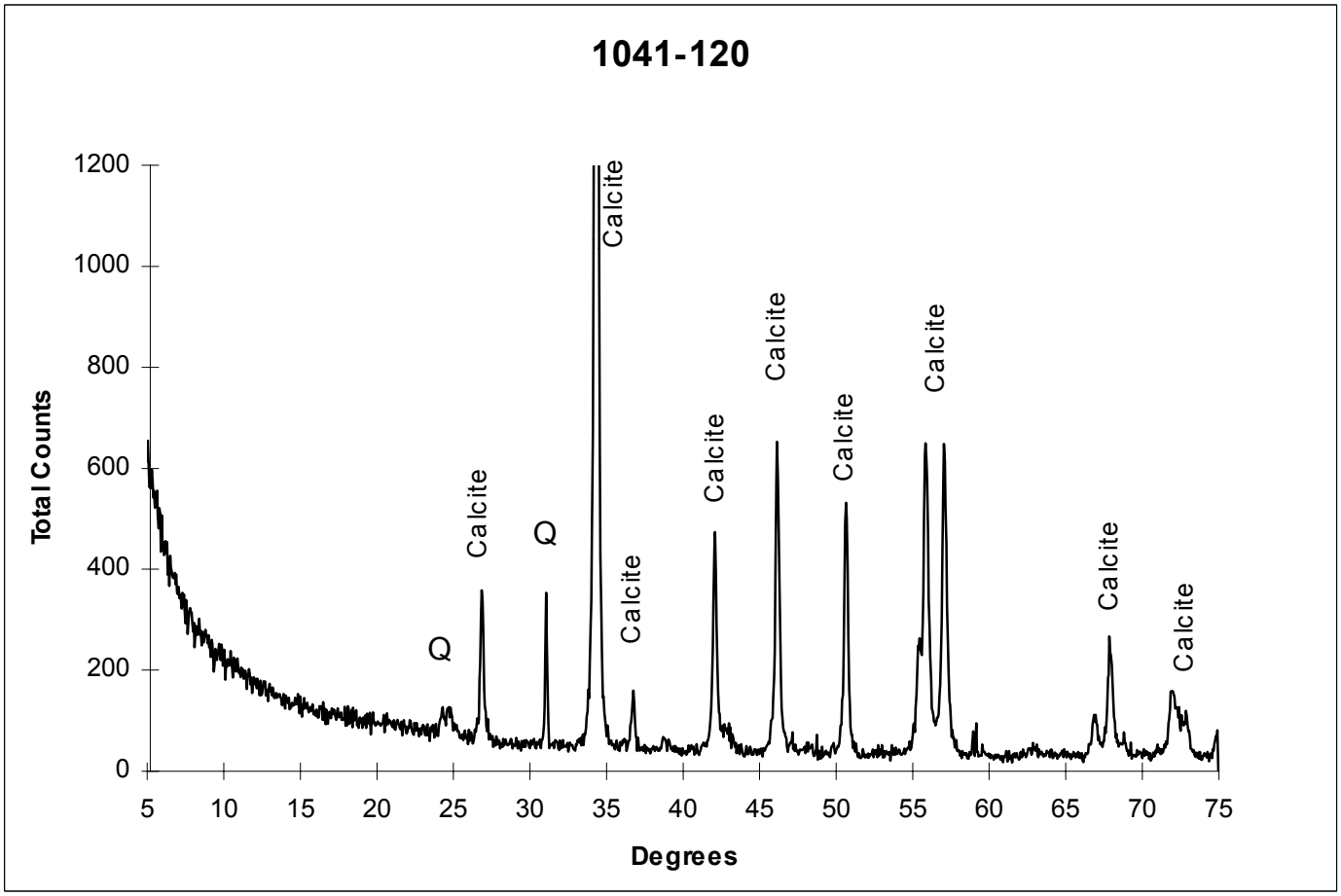

SAMPLE: 1041-140
FORMATION: Etina Formation LOCATION: Popes

MACRO: Blue-green very fine sandy limestone.

MICRO: moderate-well sorted, sub-angular grains size average 0.05mm (max.=0.08mm)
Composition: 33% Quartz, 5% Plagioclase, 14% Orthoclase, 21% Calcite, 6% Dolomite, 8% Heavy minerals/opaques, 11% Chlorite-mica/clays/mud.
Dolomite d-spacing: 2.889 - $Ca_{(1.0)}Mg_{(0.91)}Fe_{(0.09)}(CO_3)_2$

Comments: Quartz is mono-crystalline. Small overgrowth cements on quartz and feldspars are slightly etched by carbonate cements. Mineralogic and textural immaturity typical of fine grained sediment. Mica grains observed indicate negligible compaction. Carbonate, viz. dolomite, is common in detrital form. Micritc calcite is a common material binding grains.

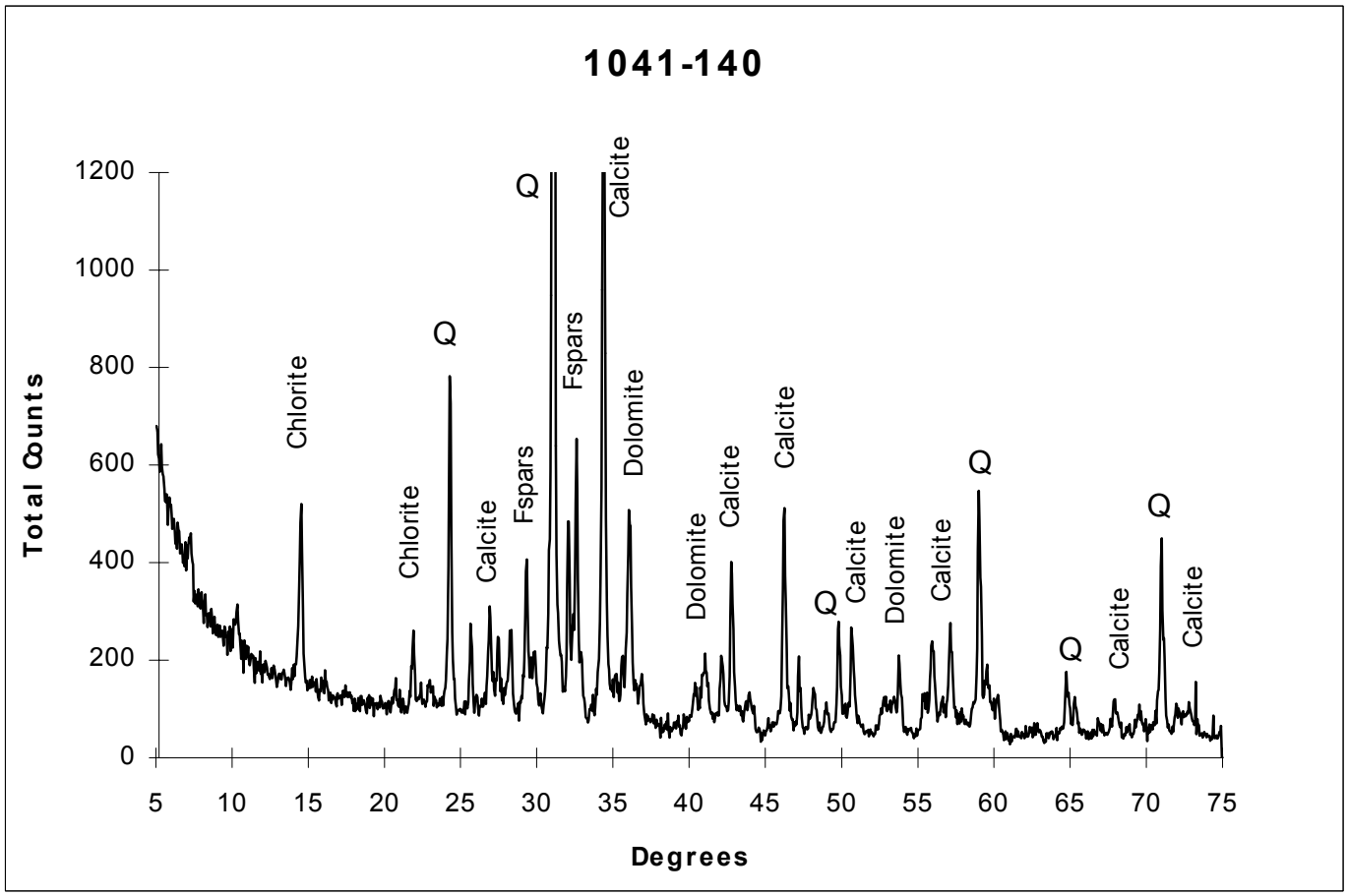

SAMPLE: 1041-141
FORMATION: Etina Formation LOCATION: Popes

MACRO: Blue fine-medium sandy oolitic limestone.

MICRO: well sorted, sub-rounded grains size average 0.2mm (max.=0.5mm)
Composition: 15% Quartz, 9% Feldspar (commonly Orthoclase), 68% Calcite (50% ooidal/micrite, 18% cement), 2% heavy minerals/opaques, 6% clays/mud.

Comments: Detrital mono-crystalline quartz and feldspars, commonly exhibit euhedral form overgrowths etched by carbonate. Feldspars show slight indication of alteration along twinning to carbonate. Ooids have largely pure calcitic-micrite cores and are generally bound in carbonate mud. Cathodoluminescence discerns dominant ooid-micritic cement from restricted dark early burial cement and rare, brightly luminescent, initially-detrital carbonate at ooid cores. Intermediate compaction has created sutured grain contacts without large amounts of mineral dissolution.

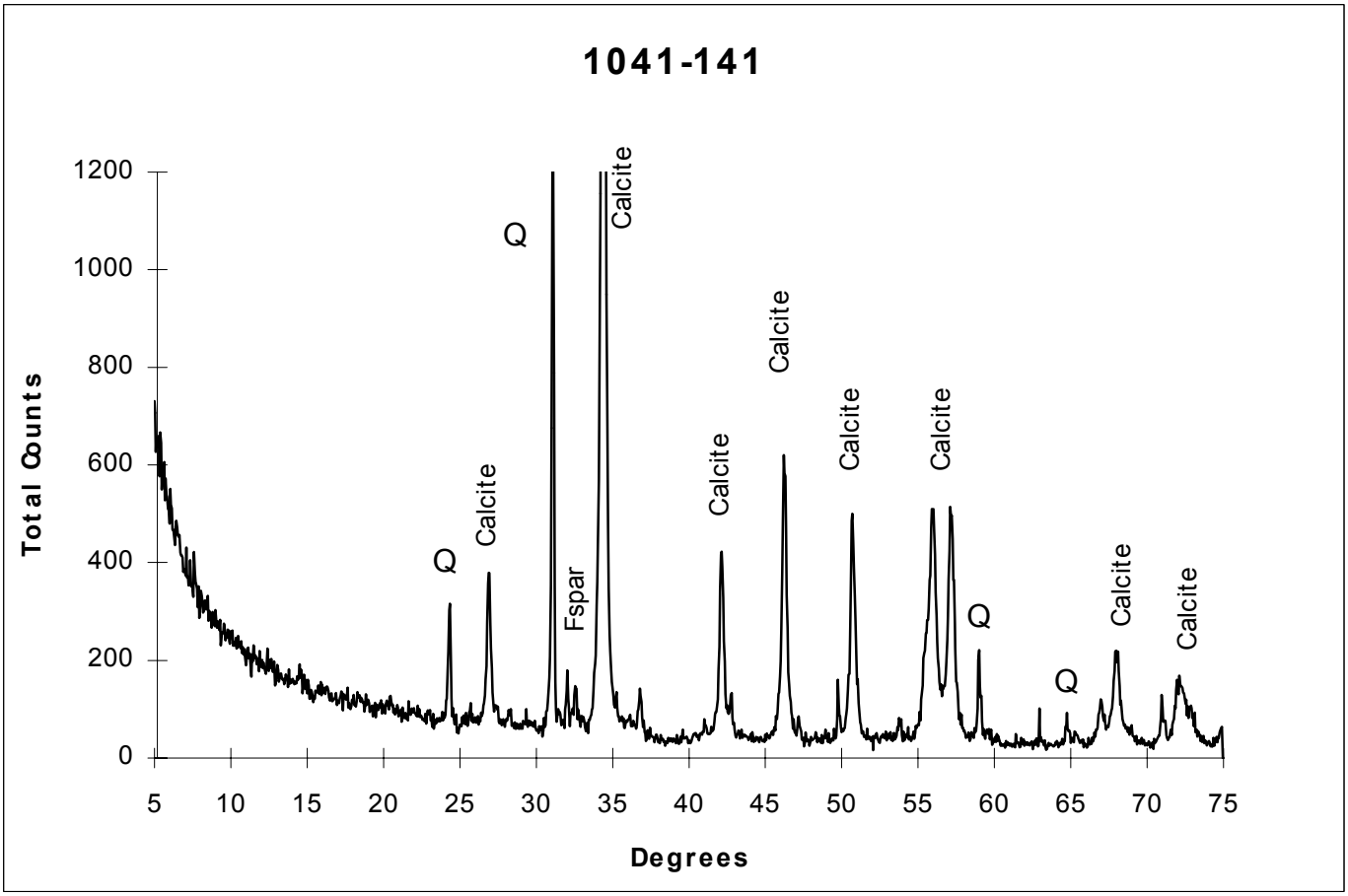

SAMPLE: 1041-142
FORMATION: Etina Formation LOCATION: Popes

MACRO: Blue medium to coarse sandy limestone.

MICRO: well sorted, rounded grains size average 0.3mm (max.=0.6mm) Composition: 15% Quartz, 9% Feldspar (commonly Orthoclase), 65% Calcite, 2% Heavy minerals/opaques, 8% Chlorite/clay/mud.

Comments: A high degree of compaction has created common sutured and concavo-convex grain contacts, stylo-laminae and mobilisation of carbonate as well as occasional fracturing of silicic grains. Generally well rounded grains have common euhedral overgrowth cements and are well etched by carbonate. Feldspars exhibit occasional alteration along twinning to carbonate. Thin ooid rims are preserved before dominant bladed-prismatic burial cement pervades. Later stage calcite cements in stylolite and vein are the same CL signature/elemental chemistry. Although not evident via XRD, green-blue authigenic chlorite coating grains in green stylo-fracture.

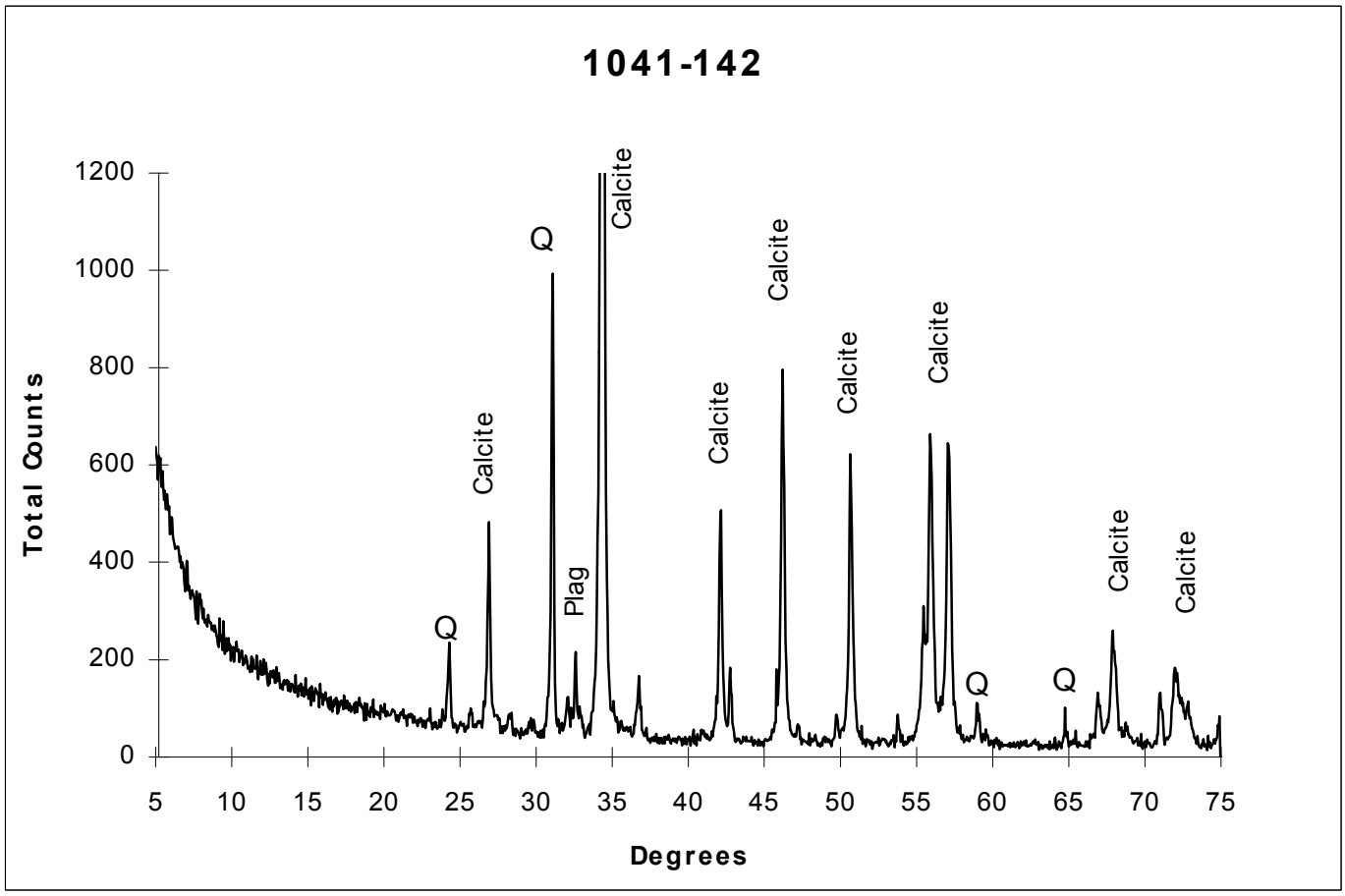

SAMPLE: 1041-145
FORMATION: Etina Formation LOCATION: Popes

MACRO: Dark blue medium sandy oolitic limestone.

MICRO: moderate-well sorted, rounded grains size average 0.4mm (max.=2.0mm)
Composition: 21% Quartz, 9% Feldspar, 60% Calcite (22% micrite, 38% cement), 2% Heavy minerals/opaques, 8% clay/mud.

Comments: Quartz is generally mono-crystalline, along with feldspar lacking overgrowth cements. Well rounded grains and peloidal-sandy calcareous ooid nuclei, slightly recrystallised in this sample. Dark rhombic forms, possibly calcite after dolomite, are observed under cathodoluminescence within peloids. Dark bladed-prismatic isopachous early burial calcite cement is dominant in the texture of this rock.

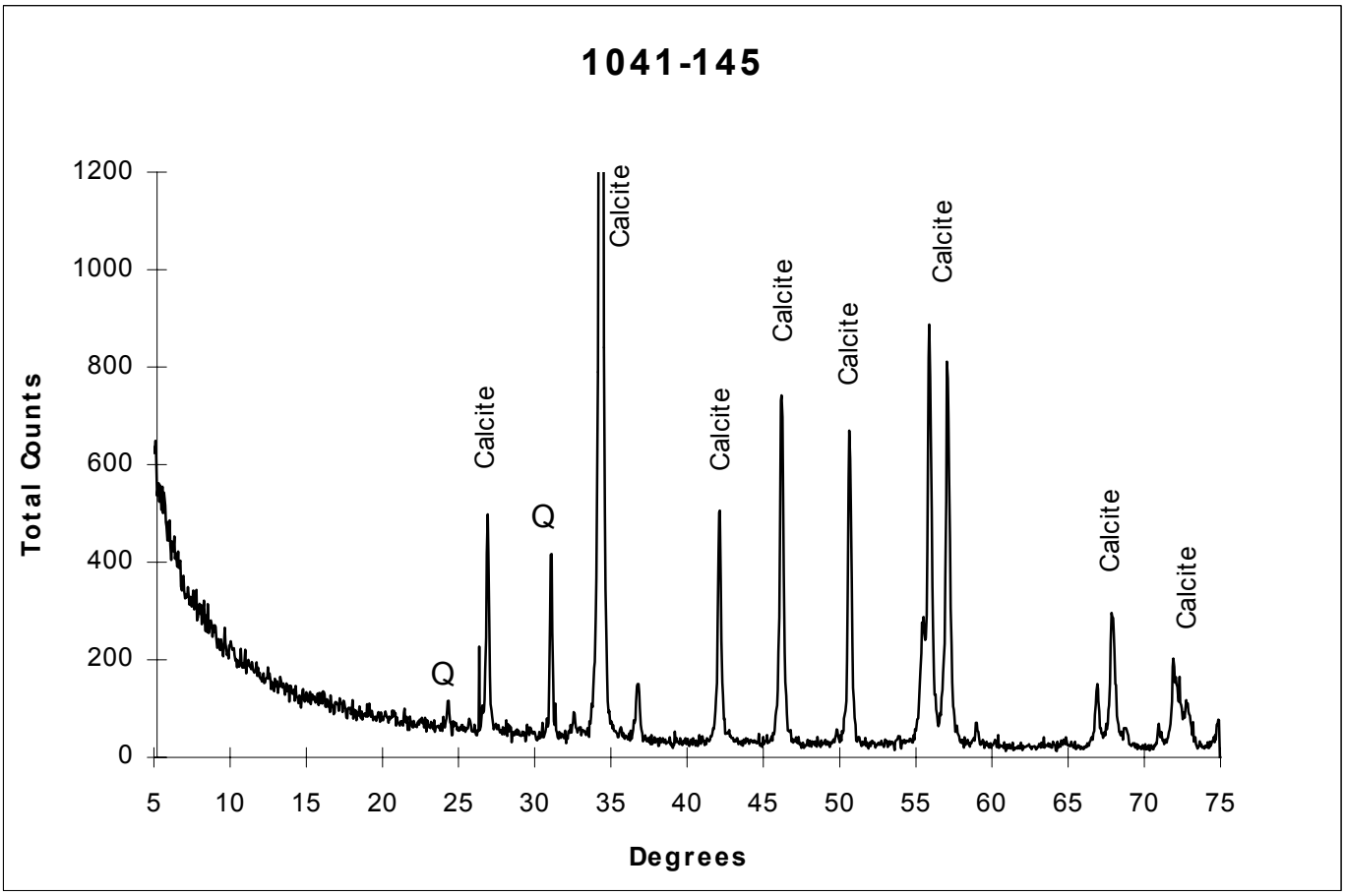

SAMPLE: 1041-148
FORMATION: Etina Formation LOCATION: Popes

MACRO: Blue-green fine sandy limestone.

MICRO: poorly sorted, sub-rounded grains size average 0.06mm (max.=0.5mm)
Composition: 15% Quartz, 8% Feldspar (commonly Orthoclase), 59% Calcite (commonly micritic, but also detrital and spar forms), 6% Heavy minerals/opaques, 12% Chlorite/clays/mud.

Comments: Quartz is generally mono-crystalline and like feldspar, lacking overgrowth cements. Well rounded grains in sandy layers include detrital calcite as well as binding spar-cement although identical luminescent signature suggests precipitation in water of same elemental chemistry. Micritic calcite is dominant in the finer grained layers. One fine (~.05mm) stylo-fracture is observed cutting bedding at oblique low angle and is filled with similar luminescent cement.

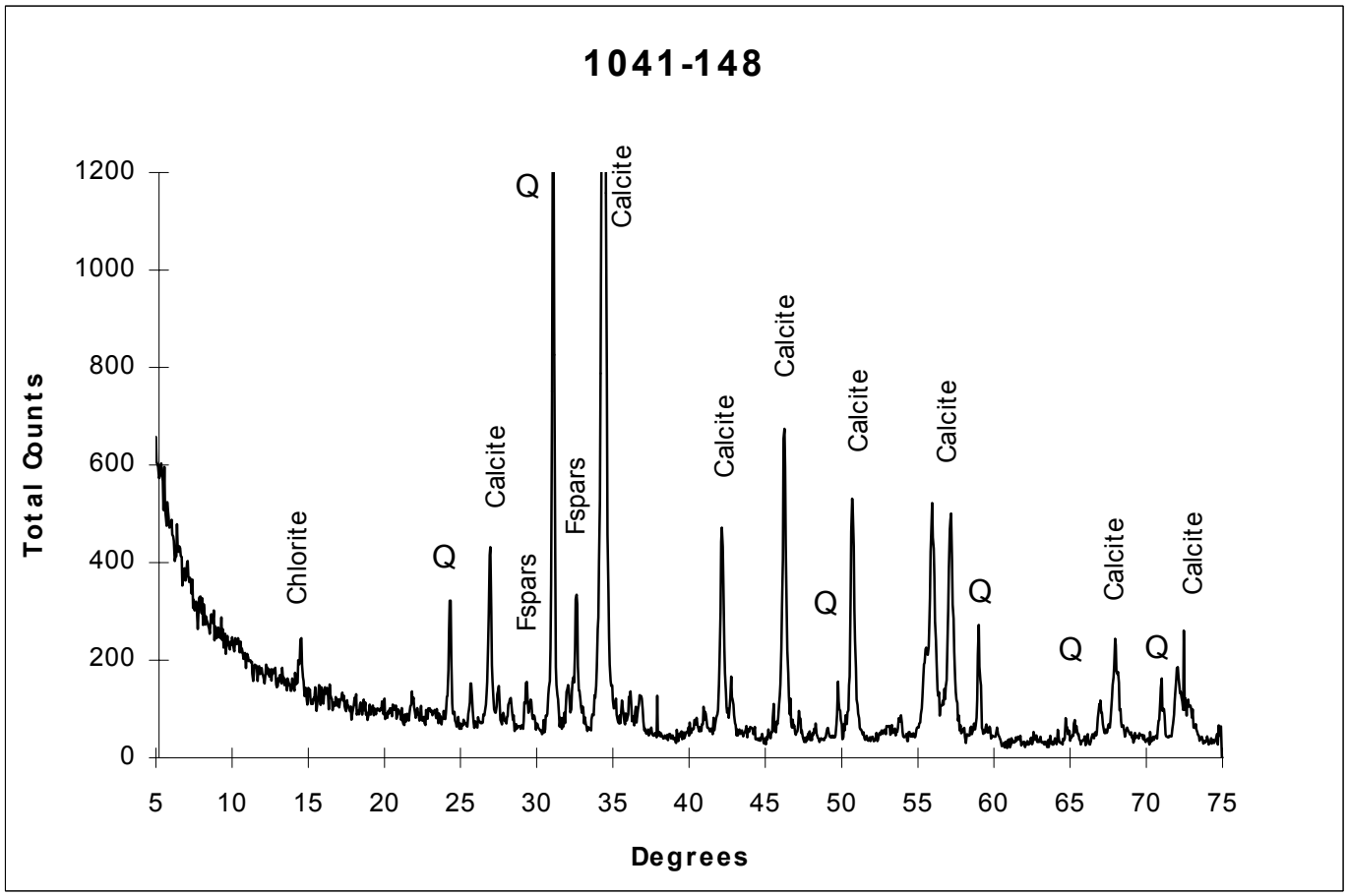

SAMPLE: 1041-160
FORMATION: Etina Formation LOCATION: Popes

MACRO: Blue-green-brown intraclastic limestone.

MICRO: moderate-poorly sorted, sub-angular grains size average 0.8mm (max.=4.0cm cyanobacterial flake)
Composition: 12% Quartz, 6% Feldspar (Plagioclase and Orthoclase), 62% Calcite, 4% Heavy mineral/opaques, 4% Dolomite (commonly detrital), 12% clays/mud.
Dolomite d-spacing: 2.881 - $Ca_{(1.0)}Mg_{(1.00)}Fe_{(0.00)}(CO_3)_2$

Comments: Grains are included in reworked clasts (very fine) as well as interstices (fine-medium). Silicic grains lack overgrowth cements. Reworked clasts generally comprise micritic calcite with diverse range of detrital grains. Detrital dolomite commonly observed outside reworked clasts. They commonly exhibit brittle fracture and are annealed by both the early burial bladed-prismatic cement and later stage carbonaceous(?) mud. Latest stage, brightly luminescent coarse mosaic spar cement is evident but uncommon.

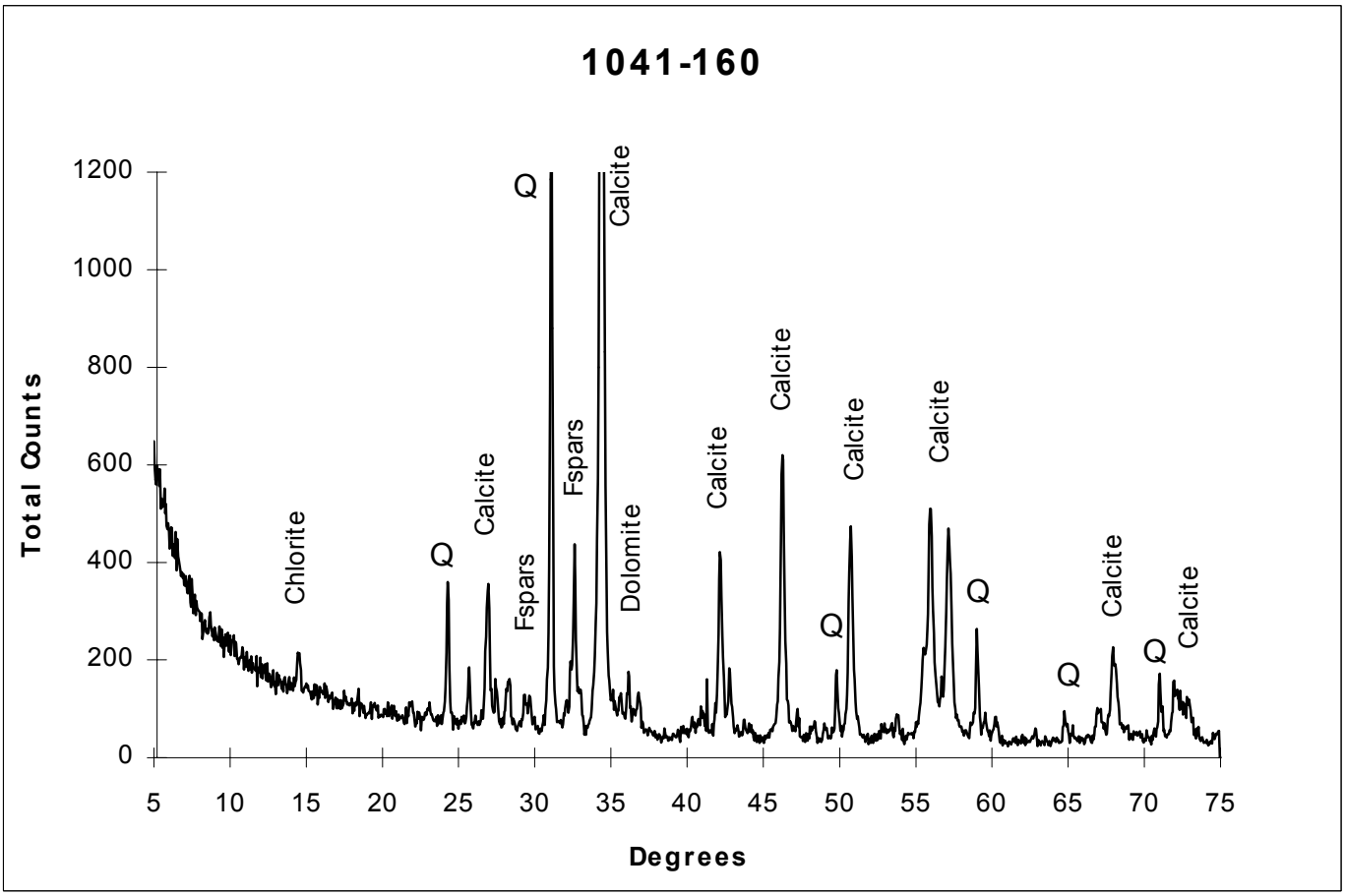

SAMPLE: 1041-165
FORMATION: Etina Formation LOCATION: Popes

MACRO: Blue medium sandy limestone.

MICRO: moderate-well sorted, rounded grains size average 0.4mm (max.=0.8mm)
Composition: 11% Quartz, 5% Feldspars (Plagioclase and Orthoclase), 76% Calcite (23% micrite, 53% spar), 2% Heavy mineral/opaques, 4% Dolomite, 2% clay/mud.
Dolomite d-spacing: 2.885 - $Ca_{(1.0)}Mg_{(0.98)}Fe_{(0.02)}(CO_3)_2$

Comments: Silicic grains in ooid cores have only very minor overgrowth cements before etching and encroachment by calcite. Preservation of ooids ranges widely, whilst cores include diapirically-derived, brightly luminescent carbonate. Reworked grains include oolite and commonly have thin oolitic rims. Rhombic forms are common within ooid cores. Moderate amounts of isopachous bladed-prismatic calcite spar cement exist before common latest stage pore occluding mosaic calcspar.